In Vivo 2-Photon Calcium Imaging
Of Olfactory Interneurons
In The Honeybee Antennal Lobe

Dissertation zur Erlangung des akademischen Grades des
Doktors der Naturwissenschaften (Dr. rer. nat.)

eingereicht im Fachbereich Biologie, Chemie, Pharmazie
der Freien Universität Berlin

vorgelegt von

Tilman Franke
aus Münster

Dezember 2009

Die vorliegende Arbeit wurde im Zeitraum von September 2002 bis April 2004 und Oktober 2004 bis Dezember 2009 angefertigt.

1. Gutachter: Prof. Dr. Dr. h. c. Randolf Menzel

2. Gutachter: PD Dr. Martin Nawrot

Disputation am 18.12.09

Abbreviations

Abbreviations used in the text:

2PLSM	2-photon laser scanning microscope / microscopy
AL	Antennal lobe
RN	Receptor neuron
PN	Projection neuron
LIN	Local interneuron
OR	Odorant receptor protein
OB	Olfactory bulb
OBP	Odorant binding protein
PBP	Pheromone binding protein
lACT	Lateral antenno-cerebralis tract
mACT	Medial antenno-cerebralis tract
mlACT	Mediolateral antenno-cerebralis tract
LH	Lateral horn
MB	Mushroom body
PMT	Photomultiplier
FWHM	Fourier-width half maximum
HX1	1-Hexanol
LIX	Binary mixture of HX1 and LIO
LIO	Linalool
OC2	2-Octanol
NO1	1-Nonanol
MIX	Binary mixture of NO1 and OC1
OC1	1-Octanol
FoV	Field of view
CSA	Curve Sketching Algorithm
TCA	Template Correlation Algorithm
SWCA	Sliding Window Correlation Algorithm

Zusammenfassung

Jeder Meßvorgang bedeutet eine Beschränkung auf das Meßbare; der größere Teil der Welt wird ausgeblendet. Mit der Methode der Elektrophysiologie können Aktionspotentiale in Nervenzellen gemesen werden, und die Zellen können in weiteren Schritten gefärbt, rekonstruiert, udn identifiziert werden. Die Methode ist jedoch blind gegenüber dem Netzwerk in dem die Nervenzellen eingebettet sind. Zeitaufgelöste Weitfeldfluoreszenzmikroskopie kann die Aktivität von ganzen Hirnregionen gleichzeitig visualisieren, aber die Raum- und Zeitauflösung ist zu gering um die Signale einzelner Nervenzellen darstellen zu können. 2-Photonen-Laser-Restermikroskopie verspricht, die Lücke zwischen diesen Meßmethoden, die in der Erforschung der Duftverarbeitung im Gehirn der Honigbiene weitlich angewandt wurden, zu schließen. Um die Erforschung der Duftverarbeitung im Gehirn der Honigbiene voranzubringen, habe ich ein 2-Photonen-Laser-Rastermikroskop für Messungen von mit dem Kalzium-abhängigen Farbstoff FURA2 gefärbten Nervenzellen im Gehirn der Honigbiene aufgebaut. Das Mikroskop erwies sich als tauglich, zeitgleich und in hoher Zeitauflösung die Signale mehrerer Nervenzellen aufzunehmen. Messungen an einzelnen Bienen konnten über Stunden durchgeführt werden, was für eine geringe Phototoxizität der Belichtung spricht. In dreidimensional aufgelösten Bilderstapeln, die in lebenden Tieren aufgezeichnet wurden, wurde eine zur Rekonstruktion und Identifikation von mehreren Nervenzellen pro Präparat ausreichende Raumauflösung erreicht. Um das Potenzial der Methode auszuloten, habe ich eine vieldiskutiete Frage bearbeitet: Warum gibt es in jeder der 160 funktionelle Einheiten (Glomeruli) im Riechhirn der Honigbiene mehrere Ausgangsneurone? Die unvollständige Konvergenz-Divergenz-Verschaltung zwischen sensorischen Nervenzellen, Nervenzellen im Riechhirn, und Nervenzellen im Pilzlörper konnte mit den oben beschriebenen bisher genutzen Methoden nicht näher untersucht werden. Dennoch wurden in der Vergangenheit verschiedene Konzepte postuliert, die den $\approx$10 Ausgangsneuronen, die jeden Glomerulus innervieren, funktionelle Relevanz beimessen. Durch die gleichzeitige Aufnahme der Nervenzellaktivität in mehreren Ausgangsneuronen mittels

2-Photonen-Laser-Rastermikroskopie werden die postulierten Konzepte testbar. Ein auf der Bestimmung von Korrelationskoeffizienten basierende Auswertungsmethode wurde angewandt, um das Maß der Synchronie zwischen Ausgangsneuronen zu bestimmen. Es konnte gezeigt werden, daß Ausgangsneurone innerhalb eines Glomerulus stark synchronisiert sind, und zwar nicht nur während duftevozierter Nervenzellsignale, sondern auch während Spontanaktivität. Synchronie wurde separat in drei Zuständen der Nervenzellen bestimmt, nämlich während Signalen von Erregung, Hemmung und während der Abwesenheit meßbarer Signale. Es zeigte sich, daß Signale von Nervenzellerregung während Spontanaktivität stärker synchronisier sind als Signale, die während der Duftstimulation auftraten. Also ist offenbar nicht der erregende Eingang von sensorischen Neuronen während Duftstimuli der synchronisierende Faktor, sondern Synchronie ist eine Eigenschaft des lokalen Nervenzellnnetzwerkes im Riechhirn. Die stärkeste Synchronie zeigte sich, wenn Zweige ein und des selben Neurons verglichen wurden. Etwas geringere Synchronie war zwischen Zweigen von unterschiedlichen Nervenzellen innerhalb des selben Glomerulus zu verzeichnen. Überaschenderweise konnten Synchrony und Asynchronie zwischen bestimmten Paaren von Nervenzellfortsätzen nicht nur während Phasen von Nervenzellerregung, sondern auch in Phasen von Hemmung und Ruhe festgestellt werden. Eine 19-38 Hz Komponente des Ruherauschens ist notwendig, um den Unterschied in der Synchronie zwischen Zweigen des selben gegenüber Zweigen von zwei verschiedenen Nervenzellen detektieren zu können.

Abstract

Each and any measurement method is tantamount to applying a filter to the world. Electrophysiology can detect action potentials and allows neuroanatomical reconstruction and identification of the measured neuron, if cells are filled after recordings. The method is, however, blind for the network that neurons are embedded in. Wide-filed imaging can visualize the activity of networks of neurons or whole neuropils, but lacks the spatial and temporal resolution necessary to identify single neurons. 2-photon microscopy promises to bridge the gap between those methods. To augment research on the olfactory system of the honeybee, I constructed a 2-photon laser scanning microscope (2PLSM) for imaging of neurons stained with the calcium-sensor FURA2. When the 2PLSM was finally operable, it proved to be capable of parallel measurements of calcium signals within multiple identifiable neurons simultaneously at a high temporal resolution. Recordings in single bees could last for hours, which is evidence for low phototoxicity. Anatomical image stacks with sufficient resolution for reconstructions of the cells were acquired *in vivo* in the 2PLSM. To demonstrate the potential of the method, I attempted to elucidate a hitherto unsolved, but much debated question: Why are there several projection neurons in each of the functional units of the primary olfactory brain center (glomeruli)? The incomplete convergence-divergence-connectivity between sensory neurons, antennal lobe neurons, and mushroom body neurons has inspired postulates about the functional relevance of the ≈10 projection neurons that innervate each glomerulus. By recording from several projection neurons in parallel during odor-stimulations and during rest, hypothetical concepts become testable. Using a correlation-based measure of synchrony, it could be shown that projection neurons that are housed within the same glomerulus are indeed synchronized to a high degree, during odor-evoked activity as during rest. Determining synchrony was done separately for three signaling states that were automatically detected in all recordings: signals of excitation, signals of inhibition, and rest. Careful analysis of synchrony across signaling states revealed that synchrony of signals of excitation is higher during spontaneous signals as compared to signals

that occurred during odor stimuli. Thus synchrony is result of the network of neurons in the antennal lobe, and not caused by input from sensory neurons. Synchrony was found to be strongest between sub-branches of a single neurons. Slightly weaker was the synchrony between branches of two distinct neurons housed in the same glomerulus. Surprisingly, synchrony and asynchrony were also found during resting phases in which recordings were void of detectable calcium signals. It could be shown that noise-like baseline fluctuations in a frequency band 19-38 Hz are essential for the detectability of the difference in synchrony between branches from the same vs. branches of different neurons in the same glomerulus.

Contents

Contents

Contents

Part 1

Introduction

Preface

This thesis stands in the tradition of both the neuroanatomical and the neurophysiological approach of neurosciences. I will report here on the results from my research project in which a rather young technique, 2-photon laser scanning microscopy (2PLSM), has been applied for the first time to a well characterized model system, namely the antennal lobe (AL) of the honeybee, *Apis mellifera*. Neurobiology is a field in which technical advances have always been of paramount importance. Ramón y Cajal, for instance, was able to confirm his neuron doctrine not before he was able to obtain results from microscopic studies featuring a silver-nitrate staining technique that he and his co-workers developed with the aim to stress the functional role of neurons, as opposed to fibrils, in the nervous system. While the technique of the light microscope was rather perfected at Cajal's time, it was a perfected staining method that was needed to settle the dispute between reticularists and followers of Cajal's neuron doctrine. Reticularism was a school of thought inspired by the fine fibrils found first by Remak (1843, 1844), in preparations of crustacean nervous tissue. When Apáthy published his study on complete fibrillar pathways across whole nervous systems (Apáthy, 1897), this strengthened the view of fibrils as the basic units in which excitation was conducted within nerve tracts, while the nerve cells would only serve protective and insulating function. Cajal on the other hand had yet to find a staining method that would allow to prove the concept of neurons as *the* basic organization principle in nervous tissue. The silver-based photographic procedure, invented by Simarro Lacabra (1900) and adapted by Cajal finally brought the evidence that the ominous fibrils were unlikely to be the basic conducting pathway within neurons (Ramón y Cajal 1903a; full account of the staining method in Ramón y Cajal 1903b).

To cut a long story short, this anecdote shows that the methods used have tremendous impact on the possible findings. In the worst case, the findings can be misleading, rendering interpretations false. This is one of the reasons why scientific communication always includes an account of the techniques used, so that reproduction of results can be attempted. But that is not enough:

Another vital mechanism to assure correctness of data and interpretations is the advancement of the techniques available. As Cajal wrote in his recollections (Spanish original in Ramón y Cajal 1923; English translation in Ramón y Cajal 1937):

> "For the histologist, every advance in staining technique is something like the acquisition of a new sense directed to the unknown."

The same holds true for new microscope techniques. Now that the fields of science became more specialized, new techniques are sometimes not developed by the same scientists that require them for their work. The most common way for a new technique into the scientist's lab starts in another scientist's lab. But more often than not, the new technique is not embraced by the sciences before it is put into a product by a commercial enterprise. This is unfortunate, because (1) the one-size-fits-all design of the enterprises might be ill suited for the scientist's purpose, (2) by this way much time passes from the development of a technique until its application to a scientific question, and (3) the product will initially be very expensive.

The story was not different for the 2PLSM. The technique has been proposed to be of use for the neurosciences in Denk *et al.* (1990); the whole spectrum of measurements that become technically feasible with the 2PLSM were conclusively described in Denk *et al.* (1994). The technique is, in Cajal's wording, like a new sense, as it allows to record images from the brains of living animals that have only been possible in fixed preparations beforehand; additionally it enables the researcher to perform optophysiological measurements of neuronal activity at a resolution that resembles the state of the art microscopic technique, the confocal microscope. The 2PLSM is also, in Cajal's wording, directed to the unknown, because until the first *in vivo* recordings with a 2PLSM, only speculation fills the gap of information that the standard techniques of wide-field imaging, confocal microscopy, and electrophysiology leave open, even if combined. Nevertheless, desirable as it may appear to put to use a 2PLSM, there are still rather few publications around that report on results from routinely acquired measurements. I mentioned above that the detour via the microscope manufacturers may account for such delay. In the case of the 2PLSM it was even worse: The technique was patented, and the patent was bought by an enterprise that did not even construct microscopes. The other microscope manufacturers were resilient to pay royalties for licensing the patented technique. Instead,

they sold no 2PLSMs at all or constructed 2PLSMs that loopholed the original patent by artificially degrading the pulse duration of the illuminating laser. Unfortunately, the use of such degraded systems was very limited. To conclude, while the technique is around for almost 20 years, it has not often been applied. Good and non-degraded 2PLSMs can be bought nowadays, but they are still not commonly used.

Following from the above considerations it is clear that the present thesis is as much an exploration of the virtues and downsides of the new microscopic technique as a scientific project with the aim to gain insight into the workings of the honeybee olfactory system. To elucidate the potential of the 2PLSM, I aimed to characterize the activity within multiple olfactory projection neurons (PNs) of the AL of the honeybee during odor stimulations and during rest. The advantage of the olfactory system of the honeybee as target structure for the 2PLSM is that it has been characterized already in detail in many studies featuring a large variety of techniques. It will be one aim of the present thesis to compare the results obtained here to the results from those studies. This cross check serves as a control for results from methodologically different studies. At the same time, comparison of the techniques will define in how far the view of the same model system is different in 2PLSM, and for which kinds of questions the new technique is best suited.

Last but not least, it will be discussed in what respect my results can add to our understanding of odor coding in the AL network.

Structure of the introduction

The introduction is structured into the following sections:

- Section 1.1, starting on page 6: **Current understanding of the olfactory system**

  In this section I will shortly summarize the key findings that led to the current understanding of olfactory systems. I will also name some assumptions on the functional significance of glomeruli in odor coding.

- Section 1.2, starting on page 10: **Revision of the antennal lobe network**

  Here I will compile the whole body of information that is relevant for the research on the olfactory system of the honeybee. To open your mind for the findings of this thesis, I will try to cast doubt on the common conception of a consistent, full understanding of the olfactory system.

- Section 1.3, starting on page 25: **2-photon laser scanning microscopy (2PLSM) in the honeybee**

  In this section I will contrast the theoretically exceeding suitability of 2PLSM for the research of the honeybee olfactory system with the small number publications from users of 2PLSM that can be found in the literature. The potential of 2PLSM is outlined and compared to other methods.

- Section 1.4, starting on page 28: **Probing the antennal lobe network with 2PLSM**

  At the end of the introduction I will, based on the information given in the previous sections, elaborate questions that can be answered in this first routine study on the honeybee olfactory system that makes use of 2PLSM.

1.1 Current understanding of the olfactory system

The first olfactory neuropils, olfactory bulb (OB) in vertebrates and AL in insects, share several common design principles, probably resulting from convergent evolution. Thus it has been implied in many studies on olfactory systems that the findings were of universal relevance; this has been especially common among researchers of the insect AL (e.g. Hildebrand and Shepherd 1997; Strausfeld and Hildebrand 1999). For the purpose of this thesis, which is comparing the results obtained with similar data that have been obtained with other methods, such universal relevance need not be claimed. Thus it will be sufficient to subsume specifically the current understanding of the network within the insect AL. Studies on the olfactory system of vertebrates that have implications for the interpretation of properties of the insect olfactory system will be cited where appropriate. Generally, studies that involve physiological measurements and neuroanatomical studies are of particular interest.

The sequence for presenting is from peripheral to central. In the AL network, three major classes of neurons interact, namely the receptor neurons (RNs), the local interneurons (LINs), and the projection neurons (PNs). Odor detection starts on the insect antennae, in olfactory sensillae.

Receptor neurons and the sorting problem

The detection of odorants starts with interaction of the airborne environmental chemical ("odor") with one or several of the odorant receptor proteins (OR) that are expressed on the surface of RN external dendrites. The dendrites of the $\approx$60.000 RNs per antenna (Witthöft, 1967) innervate the broadly dispersed olfactory poreplate sensillae (sensillae plocedeae, Lacher and Schneider 1963) on the antennal flagellum. Here, the extracellular side of the OR is in contact with the environment via the sensillum lymph. Each of the RNs expresses only one or few ORs out of the odorant receptor repertoire (mouse: Mombaerts *et al.* 1996; drosophila: Couto *et al.* 2005). Binding of target chemicals to the G-protein-coupled OR (first described in mouse in Buck and Axel 1991; drosophila: Clyne *et al.* 1999 and Gao *et al.* 2000) leads to activation of intracellular cascades and

finally to depolarization and action potentials.

Couto *et al.* (2005) found in drosophila, and Mombaerts *et al.* (1996) in the mouse model, that RNs expressing the same OR are scattered and intermingled on the antenna / in the mucosa, but project to only one specific glomerulus in the AL resp. two glomeruli in the OB of the mouse. Such wiring requires RN axons to be sorted at the entrance to the first olfactory neuropil; it is still unclear how this formidable sorting problem is solved during development (Mombaerts 2001; Zou *et al.* 2009). The following figure (1.1.1) illustrates the wiring between antenna and AL.
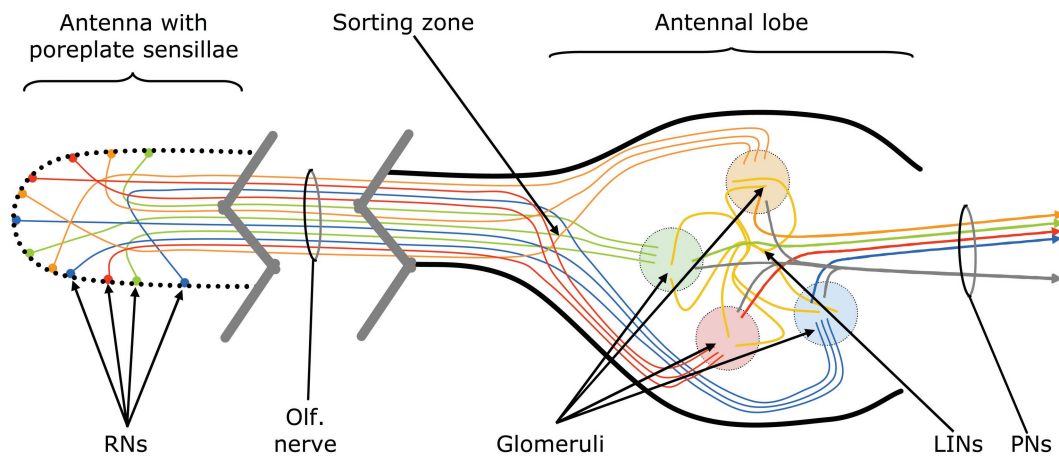
Figure 1.1.1: Schematic drawing of the wiring between RNs and AL glomeruli. 4 classes of receptor neurons and 4 glomeruli are shown.

Each OR binds several chemically different odorants (Hallem *et al.* 2004, Pelz *et al.* 2006, both on drosophila) with varying degree of sensitivity, i.e. the fit of odorant to receptor is unsharp. Axons of single RNs terminate in the outer rind (cortex) of one olfactory glomerulus in the AL (honeybee: Brockmann and Brückner 1995; *Manduca sexta*: Christensen *et al.* 1995.

The one-OR-one-RN-one-glomerulus scheme (or: chemotopic labeled line) has important implications for odor coding: because of the unsharp fit between OR and chemical, also a monomolecular odorant can bind to several ORs, leading to a distributed pattern of glomeruli that get input from RNs. For the honeybee model, Galizia *et al.* (1998) first showed that the resulting pattern of activity is symmetrical between brain hemispheres. Next, it could be shown that odor-evoked activity patterns in identified glomeruli are species-specific (morphological atlas of identified glomeruli in Flanagan and Mercer 1989 and

Galizia *et al.* 1999b). Patterns of activity have been recorded with a large panel of odors (Galizia *et al.* 1999c; Sachse *et al.* 1999; mini-review in Galizia and Menzel 2001). Maps of activity have been introduced into a functional atlas of the honeybee AL (Galizia and Menzel, 2000). This atlas will be mentioned at several instances in the remaining document; please note that with "AL atlas", I always imply the functional atlas of odor-evoked response pattern, not the morphological AL atlas of identified glomeruli.

To conclude, each glomerulus is activated by several odorants, and each odorant activates several glomeruli. Therefore, patterns are partly overlapping. It has been calculated that the possible coding space is exploited optimally. However, it remains unclear how the problem of sorting the dispersed RNs expressing the same OR into distinct glomeruli is solved during development.

Odor coding in glomerular patterns

The proposed mechanism of odor coding in glomerular patterns is beautiful and suggestive; the fact that this coding principle has been found in all glomeruli-developing species tested (e. g. rat: Rubin and Katz 1999; mouse: Xu *et al.* 2003; zebrafish: Baier and Korsching 1994, Friedrich and Korsching 1998; salamander: Cinelli *et al.* 1995; honeybee: Galizia *et al.* 1999b; carpenter ant: Galizia *et al.* 1999a, drosophila: Wang *et al.* 2003) contributes to the widespread believe that the puzzle of olfactory perception was solved. Three major functions are commonly attributed to olfactory glomeruli:

1. **Relays station**: The glomeruli are convergence sites for the high number of afferent receptor neurons. In the bee, the numeric relationship between RN input and PN output is on average 375 / 5, or 75 : 1 (assuming 60,000 RNs (Witthöft, 1967) and 800 PNs (Bicker *et al.*, 1993) divided by ≈160 glomeruli (Flanagan and Mercer 1989; Galizia *et al.* 1999b)). By summation of the RN input on the dendrites of (output) PNs, as a by-product of the relays functionality, noise is reduced and reliability enhanced (Schild, 1988).

2. **Sharpening, Sparsening**: Through local inhibitory interconnections, the amount and the relative strength of active glomeruli participating in odor-elicited patterns can be adjusted. For the honeybee, Sachse and Galizia (2002) demonstrated that at least two independent networks of local in-

terneurons (LINs) mediate global inhibition and local inhibition of single glomeruli. Sachse and Galizia (2003) demonstrated by comparing glomerular patterns of input- and output-side of the AL that the LIN network expands the range of concentrations over which the odor quality can still be reliably coded. Also, the contrast between the patterns elicited by akin odors was enhanced. The same mechanism has been discussed in connection with maintenance of an optimal ratio between silent and active glomeruli, preventing patterns of too many or too few active glomeruli.

3. **Dimensionality reduction**: The most striking feature of the AL (and OB) is that it apparently solves an impossible task: Odor space, defined by all odors that elicit a percept, cannot be mapped to any number of continuous dimensions. Furthermore, there is no inherent topographical relation between the single chemicals that fill the odor space. Nevertheless primary olfactory neuropils developed, most likely by convergent evolution, a way to map the complex sensory input onto one single dimension, namely the activity state of a given number of glomeruli.

1.2 Revision of the antennal lobe network

It cannot be disputed that glomeruli are a functionally significant organization principle in olfactory systems. But what is the role of intrinsic neurons in the lobes and bulbs? These neurons *could* in theory optimize the coding space, signify learning, and reduce noise. It has been frequently remarked that interpretations of the glomerular structure of primary olfactory neuropils might have been driven too far by aesthetic incitement; one very reasonable appeal to take into account a different explanation for the occurrence of glomeruli being the call from the group of Stuart Firestein (Zou *et al.*, 2009), who argues that the glomerular organization of the primary olfactory neuropils was in the first place a solution to the developmental problem of wiring a multi-parallel convergence-divergence network, and only secondly helping with olfactory coding. This exclamation follows after decades of work on the vertebrate olfactory bulb (first salamander species, than mouse), so it should not be put away too easily.

Therefore I regard it necessary to recapitulate in detail what is known about the cells that participate in the AL network, their functions, numbers, and their transmitter equipment. I will conject these data with results on the synaptic connections that have been revealed in studies on the ultrastructure of the insect AL. In the following section, long-known observations that are still to be appreciated by the scientific community will be unveiled. Thereby, widely believed facts about the honeybee AL will be questioned.

As already section 1.1 Current understanding of the olfactory system on page 6, also this section structured in accordance to the sequence of events that take place in the process of olfaction; from peripheral to central.

1.2.1 Odorant binding is not well understood

From odor plume to percept, uncertainty starts as early as the first molecules that get in contact with the odorant.

Odorant-binding proteins (OBPs) are known in vertebrates since the sixties. Unlike our rather extensive knowledge about OR families and expression pat-

terns, we know much less about the OBPs. The existence of OBPs in human was first deduced from specific anosmias. In the eighties, research on odorant specificity and chemical characterization of OBPs started in a variety of labs, and with several different model species. Bovine OBPs were detected and characterized chemically in Bignetti (1985). A bovine OBP was detected immunohistochemically also in rat Pevsner *et al.* (1986). This study also showed that this OBP binds several odors. Pevsner *et al.* (1988) described the cloning of a secreted OBP in the rat nasal epithelium, again showing that it selectively binds odorants.

Studies on the genetics of OBPs and research on pheromone-binding proteins (PBPs) and OBPs in a variety of insect species started in the nineties. For the hydrophobic pheromones of moths, like bombykol, PBPs have been thoroughly analyzed, including x-ray christallography for 3D-structure reconstruction, see e.g. Sandler *et al.* (2000). Vogt *et al.* (1991) describes the isolation and partly sequencing of 14 candidate OBPs from 6 moth species, showing that OBPs subfamilies of type II and III are differentially expressed in ORNs carrying specific ORs. Stengl *et al.* (1992) reviewed the possibility that odorant binding proteins may facilitate in an odor- and sensillum-specific way the diffusion of odorant molecules through the watery medium. Such locally segregated expression of a subset of specific OBPs represents a selective signal filter even before the first binding of odorant molecules with an OR.

To conclude, even the most careful analyses of ORN/OR function which are possible in Drosophila, where complete maps of antennal OR expression and identity of innervated glomeruli are established (Hallem *et al.* 2004; reviews e.g. in Dahanukar *et al.* 2005; Hallem *et al.* 2006), face the problem of insufficient knowledge of the spectrum and distribution of OBPs among sensillae. Analyzing ORs in question in parallel in the empty neuron expression system (see Van der Goes van Naters and Carlson 2007) might give us more insight into the action of OBPs in the insect olfactory system.

Several receptor neurons are bundled within sensillae

Robertson and Wanner (2006) found 170 OR genes in the honeybee genome. The AL consists of 160-170 glomeruli, therefore the finding is consistent with a general one-receptor-one-neuron-one-glomerulus relationship. A factor that renders the system potentially very complex, however, is the fact that most

insect sensillae are host to several RNs that express different ORs. Getz and Akers (1994) showed in placoid sensillae of the honeybee that the RNs are not uniformly distributed into the placodes, but that RNs responding to similar odorants are preferentially hosted in different placodes. This study also found that the RNs within the same placed do not spike independently, but appear to be electrically coupled. Kelber *et al.* (2006) found by means of whole-placode stainings and RN tracings, that the 5-35 RNs that innervate each poreplate sensillum innervate a set of glomeruli, and assumed that these RNs express different ORs. Vermeulen and Rospars (2004) modeled *in silicio* how the equipment of a sensillum with electrically coupled RNs changes the usually sigmoid dose-response curves of the single RNs. Schwarz (2006), finally, found in the drosophila antenna biogenic amine receptors for dopamine, octopamine, and tyramine. A TyrR null-mutant showed altered electro-antennograms. The thecogen glia-like accessory cell was shown to be a putative source for tyramine in the sensillum. It was hypothesized that plasticity of response properties of single sensillae might be mediated by biogenic amine *via* modulation of accessory cells that mediate the ion composition of the sensillum lymph.

Taken together, these findings point at a possible integrative role of sensillae. Experimental evidence for interdependency of RN signals has been found in the study of Akers and Getz (1992). The authors determined the average spontaneous spiking frequency of a large population of RNs to be around 16.6 $\pm$ 9.4 Hz. 90 placoid sensillae were analyzed. In each of these, the signals of several RNs could be distinguished through spike sorting. Odor-evoked responses were shown to be phasic-tonic. The frequency of spontaneous activity differed not only between individual RNs, but fluctuated over time within single RNs. RNs not directly activated by an odor often displayed increased fluctuations in their baseline spike rate during odor stimuli. Interestingly, the authors also report that signals of inhibition, e. g. a reduction of the resting spike during administration of an odor stimulus, are often encountered in RNs.

To conclude, binding of odorants to ORs is either mediated or facilitated by OBPs. The distribution of OBPs over the sensillae is not homogeneous but sensillum-specific. The responses of RNs housed within the same sensillum are not independent. Accessory cells potentially alter the ion composition of the sensillum lymph in activity-dependent or even centrally controlled fashion. Both features, the sensillum-specific OBPs as well as the electric coupling of groups of RNs, are unique to insect and unlikely to be realized in vertebrates:

OBPs that are secreted from the mucosa of vertebrates are unlikely to stay locally segregated, and there are not apparent localized groups of RNs in the mucosa. Thus, already at the periphery there are fundamental differences in the olfactory systems of insect and vertebrates. Also for the model of odor coding in glomeruli, the presence of OBPs and the integrative function of sensillae has implications: glomeruli may be convergence sites for RNs expressing the same OR, but the odor-response-spectra of single RNs might differ because of the OBP repertoire in its sensillum and/or biogenic amine mediated plasticity. Thus, the interface between odor space and RNs is not as linear as often believed, and the signals conveyed by a number of RNs to a single glomeruli are potentially not uniform. This is opposed to the common notion of independent RNs that relay redundant information to the glomerulus that is defined exclusively by the odor/OR pair, and noise.

1.2.2 Numerous neurons types are present in the antennal lobe

Once the RNs enter the AL glomeruli, they synapse onto PNs and local interneurons (LINs). RNs terminate in the outer cap of the glomeruli ("cortex", Galizia *et al.* 1999b). On average, 375 of the total of 60,000 RNs (Witthöft, 1967) enter each of the 160 glomeruli (Flanagan and Mercer 1989 and Galizia *et al.* 1999b). The output neurons of the antennal lobe are PNs, which travel through the protocerebrum in three tracts. 800 PNs (Bicker *et al.*, 1993) run through the lateral antenno-cerebralis tract (lACT). It has been estimated that the other large tract of PNs, the medial antenno-cerebralis tract (mACT), contains the same number of axons (Dr. Jürgen Rybak, personal communication). The number of PNs per glomerulus is thus larger than the commonly assumed ≈ 5. Abel *et al.* (2001) could show that in each AL, two large populations of glomeruli are defined by the tracts in which their RN afferences and PN efferences run. lACT PNs innervate mainly a frontally positioned population of $\approx$70 glomeruli. These glomeruli are also target for a sub-population of RNs which send their axons through the antennal tract T1 ("T1-glomeruli"). mACT PNs, in turn, innervate a posteriorly positioned population of $\approx$70 glomeruli which are target for RNs which send their axons through the antennal tract T3 ("T3 glomeruli"). PNs running in the lACT and the mACT each innervate only one glomerulus

(uniglomerular PNs), as opposed to the multiglomerular PNs that run in the three small mediolateral antenno-cerebralis tracts (mlACTs). Summing up, each T1- and T3-glomerulus is innervated by $(800/70 =)$ 11.4 uniglomerular PNs, and by a potentially large quantity or multiglomerular PNs, the exact number and innervation patterns of which have yet to be determined. Fonta *et al.* 1993 estimated that each multiglomerular PN innervates more than 50% of all glomeruli.

Glomeruli are each also innervated by a potentially large subset of the pool of up to 4000 LINs (Witthöft 1967; but in an unpublished immunohistochemical study performed at the neurobiology department of the FU Berlin only 2000 could be found). Fonta *et al.* (1993) found that two morphological variants of LINs each innervate 1/3 to 2/3 of all glomeruli. LINs innervate glomeruli with either homogeneous density of fibers ("homo-LINs", only arborizing in the core of glomeruli) or one of all innervated glomeruli is innervated more densely than the others ("hetero-LINs", arbor also reaching into the outermost parts of one densely innervated glomerulus). Depending on the assumed number of LINs, between $(0.5 * 2000 =)$ 1000 and $(0.5 * 4000 =)$ 2000 LINs arborize in each glomerulus. Assuming that half of the LINs are heterogeneous LINs, on average $(0.5 * 2000/160 =)$ 6.25 to $(0.5 * 4000/160 =)$ 12.5 dense arbors of hetero-LINs must be present in each glomerulus.

To sum up, each glomerulus contains on average

- axonal projections of 375 RNs (cortex),

- sparse processes of 1000-2000 LINs (Core),

- 6.25-12.5 dense arbors of hetero-LINs (cortex and core),

- 11.4 dendritic innervations of uniglomerular PNs (cortex and core))

- dendritic (and terminal? see below) branches of an unknown number of multiglomerular mlACT PNs.

Several central neurons innervate the antennal lobe

Central neurons that are known to send afferences into the AL are the VUM-mx1 neuron (ventral unpaired medial cell of maxillary neuromere 1, see Hammer 1993 and), the ALF-1 (antennal lobe feedback neuron 1, see Rybak and

Eichmüller 1993 and Kirschner *et al.* 2006), and a sub-population of GABAergic neurons running through the mlACT tract, but with opposed polarity (Jürgen Rybak, unpublished observation). Iwama *et al.* (1995) described the Pc(m) neuron (projection neuron with axon in central antenno-cerebralis tract) with multiglomerular arborization in both ALs. Its neurite enters the contralateral AL through the AL commissure before continuing further until the contralateral lateral horn. In personal communication with Jürgen Rybak, finally, I learned that a type of neuron exists that innervates one glomerulus in the ispilateral AL and the coarse neuropil in the interior of the contralateral AL; the interconnecting neurite runs in the protocerebrum.

To conclude, several central neurons send afferences into the AL neuropil, but the function of most of them is unknown. Hammer (1993) could show that the VUM-mx1 neuron encodes the presence of a sucrose stimulus and, after associative conditioning of an odor-sucrose forward pairing, its activity accompanies the response specifically to the rewarded odor. The VUM-mx1 neuron apparently branches in all glomeruli (Schröter *et al.*, 2007), but the question for the the postsynaptic partners is open for speculation; it may be LINs or PNs.

1.2.3 Knowledge about connectivity is vague

The ultimative goal in this study is to relate physiological measurement data to the structure and function of the AL neuropil. It would be extremely helpful to have an overview about the precise wiring and connectivity of the neuron families described in the previous sections. Knowledge about the distribution, number, polarity, and physiology of synapses between those cell types would facilitate interpretations of the signals measured at any stage of the network. Extensive EM studies with multiple labels for the cell types covering at least a representative sub-population of the AL neuropil would be required as a first step, but such studies are yet to be performed in the honeybee. For the time being, I will try to sketch the connectivity in the AL network by conjecting findings from several model systems on the ultrastructure and/or physiology of parts of the insect AL network.

> Which are the major postsynaptic partners of receptor neurons?

All RNs send their axons into the deuterocerebrum *via* the antennal nerve. The antennal nerve is structured into 6 tracts named T1 to T6, which each project into a distinct neuropilar region (Arnold *et al.*, 1985). Tracts 1 through 4 terminate in separate groups of egg-shaped olfactory glomeruli in the AL. T1 innervates 71 glomeruli at the frontal surface of the AL ("T1-glomeruli, average diameter 44 μm), T3 innervates 81-90 slightly smaller glomeruli at the posterior surface ("T3 glomeruli", average diameter 39 μm). Tracts T2 and T4 each innervate only small populations of glomeruli (T2: 6; T4: 7). One of the T2 glomeruli is different from all other glomeruli in being positioned not at the outer perimeter of the AL, but inside of the layer of glomeruli in the inside of the lobe. The T4 glomeruli differ from other glomeruli in their lack of an anatomical separation into cortical and core region. In T1, T2, and T3 glomeruli, on the contrary, RNs terminate in the outer rim ("cortex") of the glomeruli, leaving 70% of the glomerular volume void of RN terminals.

Extrapolating from the above information, the RN population of 60.000 RNs per antenna each send spontaneous spikes at a frequency of 16.6 Hz to the AL, totaling $\approx$ 1.000.000 spikes per second. Several synapses are made between RNs and postsynaptic neurons (Boeckh and Tolbert 1993 estimated several hundred en-passant synapses per RN for the cockroach; Gouwens and Wilson 2009 also implemented several output synapses per RN in their model on drosophila PNs), so the effective frequency is even higher.

Astonishingly, while it is commonly believed that the RN::PN synapse was prevailing at least in the cortex of olfactory glomeruli, this has in no insect species been found to be the most frequent pairing. Instead, Malun (1991) found in an extensive electron microscopic study with labels for GABA and for RN processes, that RN::PN synapses were extremely rare in the cockroach. Hildebrand *et al.* (1992) and Christensen *et al.* (1993) found with electron microscopy and intracellular recordings in LINs and PNs in the moth *Manduca sexta*, that PNs do only rarely get direct excitatory input from the antennal nerve, which was either excited by odor stimulations or by electrically stimulations. PNs appeared to get multisynaptic input or to be activated by disinhibition rather than excitation, while LINs not only were the most frequently found postsynaptic partners of RNs, but were also activated with smaller delay and more fidelity

by the stimulation procedure compared to the PNs measured. Already before these studies, Tolbert and Hildebrand (1981) and Matsumoto and Hildebrand (1981) showed with freeze fracture electron microscopy and intracellular recordings in the moth AL that synapses in the AL are typically dyadic with two or more postsynaptic partners in each synapse, that all AL neurons are equipped with both presynaptic vesicles and postsynaptic specializations, and that serial synapses occur frequently. Delayed PN responses and frequent signals of inhibition showed clearly that the input to PNs must be polysynaptic. Krofczik *et al.* (2008), finally, showed with intracellular recordings in the honeybee AL that also in the bee LINs respond to odor stimulations with significantly shorter delay than PNs ($\approx$70.0 ms, n=6 vs. $\approx$130.8 ms, n=30).

In drosophila, however, Wilson *et al.* (2004) and Wilson and Laurent (2005) found that PNs respond with less delay than LINs. Disinhibition of PNs by the GABA-blockers PTX and CGP54626 did not affect the delay of PN responses, but only the spike rates in two separate time windows. Kazama and Wilson (2008) found strong RN::PN synapses by whole-cell-patch-clamp recordings in PNs during electrical stimulation. The response latencies were as short as to imply monosynaptic transmission. EPSC were found to consist of a fast component, evoked by direct RN input, and a slow component that was convincingly demonstrated to originate from lateral excitatory connections in the AL. Furthermore, the authors determined several parameters of the RN::PN synapse (using the technique of multiple-probability fluctuation analysis): (1) the quantal current evoked by a single vesicle of neurotransmitter was found to be 1.05 pA; (2) the vesicular release probability is 0.79; (3) the number of release sites per synapse is 51. Gouwens and Wilson (2009) created a model of a drosophila PN on the basis of an extensive body of data from patch-clamp recordings and pharmacological experiments. The model predicts that the number of synaptic contacts between each individual pair of RN and PN is 25, and that each RN forms synaptic contacts with all 3-4 PNs per glomerulus. In an earlier publication, Bhandawat *et al.* (2007) showed that the PNs amplify the RN signal, and that this amplification is non-linear: weak RN inputs are amplified much more than strong RN inputs. Furthermore, PN responses do not follow the time course of the RN spiketrain, but emphasize the stimulus onset. Thus, the drosophila PN response is shaped by excitatory and inhibitory LINs, but essentially it is driven by direct RN input.

Obviously, two fundamentally different wiring schemes are established in

the ALs of cockroach/moth and drosophila. The honeybee AL might be organized like either of these, or yet another wiring scheme might be implemented. Extensive studies on the ultrastructure of the AL and the genetic toolkit of the drosophila researchers are both unavailable in the bee, so in constructing a model wiring scheme we have to resort to the large body of physiological and immuno-histochemical data that has been acquired over the last decades. Linster *et al.* (2005) built a functional model of the honeybee AL on the basis of calcium imaging data with the aim to predict the LIN architecture necessary to explain the difference between the odor-evoked patterns of active glomeruli that are measured at the level of either RNs or PNs. In this model, RNs form synapses with both PNs and LINs. When fed with RN across fiber patterns similar to those determined in Calcium imaging of bath applied dyes, the model reproduces the patterns measured at the output (PN-) level with high fidelity. Thus, at least functionally, the proposed model mimics the transformation of the odor representations between AL input and output. The predicted architecture of the LIN network is a "functional" network, as opposed to "stochastic" or "morphological" networks; e.g. strong inhibitory connections occur not between random or neighboring glomeruli, but between glomeruli that respond to similar odors.

Are local interneurons inhibitory and polar?

Are LINs inhibitory? In all species tested, at least a part of all LINs can be visualized by immunohistochemical staining with fluorescent labeled antibodies against the inhibitory transmitter GABA (gamma-amino-butyric acid). In moth and cockroach, almost all LINs are GABAergic (Hoskins *et al.* 1986; Distler 1989). In the honeybee only 20% of all LINs were shown to be GABAergic (Witthöft 1967; Schäfer and Bicker 1986), raising the question which neurotransmitter the remaining LINs release, and if this transmitter acts inhibitory.

Barbara *et al.* (2005) showed that not only GABA, but also glutamate elicits Cl^- currents in primary culture of AL neurons (LINs and PNs). It is tempting to assume that the LINs of the two inhibitory networks that have been hypothesized to shape the AL output signals express either GABAergic or glutamatergic synapses, which both act inhibitory on the postsynaptic cells. Sachse *et al.* (2006) showed that application of histamine reversibly abolishes odor-evoked activity patterns in imaging experiments. Interestingly, Barbara *et al.* (2005)

found no effect of histamine in primary culture of AL neurons. It has thus been hypothesized that the receptors for histamine must be expressed on RNs.

Also excitatory LINs might be present in the honeybee AL, yet their existence has not yet been shown. Proof for excitatory LINs is has been brought forward in drosophila (Olsen *et al.*, 2007), where the authors could show that activity within excitatory LINs suffices to evoke a train of spikes in PNs of a glomerulus that is deafferented of RNs. Bornhauser and Meyer (1997) found a population of histaminergic LINs in the honeybee which label brightly all glomeruli of the AL. Sachse and Galizia hypothesized that histamine acts in the honeybee AL as an inhibitory transmitter in a second inhibitory network (Sachse and Galizia 2002; Sachse *et al.* 2006). The two networks, a global GABAergic one that interconnects PNs, and a histaminergic one, which interconnects RNs with RNs, could mediate on the one hand global gain control and on the other hand the specific inhibition between functionally similar glomeruli, as it is implemented in the model of Linster *et al.* (2005).

It is not entirely clear if LINs are polar. Galizia and Kimmerle (2004) performed sharp electrode recordings of hetero-LINs and could show via reconstruction of the dye filled neurons and comparison with the honeybee AL atlas that the response profile of the densely innervated glomerulus predicts the recorded activity of the hetero-LIN. Thus the densely innervated glomerulus is likely to be the (or: one) input side of a hetero-LIN. The Linster *et al.* (2005) model is based on the assumption of polar hetero-LINs that receive input only in the densely innervated glomerulus. In all of the electron-microscopy-based publications on the ultrastructure of neurons of the AL network, however, both input and output synapses were found on the arborization of LINs. Serial synapses between numerous neurons were also frequently observed. It is thus likely that hetero-LINs receive input and form output synapses in the same, densely innervated glomerulus. Only output synapses are suspected in the sparsely innervated glomeruli; but Christensen *et al.* (1993) found in a study featuring electrophysiological measurements of moth AL LINs evidence for multiple spike initialization zones within the same LIN. The authors speculate that parts of the LIN arborization might be electrically isolated, and that multiple input sites to the LIN exist. The authors could also demonstrate inhibition of LINs by other LINs and clear cases of release-from-inhibition activity in PNs that were recorded simultaneously with a presynaptic LIN. It is unclear if the LINs measured in this study were homo- or hetero-LINs. Galizia and Kimmerle

19

(2004) also recorded from LINs in their study and reported that multiple spike heights were also observed in sharp electrode recordings. Spikes of a given height had their own specific odor-response-spectra, suggesting that the source of the spikes are different glomeruli. In simultaneous calcium imaging recordings, the authors could indeed show that the spikes of a given height temporally correlated with calcium signals in one of many innervated glomeruli. Electric coupling between LINs may explain the presence of multiple spike heights in electrophysiological recordings.

PN activity is complex!

   PN responses were measured with sharp electrodes also in the studies by Müller *et al.* (2002) and Krofczik *et al.* (2008). Krofczik *et al.* reported rates of spontaneous activity of 6.8 Hz mean, 3.4 Hz median. The large difference between mean and median is caused by a very skewed distribution of spontaneous spiking frequencies in different cells. Also cells without spontaneous spiking were found. 7 lACT- and 23 mACT PNs were analyzed. lACT PNs and mACT PNs were not found to differ in their spiking frequency, which is not surprising given the large variability present in each of the groups. Müller *et al.* found spontaneous spike rates of 3.4 Hz mean (standard deviation 4.3, n=11) in lACT PNs, 10.9 Hz mean (standard deviation 6.9, n=13) in mACT PNs. The large standard deviations reported in Müller *et al.* and the large difference between mean and median value reported in Krofczik *et al.* show that the pool of PNs of both tracts must be extremely inhomogeneous with respect to spontaneous spiking behavior. In both publications, no dedicated analysis was made concerning the temporal variation of spontaneous spiking within a given neuron over time. Given that the exemplary recording traces given in the figures are representative, one can conclude that the spontaneous spikes are rarely regularly scattered, but rather appear in short bursts of 2-10 spikes. During odor stimulations, the responses are either phasic-tonic or temporally complex. There appears to be a bias towards complex responses in lACT PNs, while mACT PNs are biased towards phasic-tonic responses; yet this is not a general finding and in both populations of neurons, examples for both response shapes occur. It shall be mentioned that the publications by Müller *et al.* (2002) and Krofczik *et al.* (2008) actually aimed at the quantification of the response latencies of lACT and mACT PNs, in Krofczik *et al.* also LINs. Unfortunately, while Müller *et al.* did

find significantly different response latencies, Krofczik *et al.* did not. This my be a result of accidental sampling bias in a very inhomogeneous population of PNs. Undoubtedly the response latency of the LINs recorded in Krofczik *et al.* was shorter than the response latency of PNs; this has also been found in the works of Hildebrand *et al.* (1992) and Christensen *et al.* (1993). Also Galizia and Kimmerle (2004) found complex as well as phasic tonic response shapes in LINs as well as PNs. Furthermore, regular as well as bursty spontaneous spiking was observed. Sun *et al.* (1993) recorded electrophysiologically from a large number of LINs and PNs and stress in their data evaluation the fact that the variability between cells as well as over time is large. A whole set of response profile templates was set up and all responses were sorted accordingly. The most frequent response shape was the phasic tonic response. Yet is shall be mentioned that (1) from the total of recordings with ≈390 odor stimulations, a subset was chosen that displays "unambiguous variation of response to background activity" during the stimulation time window - but complex responses have a lower "unambiguous" difference towards background!; (2) there was no template for a complex response profile. Additional to the response shape analysis, the responses of inhibition and excitation were quantified separately: 82% of LIN responses were found to be signals of excitation, while 18% were signals of inhibition. In PNs the ratio was 51.5% to 48.5%. The sub-group of uniglomerular PNs yielded a ratio of 4:9.

To conclude: PN responses are complex. Phasic-tonic responses occur alongside all kinds of temporally dispersed brief bursts of action potentials. Often, the complex responses are reproducible during repeated stimulation with one of several odors. So the complex responses are partly odor-specific and not random. Still it can be difficult to unambiguously tell apart bursty spontaneous spiking from complex odor-evoked signals in electrophysiological recordings.

1.2.4 Conclusions on the antennal lobe network

The puzzle peaces outlined above do not fall into a coherent picture. At least two different network architectures are implemented in the range of species discussed: On the one hand there is drosophila, with its bilateral RNs, RNs on antennae and palps, excitatory LINs, and strong RN::PN synapses; on the other hand there are cockroach, moth, and honeybee, in which inhibitory LINs are

most likely the prevailing postsynaptic partners of RNs. This differentiation is not explained by the phylogenetic relationship between the species, as the exert from the phylogenetic tree in figure 1.2.1 on page 22 shows. Neither can any ecological parameter be found that differentiates the species along the same line between cockroach, moth, and honeybee vs drosophila.
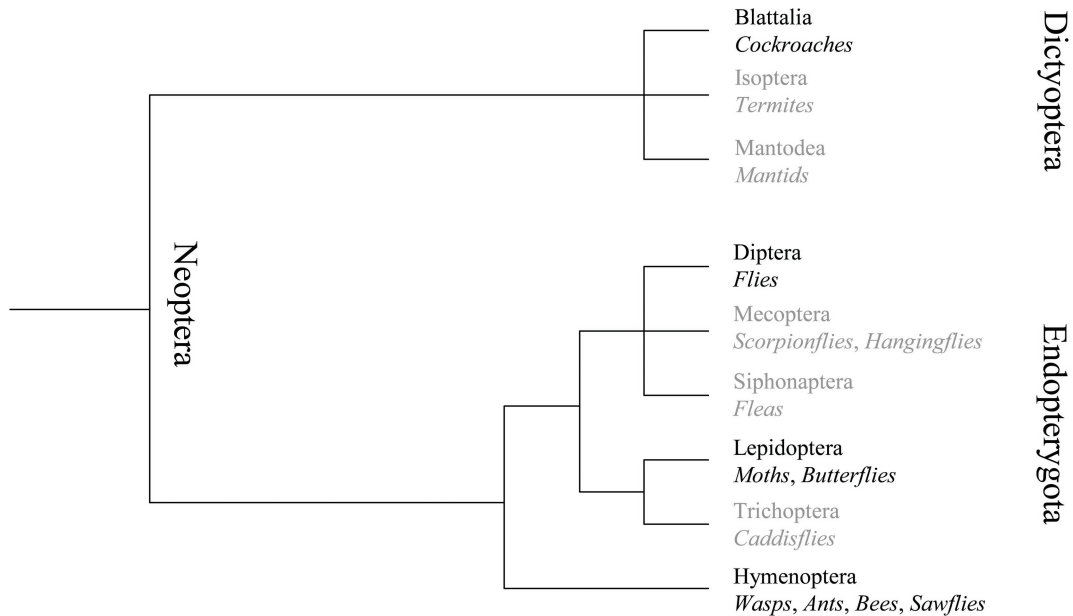
Figure 1.2.1: Phylogenetic tree showing the relevant part of the Neopteran sub-branches. Moth and fly separated most recently among the species discussed here, honeybees are the next closest species. These three species belong to the group of Endopterygota. The cockroach sub-branch belongs to another group, the Dictyoptera. Modified after The Tree of Life web project, Diverse authors (2003).

One grouping variable that does is the body size (or the brain volume); yet it appears unlikely that mere size would be the determinant of specific wiring schemes (but Eisthen argues in a review from 2002 that a larger brain with more cells requires subdivision of brain parts into more brain parts, because the amount of fiber needed to maintain the same wiring complexity increases disproportionally with the number of cells. This may explain at least the difference in the number of glomeruli in the species discussed here).

The following list concludes the findings cited in the previous sections, but excluding the drosophila-specific parts (apart from the RN synapse parameters).

- An estimated 1,000,000 spikes per second is generated in the RNs of each antenna (6250 per glomerulus and second).

- Each RN forms many synapses (estimation: 100), each with several (51 in drosophila) release sites and a high release probability.

- The RN::PN synapse might outbalance its low relative count with high synaptic strength.

- RNs form synapses with LINs more often than with PNs.

- The prevalent input to PNs is inhibition by LINs.

- LINs respond with lower latency than PNs.

- The population of uniglomerular PNs (mACT and lACT PNs) is very inhomogeneous in all aspects of resting- and odor-evoked activity, but complex responses can still be reproducible and odor specific.

- Two inhibitory networks of LINs exist, one of these might be global while the other interconnects glomeruli with similar response spectra.

- Excitatory LINs might exist in the honeybee AL.

- Disinhibition, leading to rebound effects might be a source of PN activity.

- Serial synapses that might mediate feed-forward disinhibition have been found in several studies.

These findings could be used as rules for the construction of several putative wiring schemes. Computer models could be used to compare parameters of cellular activity predicted by the wiring schemes with the measurement data presented in this thesis and elsewhere. These models might also explain why in cockroach, moth, and honeybee, the latencies between RN- and LIN-responses differ. Unfortunately, computer models require specific data on wiring, input activity, and electrical and chemical parameters of the simulated neurons. At present, also after reviewing all available literature, a fine-grained computer model with realistic numerical relationship of the simulated neurons ans synapses would be based largely on assumptions. A coarse model, on the other hand, that one might want to create to demonstrate how the two LIN populations would have to be wired with the RNs and PNs to produce an output roughly similar to the measured data, would be of low predictive value.

I hope I could convince you of the fact that it would not be appropriate at this time to state a clear hypothesis on the wiring scheme upstream of PNs in the honeybee AL. The problem is not the the source of PN activity in PNs could not be explained with the available anatomical and physiological data, but there are too many possible wiring schemes that all could explain the delayed, complex signals reported by the publications cited.

So, to say it with Keats, researchers of the honeybee olfactory system currently need the "negative capability" to be in a state of mystery without irritability - investigating and discussing all ideas with equanimity.

1.3 2-photon laser scanning microscopy (2PLSM) in the honeybee

By adapting a rather young variant of laser scanning microscopy (LSM), namely 2-photon-LSM (2PLSM), for use with living honeybees, I recorded optically odor-evoked neuronal signals at sub-cellular resolution. Within the same setup, I recorded *in vivo* stacks of images at a resolution sufficient for identification of sub-cellular processes of neurons.

As opposed to electrophysiological sharp electrode recordings with successive single cell staining, the 2PLSM can be applied to mass stainings of neurons, enabling the experimenter to simultaneously record from multiple neurons. As opposed to widefield imaging and extracellular neurophysiology, which also yield simultaneous measurements from several neurons resp. neuropils, the neurons that are recorded in 2PLSM can later be reconstructed. For neuron reconstruction, both a high optical resolution and depth sectioning is required; it will be tested if both requirements are met by the 2PLSM. If this were so, 2PLSM would be a unique tool with the potential to gather detailed information on neuronal processing in networks of cells, rather than single cells. It has been proven in numerous publications that this s theoretically possible, but surprisingly few publications report on results from studies in which 2PLSM was applied routinely to a number of animals as high as when other methods are used (in Wang *et al.* 2003, Wang *et al.* 2004, and Root *et al.* 2007 the authors indeed did perform measurements routinely with 2PLSM in the drosophila AL and MB; Wachowiak *et al.* 2004 is one of several publications on the routinely use of a 2PLSM with the zebrafish). More publications exist, however, in which in the first place the technique or variants thereof are validated or extended (Denk and Svoboda 1997 already listed a large range of possible recording modes and demonstrated their use exemplarily; review of the use of 2PLSM in Piston 1999 and Svoboda and Yasuda 2006; Stosiek *et al.* 2003 developed a new technique for staining deeper sections of mammalian brain tissue; Helmchen and Denk 2002 and Helmchen and Denk 2005 reviewed and proposed new developments of the

technique; Yaksi and Friedrich 2006 reported on a deconvolution algorithm for 2PLSM signals that produces from the measured fluorescence intensity changes the spike rates; Saggau 2006 reviewed new scanning modes for the acquisition at yet higher repetition rates; Jayaraman and Laurent 2007 related fluorescence intensity changes of a genetically encoded calcium sensor with simultaneously measured patch clamp recordings). Numerous publications cover the exemplary application of the technique to various model species (Denk *et al.* 1990; Denk *et al.* 1994; Helmchen *et al.* 2001; and numerous others). Such publications are primers, and it is astonishing how rarely these primers are followed up by question-driven research featuring the 2PLSM.

Constructing a 2PLSM on the basis of a confocal microscope is theoretically simple: Instead of a continuous mode laser, a pulsed IR laser is coupled into the microscope. Instead of confocal detection optics and photomultiplier, a more sensitive photomultiplier without confocal pinhole is placed close to the aperture of the objective together with a new beam splitter for FURA dyes and a IR band-elemination filter.

Without forestalling large parts of the methods section it must be allowed to stress the fact that it certainly is not as easy as that. Many technical and preparation issues were to be resolved until routine measurements were possible, and that this process spanned for more than half of the time that was consumed by this work. Given that constructing a 2PLSM in this (and most likely in other cases, too) culminates in almost re-inventing it, it is not so astonishing that many scientists make a virtue out of the necessity and continue working on the advancement of the method instead of using the technique for question-driven research. Also in this project, the basic setup of the 2PLSM had to be upgraded with several components that all served the need for enhanced light efficiency and reduced photo-bleaching (see methods part 2.1 on page 32 and following).

The project presented in this thesis is, however, not solely a report on the achievement of applying a 2PLSM to the honeybee model, but I report also on the results from a large number of recordings that have been routinely performed with the 2PLSM in the honeybee AL. 2PLSM has been applied in the honeybee before by Paul Szyszka in a collaboration with Rainer Friedrich at the Institute for Biomedical Research of the MPI, Heidelberg, Germany (Szyszka, 2005). Also I did visit that lab before constructing the microscope and gathered first insights into what benefits the 2PLSM might offer over other techniques.

After the first data were recorded, it was immediately clear that the recordings

of multiple distinguishable neurons and sub-branches in several simultaneously measured glomeruli yield temporally complex, rich data. The large size of the neurons in the honeybee brain, e.g. as compared to drosophila, allows for true cellular resolution while using a high N/A 20x objective that covers up to $500^2\mu m^2$, which is sufficient to record an optical section of the whole AL in one single image frame. One image frame thereby transects up to 40 of the total of 160 glomeruli; up to 10 of these are transected at a comparable relative depth (e.g. between cortex and core). The large size and robustness of honeybees, at last, allows for precise surgery with the aim to suppress brain movements. As a consequence, the animal can be left more intact, which is favorable over the situation in drosophila, which needs to be reduced to its nervous system before motion-free measurements can be performed (Wang *et al.*, 2003).

To conclude, 2PLSM promises to yield richer information than the hitherto used methods of widefield fluorescence imaging and electrophysiology.

In Galizia and Kimmerle (2004), data obtained with electrophysiology, opto-physiology, and neuroanatomy were analyzed with the aim to (1) relate calcium responses to spiking activity, and (2) relate the odor-response-profiles of single, identified PNs to the glomerulus-wide response profiles that can be retrieved from the functional honeybee AL atlas (Galizia *et al.*, 1999c). The authors found that the electrophysiological recordings in single PNs are temporally complex, i. e. that responses in PNs individually recorded with sharp electrodes often deviate strongly from the phasic-tonic signal shape. Furthermore, odor-response-spectra predicted by the AL atlas were matched only in a part of the PNs recorded. Thus the authors postulated that glomerulus-wide signals, as they were gathered for creating the functional AL atlas, are result of summation of individually deviant signals in PNs that innervate the glomerulus in question. Electrophysiology does not allow to prove this hypothesis, because simultaneous recordings from two PNs innervating the same glomerulus are presently impossible. 2PLSM, however, can reproduce both the highly averaged wide-field data and the pure single cell data by applying different kinds of spatial and temporal averaging.

1.4 Probing the antennal lobe network with 2PLSM

Accordingly, one task for this thesis is to define the complexity of signals that PNs exhibit, and to compare the responses from single, identified PNs that are housed in the same glomerulus. By recording signals from several PNs simultaneously, the assumption of summation of diverse PN responses in each glomerulus can be checked. I decided to keep the stimulation protocol (e. g. the number of odors used and the treatment of the animals) simple, which is logical given that the results shall be correlated with previous studies. As for the target of my recording efforts, I simultaneously attended two goals: (1) Check many glomeruli for their odor-response-spectra and other general response characteristics, even if the number of animals per glomerulus might be low; (2) obtain in a large number of animals recordings from few readily identifiable glomeruli to define the variability and complexity of PN signaling with finer grain.

It follows a list with hypotheses, questions and tasks for this thesis, as they unforcedly emerge from the considerations in the preceding sections.

- 2PLSM is the method of choice for the analysis of the AL network. It can bridge the gap between electrophysiology and widefield imaging.

  The minimum requirements for this would be measurements of at least 20 Hz sampling frequency. This sampling frequency would match the binning into 50 ms bins that is routinely done when peri-stimulus histograms of electrophysiological recordings are produced. Additionally, to compete with electrophysiology, the optical resolution needs to be as high as to allow recording, reconstruction, and identification of several neurons within the same visual field simultaneously.

- The results obtained with 2PLSM may elucidate which aspects of the measurement data acquired with different techniques are influenced by the respective method used, and to what extent.

Imaging PNs with a 2PLSM can answer the question if there is a diversity of odor-response-profiles among PNs within the same glomerulus, or if e.g. a general variability of the responses accounts for deviations between the AL atlas and single identified neurons.

- Phasic-tonic responses are rare in PNs, signaling is complex, inhibition occurs frequently.

  The wiring rules and the physiological data from electrophysiology suggest that PN responses are delayed, complex, or phasic, and that spontaneous activity is strong.

- Two (or three) inhibitory systems of the AL synchronize PN activity.

  Inhibitory systems are hypothesized to act on different scales, e. g. one system de-correlates PN responses from glomeruli with similar odor response profiles as hypothesized by Linster *et al.* (2005), while the other serves as global gain control, attenuating in a stimulation-dependent way the signals in all PNs (Sachse and Galizia, 2002). I should be able to detect the action of the different layers of the inhibitory systems in the measurement traces from identified PNs. By pairwise comparisons of measurement traces from either sub-branches of single PNs, from branches of different PNs within the same glomerulus, or from PNs hosted by distinct glomeruli, I will test the following hypotheses:

  - The global inhibitory network synchronizes PN responses across borders of glomeruli.

  - The reciprocal inhibitory network that mutually inhibits glomeruli with similar odor-response-spectra de- or anti-correlates PN responses.

    If pairs of glomeruli with mutual inhibition are accessible to the method applied here, I should be able to find anti-correlation between responses in pairs of PNs that are housed in different glomeruli. This anti-correlation should be strongest during odor stimulations.

  - Assuming that the RN input is homogeneously distributed to all PNs of one glomerulus, any anti-correlation of PN signals within the same glomerulus, spontaneous or odor-evoked, reveals the action of LINs that do not connect to all PNs homogeneously with the same strength,

or that specifically interconnect the PNs within one glomerulus with the aim to de-correlate them.

This kind of inhibition on the level of single PNs has been hypothesized by Randolf Menzel and Michael Schmuker (personal communication) to be part of the memory trace formed after olfactory conditioning. Up- or down-regulation of such inhibition between PNs in the same glomerulus as a result of odor learning would be an elegant solution to the AL learning problem, because (1) the global pattern of glomerular activity would remain unchanged, but (2) the AL would still generate a clear signal as a result of learning, namely the differential activity in PNs from the same glomerulus. A readout system could average the responses from all PNs originating from one glomerulus to extract the odor identity; at the same time it could detect the across-fiber-anti-correlation among the PNs from the same glomerulus to register that a learnt odor is present.

This concept stands against the conception of glomeruli as functional units. But it should be mentioned that no method has yet been applied to the AL of honeybees that would have the potential to detect a violation of the functional unity theorem in PNs. Thus, functional unity might be present at the level of RNs, but not necessarily in the rest of the olfactory system.

Part 2

Materials and Methods

2.1 Setting up the 2-photon microscope

The following sections will describe the modifications and additions that had to be made to convert the Leica TCS-4D confocal microscope (Leica, Mannheim, Germany) into a highly light-efficient 2PLSM.

2.1.1 Modifications to the basic microscope system

The ArKr-ion-laser, photomultiplier tubes, filters, and the original microscope table of the Leica confocal microscope were removed. The XY-galvo scanner was re-adjusted. A filter cube with dichroic mirror and 540/50 nm bandpass for FURA2 was installed. An IR-band-elemination filter and a collimating lens were equipped in the emission light path. A non-descanned photomultiplier was placed close to the dichroic mirror. A new microscope table was designed, built, and installed that offered increased headroom for the use of a longer objective with stepper motor. Parts of the original microscope that were not modified were (1) the objective mount; (2) the "microscope controller", which is a real-time computer running under OS9 that serves as controller for actuators in the microscope, power supply and image-readout for the photomultipliers; originally it also controlled the ArKr-laser and the acousto-optic beam splitter; the microscope controller connects to the rest of the microscope hardware mainly via a (3) "connection box", which is basically a break-out-box allocating space for the numerous connectors; (4) the "Leica-PC", a standard i386-computer that is connected to the microscope controller via serial and parallel links; it runs the software "ScanWare" for controlling the operation of the microscope system. Figure 2.1.1 on page 33 shows in black the connectivity of these components.

2.1.2 Specifications of objective and objective scanner

We equipped the microscope with an Olympus 20x water immersion objective, NA 0.95, with special coating for enhanced transmission of IR light (XLUMPFL 20XW UIS -IR; Olympus, Hamburg, Germany). The objective was mounted

32
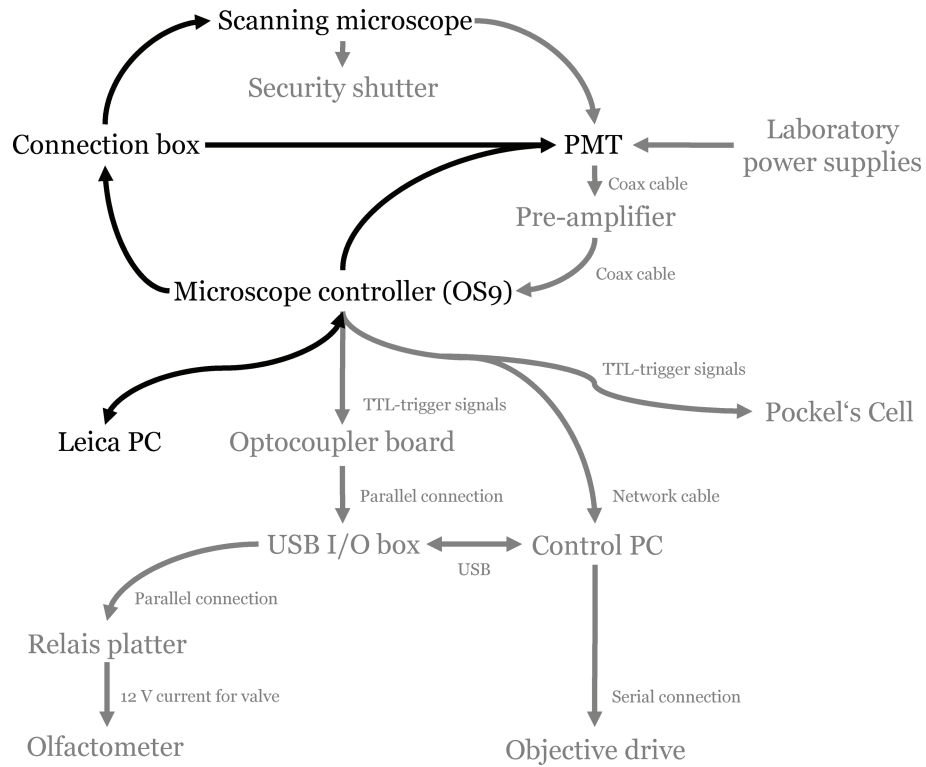
Figure 2.1.1: Sketch of the electric connections within components of the imaging system. All components that I added during the course of this project are drawn in gray. Arrows and text in small font indicate basic features of the connections.

in a piezo-electric linear motor stage ("objective drive" in Figure 2.1.1 on page 33) to allow for computer-controlled movements along the depth axis (PIFOC P-725 2 cl with capacitive sensor; LVPZT amplifier and servo controller; Physik-Instrumente, Karlsruhe, Germany). The PID servo controller of the objective scanner was adjusted to the weight of the objective until it was capable of shifting the objective within 70 ms over distances of up to 400 μm.

2.1.3 Optimizations in the emission light path

Multi photon excitation is restricted to the focal point of the objective. All fluorescent light that is emitted from the sample can be assumed to originate from this focus point. Therefore, a 2-photon microscope does not need a confocal pinhole to reduce out-of-focus light. Instead, as much as possible of the emitted light should be collected. Therefore, instead of the built-in descanned photomultiplier tubes (PMT), we installed a non-descanned PMT (R3823, Hamamatsu Herrsching am Ammersee, Germany) and a collimating lens that were positioned very close ($\approx$15 cm) to the aperture of the objective. In commercial multi photon systems, this distance is generally much larger (50 cm to 1 m, personal observation during demonstrations of the current systems by Leica, Zeiss, and Lavision Biotec in autumn 2006; Leica, Mannheim; Zeiss, Jena; Lavision Biotec, Bielefeld, Germany), reducing the efficiency of the emission light path of those systems dramatically.

2.1.4 Optimizations of power supply and output currents of the PMT

An offset between the output-currents of the non-descanned PMT and the input currents accepted by the A/D converter forced us to develop and construct a pre-amplifier. The pre-amplifier was designed such that, using analog potentiometers, we could adjust offset and gain of the PMT output. This enabled us to utilize the full 8-bit digitization range of the A/D converter independent of the amount of light from the sample, thereby increasing the dynamic range of recordings and reducing loss of information due to the quantization process.

Using an oscilloscope we detected distortions in the supply voltages that are provided to the PMTs by the original microscope controller and connection

box. These distortions lead to image artifacts (stripes). Thus we substituted these functions using stable laboratory power supplies. One power supply provided the supply voltages of ±15 V for the non-descanned PMT. Another power supply generated the 7 to 10 V which are necessary for controlling the gain of the PMT.

2.1.5 Software for objective scanner and olfactometer

A custom-written program "2-Photon-Control 2.00 by Tilman Franke", running on a PC (see next section) separate to the microscope setup, allowed manual or automated movements of the objective synchronous to the scanning process. Synchronization was achieved by reading out a TTL-trigger-signal from the microscope controller. The software allowed collecting stacks of planar images along the depth dimension ("z stack"). The software shifted the objective only during the time interval between scanning of two image planes. In manual mode, the software controlled the focus depth conveniently by either entering numeric depth values via the computer keyboard, clicking buttons on the graphical user interface, using the mouse wheel, or pressing the keyboard buttons "home", "PageDown", or "PageUp". The software was additionally used for computer-controlled delivery of odor stimuli. See section 2.2.3 Olfactometer and temperature control on page 46 for details on the olfactometer.

2.1.6 Additional devices for control and synchronization

To control and synchronize the added hardware and for running the software "2-Photon-Control", we added a further computer, the "control PC". The control PC was a standard Pentium III PC with large disc space for saving of files which were transferred *via* computer network from the microscope controller. TTL signals from the microscope controller that were in synchrony with the galvo-control of the scanning mirror (frame- and line-trigger) were fed into the control PC via optocouplers and a USB I/O box. The olfactometer was connected *via* the same USB I/O box and a relays platter. The objective drive was connected *via* serial port. Figure 2.1.1 on page 33 gives an overview over the connectivity between the components of the 2PLSM.

2.1.7 IR-laser light source and laser coupling

As light source we used a Ti:SA pulsed IR laser (Kapteyn-Murmane Griffin oscillator with fibre-coupled Spectra Physics Millennia Nd:YAG pump laser; Kapteyn-Murmane: Boulder, CO, USA; Newport Spectra-Physics GmbH: Darmstadt, Germany). The laser was placed on the same optic table as the microscope. We coupled the IR laser into the microscope directly through the air using a periscope turret on the optic bench. Instead of coupling the IR laser into the existing ArKr-Illumination light path by using a dichroic mirror, we targeted the scanning mirror directly, reducing the loss of laser power to a minimum. Therefore, we had to remove the ArKr illumination light path, excitation and emission filters, and the de-scanned photomultiplier unit.

2.1.7.1 Optimization of laser parameters and beam conditioning

Final laser parameters were the result of intense optimizations. Our aim was achieving near-transform-limited laser pulses of suitable central wavelength, FWHM, and energy in the focus plane under the objective.

Short pulses of laser light are not monochromatic. A linear relationship describes the broadening of the FWHM as the pulses get shorter. The $\approx$45 fs pulses that we found to optimally excite the 380 nm absorption peak of the dye FURA2 lead to a broadening of the 800 nm laser line to a Gaussian wavelength function of 25 nm FWHM (Fourier Width Half Maximum). Because the wavelengths are slowed to a differently degree when the light travels through air or glass due to 1st order material dispersion, in an uncorrected illumination light path the longer-wavelength portion of the pulse would reach the focus plane much earlier than the shorter-wavelength portion, leading effectively to a broadening of the laser pulse in time. This effect, also called "chirp", must be corrected for if pulse durations near to the initial 45 nm shall be preserved in the focus plane under the objective. Therefore we built up a so-called prism compressor that induces negative chirp (that is, longer-wavelength light is slowed down less than the shorter-wavelength light). Once optimally adjusted, the negative chirp ("pre-chirp") from the prism compressor and the linear chirp induced by material dispersion in the microscope and objective cancel out. Perfect adjustment of the distance between the prisms of the compressor is crucial. To find the optimal settings, we applied two separate strategies, both leading to the

same setup of the compressor: (1) we directly measured the pulse length in the focus plane of the objective using an auto correlator (see Figure 2.1.3 on page 40 for the pulse measurement set-up); (2) we shifted the prisms while imaging FURA2-stained neurons in the brain of a honeybee *in vivo*. At optimal settings, the 45 fs pulses exiting the oscillator reached the focal plane under the objective with 50 fs pulse length; this is as close to the Fourier limit as one can get when only 1st order dispersion is corrected.

Parameter	Final value	Range tested
Central wavelength	800 nm	760 - 805 nm
Average power	450 - 500 mW	150 - 550 mW
Pulse length	45 - 50 fs	45 - 100 fs
Pulse repetition rate	85 MHz	85 MHz
Energy per pulse	7.5 nJ	2 - 7.5 nJ
FWHM	25 nm	14.5 - 33 nm

Table 2.1.1: Laser parameters found to be optimal for exclusive excitation of the 380 nm absorption peak of the dye FURA2. The column "Range" shows the minimum and maximum values of parameter space that we experimentally tested when optimizing the laser system specifically to FURA2-stained neurons in the honeybee brain.

Also the central wavelength of the IR laser was subject to optimizations. The ratiometric dye FURA2 absorbs at two separate absorption wavelengths 340 nm and 380 nm, emission is always at 475 nm. When excited at 340 nm, fluorescence efficiency increases with the calcium concentration. The opposite is true for the 380 nm absorption peak. We chose to excite the higher absorption wavelength, because intracellular calcium concentrations are usually low; therefore bright anatomical images can be recorded in resting animals. Calcium influx leads to a reduction of fluorescence efficiency, thus active neurons appear dark.

The rule of thumb for finding the optimal excitation wavelength under 2-photon illumination is $\lambda_{2-photon} = \lambda_{1-photon} \cdot 2$. In the case of the upper wavelength of FURA2, this would be 760 nm. We tried illuminating stained bee brains with this wavelengths and were not surprised to find that there was very high background brightness. The background was apparently caused by (1) autofluorescence, because also unstained bee brains could be visualized at that wavelength and (2) extracellular dye, because stained bee brains were even brighter, but not only in the ALs, but also in unstained regions of the brain. The extracellular dye that diffused out of the injection site should be almost
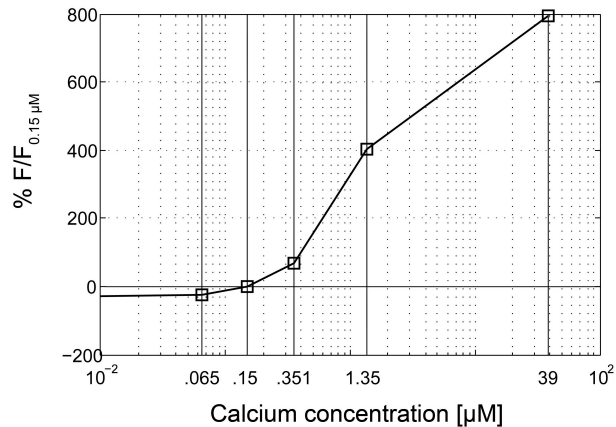
Figure 2.1.2: FURA2 fluorescence over a range of calcium concentrations, denoted as % of fluorescence at 0.150 μM [calcium]. Abscissa is logarithmized.

non-fluorescent when the upper absorption wavelength is excited, because it is in a medium with high calcium-concentration. At the lower wavelength, however, calcium binding leads to high fluorescence efficiency. Xu *et al.* (1996) demonstrated that at 2-photon illumination the absorption peaks are extremely much broader than under 1-photon illumination. Therefore the peaks overlap much more if illumination is achieved *via* the 2-photon process. We thus hypothesized that both the lower and higher absorption wavelength of FURA2 were excited at 760 nm laser wavelength.

We tested the hypothesis with a FURA2 calibration kit (F-6774 Fura-2 Calcium Imaging Calibration Kit, Molecular Probes, Leiden, The Netherlands). The kit consisted of buffered solutions of FURA2 in different concentrations of calcium. In an ordinary microscope, the kit solutions are measured on a standard microscope slide under a cover slip with beads as spacers. In a 2PLSM, it is difficult to compare absolute brightness values between independent measurements, because reflections in the glass surfaces often lead to long-lasting fluctuations in laser power. We thus filled solutions of different calcium concentrations into glass capillaries and measured them pairwise. From these pairwise data we reconstructed the absolute range of fluorescence strengths. The result was that almost no difference between the fluorescence was seen between FURA2 in calcium-free solution vs. FURA2 in 39μM calcium. This result affirmed the hypothesis that we excited both absorption wavelengths of FURA2 when we set the laser to 760 central wavelength.

We then shifted the laser wavelength in small steps towards 805 nm. During

each step, before being able to measure again, the laser had to be tuned to the same output power again, it had to be stabilized, the prism compressor needed to be re-adjusted and the laser coupling had to be repeated. With each step, the background brightness of stained tissue receded, the clarity of stained structures increased, and the overall image quality improved. At wavelengths of >800nm, the overall image brightness decreased again; thus a final value of 800 nm was used for the honeybee experiments. We also repeated the measurement of the FURA2 calibration kit. Figure 2.1.2 on page 38 shows the fluorescence efficiency of FURA2 at 800 nm excitation over a broad range of calcium concentrations.

Even more complicated was the determination of the optimal pulse length. Changing the pulse length is intricate and involves a complete recalibration of the IR laser. It is extremely difficult to achieve similar laser power over a range of pulse lengths. Furthermore, as already described for the optimization of central wavelength, the prism compressor and laser coupling had to be re-adjusted in each iteration. We found two important aspects when varying pulse length: (1) There is an absolute limit of pulse length when measured under the objective. At incident pulse lengths of < 45 fs, the correction for first order dispersion by the prism compressor did not suffice to preserve the pulse brevity. Thus a lower limit of 45 fs defines the lower limit of pulse lengths that can be achieved. (2) Pulse lengths of >50 fs lead to increasingly dark images of stained bee brains at the same input power. Thus, notwithstanding the great efforts necessary to regularly check and preserve the short pulse length, we settled at a pulse length of 45-50 fs.

We repeatedly adjusted the parameters wavelength and pre-chirp from scratch. The respective optimal settings did not differ between trials. The laser parameters we finally chose for honeybee imaging are collectively displayed in Table 2.1.1 on page 37.

2.1.7.2 Setup for measuring pulse length

Achieving an effective pulse length of minimal duration is crucial for the light efficiency of a 2PLSM. The pulse length is inversely proportional to the likelihood for the 2-photon process, thus, at a constant amount excitation light, the amount of emission light that is evoked is doubled when the pulse length is halved. It is therefore advised to aim for very short pulses in the pulsed IR laser, and to pre-chirp (see section 2.1.7.1 on page 36) the pulsed laser light such that

the effective pulse length under the objective is as close to the original pulse duration as possible.
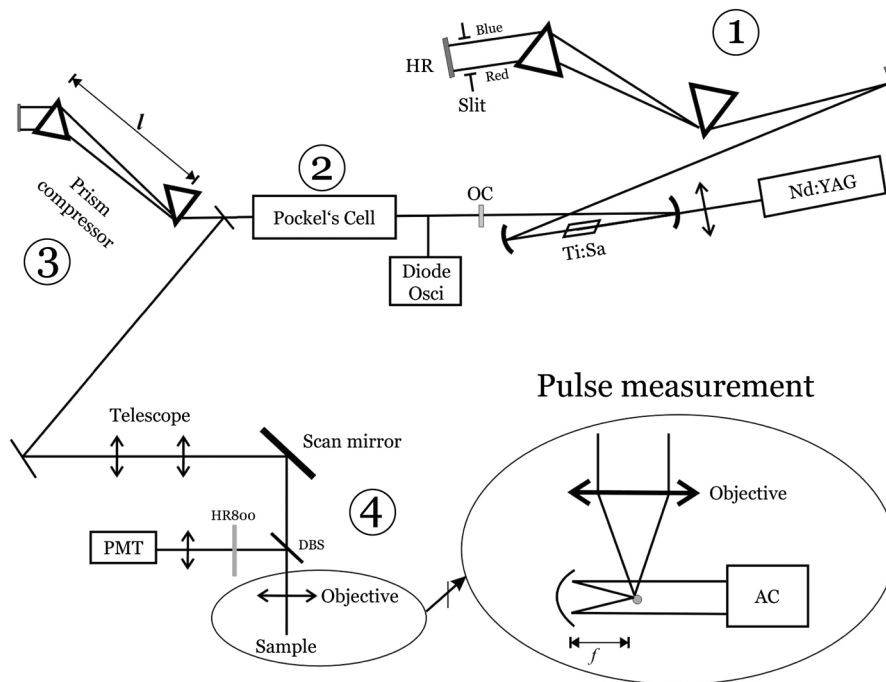
Figure 2.1.3: Complete light path on the optic table and inside the microscope (lower left corner). The inset shows the setup of the pulse length measurement. See text for details. Description of the features along the light path: **(1)** The frequency doubled Nd:YAG laser pumps the Ti:Sa oscillator. A slit in the Fourier plane was used to adjust the FWHM of the generated pulses. Stability and amplitude of the pulses was controlled by a photo diode connected to an oscilloscope. **(2)** Pockel's Cell, see section 2.1.7.3 on page 41 for details. **(3)** Prism compressor and telescope. The telescope was applied to optimized divergence and diameter of the laser beam. The mechanical security shutter was placed behind the telescope (not shown). **(4)** Scanning microscope. The beam was coupled directly onto the scan mirror. Fluorescent light from the sample was deflected at the dichrioc beam splitter (DBS), low pass filtered (HR800), and focused onto the photomultiplier tube (non-descanned photomultiplier, PMT).

We devised a method to measure pulse length under the objective without glass in the light path (further glass in the light path would lead to false readings of pulse length because of additional linear chirp!): a spherical light wave was generated on a small scattering element in the focus of the objective and parallelized on a spherical mirror. The resulting parallel beam was coupled into an auto correlator (AC) that measured the pulse length as present at the focal

plane of the microscope. See figure 2.1.3 on page 40, inset, for a sketch of the pulse length measurement approach. In this way we were able to optimize the prism compressor and the laser settings such that a pulse length as low as 50 fs could be achieved under the objective. It should be noted that this intricate method for determining the real, effective pulse length is unprecedented. Other 2PLSMs are rarely equipped with a prism compressor at all, and even the rare systems that do feature a prism compressor are not adjusted under control of an auto correlator. We are thus sure that no other 2PLSM exists that achieves a comparable light efficiency in the excitation light path. I explained already in section 2.1.3 on page 34 that also the emission light path is principally superior to other systems because of the very close distance between objective and PMT.

2.1.7.3 Flyback blanking reduces incident power

The average laser power of $\approx$500 mW is too high for the illumination of biological samples. We reduced the incident power using a Pockel's Cell (M302 AOM with M350-80 BK driver; Polytec, Berlin, Germany; (2) in Figure 2.1.3 on page 40). Pockel's Cells can switch between blanking and transmitting in a time interval as short as 10 μs, allowing for blanking of the laser beam synchronous to the scanning process ("flyback blanking"). Synchronization was achieved by feeding the line trigger of the microscope controller, which is synchronous to the scan mirror movements, into a delay generator. The adjustable analog delay generator was custom build to our order in the electronics workshop of the Physics Department of the FU Berlin. The delay generator finally controlled the -450 to +450 V output voltage of the Pockel's cell driver.

The laser was attenuated by the Pockel's Cell at all times when the laser light was not required for illumination of the image plane: the return points at beginning and end of each scanned horizontal line, the return to vertical start point after a whole image has been rastered. Thereby we reduced the amount of energy beamed into the tissue by a factor of three. Thus, even at full laser power the tissue would be exposed to only $\approx$166 mW IR light. For further attenuation of laser light we used an analog 10-turn potentiometer that controlled the switching current of the Pockel's cell. The attenuation was continuously adjustable between 1 and 100% laser power. A power of 20 mW in the focus plane under the objective was never exceeded during the experiments.

For the sake of security of operation, we additionally introduced a custom-

built mechanical laser shutter into the illumination light path. The built-in shutter controller of the microscope controller triggered switching of this shutter.

2.2 Experimental procedure

2.2.1 Honeybee administration and staining protocol

Honeybees were collected from an indoor hive during the period from February 2007 to middle of April 2007. From then on, we obtained bees at the entrance of an outdoor hive in the institute's garden. Indoor bees were collected in glass vials, while outdoor bees were caught using a UV-transparent Plexiglas pyramid at the hive entrance.

For each bee, I kept log of the amount and color of mandibular glands that covered the brain. This allows for a rough estimate of age and chaste affiliation. As a rule of thumb, young bees employed with nursing have the most gland tissue and a high hemolymphe pressure. Gland- and brain tissue are colorless and soft. The gland volume and hemolymphe pressure decreases with age; smaller glands appear more firm to the touch. Also the texture of the brain tissue appears more firm in older animals. Pollen foragers have small, more or less strongly colored glands. Depending on the plant the bee collects from, the glands may appear yellow, greenish, or brown. Finally yet importantly, dotted glands (sometimes only unilateral) are a sign of parasitic infection of the glands.

Bees from the collection pyramid were transferred into glass vials. Within 10 minutes after collection, I chilled the bees in the glass vials one by one on ice. Just before movements ceased completely, I transferred the bees into Plexiglas stages (Figure 2.2.1 on page 44). Chilling never took longer than 5 min.

Once a bee was mounted in the stage, I surrounded the head with soft dental wax (Boxing Wax Sticks, Kerr GmbH, Karlsruhe, Germany). The wax, which is plastic already at room temperature, was used to (1) immobilize the head of the bee, (2) seal the gap between stage and head to waterproof the preparation, and (3) to create a wax surface for insertion of preparation needles. The needles have been used to reversibly fix the antennae during operations in the head capsule and during measurements. The needles have been removed at all other times, allowing for free movement of the antennae.

I opened the head capsule using a blade holder with a suitable fragment of
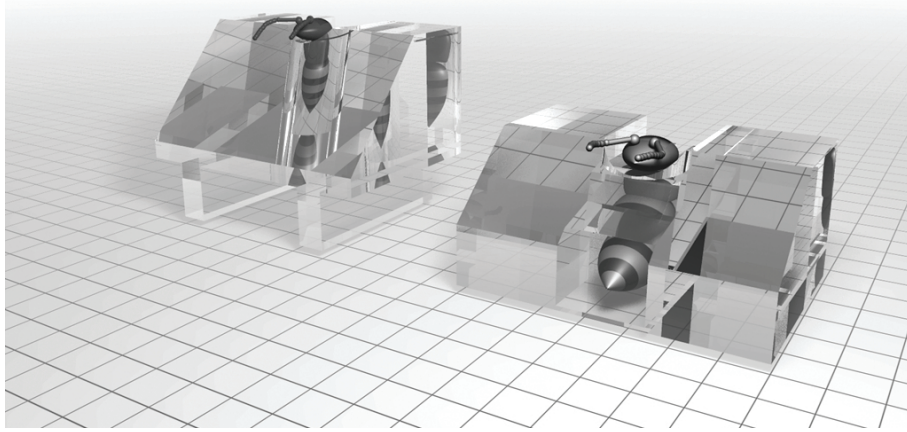
Figure 2.2.1: Plexiglas stages used for *in vivo* imaging. **Left**: Old version, 3.5 x 2.5 cm, 2.7 cm high. The abdomen hangs free in the air. **Right**: New version, same width and depth, but only 1.7 cm high. The floor of the stage suspends the abdomen.

a standard razor blade. The resulting peace of cuticula was stored for later re-use. I prepared only right halves of the brain. Glands were pushed aside to reveal the target site for injection of FURA. I removed the tracheal sheath only locally and only if necessary for clean injection. Excess hemolymphe was removed using little peaces of laboratory wipers (Kimtech Precision Wipes 7552; by Kimberly-Clark, Roswell, GA, USA) if necessary. It was not necessary to dry the brain surface completely before injections.

The dye injection was performed with 1 mm glass electrodes. Electrode production and dye application is described under Dye preparation, page 10. Figure 2.2.2 on page 45 shows the injection site as a red cross on schematic drawings of the bee brain within the head capsule.

Under visual control in a dissection microscope (Wild M3Z; by Leica, Wetzlar, Germany) the brain was punctured with the tip of the electrode between the medial and lateral mushroom body calyx. The electrode was pushed in at an angle of $\approx 45°$ to the surface, in the direction of the lateral surface of the right AL (red dotted lines with arrowheads in Figure 2.2.2 on page 45). In so doing, I aimed at the lACT (blue line in Figure 2.2.2), halfway between the AL and the mushroom body calyxes. To let the dried dye pellet dissolve, the electrode was held in place for at least 10 seconds.

Upon retraction of the electrode, the punctuation closed. I covered the brain with fresh Ringer solution (130 mM NaCL, 7 mM $CaCl^2$, 6 mM KCl, 2 mM
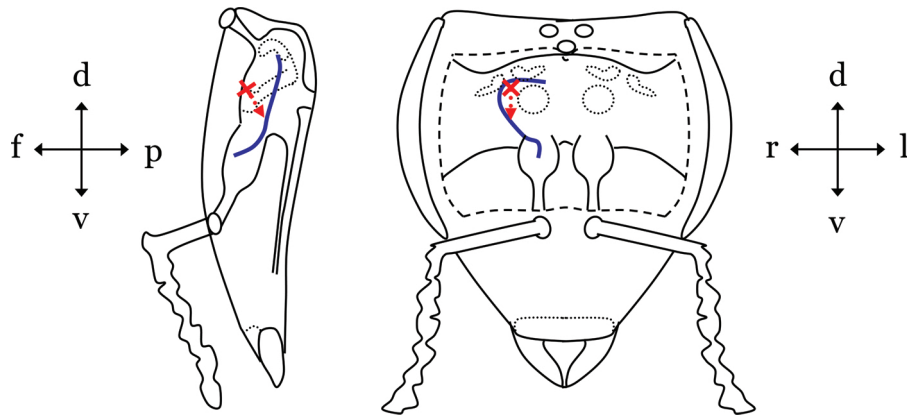
Figure 2.2.2: Schematic drawing of the brain within the head capsule. **Left**: sagittal section, f = frontal, p = posterior, d = dorsal, v = ventral; **Right**: frontal view of the preparation as seen in the dissection microscope. R = right, l = left, d = dorsal, v = ventral. The **red cross** marks the punctuation site; the **dotted line** with arrowhead shows the direction of injection.

MgCl^2, 160 mM sucrose, 25 mM glucose, 10 mM HEPES, pH 6.7, 500 mOsmol) only if a low amount of hemolymphe made this necessary; normally there was enough hemolymphe so no application of Ringer solution was necessary at this point. The head capsule was then covered with the original peace of cuticle. Sealing of the cleft was unnecessary because the original pieces of cuticle fit tightly. Bees were immediately transferred to a wet chamber after injections.

One to two hours after staining (2-3 h after collection of the bees), the bees were shortly removed from the wet chamber for feeding with sucrose solution. Feeding was done with a pipette (variable Research 10-100 μl; by Eppendorf, Hamburg, Germany). I kept log of the amount of 30% W/V sucrose solution that the individual bees ingested. Bees were allowed to feed up to 20 μl solution ad libitum. In most cases, the bees ingested the whole 20 μl.

Bees caught in the afternoons were not fed again before the night. Bees that I caught in the mornings were fed as described above before the night, usually around 8 pm. The bees were left in the wet chamber over night and fed in the following morning around 8 am. Bees that had to wait for measurement for more than 12 hours were fed once more around 8 pm. Staining times were between 16 and 40 hours. Staining quality and quantity did not correlate with staining times.

2.2.2 Preparation of dye-coated electrodes for retrograde stainings

FURA2 dextran (FURA2 dextran F-3029, potassium salt, 10,000 MW, anionic; by Molecular Probes, Leiden, The Netherlands) was prepared for coating by (1) dissolving 0.5 mg of the lyophilized dye crystals in 1 μl aqua dest., (2) addition of 1 mg bovine serum albumin, and (3) letting the mixture dry on a microscopic slide at room temperature. The slides were stored at -20°C.

Glass electrodes were produced in a Sutter electrode puller (Model P-97, Flaming/Brown micro pipette puller; by Sutter Instruments, Novato, CA, USA). The pulling protocol was designed to yield very thin and long tips with extremely low taper angle. The last 1-2 mm of the tips was then broken to get an extremely sharp tip.

Glass electrodes were coated with dye by bathing the electrode tip in the dye solution under visual control. A suitably sticky consistence of dye solution emerged automatically through condensing water on the cold slide. The diameter of the drop of dye that sticked to the electrode tip was between 50 and 100 μm. Through surface tension of the dye drop, the drop dried not at the very tip, but migrated to a position $\approx$250 μm behind the tip. Thus, when injecting the electrode into the brain, the surface was punctured not by a blunt spherical, but rather a very thin and sharp pike followed by the dried dye drop. Furthermore, the lower cuticle of the head capsule could thus be used as a guidance cue for determining the correct injection depth: it turned out that, as soon as the lower cuticle of the head capsule can be sensed, the dye droplet is in the correct depth for staining the lACT.

2.2.3 Machinery for odor stimulations and temperature control

Odor stimuli were applied by a custom-built olfactometer. I designed the olfactometer to deliver odor stimuli in synchronization with the scanning process without mechanical artifacts (Figure 2.2.3 on page 47).

I used Teflon tubing and connections wherever possible; only the connections between valve and odor sources and the tube of the resting air stream between flow meter and glass rod were silicon tubing. The tubing between valve and
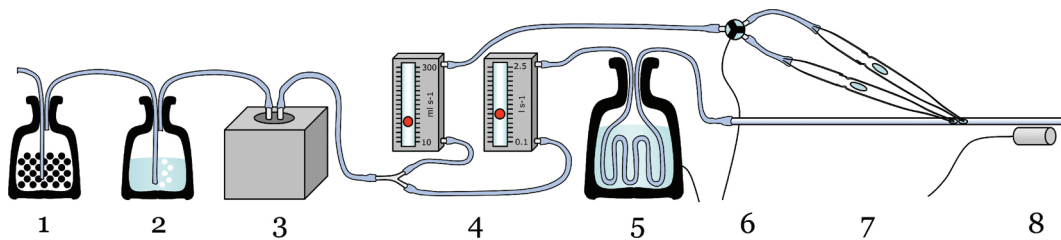
Figure 2.2.3: Layout of the olfactometer. **1**: Air is drawn in and filtered through activated charcoal. **2**: The filtered air is lubricated by bubbling through water. **3**: Air pump. **4**: The air flow is divided up into constant background air stream and stimulation air stream. Flow meters are used to adjust the streams to 1 l/min and 100 ml/min, respectively. **5**: The background air stream is guided through 2 m of tubing which are submersed in a bottle of heated water (45°C). **6**: A computer-controlled valve (Emerson, Ölbronn-Dürrn, Germany) switches between the odour source and the dummy pipette containing only a dry filter paper. **7**: Pasteur pipettes equipped with 1 ml pipette tips (Eppendorf-Pipettenspitze blau; by Eppendorf, Hamburg, Germany) are used as air channel and odor source. The stimulation air stream is lead into the 30 cm long glass rod which carries the background air stream. The entry point is located 20 cm from the outlet to assure smooth mixing of odorous air with background air stream. **8**: the external probe of a thermometer is positioned right at the outlet of the olfactometer, allowing for control of air temperature.

odour sources was exchanged frequently. The tube leading to the glass rod was never changed, for contamination was unlikely: the air flow was never switched off, so an air current constantly flushed odors away from this tube.

The heating bottle (Figure 2.2.3 on page 47, Nr 5) was positioned in direct vicinity of the microscope table, thereby heating not only the air inside the olfactometer tubing, but also the air under a curtain that enveloped the complete microscope. The air stream of the olfactometer was directed to the antennae of the honeybee. The distance between outlet and antennae was 1 cm in all experiments. Behind the bee, flexible tubing of 10 cm diameter was used to remove odorous air at a constant, low flow rate (not shown in Figure 5). The temperature inside the air removal pipe was also controlled with a thermometer so that we were able to adjust the air temperature at the microscope stage to the same temperature as the stimulation air. It took 12 h for stable temperatures to develop, so the heating system was never switched off during the course of the experiments. The temperatures of both the air around the microscope stage and air from the olfactometer were $27\pm0.5\,^\circ$C.

The volume inside the odor source is 3.5 ml, so the head space over the 1 cm^2 filter paper soaked with 5 μl of pure odor substances allowed for odor stimulations of 2 seconds length without reduction in odor concentration. Odor concentration was adjusted by diluting the head space of the odor source 1:10 in the resting air stream. The overall flow rate was 1.1 l/min.

The software "2-Photon Control 2.00" controlled the valve that switches between an empty pipette (air channel) and a pipette with odor-soaked filter paper (odor source). The software synchronizes odor delivery to the scanning process through read-out of the frame trigger of the microscope controller. The user can enter delay and duration of odor delivery. The detailed record of an odor stimulation is as follows: The desired odor source is placed in the olfactometer. The user enters delay and duration of odor delivery into the corresponding fields in the program window of "2-Photon Control 2.00" and activates standby for measurements (button "Wait for trigger"). On the Leica-Control-PC, the user clicks on "Series" to start acquisition of one or several images. The start signal runs via a serial connection to the microscope controller which than starts the measurement by activating the galvos and opening the shutter via the breakout box. The frame trigger of the microscope controller is set to high, so that via TTL trigger, optocoupler, and finally USB the control PC senses the trigger and starts the timer. At the stimulation time point, 2-photon

control switches the valve of the olfactometer via USB I/O box and relays platter. I estimate the overall delay of the complete sequence to be 16.5±11.5 ms. The delay is caused (1) by the windows system which runs the 2-photon control software and induces a cumulative delay of 5 to 8 ms; (2) by the USB connection which runs at 200 Hz tact and thus induces a delay of theoretically 0 to 5 ms (twice, at sensing of the trigger and when switching the relays). The relays finally causes a stable delay of 1 ms. Overall, the olfactometer control is fast enough: at the fastest scan frequency used here of 76 Hz in linear scan mode, the time interval of 13.158 ms between line acquisitions is approximately as long as the delay induced by the olfactometer; the temporal jitter is in the order of magnitude of maximum two scanned lines between successive odor stimulations.

2.2.4 Odors and mixtures for honeybee stimulation

1-Hexanol (HX1) was obtained at the highest available purity from Merck (Merck, Darmstadt, Germany); 1-Octanol (OC1), 2-Octanol (OC2), 1-Nonanol (NO1), and Linalool (LIO) were obtained from Sigma (Sigma-Aldrich, Deisenhofen, Germany). Additionally to the set of pure odors, a mixture of NO1 and OC1 (named MIX) and a mixture of HX1 and LIO (named LIX) were used. As control stimulus, we used a pipette with a dry filter paper (AIR).

The odor set was chosen to comprise many alcohols because their glomerular activity patterns are known from earlier imaging studies (Galizia *et al.*, 1999c). Following the results from these studies, the patterns should overlapping especially on the prominent glomeruli 17 and 33, but also glomerulus 28, all of which are positioned frontally on the AL. I aimed to invoke overlapping activity to be able to collect a large pool of data by imaging limited number of glomeruli, and to detect non-linearities in mixture interactions on single PNs within a glomerulus that is activated by both odors of the mixture.

The second mixture of HX1 and LIO was used because there might be important differences in mixture coding depending on how similar the components of the mixture are. Not much is known about the repertoire of receptor proteins that bind NO1, OC1, HX1, and LIO, but one of many possible assumption is that the alcohols OC1 and NO1 activate an overlapping repertoire of receptor cells, so that mixture interactions might appear already at the very input to the

olfactory system, in the sensillae. HX1 and LIO on the other hand are chemically very distinct, thus one might be tempted to hypothesize that mixture interactions would start not before the level of the local interneurons of the antennal lobe.

Odors were delivered in blocks of eight, every time the same sequence HX1-LIX-LIO-OC2-NO1-MIX-OC1-AIR with 1 min inter trial interval. Preliminary experiments showed that scrambling of the odor sequence does not alter the responses. This block of 8 odor stimuli was repeatedly administered in each measurement region.

2.2.5 A preparation that yields motionless brains

To achieve a motion-free *in vivo* preparation, I cut the abdomen of the bees and fixed the legs to the wall of the Plexiglas stage using molten dental wax (Dental Wax 8060.0027, melting point $\approx 50°$C, Beauty Pink soft; by Ubert, Lohfelden, Germany). Then I removed the esophagus though a window in the head capsule between antennae and mandibles. In this location, also muscles running through the head capsule towards the mouth parts were disrupted. I sealed the opening with Eicosan (CH3 (CH2)18 CH3, melting point 35-37°C; by Sigma-Aldrich, Steinheim, Germany). Next, the antennae were fixed by modeling a bridge of soft dental wax (described in section 2.2.1 Honeybee preparation and staining, page 43) over the scapi of the antennae. The wax bridge also served as a barrier against loss of Ringer solution that I used as immersion fluid during the imaging experiment. I removed gland tissue and tracheae only if they covered the antennal lobes. To avoid leakage of mandibular fluids into the head capsule, glands were never removed in part, but always as a whole. Finally, I sealed the slit in the Plexiglas stage through which the bee head had been initially inserted with soft wax, rinsed the preparation with Ringer solution, and proceeded to the microscope.

2.3 Measurement protocol

Cellular calcium concentration varies in time and space. To understand the action of networks of neurons, one wants to measure on several points of a neuron, several neurons and glomeruli simultaneously, at very high frequency. Because it is not yet possible to achieve this within one measurement, I acquired two fundamentally different datasets: (1) planar scans and (2) linear scans. In the first case, I recorded several successive images over time at high spatial resolution, large field of view, but poor temporal resolution. These measurements were used as guidance for finding the optimal Field of view (FoV), but were otherwise not (yet) exploited. In the second case, I recorded the same line of an image repeatedly at high frequency. The resulting square images show the scanned line as a horizontal array of pixels, while the repetitions are appended from top to bottom. The spatial resolution is as high in the single spatial dimension; the temporal resolution is very high at 13.158 ms/line. Table 2.3.1 on page 52 shows an overview of the parameters used in the two scan modes. Last but not least, high resolution 3-dimensional stacks of anatomical images were recorded for reconstructions of neurons and identification of glomeruli.

The following list enumerates the sequence in which recordings of the different types were administered.

1. Recording of an initial stack of anatomical images for overview and reconstruction of PNs

2. Measurements of odor responses in large frontal visual field featuring many glomeruli, planar scan mode

3. Measurements of odor responses in linear scan mode, preferably on frontal glomeruli 33, 17, 42

4. If at least three repetitions of the odor set had been recorded in planar and in linear scan mode, I chose a new field of view (FoV) and continued with the measurements

	Planar scans	Linear scans
Spatial dimensions	2	1
Spatial resolution	0.1 ... 1 μm / pixel, typically 0.5 μm / pixel	0.1 ... 1 μm / pixel, typically 0.5 μm / pixel
Temporal resolution	1.36...1.42 s / image = 0.715...0.735 Hz	13.158 ms / line = 76 Hz
Typical amount of data per measurement	3 mB (12 frames, 16.8 s)	256 kB (512 lines, 6.74 s)
Average number of glomeruli in FoV	12	3.74
Estimated percentage of PNs per glomerulus visible	100%	50%
Estimated number of neurons in FoV*)	82.5	15

Table 2.3.1: Technical data of the 2 scan modes. *) FoV = Field of view; assumed number of neurons per glomerulus that could be reconstructed = 5.5.

5. If responses were still stable after this point, I chose deeper regions in the AL for measurements on glomeruli that are hitherto not characterized by the functional AL atlas

6. Finally, high resolution stacks were recorded (only when the initial stack was too noisy or contained movement artifacts)

2.3.1 Stacks of anatomical images were recorded first

Recording of a depth resolved stack of images (zStack) on the stained AL. The parameters for the stack represent a compromise out of image quality and protection of the preparation: the stack had to be administered quickly without averaging and with reduced resolution along the depth axis to avoid bleaching of the tissue. Because in a large FoV the power density is lower compared to a high-resolution, small FoV, the FoV was chosen such that the whole AL would be visible. To allow for a reliable estimate of the staining quality, the resolution was set high enough to visually trace neuronal processes. Typical parameters were: 400 μm^2 FoV x 225 μm in depth, 512 pixels^2 x 180 images (= 0.78 μm^3 / voxel). Laser power was set to a rather low value of typically ¡ 5 mW for this initial stack. The stack was observed already during the scanning process. If

movements of the brain occurred, the bee was checked under the dissection microscope once more. If the staining had failed, the bee was discarded. If staining and motionlessness were satisfactory, I immediately started the odor measurements. In some cases, i.e. if Ringer solution leaked or movements of the animals were strong, the animal had to be removed from the microscope for further preparation.

Depending on the quality of the recorded stack, it was sometimes necessary to acquire another stack at higher resolution and slower scan speed after the physiological measurements were completed. If brain movements occurred during the recording, I movement-corrected the stacks with the StackReg plug-in in the Software ImageJ.

2.3.2 Planar scans provide overview

Odor responses in frontal glomeruli were measured with planar scans. Table 2.3.1 on page 52 outlines the scan parameters. Three blocks of odour stimulations (as described under section 2.2.4 odors, page 49), totaling 24 measurements, were performed in each FoV. The lateral position and the depth of the FoV below frontal surface were varied with the aim to yield a complete picture of the activity in all stained glomeruli. Depths ranged from 20 to 120 μm; I positioned the FoV such that such that cortex and core of as many glomeruli as possible were are simultaneously visible. The recordings were not only saved to disc but also observed and evaluated online with the aim to get an overview over the staining quality and arrangement of glomeruli in this animal, which was important for the choice of FoVs for later linear scan measurements.

2.3.3 Glomeruli 17, 33, and 42 were recorded most frequently

In the same depth as the measurements above, I tried to find a good position for a linear scan. The optimal position would comprise again the glomeruli 17, 33, and 42, and it would dissect them through the center so that cortex and core would be covered by the line for all three glomeruli. Because of the v-shaped arrangement of the three glomeruli of interest, this was often not possible. I then placed the line such that (with descending priority) at least one of the glomeruli

28, 52, 62, 60, or 47 would be the third fully transected glomerulus along the line. The length of the line was set to 250 or 300 μm (Table 2.3.1 on page 52 outlines the scan parameters), so quite regularly more than three glomeruli were dissected by the line. Yet neither the identity of these additional glomeruli, nor the position at which they were hit by the line could be targeted exactly for spatial reasons (linear scan field on a variable arrangement of glomeruli).

2.3.4 Balancing repetitions vs. overview: more recordings in 17 & 33 or other glomeruli

To continue the measurements, I followed two alternative routes: Either (1) I continued with linear scans on the same glomeruli, if a new position for a linear scan could be found at which the same glomeruli would be sectioned, but at a different position. Or (2), if such a line could not be found, a new FoV on any of the (still frontal) glomeruli 52, 62, 60, 47, 36, 28, 18, 35, 23, 48, 38, 29, 37, or 135 was chosen. In the latter case, I measured again first in planar scan mode, then in linear scan mode. In any case I collected three times the complete odor set in each FoV and scan mode.

2.3.5 Scans in deeper glomeruli reveal activity in integrative segments

At this point, the bee has been stimulated with odors 72 or 96 times. If the responses were still stable, I continued the measurements, but changed the AOI towards glomeruli from deeper regions of the AL, preferably ones which were arranged such that a linear scan could dissect the glomerulus along the distal-proximal-line. In such cases, a linear scan could capture the calcium transients in the primary neurite, the integrative segment, in the core, and in the cortex simultaneously.

2.3.6 More stacks of anatomical images at higher resolution and averaging setting

At the end of the experiments, I acquired more image stacks at higher resolution and with line- or frame-averaging to yield increased image quality for later

reconstructions of neuropils or neurons. The position, size, and resolution of the stacks were chosen such that the fields of view of the earlier odour measurements would be represented together with the immediate surrounding tissue. The recording of stacks that comprise hundreds of images and high averaging could take up to 1 hour to complete. During this time the next bee was prepared for recording.

2.4 Automated registration of calcium signals

Two different algorithms were employed for the automatic registration of signals. To detect all spontaneous signals in signal traces from linear scan measurements, I created an algorithm that reliably finds the exact onset, rising slope and amplitude of isolated, successive signals. At the core of this algorithm is the detection of zeros crossings of the differential of the measurement trace. This algorithm has a weakness concerning the detection of the duration of long, tonic signals with shallow slope at the end of the signal. Yet such long signals are only encountered during odor delivery. So this weakness plays no important role for the registration of spontaneous signals. The strength of this algorithm is its ability to detect signals also when they occur in quick succession. There is nor resting phase before or after the signal required for reliable detection. For the rest of this document, I will term the algorithm for the detection of spontaneous signals by curve sketching "curve sketching algorithm", CSA.

The other algorithm for the detection and characterization of spontaneous and odor-evoked signals is based on correlation of linear scan measurement traces with signal-like templates of variable length and shape; it is thus called "template correlation algorithm", TCA. The detection threshold is slightly higher compared to the curve sketching algorithm, and trains of signals with brief pauses are often registered as one single signal. The benefit is that more parameters can be extracted: the algorithm extracts not only the onset and amplitude of the signals, but it also determines the exact duration and the slope of the falling phase. Additionally it can detect signals that are not isolated, i.e. a phasic signal that occurs during a tonic signal. Last but not least, this algorithm can detect also signals of inhibition just as well as signals of excitation.

2.4.1 Use of curve sketching for the detection of signals: CSA

As pointed out above, the aim of this algorithm is to extract spontaneous signals. The main characteristic of spontaneous signals is that they do not occur at fixed

time points. Because of variable noise levels, variable signal amplitudes, and fluctuating or sagging base lines across different glomeruli and animals, a simple amplitude threshold yields unsatisfactory amounts of false-positive and false-negative detection events. I devised instead an algorithm that detects signals by analyzing the differential of a smoothened copy of the raw signal trace. Zero crossings of the differentiated trace signify points in time when a rising phase ends and a falling phase begins and vice versa. When optimizing the algorithm, I constantly observed the impact of changed parameters with randomly chosen measurement traces. Figure 2.4.1 on page 58 shows the graphical output that the algorithm generates for this purpose.

The graph is helpful for the explanation of the sequence of steps in this part of the signal detection process. The analysis starts with the raw measurement trace (see figure 2.4.1 on page 58, label raw signal trace). The example shown in the figure displays strong signals at a rather high frequency of ≈1.5 Hz. The noise level is substantial, and the baseline is shifted to a negative value of ≈3% $\Delta F/F$. The latter is an artifact from the bleaching correction which tends to shift the measurement traces such that their sum is zero. The algorithm performs several consecutive steps to finally create a list of putative signal start points, rising slopes, and amplitudes:

- **Smoothe**: First the raw measurement traces are smoothened by application of two successive running average filters. Shown in figure 2.4.1 on page 58 are three iterations of a running average filter. Labelled with "running average 1" is the result after filtering with a 5 samples running average filter. The trace labelled "running average 2" shows result of filtering "running average 1" once more with a 7 samples running average filter. This amount of filtering turned out to be best suited. The trace labelled "running average 3" is smoothened once more with a 10 samples running average filter, but it has not been used further in the analysis.

- **Differentiate**: Next the algorithm differentiates the trace "running average 2" by calculating the difference between adjacent samples. The result is shown in the figure at the label "differentiated trace".

- **Detect zero crossings**: Zero crossings (= change of sign) of the differentiated trace are journalized. The direction of the change of sing is registered as well. Each change of sign from negative to positive represents a putative
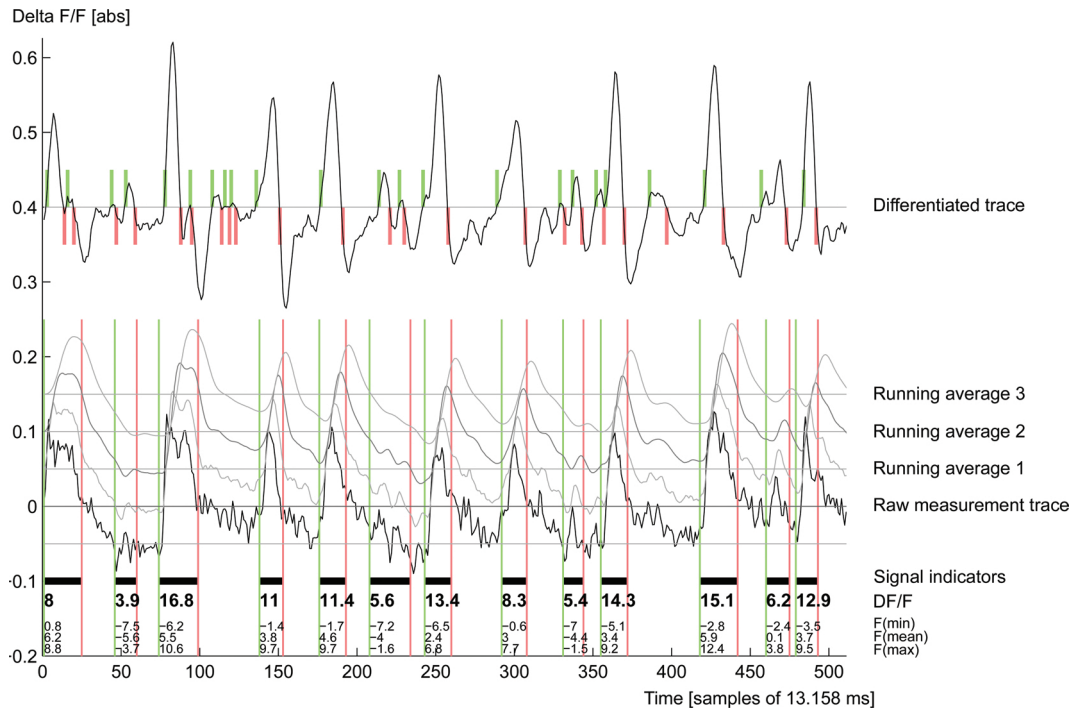
Figure 2.4.1: Representation of an exemplary measurement trace (animal 7228‗07b, glomerulus 12, no stimulus) and filtered / differentiated curves as calculated by the curve sketching algorithm. Raw traces, running-average filtered traces, and the differentiated trace are labeled at the right hand side of the figure. At the bottom, thick horizontal lines mark putative signal phases. The numbers below these lines quantify the minimal, mean, and maximal amplitudes of the measurement trace around the current putative signal. In bold letters, the signal amplitude as shown as $\%\Delta F_{max} - \%\Delta F_{min}$. The thick short colored vertical lines behind the differentiated trace mark the zero crossings (green for negative to positive sign change and vice versae for the red lines). Thin colored vertival lines in the lower half of the figure mark the onset and offset of putative signals before filtering out non-signals by thresholding and end-of-signal optimization.

signal onset, and vice versa. The actual sample number that is journalized as signal onset / signal offset is the point of the differential trace with the highest / lowest incline.

- **Apply threshold**: For all putative signal onsets, the slope of the incline and the amplitude of the signal compared to a phase before the onset are calculated. Only signal onsets after which a signal of more than 3% $\Delta F/F$ develops, and that rise with more than 0.3% $\Delta F/F$ per sapmple, are kept. Amplitudes are determined in the raw measurement trace as the mean of the three samples around the maximal amplitude minus the mean of three samples around the minimal amplitude in a small time window before the signal onset. Please note that during this filtering step, many of the signals which are marked in the bottom row of figure 2.4.1 on page 58 are rejected.

- **Optimize end-of-signal detection**: Because the inclines of the falling phases are usually shallower than the rising phases, the precision of the detected signal offset time points is low. The offset time points thus have to be corrected for each signal by a simple algorithm which searches in all measurement samples after the signal onset for the first sample which falls below the half-maximal amplitude. Rather often two separate signal onsets are assigned the same signal offset time point. In this case the signal onset with the steeper rising slope is kept, the other rejected.

- Δ **F/F** → **standard deviations**: At this point, reliable start- and end points of signals are found. The algorithm can now determine the true base line of the measurement trace by taking the mean of all samples that do not fall into a signal phase ("resting phase"). At the same time, the standard deviation of the resting phases is calculated. The algorithm now divides the % $\Delta F/F$ amplitude values of all signals in the journal by the standard deviation. The measure of amplitudes is thereafter *multiples of baseline standard deviation*, which is a kind of signal-to-noise factor representation. The conversion allows to filter the signal list again with a standard deviation threshold in the next data evaluation step.

To conclude, the curve sketching algorithm creates for each measurement in each glomerulus a list of signals, which are quantified with start- and end-sample, % $\Delta F/F$ min/men/max, baseline standard deviation, and signals

amplitude as multiple of the baseline standard deviation. In measurements with odor stimulation, only the two seconds before odor stimulation are analyzed.

The lists of signal parameters that are created by the curve sketching algorithm are saved in a convenient data format in MatLab, called "struct". This struct is used as database for descriptive statistics on various parameters of spontaneous activity, i.e.

- Frequency

- Regularity

- Amplitude

- Duration

These parameters are compared between grouped datasets. To describe the basic parameters of spontaneous signals, data were grouped by animal and by glomerulus. Also checking for correlations between parameters is possible; i.e. dependency of regularity on frequency, correlation of amplitude with signal duration, or change of the regularity value when only signals of ≥ 3 standard deviations are taken into account.

2.4.1.1 Lists of signals are checked for regularity and frequency

Frequencies F of signals are either determined as instantaneous frequencies F_i between two time points:

$$F_i = \frac{1}{t_2 - t_1},$$
(2.4.1)

or if the frequency of spontaneous events in a whole measurement is quoted, than the frequency is calculated as n-1 events divided by the length of the time window from the first to the last event (t_1 to t_n:

$$F = \frac{n-1}{t_n - t_1}.$$
(2.4.2)

Regularity R is calculated as 1 minus the mean deviation $\overline{D}$ from perfectly regular inter-signal intervals divided by the mean interval $\overline{I}$:

$$R = 1 - \overline{D}/\overline{I},$$
(2.4.3)

where $\bar{I}$ is the mean temporal interval between signals

$$\bar{I} = \frac{1}{n} \cdot \sum_{1 \to n} I_n, \tag{2.4.4}$$

and $\overline{D}$ is the mean of all (modulus) differences between the intervals I_n and the mean interval $\bar{I}$

$$\overline{D} = \frac{1}{n} \cdot \sum_{1 \to n} \left| I_n - \bar{I} \right|. \tag{2.4.5}$$

R has been designed to range from 0 to 1. If the observed signal train is perfectly regular, $\overline{D}$ becomes 0, thus R would be 1. If the mean deviation of the actual intervals I_n from the mean interval $\bar{I}$ becomes large, R becomes smaller. If the mean deviation is as large as the mean interval, R becomes 0. If the mean deviation becomes larger than the mean interval (which could happen in theory, i.e. if the observation period is very long but all but one signals appear only during a specific time window), R might even get a negative value. For the data presented here, this was never the case. R is a robust measure of regularity, for it is showing the relative, not absolute jitter of events irrespective of the frequency / inter-event-interval of events. Thus, at with rising frequency, R stays constant, if the relative regularity stays constant.

R could as well be expressed as % deviation from a perfectly regular train of signals:

$$\%Deviation = 100 \cdot (1 - R) \tag{2.4.6}$$

2.4.2 175 templates for detection of signals: TCA

The second automatic signal registration algorithm has been designed with the aim to characterize also the temporal structure of signals. Especially during the time window of odor stimulation the signal shapes can be complex, i.e. phasic-tonic. The algorithm represents such complex signals as the sum of a number of elementary signals. The representation of a phasic-tonic signal would be one long, smaller signal that is overlain with a sorter, larger signal in the beginning. The second important difference is that his algorithm registers signals of pre-synaptic inhibition as well.

To achieve these goals, the algorithm pursues, compared to the curve sketching algorithm, a completely different approach. At the core of this program are

signal-shaped templates of variable length, and slope. The templates are shorter than the measurement traces. To cover the whole length of a measurement trace, the templates are shifted sample-wise over the recordings. The algorithm computes the correlation coefficient of the measurement traces with all templates in all time points. Consecutively, the best matches are analyzed in detail to find the exact sample that fits a given signal the best. The algorithm is thus called "template correlation algorithm", or TCA. It follows the description of the steps necessary to produce a full set of correlation coefficients for all measurements.

- **Produce templates**: Two sets of templates are created. The first set contains 75 templates with 250 ms long tails before and after the signal waveform and 26 to 461 ms long plateau phase. Because of the short tails and plateaus, the templates from this set are suited for the detection of short signals. The second set with 500 ms long tails aims at the detection of long signals. The plateau phases of the 100 templates are from 52 to 1974 ms long. In both sets of templates, the signal end is modeled with 5 different declining slopes. The slopes are produced such that they are correlated to the length of the plateau phases. Figure 2.4.2 on page 63 shows all templates.

- **Walk**: In each of the 3015 measurement traces, all 175 templates are sample-wise shifted over the length of the recording. One recording consists of 512 samples, but the number of correlation coefficient calculations is lower, because no coefficient is calculated if the shifted sample exceeds the length of the recording.

- **Correlate**: In each walking step, the correlation of all templates with the current stretch of measurement trace is calculated. It is worth noting that absolute amplitude differences so not play a role in calculating the correlation coefficient: The correlation of an array [0 0 0 1 1 1 0 0 0] with [0 0 0 10 10 10 0 0 0] yields a correlation coefficient of 1. It is also worth noting that the same samples can detect positive and negative signals: The correlation of an array [0 0 0 -1 -1 -1 0 0 0] with [0 0 0 1 1 1 0 0 0] yields a correlation coefficient of -1. By using two thresholds, one in the positive, one in the negative, one can detect excitatory signals and inhibitory signals with one and the same template.

- **Save in 3D-matrix**: the correlation coefficients are saved in 3D-matrices, one matrix per measurement trace and template set. The matrices have the dimensions time, template length, and slope. I will refer to this matrices as "3D-correlation-matrices". Creating a complete set of results matrices takes 8 h to complete on an Athlon64 1.8 GHz computer and produces 1.56 GB of data.
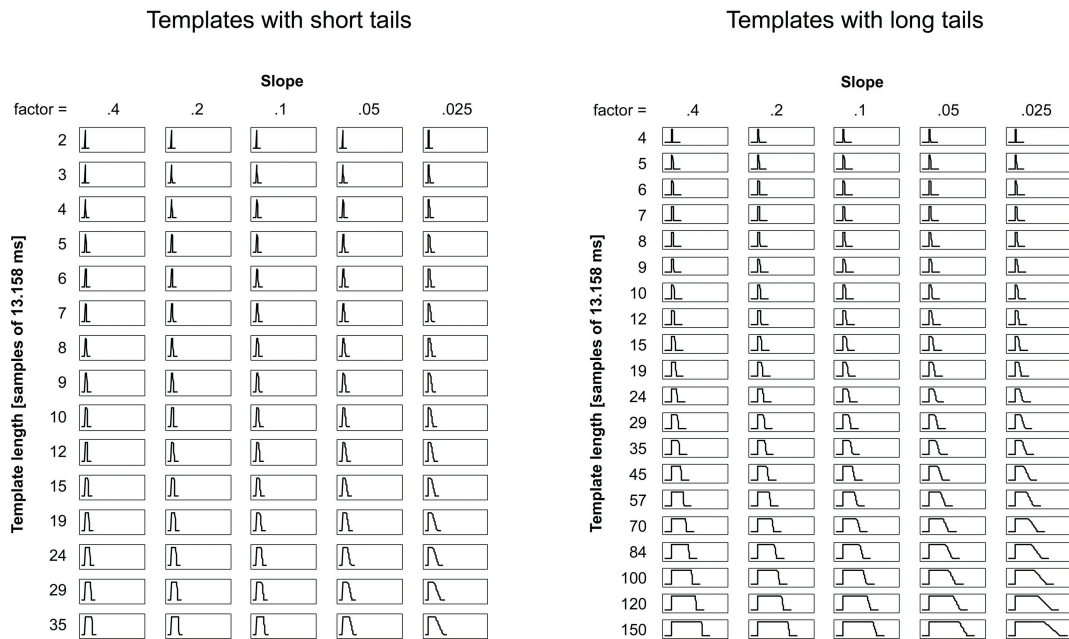

Figure 2.4.2: All 175 templates that were used by the walking template correlation algorithm. Templates are sorted such that from top to bottom, the length of the plateau phase increases, and from left to right, the slope factor of the falling phase decreases.

The matrices created by the walking template correlation algorithm contain the information to find for each signal the template that fits best. But it is not trivial to retrieve this information from the 3D-matrices. Figure 2.4.3 on page 64 shows one exemplary measurement trace and the 2D-image representation of the correlation coefficient matrix. The image planes that are arranged along the z-axis in the 3D-matrix are appended vertically. See figure legend for information on what to find where.

Knowing how to read the correlation matrix is useful for the understanding of the next steps in the analysis. I will walk you through this by focusing on one of the signals of the exemplary measurement trace shown in figure 2.4.3 on
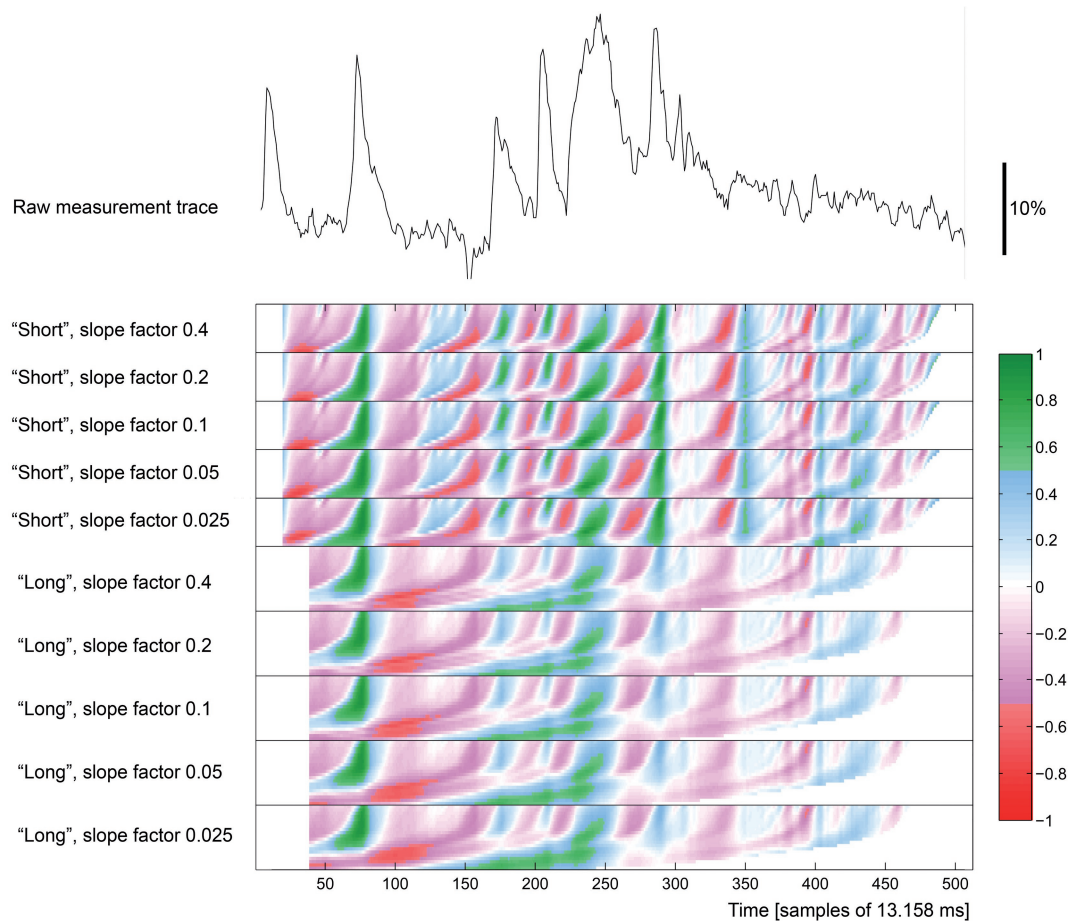
Figure 2.4.3: Measurement trace (on top) and 2D-image representation of the correlation coefficient matrix (below) for one exemplary measurement (7314_02 glomerulus 33, stimulation with OC2). Each of the 10 horizontal strips of the 2d-image contains the correlation coefficients for all temporal positions (along the x-axis, sample indication is valid for the raw trace too) and all lengths (along the y-axis, short to long templates are arranged from top to bottom), and one slope function of the test templates. The various slope functions and template identities are quoted at the left of the figure. The correlation coefficients are color coded with the color table shown at the right side of the figure.

Locate the second phasic signal of the raw measurement trace, it starts at sample 70. In the correlation matrices below the signal, saturated green areas mark correlation coefficients of ≥ 0.5. After visual inspection of hundreds of signal traces and their correlation matrices I determined this threshold to be best suited for visual detection of signals. The problem is that there are many correlation coefficients of ≥ 0.5. Obviously, if the signal is as clear as in this example, many of the templates fit rather well. But the perfect match should stand out. One of the correlation coefficients for this signal must be the highest. Determining the highest correlation coefficient from the entire matrix would yield only one template for one signal. Therefore, the correlation matrices need to be analysed in three steps: (1) locate the temporal position of signals roughly; (2) from the rough position, generate a search window within to determine the maximal correlation coefficient; (3) remove false positive matches. This is exactly the sequence of steps that the next analysis program takes.

(I will come back to the example measurements and show the results from the next analysis steps further below. First comes the description of the next steps in the analysis.)

- **Reduce dimensionality**: For each time point, all correlation coefficients are averaged, creating a 1-dimensional curve of mean correlation over time ("correlation curve").

- **Fit Spline**: In the next step the program needs to find maxima and minima in the correlation curve, but the curve is not necessarily equicontinuous. Smoothing with a running average filter is unsatisfactory because to be sure that in none of the 3015 measurements any false positive peaks are registered, quite strong smoothing would be necessary, which would again lead to false negatives. A better method is fitting a spline to the raw correlation curve. Therefore, the average correlation trace is serially averaged over 6 samples, resulting a 85 supporting points for the spline fitting algorithm. Now, the MatLab function "interp1" interpolates over the supporting points to re-establish a 512 samples long representation of the average correlation trace, the chosen method for interpolation is cubic spline interpolation. The resulting curve ("spline smoothened curve") is very smooth and allows for reliable detection of all maxima and minima.

- **Detect zero crossings**: As in the curve sketching algorithm, maxima and

minima of the spline smoothened curve are registered by differentiation and successive detection of zero crossings. These maxima and minima point at the rough location of the highest correlated template *for single signals*.

- **Pick best fitting template**: In a time window of 11 samples around the detected maxima and minima, the highest correlation coefficient is determined in the 3D-correlation-matrix. If the maximum correlation coefficient that is found is ≥ 0.55 or $\leq$ -0.55 (signals of inhibition), the program retrieves the template that produced the optimal match. Retrieving the templates is easy, because the position of the highest correlation coefficient in the 3D-matrix directly corresponds to a certain delay, length, and slope of one of the templates.

- **Create list of signals**: At the temporal positions of the best-fitting templates, there are signals in the raw measurement trace. From the raw signal traces and from the matching template, the walking template correlation algorithm creates a list of signals with the parameters

    - Description: excitation/inhibition
    - Sample number of signal onset
    - Sample number of signal offset (half-maximum of the falling slope)
    - Signal amplitude as mean ΔF abs. during the plateau phase
    - Background amplitude as mean ΔF abs. directly before and after the signal (during the template's tail phases)
    - Absolute signal amplitude as $\overline{\Delta F_{plateau}} - \overline{\Delta F_{before\&after}}$
    - Signal amplitude in multiples of baseline standard deviation
    - Baseline standard deviation

    Obviously, to fill the last two positions of the list, the same approach as in the curve sketching algorithm can be used: Determine the standard deviation of all samples that are *not* part of a signal as indicated by the best fitting templates; divide the absolute signal amplitude by this standard deviation measure.

- **Remove duplicates**: In some cases, two partly overlapping templates fit onto one and the same complex signal. Often this is wanted, because

it allows analyzing for example the phasic and the tonic component of a complex signal separately in a later step. But after visual inspection of hundreds of signal traces with their appointed templates, I realized that some of these duplicate matches must be removed from the signal list, because both templates overlap largely and fit the same signal without adding usable information about the signal's temporal structure. I programmed an algorithm that checks the signal list for pairs of signals with an overlap that exceeds 50% of their average length. Thus, a 10 samples short signal on top of a 100 sample signal would *not* be excluded because the overlap of 10 samples is smaller than 50% of the average of their lengths (= 27.5 samples). Oppositely, if two signals are rather equal in length and overlapping with more than 50% of their average length (i.e. two 50 samples long signals that overlap at 40 samples), the template with the lower correlation to the trace is removed from the list.

- **Adjust standard deviation**: After removal of duplicate signals, there are more samples between signals available for determining the baseline standard deviation. So the standard deviation is calculated once more, and the respective fields in the signal lists are corrected.

It is worth noting that not only the robust signal detection and characterization realized by this method, but also the reliable detection of phases with no signal are equally important for later analyses.

2.5 Data grouping by multiple hierarchical criteria

No differentially treated groups of animals are to be compared in this thesis. The body of data nevertheless benefits from group-wise analysis. Some grouping criteria are effortlessly found in the data structure: one could compare the identified glomeruli or individual test animals. Within the group of all measurements belonging to the same glomerulus, one might determine the average increase in activity at stimulation with a certain odor. The aim of such group-wise analysis would be to determine glomerular activity patterns, for example for comparison with the published activity patterns from the functional AL atlas.

These criteria have been used for grouping of data in the data analysis:

- Morphology
    - Identified glomeruli
    - Identified neurons and their dendritic branches

- Stimulation
    - No stimulus
    - Odor stimulus
    - Odor mixture stimulus
    - Stimulation with activating odor (i.e. according to AL atlas patterns)

- Measurement time window
    - Before stimulation
    - During stimulation
    - After stimulation

- Circumstances of the measurements
    - Simultaneously measured pairs of glomeruli (synchrony)

- – Number of pixels that a given target structure fills in the measurement plane or line

  – Laser power / fluorescence strength

  – Signal to noise ratio

- Parameters extracted from the measurement traces

  – Signal amplitude

  – Signal duration

  – Signal frequency

  – Regularity of spontaneous signals

  – Temporal signal shape

  – Signals of inhibition

  – Delay of responses

In the following sections I will describe in how PNs were identified, how the recordings were segmented by the odor stimulus, and how different kinds of signals were treated.

2.5.1 PN processes were reconstructed in Amira

Using the anatomical image stacks recorded before and after the physiological measurements, I reconstructed between 2 and 8 individual neurons in 10 single glomeruli from 7 different animals. Already during the data acquisition I concentrated most on glomerulus 33 and took care to transect it with the scan line in the geometric middle. Consequently I reconstructed PNs mostly within this glomerulus.

The neuron reconstructions are the key to an analysis that takes into account all structural levels of the antennal lobe. Table 2.5.1 on page 70 recapitulates the structural levels that are, as opposed to any other physiological measurement method, simultaneously accessible in 2-photon microscopy.

Between 2 and 8 neurons could be reconstructed per glomerulus. Reconstructed branches of the PN dendrites dissected the scan line between 1 and 3 times. See Table 2.5.2 on page 70 for an overview of the numbers of neurons / branches per glomerulus and animal.

Structure:	Glomeruli	PNs	Branches
Signal:	Pattern of activity	PN activation	Localized signals
Measured by:	Planar scans, linear scans with averaging in space; also wide-field fluorescence microscopy	linear scans	linear scans
Extracted information:	Multi-unit activity, ignoring neurons	Single unit activity	local calcium, EPSPs, IPSPs

Table 2.5.1: Hierarchical tree of structures within the antennal lobe. The row "Extracted information" shows what information can be obtained when analyses are carried out on a specific level of structure.

Glo.	7302_02	7308_11	7310_02	7314_02	7314_06	7330_02	7511_08
17			4 / 5	5 / 10			
33	8 / 16	4 / 6		7 / 8	6 / 9	5 / 8	
42					3 / 5		
62							2 / 4
82							3 / 6

Table 2.5.2: Amount of neurons / branches reconstructed in glomeruli of 7 different test animals.

The first step in the PN reconstruction process was the assemblage and arrangement of all necessary data in Amira:

- Image stack(s)

- Overview frames of the areas of interest (AOI)

- Representations of the linear scan images

I created a bounding box, ortho slices, and a Voltex volume rendering to gain an overview over the properties of the anatomical image stack. If the glomerular boundaries were not easily recognizable, I used the image segmentation tools to create 3D-surfaces of the glomeruli within range of the AOIs. The segmented outlines of the glomeruli served as orientation help when reconstructing the PNs.

The AOI images were loaded into the Amira workspace and positioned at the corresponding position of the anatomical image stack using the crop editor

and the transform editor. One central strip of each AOI was duplicated as a representation of the linear scan position. Figure 2.5.1 on page 71 illustrates the various data objects in the Amira workspace ("pool").
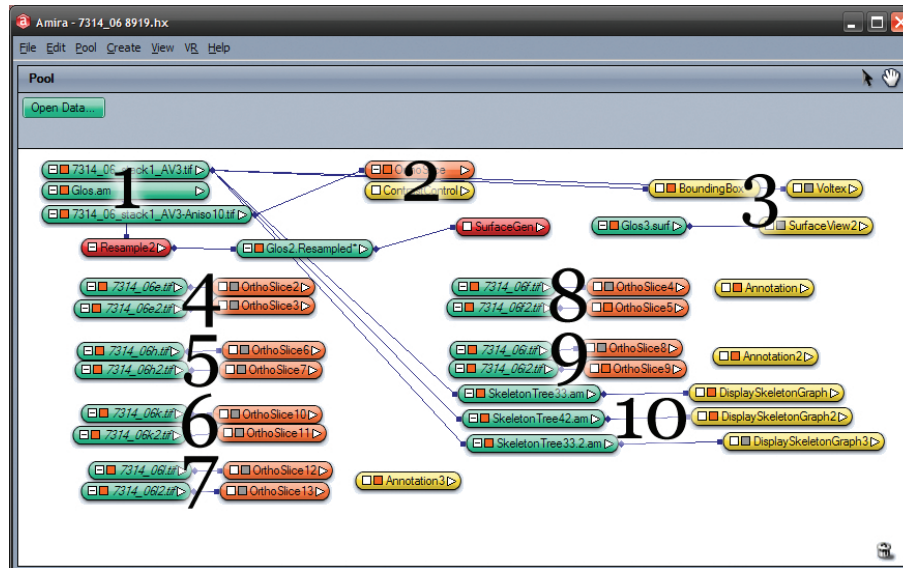

Figure 2.5.1: Network of data and display modules in the Amira pool. **1**: anatomical image stack of bleach corrected, but otherwise raw image data. This data was used for the creation of the PN dendritic skeleton trees. For visualization I created another stack with various filters applied that reduced noise and increased visibility of the neurons; **2**: visualization modules for the stacks: ortho slice and contrast control; **3**: bounding box and volume rendering; **4-9**: two data objects (green) and visualization modules (red) for each AOI, once for the overview image, once for the representation of the scan line; **10**: skeleton tree objects with their visualization modules.

Tracing of PNs was done on the basis of bleach-corrected, but otherwise raw stacks of anatomical images, because the "snakes-algorithm" that allows to semi-automatically construct skeleton trees of the PN dendrites is not optimized for strongly filtered images. The opposite is true for the human eye; fortunately Amira allows to use one stack for visualization, but another one for creation of the skeleton trees. Figure 2.5.2 on page 72 shows the visualization of all data objects used during the reconstruction process of one animal in the Amira viewer. Figure 2.5.3 on page 72 shows 9 reconstructed PNs out of two glomeruli (33 and 42) on top of an ortho slice view of the anatomical image stack.

I determined pixel coordinates for each branch of the reconstructed dendrites based on the skeleton graphs in Adobe Photoshop. To simplify further analyses and comparisons of the physiological responses in the single branches, I always
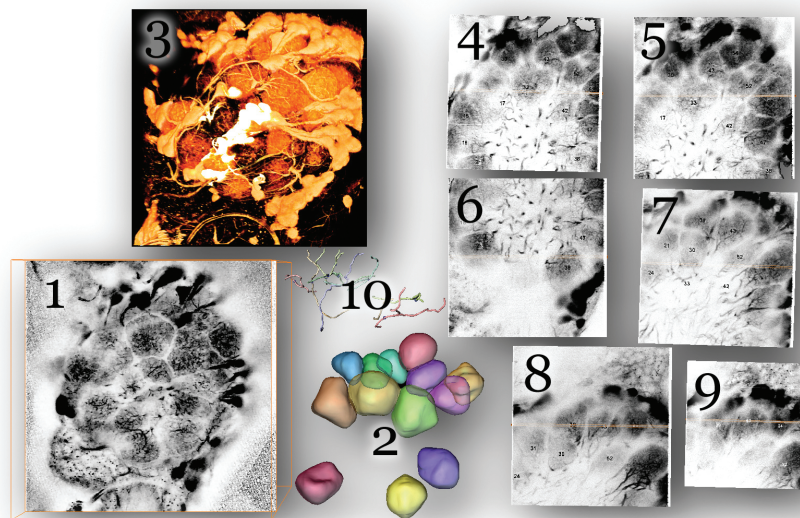
Figure 2.5.2: Data objects of one animal in the Amira viewer. All objects but the skeleton graph are to the same scale. **1**: ortho slice display and bounding box (orange) of the filtered stack of anatomical images; **2**: surface view of all glomeruli that were transected by the linear scans; **3**: direct volume rendering display of the stack of anatomical images; **4-9**: ortho slice display of all AOIs and the representations of the scanned line in the middle of each of them; **10**: skeleton graph display of the skeleton trees of 9 neurons that I reconstructed within 2 glomeruli (33 and 42), slightly enlarged.
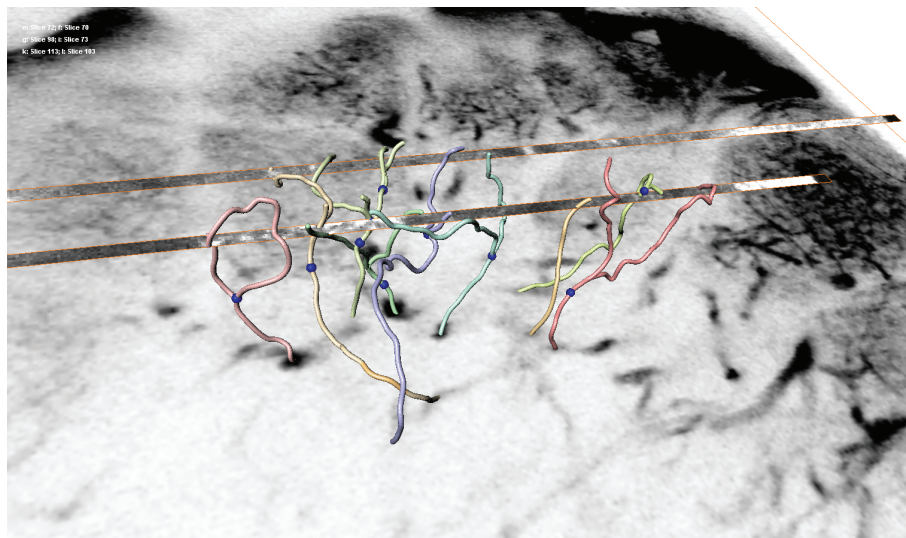

Figure 2.5.3: Skeleton graphs of 9 reconstructed PNs out of two glomeruli (33 and 42) on top of an ortho slice view of the anatomical image stack. Two 7 pixels wide strips out of the AOI images show the position of the linear scans in the 3D volume.

defined 10 pixels wide columns. The coordinates were later used in MatLab for the evaluation of responses on the level of single neurons and branches. Figure 2.5.4 on page 73 shows an example of a Photoshop file for two glomeruli in one AOI. The branches are named by letters of the alphabet followed by a number. The letter is unique for each neuron in the current glomerulus while the number defines the current branch of that neuron. The full name of a branch of a PN is thus, together with the name of the animal: YMDD_ij_xklYm, where Y stands for the last digit of the year, M for the month, DD for the day of the month, ij is the number of the animal, x defines an AOI, kl is the number of the glomerulus, Y is a capital letter defining a neuron, and a single digit number m defines the branches of the neuron; i.e. 7314_02_d33B1 for branch 1 of neuron B within glomerulus 33, AOI d, animal 02 of March 14th, 2007.
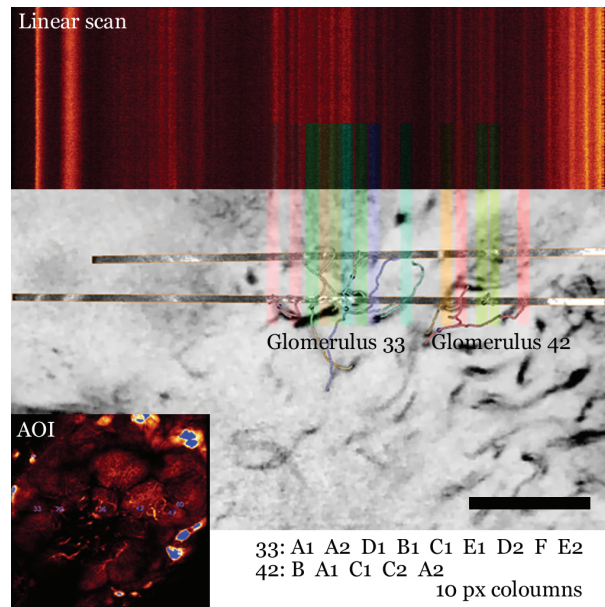
Figure 2.5.4: Photoshop image for determination of pixel coordinates from the skeleton graphs. The skeleton graph, the representative strips of the linear scan positions, a smaller version of the AOI image, and one example of a linear scan measurement are arranged such that the columns of each branch can be positioned conveniently. The text layer at the bottom right contains the neuron/branch names for each glomerulus.

2.5.2 Recordings comprise 5 temporal phases that are defined by the odor stimulus

The odour stimulus separates each measurement into three major phases: (1) pre-stimulation, "Before", (2) stimulation, "During", and (3) post-stimulation, "After". The odors were delivered in a 2-second interval that started 2 seconds after the start of the measurement in linear scans. The "after" phase was 2.737 seconds long. In planar scans, the odor stimulation interval was 3 seconds, with 4 seconds offset to the start of the measurement. The odor stimulation was trailed by a 9.92 seconds long "after" phase.

Additionally to the three major measurement phases, I implemented two more time windows that cover the transition phases just after the beginning and just after the end of the odor stimulation: (4) 500 ms window after the beginning of odor stimulation, "ON"; and (5) 500 ms window after the end of odor stimulation, "OFF".

2.5.3 Telling apart spontaneous vs. odor-evoked signals

Spontaneous activity is all activity within the PNs that is not directly or indirectly evoked by an odor stimulus. To investigate spontaneous activity I measured in each block of stimulations with odors once with an empty odor source (AIR measurement). If we assume that odor-evoked signals have ceased during the 1 minute inter trial interval, all signals measured in the AIR measurements should be caused by spontaneous activity. Following the same argument it is safe to assume that signals that precede the stimulation time window (i.e. the first 2 seconds of each measurement) in the odor measurements are spontaneous signals.

Deciding if a signal is odor-evoked or spontaneous can be difficult. I refrain from simply calling all signals that occur during the time window of odor stimulation "odor-evoked".

For the calculation of glomerular odor-response profiles, I applied the same calculation that Sachse and Galizia (2002) used; it comprises two consecutive steps: first the decision is taken if the odor elicited a response. This is the case if the peak amplitude during the odor stimulus exceeds the peak amplitude in the time window before the odor stimulus. From the ratio of responses to non-

responses, the reliability is calculated as a fraction and expressed in percent. In the second step, within each animal, the median of the single peak amplitudes is calculated from all trials with a response (non-responses are omitted here!). The results from all test animals were averaged per glomerulus and the standard deviation were calculated.

In the post-stimulation phase, the signals are either after-effects from the odor stimulus (e. g. release-from-inhibition signals, off-responses, off-inhibition), or spontaneous. Therefore it is impossible to decide if signals in the "after" phase are odor-evoked or not.

2.6 Quantifying synchrony between PN branches

In this section I will describe the method I developed to test for synchrony between simultaneously measured traces from sub-structures of identified PNs. The analysis is performed on three levels: comparison (1) between pairs of dendritic sub-branches of individual PNs, (2) between pairs of sub-branches of two distinct PNs which reside within the same glomerulus, (3) between pairs of sub-branches of PNs which reside in different glomeruli. A fourth level is the correlation of pairs of traces from sub-branches of PNs between consecutive measurements. Because the magnitude of the correlation coefficient is a measure of synchrony of events, there can be only accidental correlation between traces that were not measured simultaneously. Thus the last group serves as a negative control. To keep the wording simple, let me introduce a simplified terminology: When I speak about the correlation analyses in one of the four levels, I will express this as correlation between...

- "Branches": Pair of branches of one identified PN

- "Neurons": Pair of branches of two PNs within the same glomerulus

- "Glomeruli": Pair of branches of two PNs that innervate two glomeruli

- "Control": Comparison of two measurement traces from the same branch between successive measurements

See figure 2.6.1 on page 77 for a sketch of the four comparison levels.

The absolute correlation between the different structural levels (or measurements) may already answer the initial question about whether the neurons within the same glomerulus are synchronized, and whether the synchrony between traces from two neurons is as high as the synchrony between branches of one and the same neuron. Yet it is feasible to filter the data by several semantic criteria to understand better i.e. at which time points during the measurements which levels of synchrony can be observed between which structures, and if the amount of synchrony is different for different states of activity. Thus I implemented filtering of data by the following criteria:
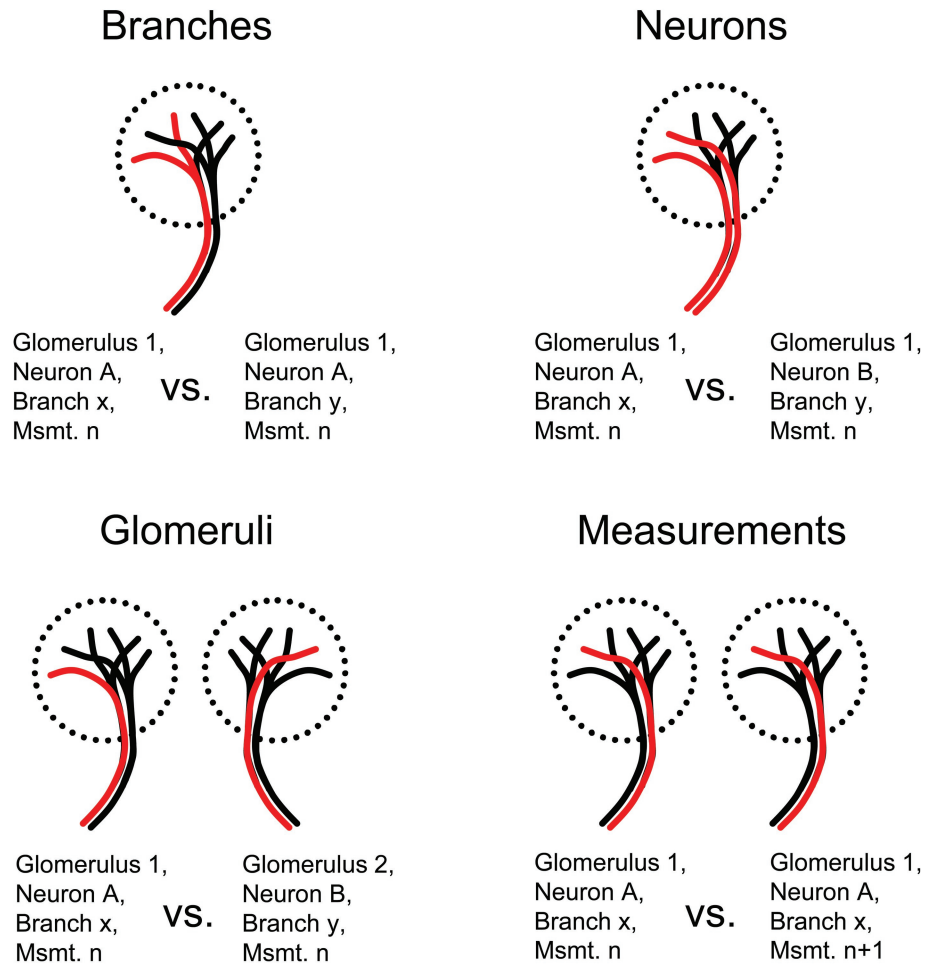
Figure 2.6.1: Sketch of the four levels of structure between which correlation analyses were carried out.

- Time windows of the measurements (see also section 2.5.2 on page 74):

  – Before stimulation

  – During stimulation

  – After stimulation

  – On-responses

  – Off-responses

- States of activity (involvement of odors is discussed in section 2.5.3 on page 74; TCA for extraction of the indices to the signaling episodes described in section 2.4.2 on page 61):

  – No signal

  – Spontaneous signals (in "before" phase)

  – Odor-evoked signals (in "during" phase)

  – Signals of inhibition

In the next section, I will describe the algorithm that I developed for determining the correlation coefficients.

2.6.1 The Sliding Window Correlation Algorithm SWCA

The aim of this data evaluation algorithm is to reliably determine the amount of synchrony between pairs of measurement traces. Pairs of traces belonging to the four levels described above) are processed sequentially. Within each pair of traces, a large number of correlation coefficients is calculated by serially correlating short, simultaneously measured stretches of the measurements. High correlation coefficients are indicative for synchronous events in the pair of traces.

In a measurement with 512 samples, using a window size of 16 samples (= 210.5 ms), and with an increment for moving the correlation window over the pair of traces of 1 sample, the number of correlation coefficients would be $n = 512/1 - 16 = 496$. The result is a time-resolved trace of 496 correlation coefficients. Each of the correlation traces is segmented according to the time windows mentioned above, i.e. before/during/after stimulation or during different states of activity. Each of the segments still consists of several correlation

coefficients. To reduce these correlation coefficients to single indicative numbers, the algorithm takes into account the t-test that is performed while the correlation coefficient is calculated. For each time window, the Sliding Window Correlation Algorithm counts into three bins (1) all occurrences of positive correlation coefficients that exceed a significance level of $p < 0.05$ ("correlated"), (2) all occurrences of negative correlation coefficients that exceed a significance level of $p < 0.05$ ("anti-correlated"), and (3) all occurrences of correlation coefficients with an accompanying p value of > 0.05 ("de-correlated").

Figure 2.6.2 on page 80 shows sliding window correlation traces for two pairs of fabricated measurement traces. Those traces were generated with the aim to exemplify the benefits of the method, i.e. the robustness of the detection of synchrony, the ability to detect also synchronous, but anti-parallel signals, and the use of the built-in t-test to generate the bins mentioned above. The demonstration traces have been generated pairwise by scrambling for each pair the same 250 samples of artificial noise. Without the scrambling, the traces would be identical; in two separate random scrambling steps, two unequal, but related traces are created. For each of the 250 samples of the resulting fabricated trace, the scrambling algorithm "randperm" picks at random one of the noise samples from the vicinity of the current trace sample. Example: the noise samples [0.0950, 0.0231, 0.0607, 0.0486, 0.0891, 0.0762] at positions [101, 102, 103, 104, 105, 106] of the noise trace are scrambled in sequence to [0.0607, 0.0231, 0.0762, 0.0486, 0.0950, 0.0891] by permutating the sample indices to [103, 102, 106, 104, 101, 105].

The first pair of traces consists only of the artificial, scrambled pair of noise traces. The other pair of traces has a pattern of fabricated signals at the background, which is overlain with the artificial noise and scrambled as a whole. Thus, a strong jitter is imposed onto the fabricated signals. The resulting pairs of traces look very much like the traces that I actually measured and are well suited to demonstrate the Sliding Window Correlation Algorithm.

Much time and effort was invested in the estimation of the optimal parameters for the detection of synchrony by the SWCA. Important parameters are (1) the number of samples in which the calculation of correlation coefficients is performed ("window size"), (2) the averaging that is applied to the traces prior to the calculation of correlation, (3) and the way in which the algorithm decides if a correlation result scores as "significant".

The **window size** turned out to be the least sensible parameter. Increasing the
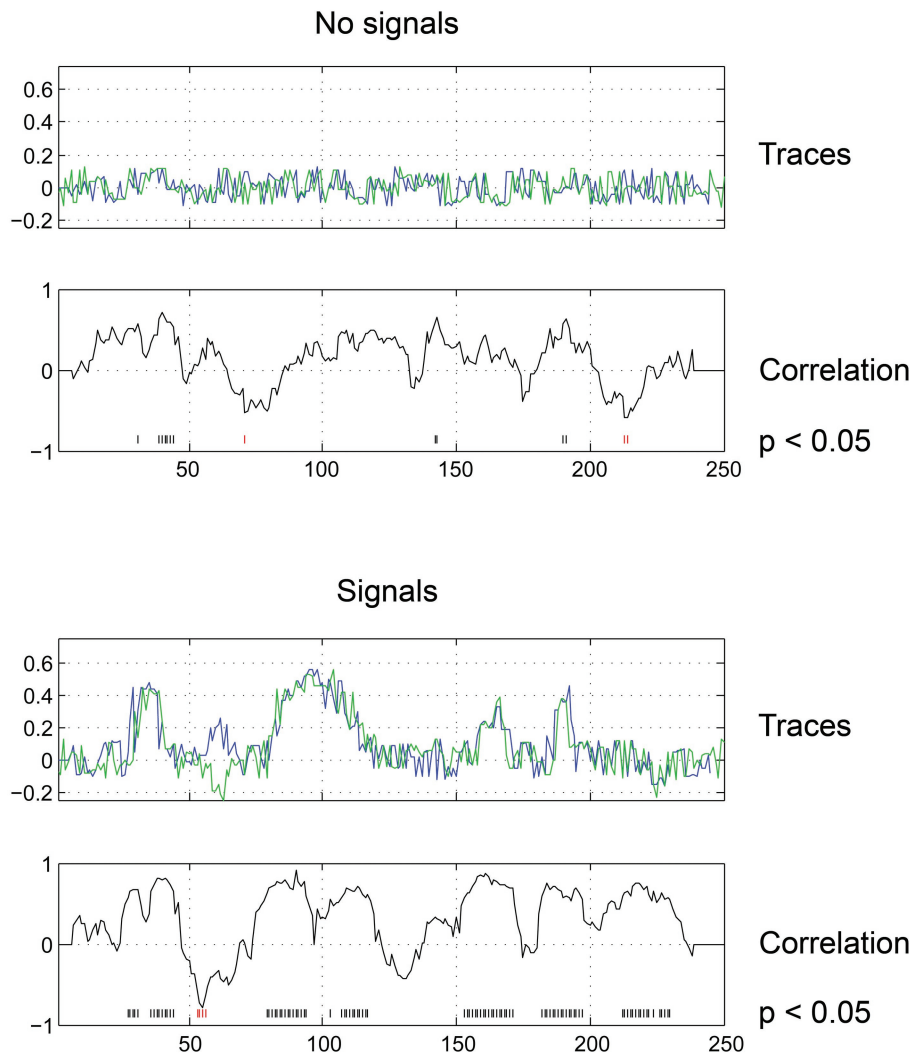
Figure 2.6.2: Fabricated pairs of measurement traces and their pairwise correlation traces. Top, "Traces": two permutations of a trace of 250 samples of noise. "Correlation": The correlation trace, resulting from the correlation of overlapping stretches of 14 samples from the two traces above. Note that the correlation coefficients are between -0.7 and 0.7, and that significant correlation does occur, but rarely (black / red vertical lines at bottom of the correlation figure). Bottom, "Traces": pair of traces with 6 fabricated signals at samples 24 to 34, 55 to 65, 80 to 110, 155 to 165, 185 to 190, and (inhibition!) 215 to 225. The signal at samples 55 to 65 has been inverted to show how the correlation analysis detects anti-correlation. Note that the rising and falling phases of the signals are found reliably, and that the anti-parallel signal leads to significant negative correlation coefficients.

window size in the first place reduces the number of possible comparisons in each pair of traces, because the SWCA needs to exclude (window size)/2 samples before and after each time window (before, during, after etc.). Furthermore, increasing the window size leads to increased correlation coefficients reported by the SWCA. I decided for a window size of 16 samples. This is a rather small window size, thus the reported % correlation scores are only in the range of 10%. But the high number of comparisons possible because of the smaller number of excluded samples leads to more solid statements on the correlation, especially when the SWCA is combined with the results from the TCA (see section 2.4.2 on page 61) to generate separate sets of results for the different states of ativity. The 16 samples that I chose for the window size correspond to a timespan of 210.5 ms.

Averaging is to be avoided. Running averaging even with the smallest kernel size of 2 samples destroys the most important aspects of the group differences demonstrated in the section on the results from the SWCA in the results part (3.3.4 on page 146).

The correlation coefficients and the p-values are computed by the MatLab function "corrcoef" which I use to calculate the correlation coefficients. They are the result from transforming the correlation to create a t statistic having $n - 2$ degrees of freedom, where n is the number of samples in both traces. The confidence bounds are based on an asymptotic normal distribution of $0.5 * log((1 + R)/(1 - R))$, with an approximate variance equal to $1/(n - 3)$. While I can not guarantee normal distribution of all pairs of samples, I still prefer this approach over the application of a fixed threshold, which I also tried. The MatLab script that compiles the statements on the amount of correlation in a pair of traces was written such that visual inspection of the process was possible. The fixed threshold leads to large amounts of false positive and false negative statements on correlation. No single correlation coefficient threshold can be found that determines optimally and equally in all measurements the amount of correlation.

2.6.2 Plotting correlation values

For plotting of single bars per level of analysis and group, the correlation values from the previous analysis have to be combined into single parameters. The

best method for this proved to be the introduction of measure "% significant correlation" or "correlation score". This measure is calculated per correlation trace as the number of correlated / anti-correlated / de-correlated events divided by the total number of correlation values in the current measurement and time window. The value is expressed as multiplied by 100, yielding percent values. The significant correlation scores of all correlation traces of the respective group are then averaged, resulting in one percent value per group and time window.

Because of the large number of groups in multiple hierarchical layers, there are many bars to be plotted: 2 bars for correlation score and anti-correlation score * 4 levels of comparison (between branches, neurons, glomeruli, and measurements) * 5 measurement time windows (before, during, after, ON, OFF) * 4 signaling states (during the complete measurement traces, only during signals of excitation, only during signals of inhibition, only during rest) = 160.

I divided the 160 correlation scores in 4 groups by the signaling states. So there will be one plot for the total correlation scores (1), and one plot each for the correlation scores of the signaling states excitation (2), inhibition (3), and rest (4). All bars of the same level of comparison are grouped and colored in the same hue: shades of red for comparisons between branches, yellow for comparisons between neurons, green for glomeruli, and blue for the negative control where the same branch is compared to the trace within the same branch in the successive measurement.

Part 3

Results

3.1 Demonstration of scan modes used

The microscope system offered three different scan modes: linear scans in which one single line was scanned repeatedly at high frequency (1 spatial dimension), planar scans in which square image frames were recorded at lower frequency (2 spatial dimensions), and stacks of planar scans (3 spatial dimensions) that took minutes to complete. See methods section 2.3 on page 51 for details on the parameters of the scan modes.

By successive application of several of the scan modes a detailed picture of the living honeybee brain can be constructed. The following sections describe the contribution of the single scan modes.

3.1.1 Anatomical image stacks reveal high spatial resolution

The image stacks of the antennal lobes usually covered a volume of 400 x 400 x 180 μm, which is the entire upper half of the lobe. The stacks were rastered with 0.8 μm^3 per voxel in all room dimensions. In most cases, no multi sampling was necessary to yield sufficient image quality; thus recording of a stack took only about 5 minutes.

Figure 3.1.1 on page 85 shows a single image out of a stack of 180 images. Somata, dendritic arborizations and axons of PNs are clearly visible. The pattern of glomeruli allows for identification according to the morphological AL Atlas (Galizia *et al.*, 1999b).

With increasing depth of recording, the image brightness decreased. Only in rare cases was it possible to detect structures at depths greater than 200 μm without increasing the laser power. To achieve homogeneous brightness of all images of a stack, a bleach-correction algorithm was abused. Regardless of the correction of brightness-loss, there were rarely any PNs or glomeruli recognizable in depths greater than 150 μm. Figure 3.1.2 on page 86 suggests that this is not only caused by technical reasons (penetration of excitation light, scattering of fluorescent light), but that also due to general lack of labeling of deep (T3) glomeruli. In the images recorded at depths greater than 120 μm,
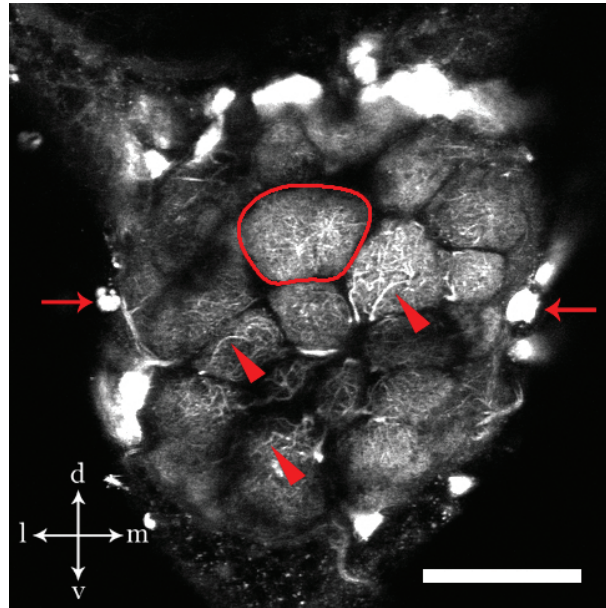
Figure 3.1.1: Single image from a stack of 225 images, recorded at 400 x 400 x 180 μm^3. The image shown has been recorded in a depth of 42 μm. The complete stack that this image is taken from is shown in Figure 5. Arrowheads: thick branches of PN dendrites; arrows: PN somata; line: encircles glomerulus 33. Scale bar = 100 μm. d is dorsal; v is ventral; m is medial; l is lateral.

only 2 glomeruli are strongly labeled. The morphological AL atlas suggests that these are the T3-glomeruli 31 and 45 or 52. Apparently these T3-glomeruli project to the protocerebrum via the lACT, because the mACT PNs, which are reported to innervate T3-glomeruli, have never been stained in this study.

In all glomeruli that were recorded in this thesis, more than one PN per glomerulus was stained. Especially in the case of the large glomeruli 17, 33, and 42, I often found more than 5 distinct neurons innervating the same glomerulus. Figure 3.1.3 on page 87 shows a close-up on glomerulus 33. Note the clear labeling of individual PNs. While the labeling is diffuse in the distal cap region of the glomerulus, there are numerous branches of several PNs visible in the core and integrative segment region. In Figure 7 I show with the same data some of the display modes that the Amira software offers. The projection- and volume rendering pictures give an overview over the image stack. The sections through the sagittal, coronal, and transversal planes proved most valuable when reconstructing PNs.
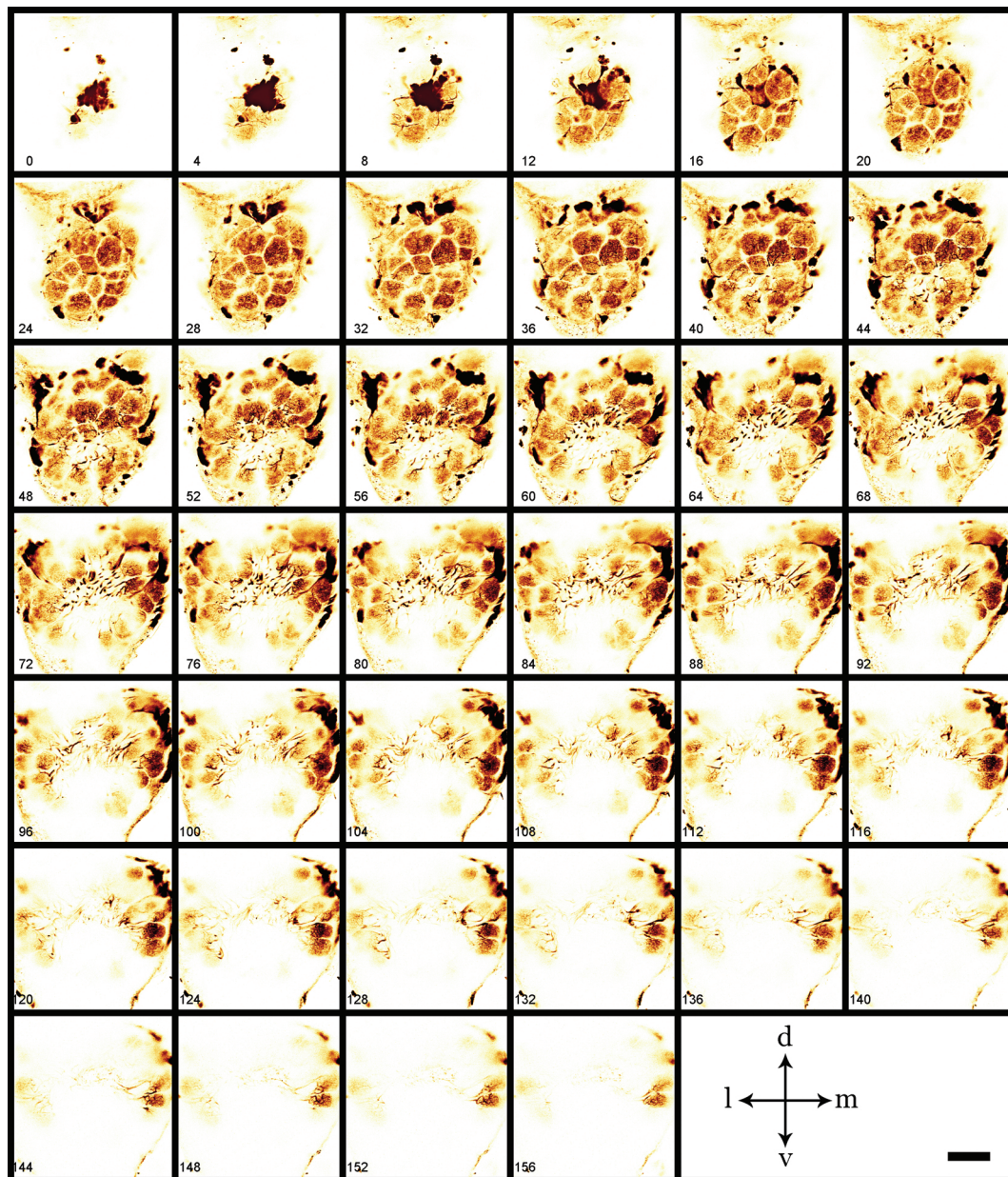
Figure 3.1.2: Image stack, acquired in vivo before odor responses were recorded. The image stack shows 400 x 400 x 160 μm of the right antennal lobe, rastered with 512 x 512 x 225 pixels. Each image shown is an average of 5 images that spanned 4 μm in depth. Frontal glomeruli in depths up to 80 μm are clearly and homogeneously labeled. In greater depth not only the general image brightness but also the number of labeled glomeruli decreases. Scale bar = 100 μm. d is dorsal; v is ventral; m is medial; l is lateral. The images are inverted and false-colored to increase visibility.
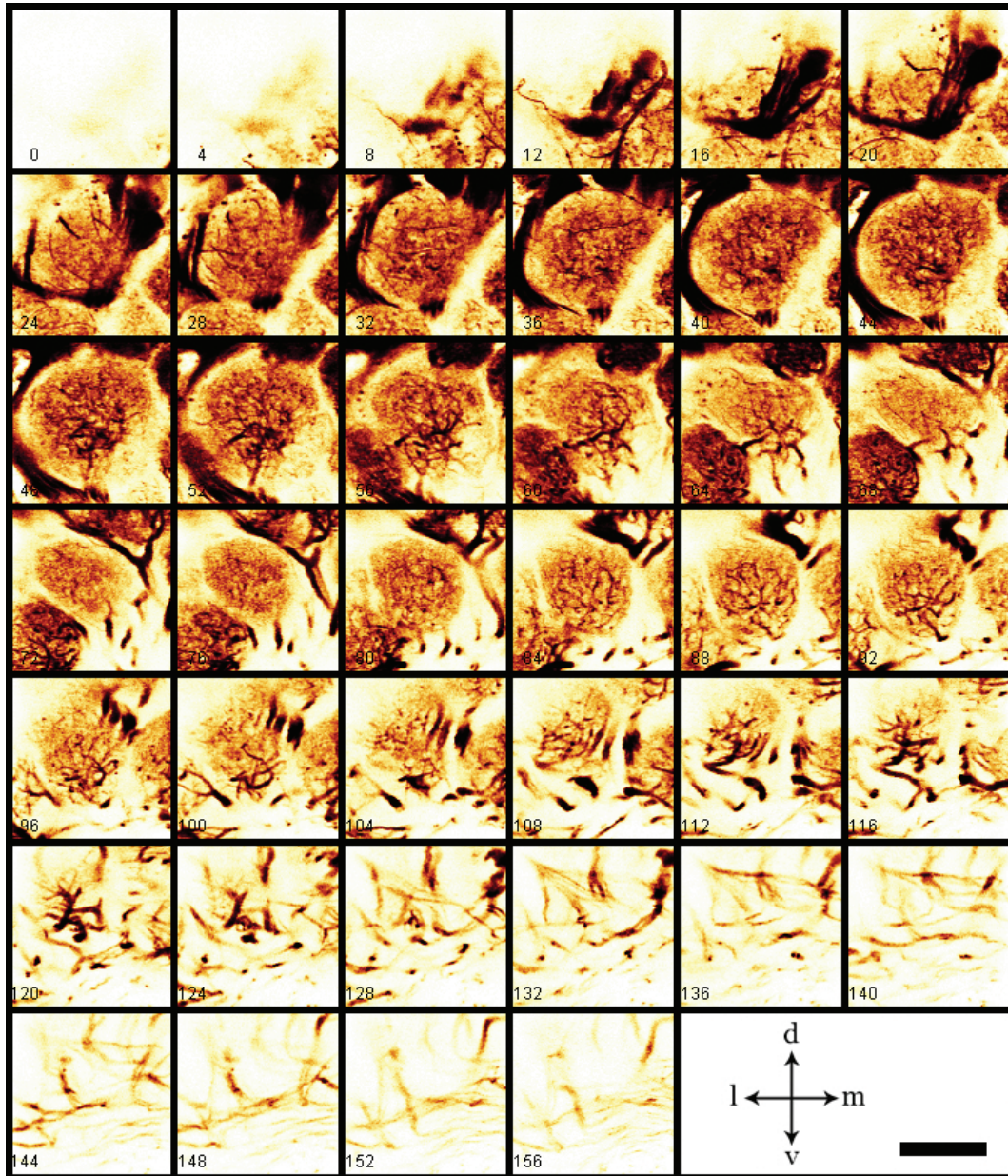
Figure 3.1.3: Close-up on glomerulus 33. 96 x 96 x 160 μm out of a stack of 400 x 400 x 180 μm are shown. Resolution, color and labeling as in Figure 5, but scale bar is 50 μm. Note that glomerulus 33 ends around 64 μm in depth; there is another glomerulus below it (possibly glomerulus 30).
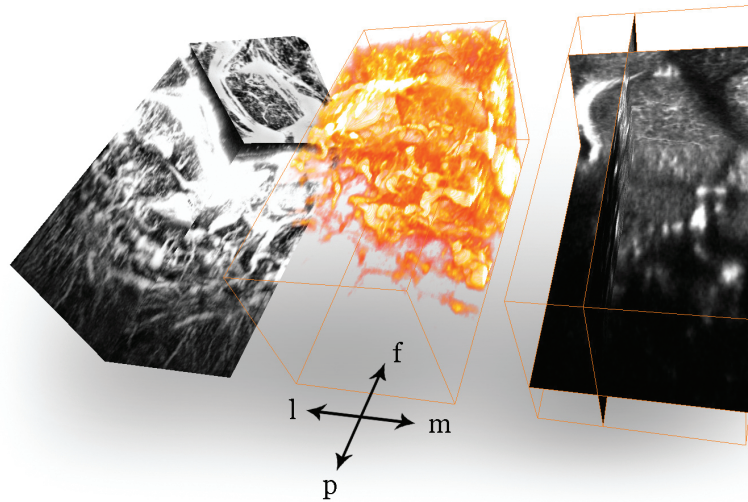
Figure 3.1.4: Same stack as shown in Figure 3.1.3 on page 87, but displayed using Amira. Left: projection view. Middle: volume rendering. Right: sagittal, coronal, and transversal planes through glomerulus 33. f is frontal; p is posterior; l is lateral; m is medial.

3.1.2 Planar scans reveal multiple glomeruli at once

1553 planar scans were recorded in 21 honeybees. Taken together, the planar scans contain a rather complete picture over the glomerular patterns of spontaneous and odor-evoked activity in the whole frontal hemisphere of the AL. However, the planar scans suffer from the low acquisition frequency of only 0.715 Hz. Thus the planar scans were only used online as a guidance cue when choosing FoVs for linear scan measurements, and not evaluated further. Figure 3.1.5 on page 89 shows the single frames of a representative planar scan measurement. In this animal, the spontaneous activity levels were low, so not before the odor stimulus at frame 4 (time stamp 4.08 s) is any activity visible. Starting with the odor stimulus the glomeruli 28 an 36 show a prolonged signal of excitation. Glomeruli 33 and 52 are inhibited at the same time. Note that the inhibition of glomerulus 33 vanishes at exactly the same time as the excitation of glomerulus 36 ends. The phenomenon of inhibition that appears to be synchronized to the activity of a certain glomerulus has been observed frequently, also during spontaneous activity.

The analysis of the linear scan data might be well suited for testing the
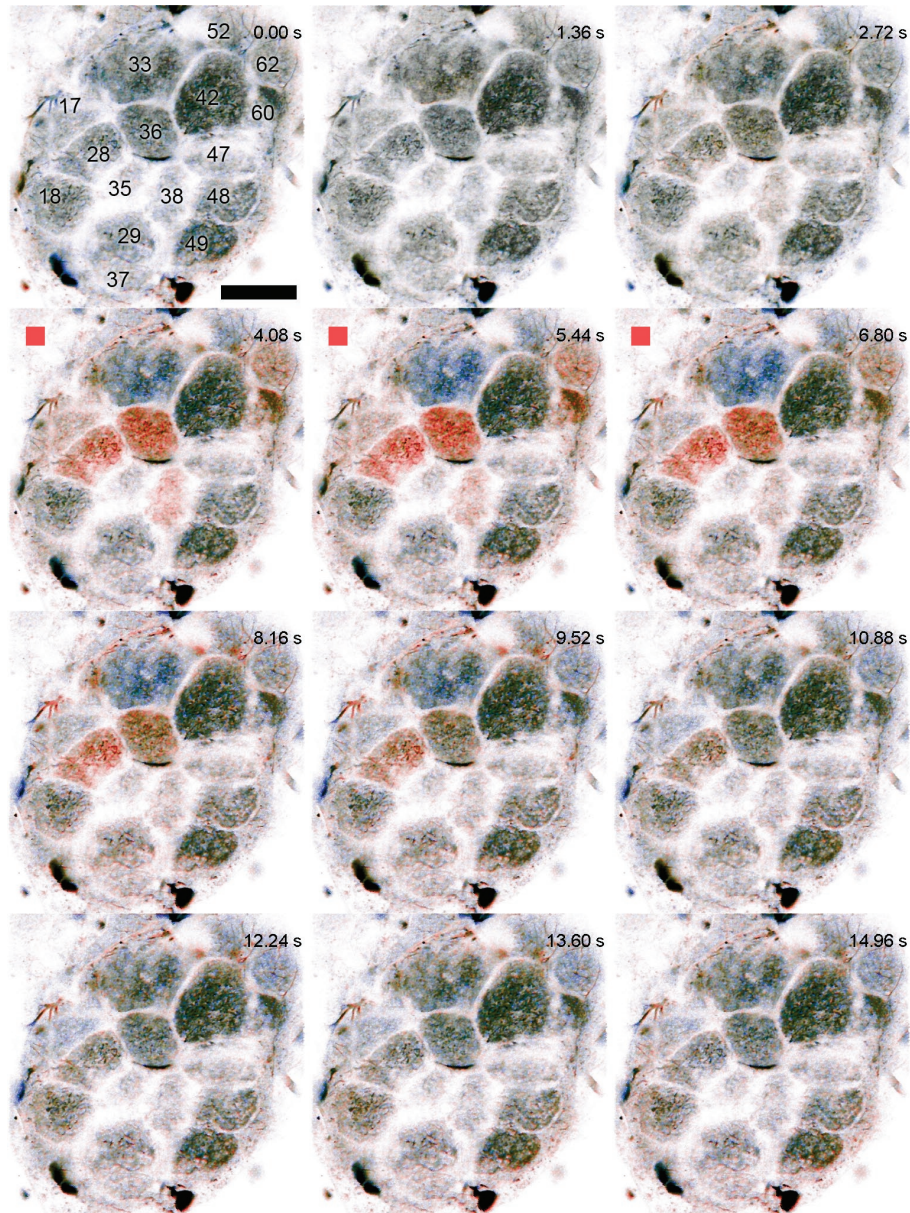
Figure 3.1.5: Montage of single frames from planar scan measurement with odor stimulation. False color representations of calcium signals are mapped onto inverted gray image of the AoI. Red color indicates strong excitation, blue color marks inhibition. A red box in the top left of three image frames marks the frames during which the odor stimulus HX1 was delivered. The number in the top right of each image is the time stamp of the measurement frame. Scale bar in top left image is 100 μm. The numbers in the top left frame are the numbers of identified glomeruli.

hypothesis of inhibition between specific groups of glomeruli with similar odor-response-spectra that was proposed in Linster *et al.* (2005); this analysis, however, has yet to be done.

3.1.3 Linear scans reveal spontaneous- and odor-evoked activity in unprecedented clarity

I obtained 801 linear scan recordings in 21 honeybees. The number of measurements per animal ranged from 9 to 210. In the 21 animals, a total of 48 separate areas of interest (AOIs) were scanned. Each AOI transected between 2 and 6 (average 3.74) glomeruli, so cumulative sum of measurements in all glomeruli is 3015. The AOIs were chosen such that (1) many different glomeruli would be measured to achieve a broad overview over a large population of glomeruli and (2) responses in the prominent and well characterized and large glomeruli 17 and 33 would be measured as more often to allow for a more detailed characterization. A total of 29 glomeruli have been scanned. Glomeruli 17, 33, and 42 have been measured 271, 281, and 203 times, respectively. See Figure 3.1.6 on page 90 for a detailed account of the number of measurements per glomerulus and odor.

For an example of a linear scan recording, please refer to 3.3.1 on page 134.
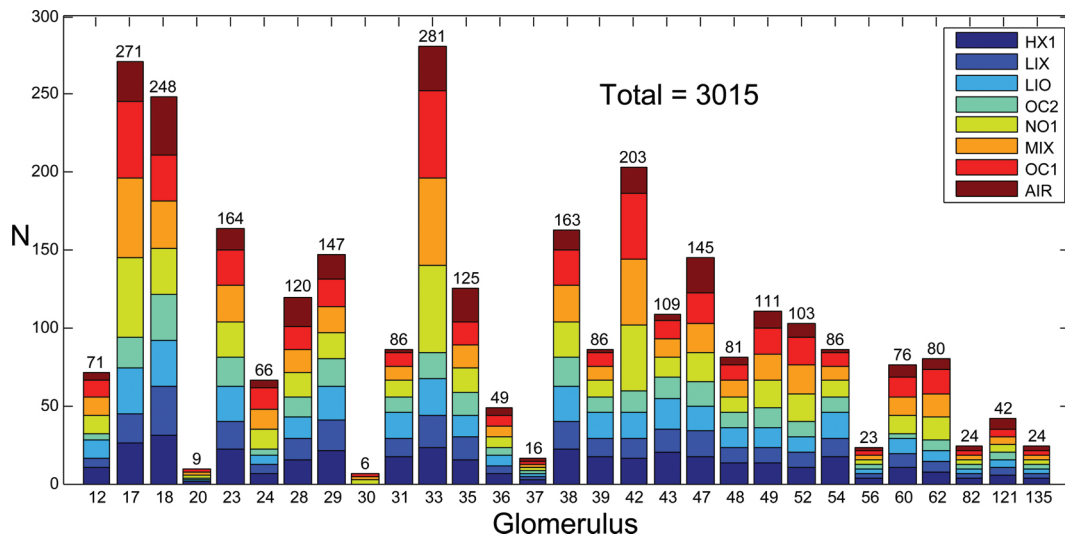

Figure 3.1.6: Number of measurements per glomerulus. The coloured subsections of the stacked bars show the number of measurements per odor in the glomerulus.

According to the functional AL atlas, glomeruli 17 and 33 are activated most strongly by the odors 1-Octanol and 1-Nonanol. Thus I applied these odors and their binary mixture MIX more often than the other test odors when measuring glomeruli 17 and 33. Figure 3.1.7 on page 91 shows how often each odor has been applied in which of the 21 animals tested.
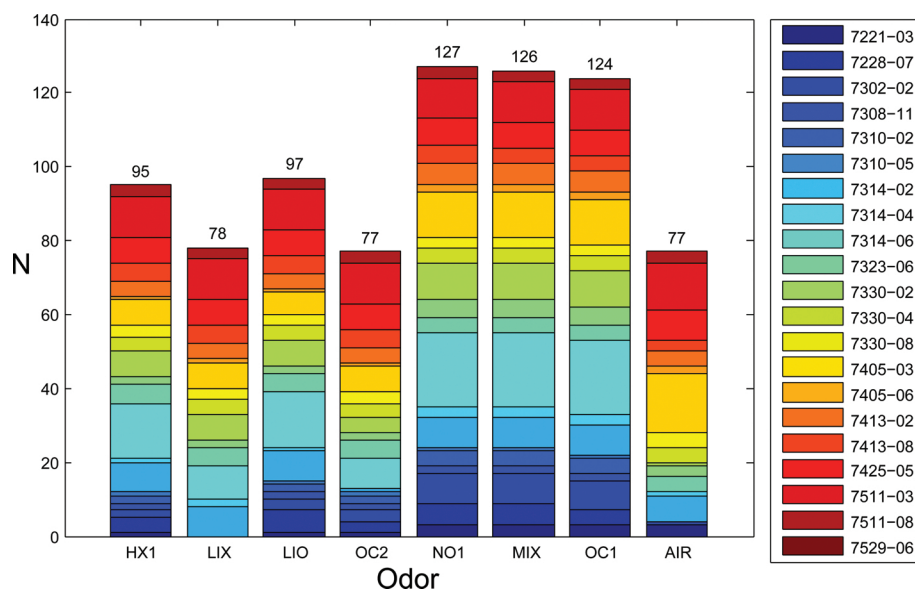
Figure 3.1.7: Number of measurements per odor. The coloured subsections of the stacked bars show the contribution of each test animal. The names of the animals shown in the legend reveal the date of the experiment (year - month - day: YMDD).

The linear scan measurements acquired in this study give a detailed picture of spontaneous and odor-evoked activity in PNs. Evaluated on the glomerular level, the data show that (1) the majority of PNs is spontaneously active; (2) phasic-tonic signals are not predominant but most signals are phasic; (3) the delay between odor stimulation onset and rise of intracellular calcium levels is large; (4) the rise-times of calcium signals are brief; (5) Inhibition can be revealed indirectly. This part of the data analysis can be found in section 3.2 Glomerulus-based analysis on page 92.

Later, I report on the analysis of linear scan data on the level of single PNs in section 3.3 on page 133.

3.2 Glomerular signals during odor stimulation and rest

Many aspects of odor coding and the role of the inhibitory system within the AL can be demonstrated on the level of glomeruli. In the following analyses, I spatially averaged all pixels of the linear scans that transected the surface of the same glomerulus down to a single data point. The temporal domain was thereby untouched. Advantages of this data evaluation approach are:

1. More animals are available for analysis, because only in a fraction of animals I was able to reconstruct individual PNs.

2. The process of spatial averaging increases the signal-to-noise ratio.

3. As opposed to wide-field imaging, the process of spatial averaging does not reduce the temporal resolution.

This section is subdivided into two large parts. First I will analyze all accessible aspects of spontaneous activity within the glomeruli. In the second part I will address odor-evoked signals. Both sections rely largely on the results from the automated signal registration program CSA (see methods part section 2.4.1 on page 56) and on exemplary measurement traces that illustrate important aspects of PN signaling.

3.2.1 Spontaneous activity is strong

The spontaneous activity measured here appeared to be structured. On average, sharp peaks with large DF/F amplitudes were rather regularly scattered at 1.3 s intervals. The frequency of large signals of $\approx$0.75 Hz is lower than the average resting spike rate on PNs that was reported elsewhere (Sun *et al.* 1993, Müller *et al.* 2002). However, also smaller signals can be observed in between the large spontaneous signals, so the total frequency of detectable signals is higher. The duration of the spontaneous calcium signals varied little within measurements,

but more between different glomeruli and different animals. See Figure 3.2.1 on page 93 for examples of spontaneous activity. Bursty spontaneous spiking is a known feature of PNs; I therefore refer to the peaks as "bursty" signals.
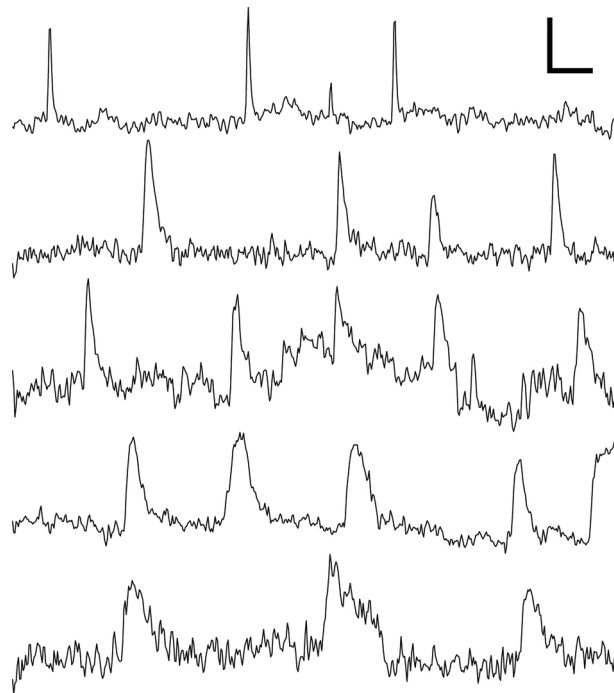
Figure 3.2.1: Examples of spontaneous activity. From top to bottom: measurements without any odor stimulus in glomeruli 49, 48, 17, 82, 33. All recordings are from different test animals. Sorting from top to bottom is by average length of bursts. The scale bar (top right) shows 10% $\Delta F/F$ (vertical) and 500 ms (horizontal). In A4 printouts, 1 cm corresponds to 1 second in the measurement. The traces shown are smoothened with a 2px running average filter. The lengths of the bursts shown here range from 50 ms to 650 ms; most commonly I observed 200 to 250 ms.

The same kind of bursting activity was observed during the time window of odor stimulation. Odor-evoked signals were thus only identifiable by the temporal relation of beginning, end, or length of calcium signals to the odor stimulus. Sometimes a phasic-tonic response was overlaid with bursts, but the typical odor response consisted of an arrangement of phasic signals that were sometimes difficult to tell apart from the spontaneous signals before the odor stimulation. Cases of pure phasic-tonic responses without any bursts also exist, but they are rare. Bursting is thus not only the typical signal shape for spontaneous, but also for odor-evoked signals.

Additionally, I observed odor-evoked inhibition of spontaneous activity in

many cases. In the most obvious cases steady spontaneous bursting was completely suppressed during the odor stimulation. See section 3.2.2.4 on page 128 for a more detailed description of inhibitory signals in the linear scan data.

As quantification of spontaneous activity I determined the frequency of spontaneous signals and their regularity in all glomeruli that have been measured in three or more animals. The figures 3.2.2 on page 94 and 3.2.3 on page 95 show the average frequency and regularity of spontaneous signals separately per glomerulus. Basis of this analysis are all measurements, filtered by the following criteria: (1) only signals counted that occurred in the PRE phase of each measurement until odor stimuli were delivered plus (2) all signals within measurements with plain AIR as stimulus; (3) only signals larger than 2 standard deviations of the baseline noise were counted; (4) only glomeruli that have been measured in 3 or more animals were included in the analysis.
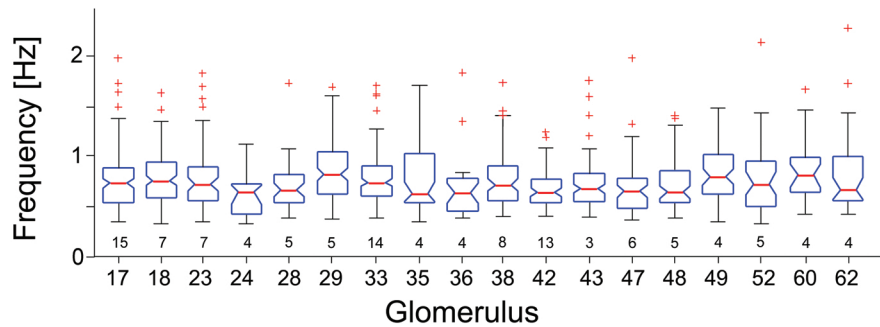
Figure 3.2.2: Box plots of the frequencies of spontaneous signals in the PRE phases of all measurements and the AIR trials within all glomeruli with an n of 3 animals or more. The number of animals per glomerulus is stated in the numbers above the ordinate. The box plots show the median values (red horizontal line in the middle) and lower and upper quartiles (lower and upper end of the box) of the underlying data. Lines ("whiskers") extend from the ends of the box to show the extent of the rest of the data. Outliers (red crossed beyond the ends of the whiskers) are all data points outside 1.5 x the interquartile range. The notches represent an estimate of the uncertainty about the medians for box-to-box comparison.

This analysis shows that the frequency of signals with an amplitude of > 2 standard deviations of baseline noise was on average 0.75 Hz, with very little variation between the glomeruli tested. More variability can be reported for the regularity measure, which quantifies the normalized deviation from a perfectly regular train of signals. A particularly low regularity value of 0.56 was found in glomerulus 24, all other glomeruli ranged between 0.6 and 0.8, mean 0.70. The
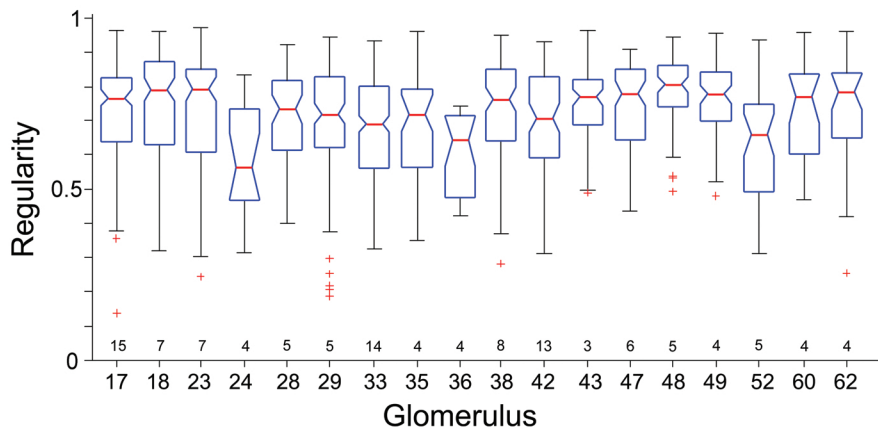
Figure 3.2.3: Box plots of the regularities of spontaneous signals in the PRE phases of all measurements and the AIR trials within all glomeruli with an n of 3 animals or more. See legend of Figure 3.2.2 on page 94 for information on box plots.

average regularity is thus very high. As described in the methods part, section 2.4.1.1 Frequency and regularity of trains of signals on page 60, regularity can also be expressed as the average deviation from a perfectly regular train of signals. For the signals with amplitudes of > 2 standard deviations of baseline noise the % deviation is only 20-40 %.

The previous analysis excluded all glomeruli that were measured in less than three animals, and signals of small amplitude. Because I want to give a full overview over the characteristics of spontaneous activity in all glomeruli and also obtain information on the smaller signals, I repeated the analysis without excluding any animals or glomeruli. All signals in PRE phases and AIR measurements with an amplitude of > 1 standard deviation of baseline noise were counted.

I extracted the descriptive parameters regularity, frequency, duration (time point of maximal slope in the inclining phase until time point of half-maximal amplitude), and amplitude (as multiple of the standard deviation measured in between signals) in all measurements. A total of 12754 spontaneous signals occurred in 7047,89 seconds (1:57:27.890 h:mm:ss.ms) of measurement time in PRE phases and AIR measurements. The average frequency of spontaneous signals was thus 1.810 Hz. For the presentation in bar graphs, the data were averaged for each glomerulus.

Now that glomeruli that were measured only in few animals are part of the analysis, it is important to check for between-animal differences. Therefore,

in a separate analysis, I averaged the parameters once more, but this time all glomeruli that were measured in each test animal were averaged.

3.2.1.1 Frequency and regularity are coupled

Figures 3.2.4 and 3.2.5 on pages 96 and 97 show the average values for regularity (R) and frequency (F) that were obtained in all spontaneous signals. Figure 3.2.4 shows the data per glomerulus, after averaging of data from all animals in which measurement were obtained in this glomerulus. Figure 3.2.5 shows the data per animal, after averaging of data from all glomeruli which were measured in this animal.
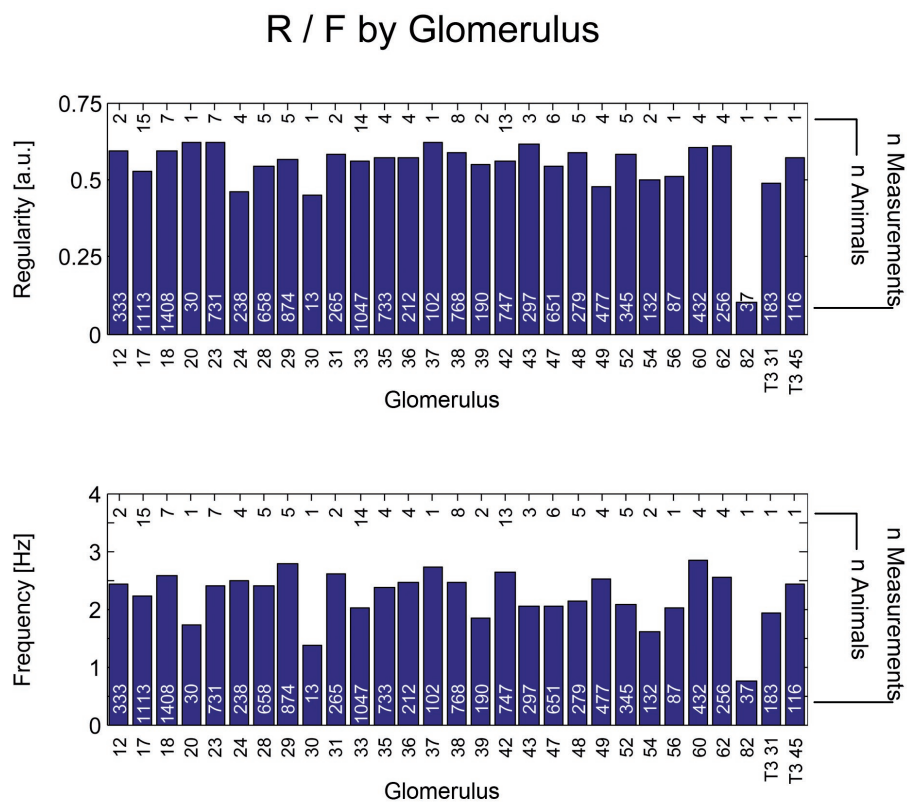
Figure 3.2.4: Bar graphs depicting the mean regularity (top) and frequency (bottom) of spontaneous signals after averaging per glomerulus. The number of animals / glomeruli behind each bar is shown above the bars. The total number of measurements per bar is shown within the bars.

The observed regularity values range between 0.101 and 0.620 (mean 0.543, standard deviation 0.097, median 0.568, interquartile range 0.066), the frequency

ranged between 0.736 and 2.854 Hz (mean 2.240, standard deviation 0.467, median 2.416, interquartile range 0.480).
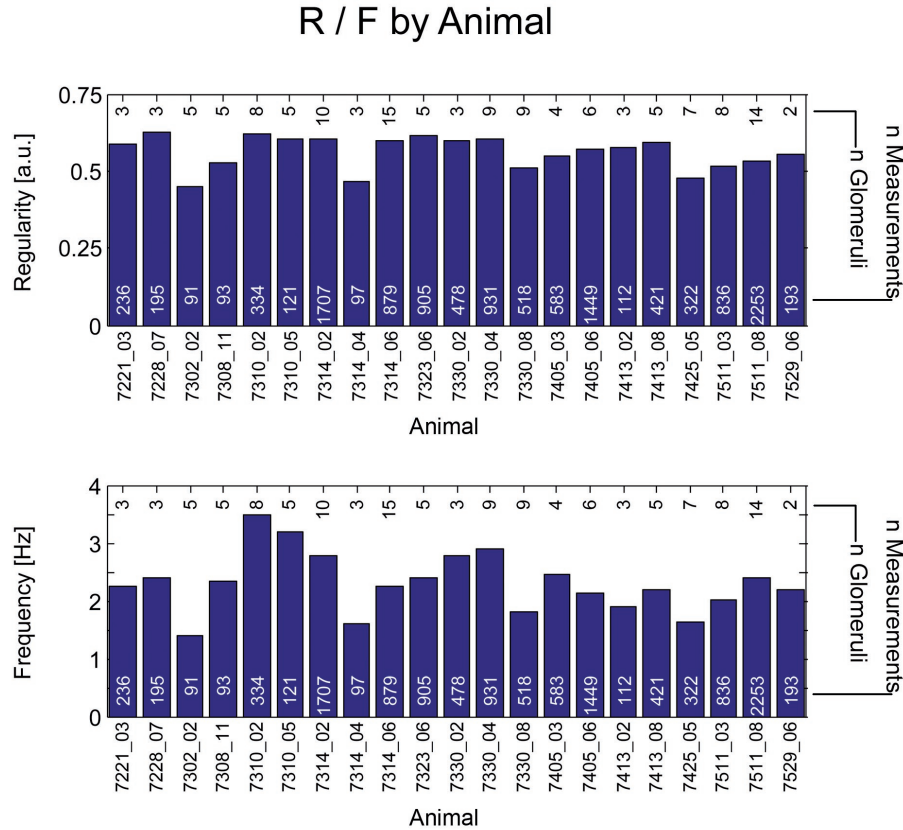
Figure 3.2.5: Bar graphs depicting the mean regularity (top row) and frequency (middle row) of spontaneous signals after averaging per animal. The number of animals / glomeruli behind each bar is shown above the bars. The total number of measurements per bar is shown within the bars.

At a glance the mean regularity per glomerulus appears again rather constant. The mean frequency shows more variation. Glomerulus 82 has an exceptionally low frequency of spontaneous signals and also the lowest regularity among all glomeruli. Apart from the glomeruli 82 and 30, which were measured each in only one animal, the data are distributed narrowly around the mean. The mean value for regularity of 0.543 is considerably lower than the mean regularity of 0.70 that was found in the high-n glomeruli and under exclusion of signals < 2 standard deviations of baseline noise.

Notably, the antennocerebral tract 3 ("T3") -glomeruli T3-31 and T3-45 do not show deviant frequency or regularity of spontaneous signals. All other glomeruli belong to antennocerebral tract 1 ("T1").

The analysis of data averaged per animal figure (3.2.5 on page 97) reveals that the variability between frequency and regularity values among test animals is as high as the variability between glomeruli. Table 3.2.1 on page 98 concludes the means, median, standard deviations, and interquartile ranges of the parameters regularity and frequency, once obtained from the data in groups of glomeruli, once obtained from the data per animal.

Measure	R (glom.)	R (anim.)	F (glom.)	F (anim.)
Mean	0.543	0.560	2.240	2.347
Standard deviation	0.097	0.056	0.467	0.511
Median	0.568	0.582	2.416	2.283
Interquartile range	0.066	0.082	0.480	0.573

Table 3.2.1: Means, medians and the accompanying measures of spread of data for the parameters regularity and frequency, based on spontaneous signals registered during PRE time windows and AIR measurements. Data derived from parameters grouped by glomerulus ("glom.") or test animal ("anim.").

I was interested to see if the parameters frequency and regularity were interdependent, e. g. if glomeruli with high frequency of spontaneous signals would also display higher regularity. Figure 3.2.6 on page 99 shows scatter graphs in which the regularity and frequency data pairs that were obtained after averaging by glomeruli or by test animal are shown together with a robust regression fit.

The relation of frequency and regularity, depicted as scatter plots with robust regression line in figure 3.2.6 on page 99, shows positive correlation of frequency and regularity. Because of the way in which the regularity measure is calculated (see methods section 2.4.1.1 on robust calculation of regularity on page 60, formulae 2.5.3 to 2.5.5), the positive correlation is not the trivial result of the shorter inter-signal-intervals at higher signal frequency. Rather, the regularity increases stronger with frequency than this trivial relation would explain.

To conclude, regularity and frequency are rather narrowly distributed around mean values of 0.543 and 2.240 Hz. There is a positive correlation between the parameters. When only glomeruli that have been recorded in more than three animals and signals with amplitudes of >2 standard deviations of baseline noise are analyzed, then the regularity is on average much higher with 0.70, while the frequency of the remaining large signals is 0.75 Hz. Apparently, the large signals are much more regularly distributed than the small signals.
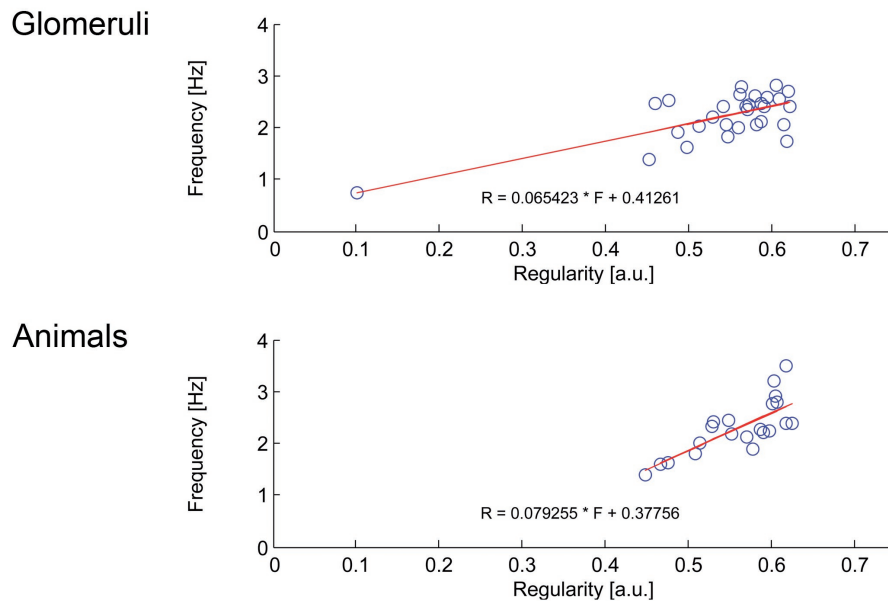
Figure 3.2.6: Scatter plots of regularity and frequency data pairs that were obtained after averaging by glomerulus (top) or by test animal (bottom). Robust regression fits are shown as red lines. The formulae are shown in the plot.

3.2.1.2 Signal amplitude and signal duration are independent - and narrowly distributed

In this section I will compare amplitude and duration of spontaneous signals. Again, the aim is to detect possible differences between glomeruli. As a control a comparison of amplitude and regularity between signals that are average per test animal is shown.

Figure 3.2.7 on page 100 summarizes the range of amplitudes and durations of all 12754 signals. All in all, the observed signal amplitudes range between 1.27 and 3.72 standard deviation of baseline noise (half maximum of log-normal fit of all signals), the peak of the fit is at 2.14 standard deviations, the mean is 2.94. The large difference between peak and mean value reveals the extreme longtailedness of the distribution. The durations range between 88.7 and 266.0 ms (again half maximum of log-normal fit), the peak is at 152.6 ms, the mean is 208.4 ms.

The parameters for each of the spontaneous signals are additionally plotted as scatter plot in figure 3.2.8 on page 101. The scatter plot shows that for spontaneous signals there is no strong correlation between the parameters duration and amplitude. Smaller signals (at the left side of the plot) display a
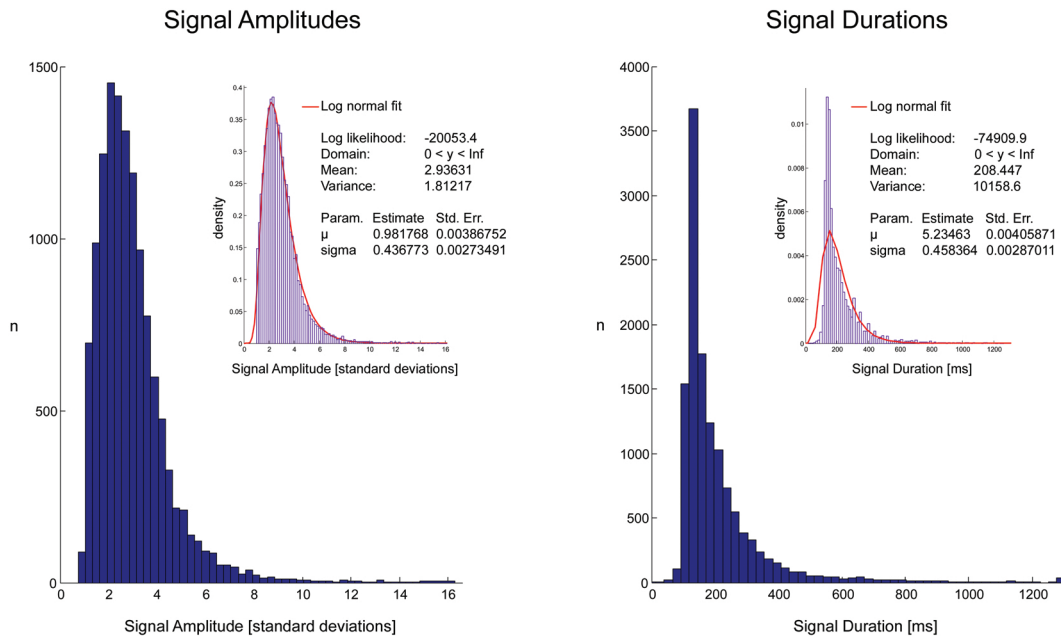
Figure 3.2.7: Histograms of signal amplitudes (left panel, calculated as multiples of standard deviation of baseline noise) and signal durations (right panel, duration calculated as time point of maximal slope in the inclining phase until time point of half-maximal amplitude). 50 data bins in each histogram. Insets: log-normal fits of the same data (red curves). The fitting parameters are shown next to the fits.
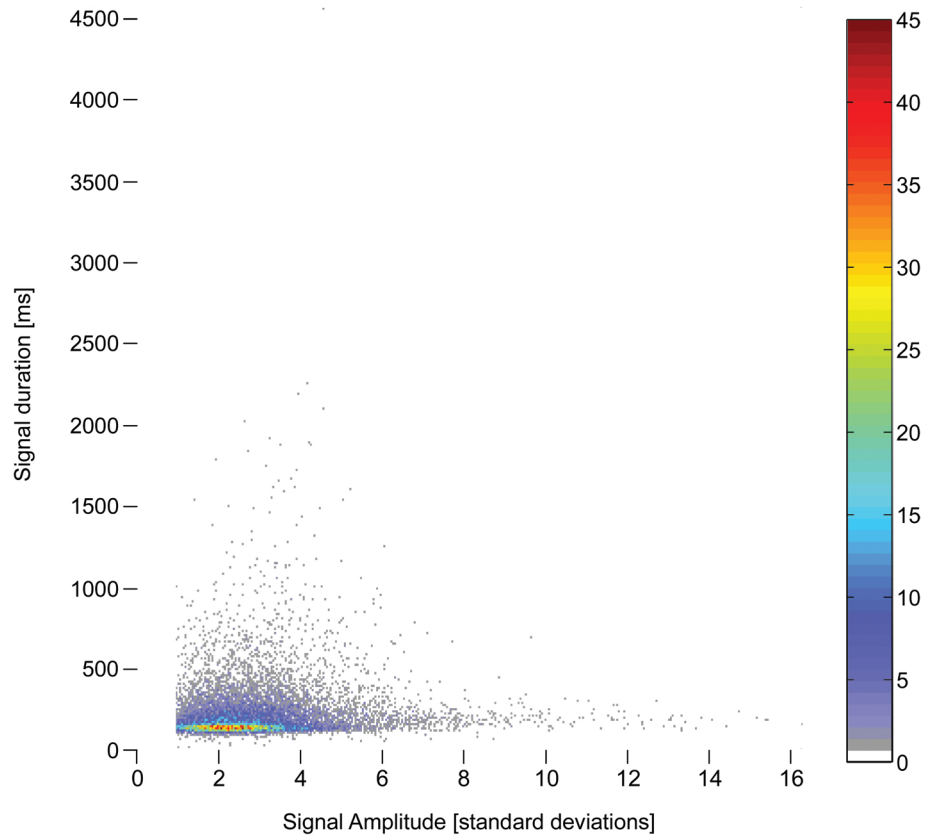
Figure 3.2.8: Scatter plot of all signals, showing both signal amplitude and duration for all 12574 signals. Because many signals cumulate and overlay each other in the lower left corner of the plot, I color coded the scattered points such that the number of stacked data points is reflected in the color of the point (refer to the color bar (right) for the numbers).

larger range of durations than large signals. The most signals come to lie in the lower left corner of the plot, i.e. the most signals have an amplitude of about 2.5 standard deviations of baseline noise and a duration of around 209 ms.

The presence of data points in the extremes of the parameter ranges proves that the signal detection algorithm SCA can detect very short and very long signals. Thus the absence of data points in the upper half of the figure is not an artifact of the data evaluation. Towards the left of the plot, the signal detection threshold of 1 standard deviation is visible as a cut-off in the otherwise homogeneous distribution of data points.
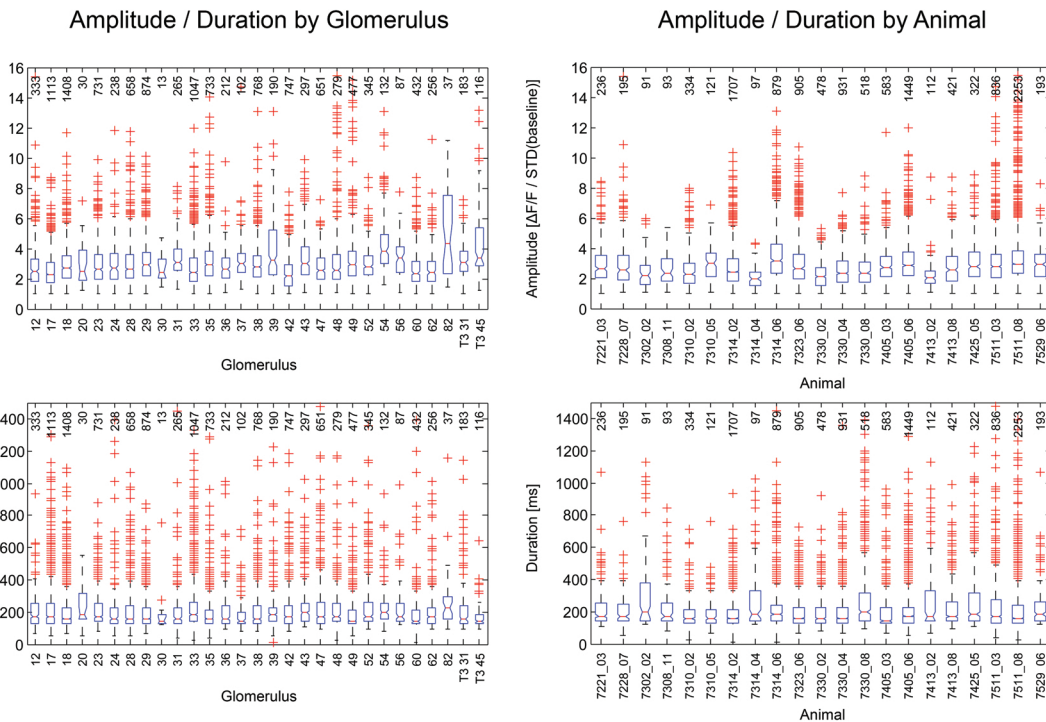
Figure 3.2.9: Amplitude and duration of spontaneous signals. Boxplots of all signals per glomerulus (left panel) and per animal (right panel). Outliers are depicted with red crosses. The number of samples per group is shown at the top of the sub-figures.

To analyze the amplitudes and durations of spontaneous signals between glomeruli and animals, it is necessary to find a way to pool the amplitude and duration measures of all measurements within the same glomerulus/animal. Because the distribution of the samples is extremely long-tailed, care must be taken when choosing the measure for pooling. The mean or median would be a problematic choice, for both measures point not at the peak of the data

distribution but at a value between the peak and the tail of the distribution. I first tried to display the duration and amplitude data in boxplots. Figure 3.2.9 on page 102 shows boxplots of signal duration and amplitude after pooling the data per glomerulus or per animal.

The boxplots show in the first place that the asymmetrical distribution of the data lead to a large number of outliers in all groups. This is unfortunate, because there is no scientific reason for treating the larger signal durations and stronger amplitudes as outliers.

The boxplot algorithm in MatLab excludes outliers from the calculation of the quartiles and medians. All data samples that are more than 1.5 times the interquartile range apart from the 75% quartile (upper boundary of the box) are counted as outliers. After removing the outliers, the skewedness of the data is drastically reduced, allowing for calculation of median values. The median is now less influenced by the tail of the distribution. The problem with this is that (1) the number of samples that are to be pooled influences the number of samples that are counted as outliers and (2) there is no reason to treat the extreme values as outliers.

A more robust integrating measure than the mean, the median, or the median after removal of outliers is the mean of a fitted log-normal distribution. The calculation of the mean values has been done with the lognfit function in MatLab and yielded mean and standard deviation values. These are plotted for data averaged in glomeruli in figure 3.2.10 on page 104. Both amplitude and duration of spontaneous signals do not reveal large differences between individual glomeruli. Compared to the rest of the glomeruli, only glomeruli 54, 82, and T3-45 show stronger signal amplitudes. The distribution of signal durations is apparently even more narrow.

Larger differences can be observed when when pooling the responses within animals (as opposed to within identified glomeruli), as shown in figure 3.2.11 on page 105. Animals 7314_04 and 7413_02 show smaller signal amplitudes while the amplitudes in animal 7314_06 are larger. Again, the signal durations vary less than the amplitudes.

Table 3.2.2 on page 106 concludes the results from the analysis of amplitude and duration of spontaneous signals. The variance between duration values between animals is higher than between glomeruli.

The analysis of amplitude and duration in groups of glomeruli or animals demonstrated that the spread of the parameters is low. A typical spontaneous
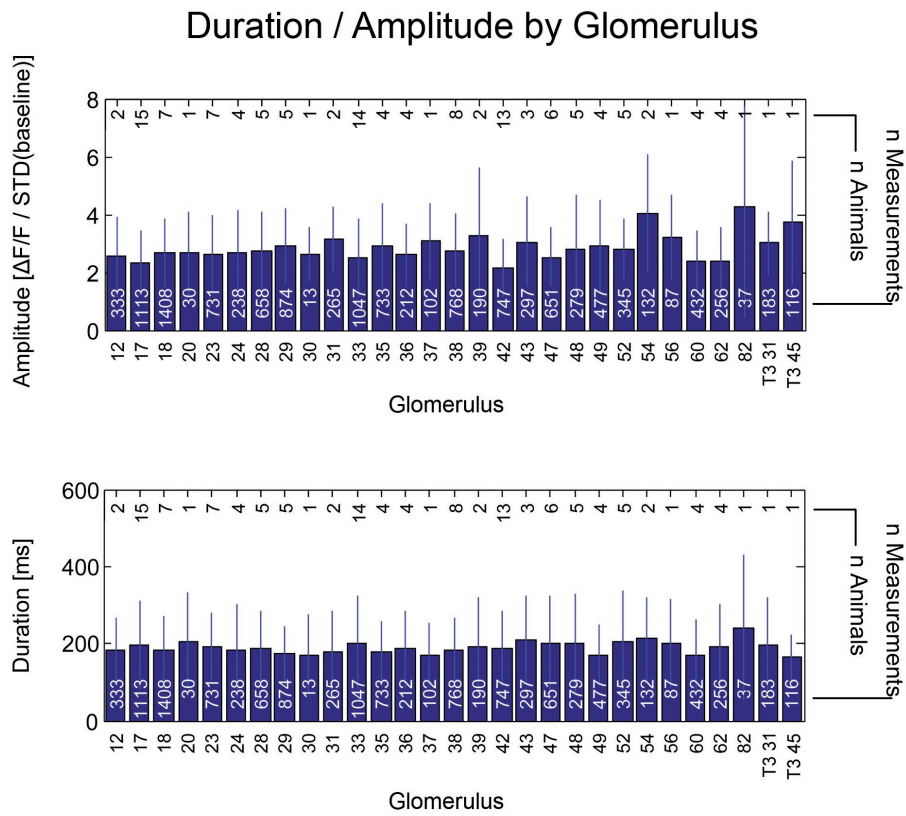
Figure 3.2.10: Bar graphs of amplitude (top) and duration (bottom) of spontaneous signals after averaging per glomerulus. In each bar, the plotted values are the mean values of log-normal distributions that have been fitted to the groups of data samples. The errorbars show the standard deviation.
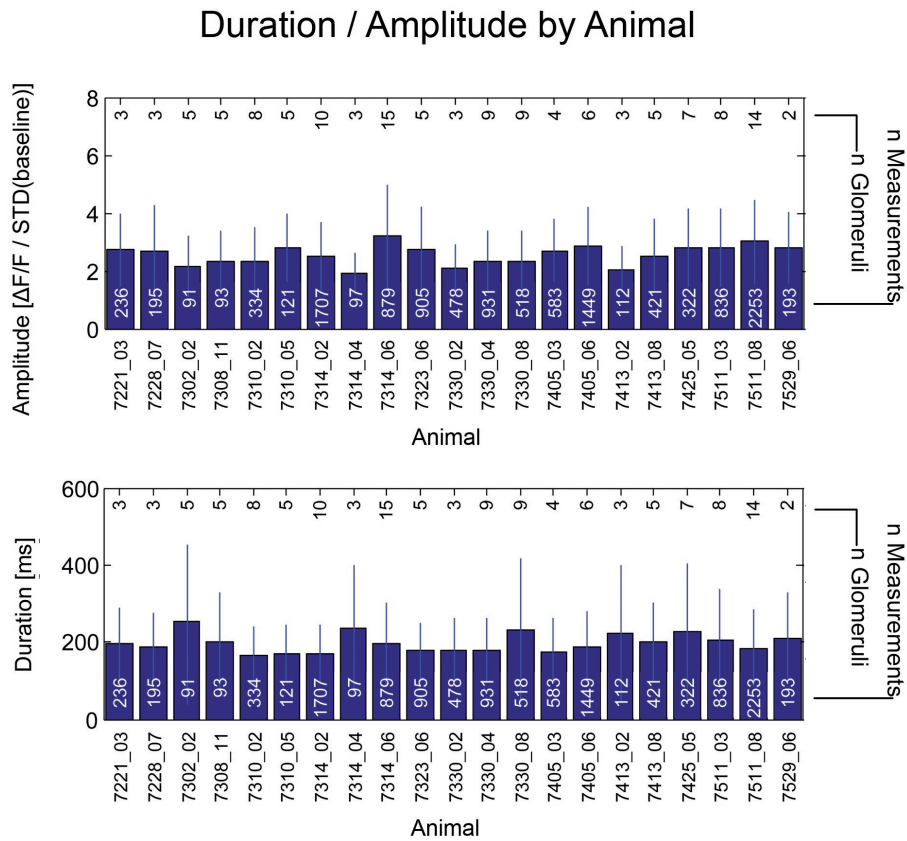
Figure 3.2.11: Bar graphs of amplitude (top) and duration (bottom) of spontaneous signals after averaging per glomerulus. In each bar, the plotted values are the mean values of log-normal distributions that have been fitted to the groups of data samples. The errorbars show the standard deviation.

Measure	A (glom.)	A (anim.)	D (glom.)	D (anim.)
Mean	2.729	2.380	188.32	195.82
Standard deviation	0.514	0.372	16.25	23.82
Median	2.606	2.441	187.40	193.10
Interquartile range	0.383	0.562	20.62	31.81

Table 3.2.2: Means, medians and the accompanying measures of spread of data for the parameters amplitude and duration, based on spontaneous signals registered during PRE time windows and AIR measurements. Data derived from parameters grouped by glomerulus ("glom.") or test animal ("anim.").

signal is ≈200 ms long and has an amplitude of 2.5 standard deviations of baseline noise. As for the parameters regularity and frequency, I also searched for correlation between the parameters amplitude and duration. No relation between duration and amplitude was apparent in figure 3.2.8 on page 101, where all parameter pairs have been analyzed in a scatter plot without pooling by glomerulus or animal, but to be sure I repeated the scatter plot analysis, which is shown in figure 3.2.12 on page 107. There is a weak positive relation between signal amplitude and duration when data are averaged per glomerulus; when pooling by animal, there is a weak inverse correlation between the parameters. Thus, an animal with stronger average signals is likely to show shorter average signal durations at the same time. Within a given glomerulus, however, stronger signals are accompanied by slightly longer signal durations.

Conclusion: As already shown for regularity and frequency, also the parameters amplitude and duration are narrowly distributed. The correlations between parameter pairs reveal weak interdependency of the parameters: the regularity rises with the frequency of spontaneous signals; the duration of signals is positively correlated with the signal amplitude when data are averaged by glomerulus, but inversely correlated when data are averaged by test animal.

3.2.1.3 Ignoring small signals does not change the picture

In the previous sub-sections, all signals larger than one standard deviation of the baseline noise have been taken into account. The data analyses aimed to robustly reveal inhomogeneities in the data, and to search for correlations between parameter pairs. The analyses were performed on a very high number of data samples. All glomeruli as well as all test animals appear rather identical, which is not surprising given the fact that numerous publications exist that
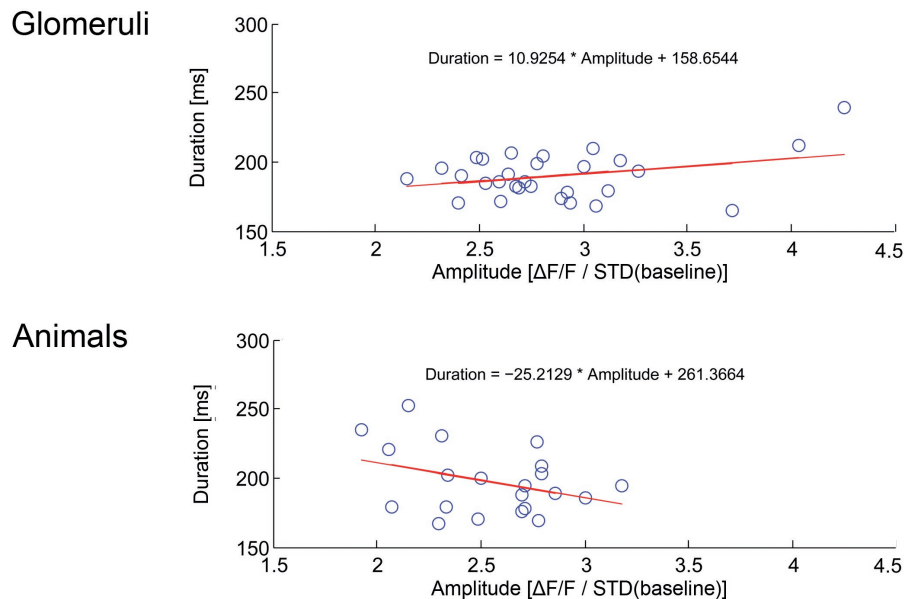
Figure 3.2.12: Scatter plots of amplitude and regularity data pairs that were obtained after averaging by glomerulus (top) or by test animal (bottom). Robust regression fits are shown as red lines. The formulae are shown in the plot.

claim that identified glomeruli are functionally identical between animals.

I was now interested to see how the findings change when only large signals are analyzed. In this analysis, all animals and glomeruli are included, but only signals with amplitudes of >4 standard deviations of baseline noise are taken into account. Figure 3.2.13 on page 108 shows the results for the 4 parameters duration, amplitude, regularity, and frequency after averaging per glomerulus data from all animals. Trivially, the mean amplitudes of spontaneous signals are higher after the signals smaller than 4 standard deviations of baseline noise have been excluded. The mean signal durations however are still in the 200 ms range. The durations appear to be as constant as in figure 3.2.10 on page 104, where the same analysis included all signals over 1 standard deviation of baseline noise. The frequency of signals with sufficient amplitude is lower, and in some glomeruli, there were not enough signals with the same measurement to calculate frequencies or regularities at all. This explains the high variability that the glomeruli exhibit in these two parameters. The regularity is in some glomeruli very high at around 0.75, e. g. in glomeruli 12, 37, 54, 60, and T3-45. The remaining glomeruli yield regularities of 0.25 to 0.6. The signal frequencies are around 1 Hz.
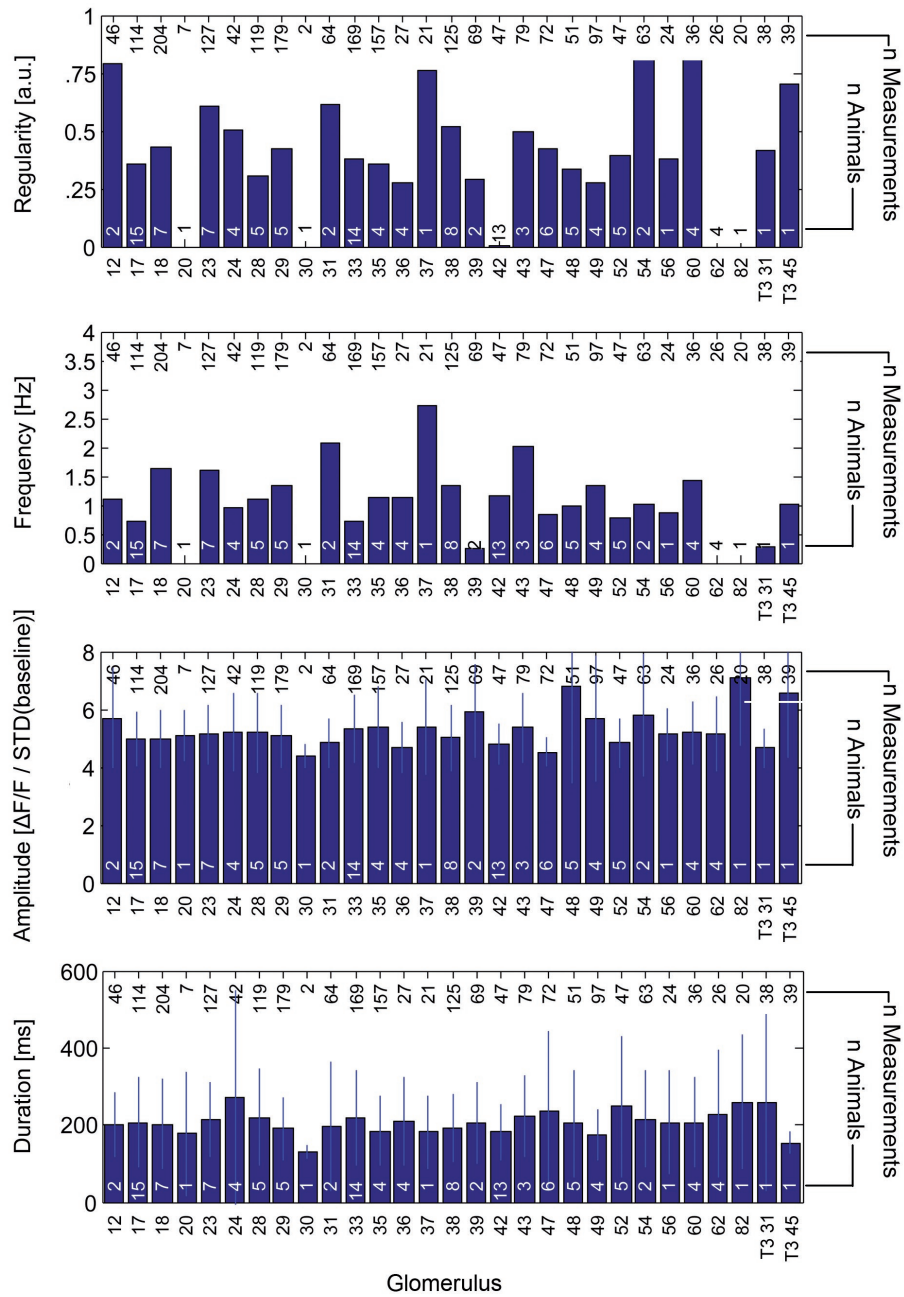
Figure 3.2.13: Amplitude, duration, frequency, and regularity of spontaneous signals averaged per glomerulus. Only spontaneous signals of ≥ 4 standard deviations of baseline noise were included. The numbers of animals and measurements per glomerulus are shown within and above the bars.
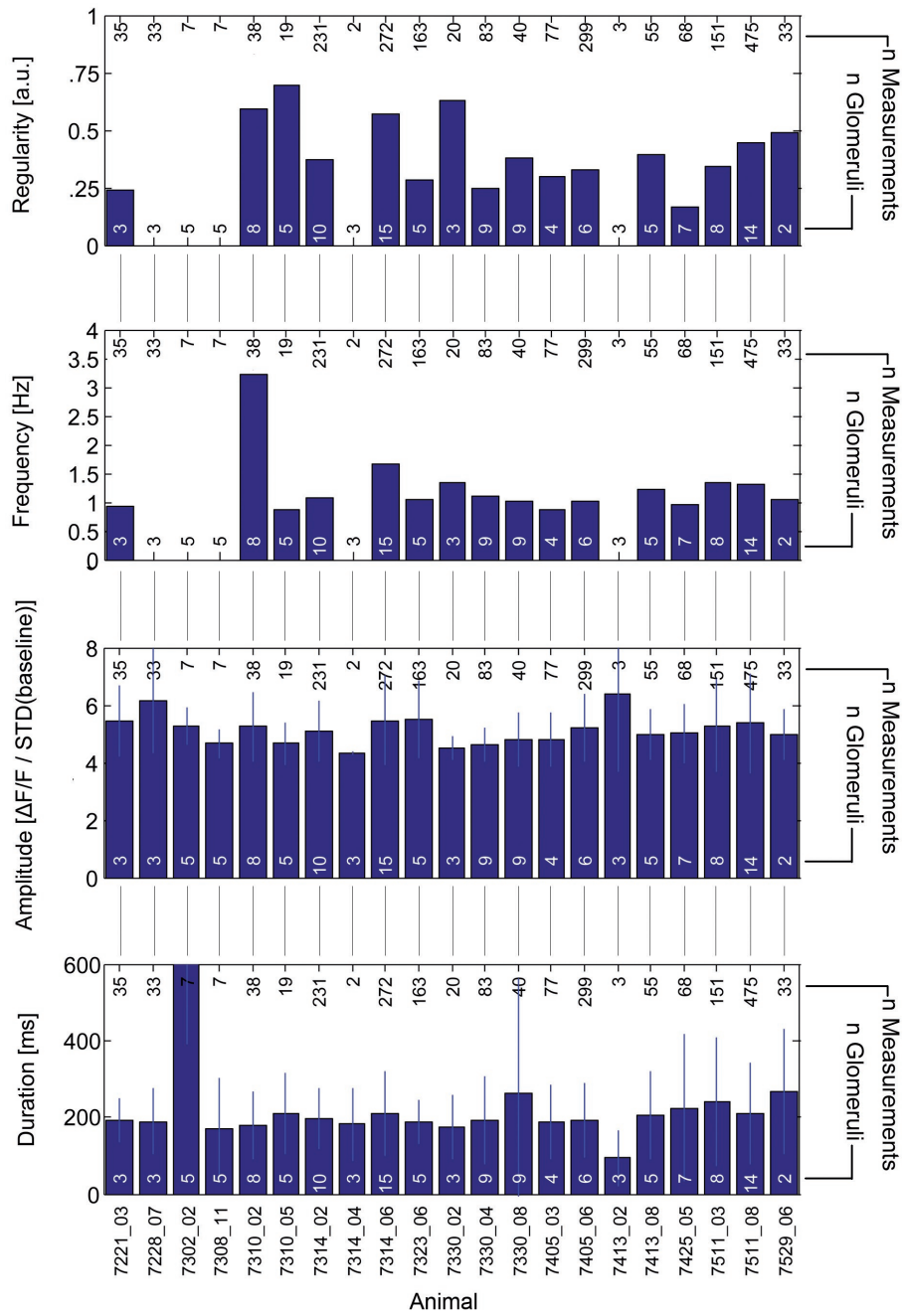
Figure 3.2.14: Amplitude, duration, frequency, and regularity of spontaneous signals averaged per animal. Only spontaneous signals of ≥ 4 standard deviations of baseline noise were included. The numbers of glomeruli and measurements per animal are shown within and above the bars.
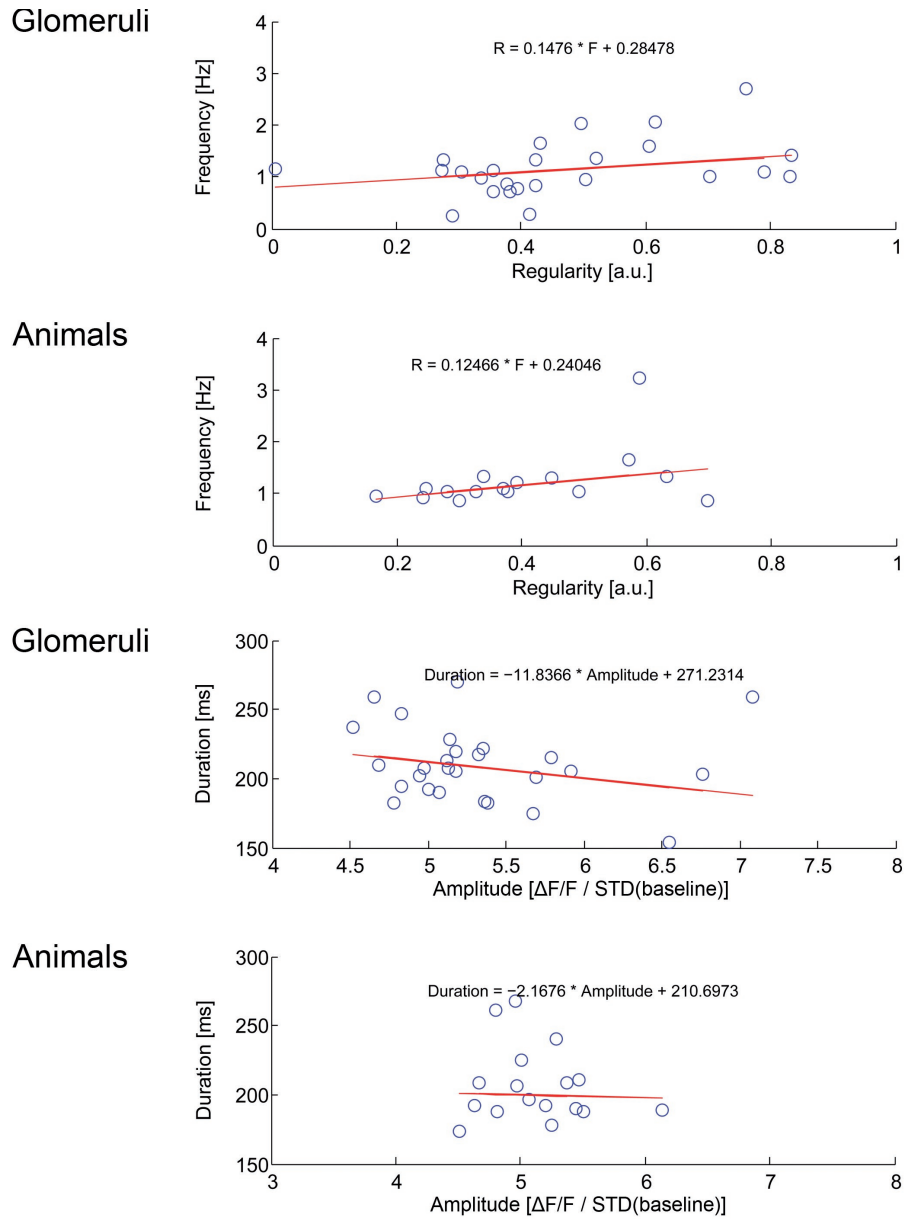
Figure 3.2.15: Scatter plots of frequency vs. regularity (top) and amplitude vs. duration (bottom) of spontaneous signals of ≥ 4 standard deviations of baseline noise. For each pair, two scatter plots are shown: the respective upper on contains the data averaged per glomerulus, the lower one contains the data averaged per animal. Formulae for the robust regressions are shown in the plot area.

Figure 3.2.14 on page 109 concludes the same analysis after averaging the data obtained in all glomeruli that have been measured in each test animal. There are two animals, both with a very small number of sufficiently large spontaneous signals, that display exceedingly high (animal 7302_02) resp. low (animal 7413_02) signal durations. All other animals display the same ≈200 ms signal duration that was reported by the previous analyses. Also the amplitudes are narrowly distributed. Frequency and regularity of signals are variable, and as before in the analysis on the level of glomeruli, some animals do not yield high enough signal frequencies within the same measurement to allow for calculation of frequencies and regularities at all. The mean values of regularity and frequency are nevertheless comparable to the analysis on glomerulus level.

Figure 3.2.15 on page 110 shows scatter plots of the parameter pairs frequency vs. regularity and amplitude vs. duration. Compared to figures 3.2.6 and 3.2.12 on pages 99 and 107, where a lower signal threshold was used, there is a non-trivial correlation between the parameters regularity and frequency also within the large signals. Amplitude and duration, however, which appeared to be positively correlated within glomeruli, appear inversely correlated here. In the analysis on the level of test animals the slope of the robust fit function is less steep here as compared to the analysis that included more signals.

To conclude, regularity and frequency could not be analyzed in glomeruli 20, 30, 42, 62, and 82 and in test animals 7228_07, 7302_02, 7308_11, and 7314_40. The remaining data suggest higher variability in both frequency and regularity, and small interdependency between the parameters amplitude and duration of signals. The values of both parameters frequency and regularity are much lower than in figures 3.2.10 and 3.2.11 on pages 105 and 104, where all signals larger than 1 standard deviation of baseline noise were taken analyzed. The frequency decrement is the trivial result from excluding many (all small) signals from the analysis; the lower regularity values (I pointed out before that this measure is independent of the absolute frequency) point at higher absolute variability in the inter-signal-intervals of very large signals. Compared to the very first analysis in this section, where boxplots were shown for the regularity and frequency of signals that were obtained in glomeruli that have been measured in more than 3 animals and that yielded an amplitude of >2 standard deviation of baseline noise (figures 3.2.2 and 3.2.3 on pages 94 and 95), the variability is higher. Thus, the inclusion of all glomeruli and the higher threshold for signals reduced the regularities obtained.

3.2.1.4 Examples for spontaneous activity illustrate complexity

The previous analysis of four signal parameters demonstrated that durations of spontaneous signals are, when averaged by animal or by glomerulus, quite narrowly distributed. Other parameters showed more variation, but taken together we can conclude that (1) parameters of spontaneous signals of all animals and glomeruli analyzed are comparable and that (2) it is advised to show representative examples of spontaneous activity to convey a more detailed image of how recorded measurement traces appeared within single animals and glomeruli.

Figure 3.2.16 on page 112 serves as example for "normal" measurement traces - i.e. the amplitude, duration, regularity and frequency of the spontaneous signals are well enclosed by the parameter distributions reported in the previous sections.
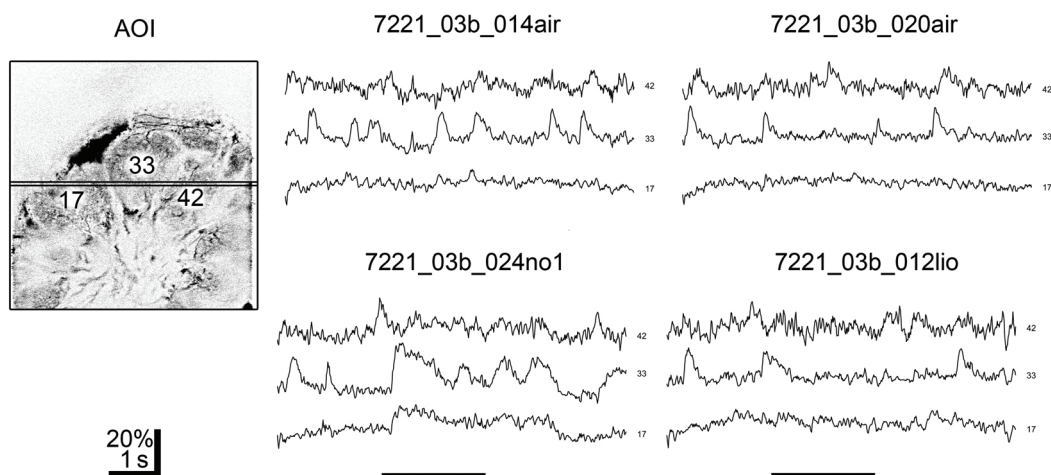
Figure 3.2.16: Example for "normal" spontaneous activity. Left: overview image from the measurement region. The linear scan was positioned between the two horizontal lines. Middle/right: 4 sets of raw measurement traces from three glomeruli 17, 33, and 42, which were positioned under the scan line in animal 7221_03. Top row: Two AIR measurements showing spontaneous activity. Bottom row: Two measurements with odor stimulation are shown for comparison. The black horizontal bar under the latter measurement traces marks the timespan of odor stimulation with NO1 (left) and LIO (right). The scale bar (bottom left) shows 20% $\Delta F/F$ (vertical) and 1 s (horizontal).

The three glomeruli that have been measured simultaneously in this area of interest, namely 17, 33, and 42, show different characteristics. Glomerulus 17,

which is the bottom trace in each set of measurement traces in figure 3.2.16, shows small spontaneous signals in the two air measurements, and a clear phasic response to the odor NO1. Glomerulus 42 (upper trace in each set) shows a rather shaky baseline with spontaneous signals on top of it. The noise level is higher than in the glomeruli 17 and 33, because the part of the glomerulus that was transected by the scan line was darker than the other glomeruli measured in this FoV. This example shows how demanding it can be to separate signals from baseline from noise. The spontaneous signals in this glomerulus are small but otherwise "normal". There are no spontaneous signals during stimulation with the odor LIO, but exactly at the end of stimulation there is a spontaneous signal which one might want to understand as off-response. Glomerulus 33 shows the highest frequency and amplitude of spontaneous signals, and also the most pronounced odor response in the NO1 stimulation. Strikingly, glomerulus 33 not only does not show an odor-evoked response in the LIO stimulation, but even displays repression of the otherwise regularly occurring spontaneous signals.

There is no obvious synchrony between spontaneous signals in the three glomeruli measured in this example. The odor-evoked response to NO1 leads to a response in both glomeruli 17 and 33. The onset of the response is synchronous, but the shape of the signal differs: both glomeruli respond with a large signal 200ms after the beginning of the stimulation, but in glomerulus 17 the response appears tonic and outlasts the stimulation time window, while in glomerulus 33 the recording traces recedes to baseline before the end of the stimulus. This phase is then followed by a train of short signals.

The example demonstrates several key findings, most of which I observed in the majority of test animals:

- Spontaneous signals are usually not synchronized between glomeruli.

- The characteristics of spontaneous activity (i.e. frequency, regularity, amplitude, duration, signal shape) differ not only between animals but also between simultaneously measured glomeruli (i.e. low amount of spontaneous signals in glomerulus 17 in all measurements in figure 3.2.16).

- The amplitude and signals shape of spontaneous signals is rather constant within each glomerulus.

- Responses to odors differ from spontaneous signals by a slightly higher amplitude and sometimes a longer signal duration; see response to NO1 in glomerulus 17.

- If an odor does not elicit a response in a glomerulus, the spontaneous activity in this glomerulus is often suppressed during the stimulation; see glomeruli 33 and 42 in the LIO stimulation.

- The amount of spontaneous activity may change over time, see the two air measurements.

Figure 3.2.17 on page 114 shows another example of spontaneous activity during air measurements. 5 glomeruli have been measured simultaneously, two of which are the same identified glomeruli 17 and 33 as in the previous example. The characteristics of the spontaneous activity in this example are "complex".
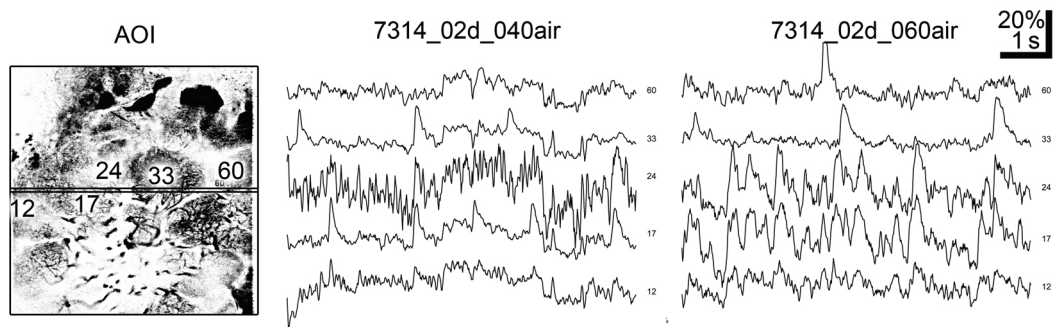
Figure 3.2.17: Example for "complex" spontaneous activity. Left: overview image from the measurement region. The linear scan was positioned between the two horizontal lines. Middle/right: raw measurement traces from the 5 glomeruli 12, 17, 24, 33, and 60 (traces from bottom to top), which were positioned under the scan line in animal 7314_02. The scale bar (top right) shows 20% $\Delta F/F$ (vertical) and 1 s (horizontal).

Most obviously, there is an elevation in the baseline in all 5 glomeruli in the first air measurement 040 (left). After second 3 of the measurement, there is a synchronous rise of the baseline to a plateau of $\approx$8% $\Delta F/F$ that lasts for about 2 seconds. This rise is followed by a drop of the baseline below zero. No odor stimulation took place in this example, so this peculiar (and rare) finding is part of the repertoire of spontaneous signals in PNs.

Furthermore, the characteristics of spontaneous activity differ largely between the two measurements in the glomeruli 17 and 24. Glomerulus 17 displays

"normal" spontaneous activity in the air measurement 040 (left), and the spontaneous signals are only partly synchronized to glomerulus 24. In measurement 060 (right), this changes: now both glomerulus 17 and 24 display high-frequency, mostly synchronized spontaneous activity. Also the spontaneous activity in glomerulus 12 partly resembles the signal traces of glomeruli 17 and 24, yet the signal amplitude is smaller and the synchrony is lower than between those two.

In glomeruli 33 and 60 the frequency of spontaneous activity is lower than average. In glomerulus 12 also the signal amplitudes are smaller than average, no matter if evaluated as absolute % $\Delta F/F$ or as multiples of baseline noise (not shown). Nevertheless it is rather obvious that not only in measurement 060, but also in measurement 040, the activity within glomerulus 12 is synchronized to glomerulus 17.

To conclude,

- The signal traces show spontaneous activity of either higher (glomeruli 17 and 24 in measurement 060) or lower (glomeruli 33 and 60) frequencies compared to the average frequencies.

- There are several synchronous signals in several glomeruli during the measurements shown. Glomeruli 12 and 17 appear synchronized in both measurements, while the striking synchrony of glomerulus 24 to glomerulus 17 appears only in the later measurement 060.

- At the first glance the trace of glomerulus 24 in measurement 060 appears very noisy. But the fact that the same glomerulus shows a much cleaner baseline at a later time point renders this interpretation false.

3.2.1.5 Conclusive remarks on spontaneous activity

The analyses and examples presented in the previous sections reveal several important facts about spontaneous signals in PNs. The fundamental findings are summarized in the following list.

- Spontaneous activity consists of brief, uniform, $\approx$200 ms long bursts-like signals that resemble the spontaneous bursts of action potentials that are found in sharp electrode recordings of PNs. The frequency of such periodic burst-like signals is on average 0.75 Hz.

- Additionally, I could demonstrate the existence of smaller signals that exhibit a broader range of signal durations. The mean duration is also around 200 ms. Together with the larger signals, the total frequency of spontaneous signals is ≈2.5 Hz, and the regularity is lower.

- Extraction of the descriptive parameters amplitude, duration, frequency, and regularity followed by averaging of data by animal or glomerulus reveals that the animals and glomeruli uniformly express a comparable score. A low number of measurements in some animals or glomeruli can often explain aberrant results in single analyses.

- The examples of measurement traces demonstrate the variability that is hidden in the descriptive parameters. The complexity and density of spontaneous signals is overwhelming and impossible to encompass in descriptive numbers or text.

3.2.2 Odor-evoked activity is complex

In this section I will describe PN signals that occurred during the time window of odor stimulation. I will demonstrate that it is often difficult to decide if a given signal is odor-evoked or spontaneous. Still, an atlas of glomerular odor-response-profiles can be unforcedly generated that resembles the functional AL atlas of odor-evoked response patterns (Galizia *et al.*, 1999b). A number of exemplary measurement traces will finally be shown to demonstrate important findings which can not be grasped by descriptive parameters and profiles.

3.2.2.1 Regularity, Frequency, Amplitude, and Duration are unchanged during odor stimulation

The first step in this section on signals during the odor stimulation time window must be the comparison with spontaneous activity. Therefore I repeated the same analysis as in section 3.2.1 Spontaneous activity on page 92, where the parameters regularity, frequency, amplitude, and duration were calculated in a large pool of signals. All signals detected by the CSA were included that fall into the time window of odor stimulation and exceeded 1 standard deviation of baseline noise.
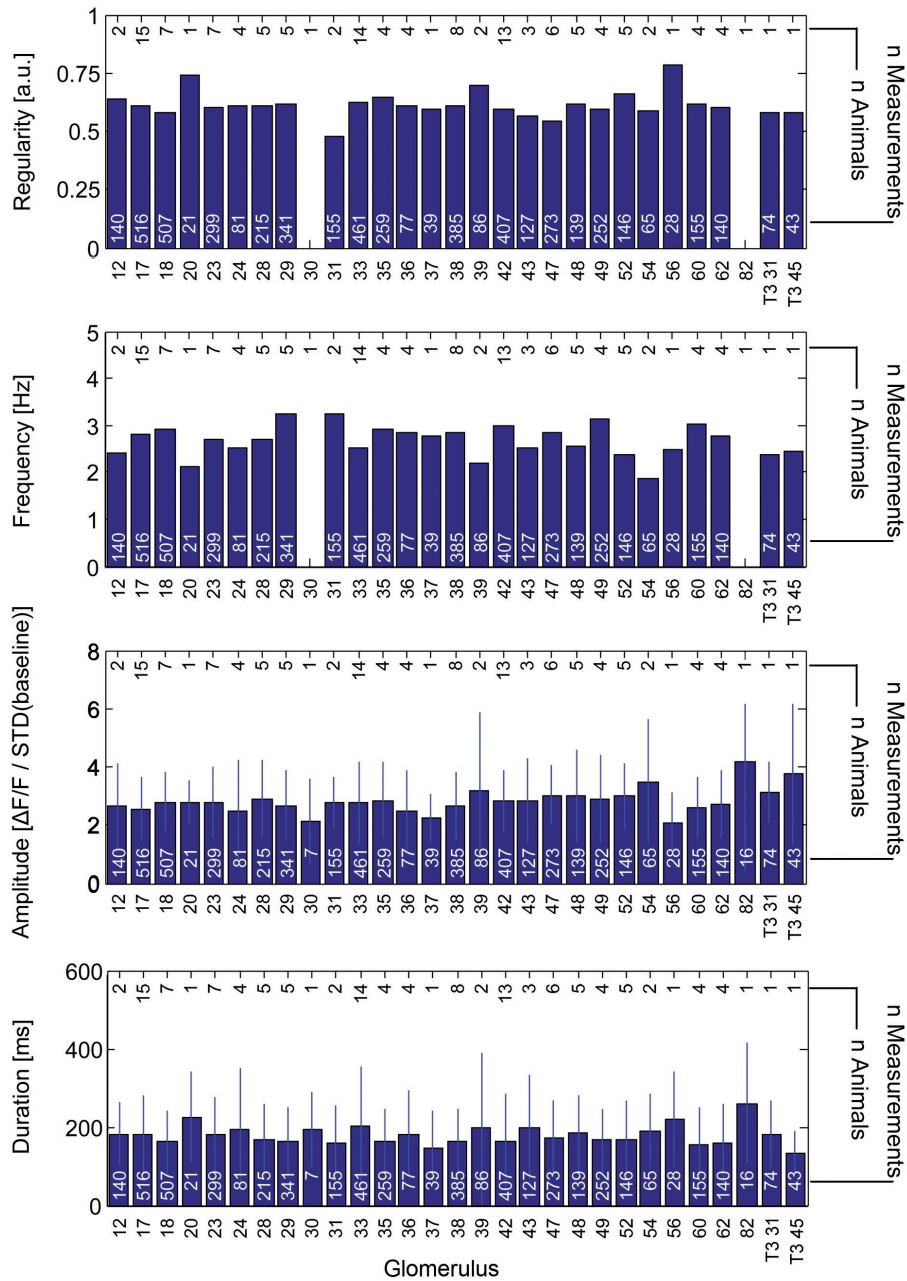
Figure 3.2.18: Amplitude, duration, frequency, and regularity of signals during the odor stimulation time window averaged per glomerulus. Only signals of $\geq$ 1 standard deviation of baseline noise were included. The numbers of animals and measurements per glomerulus are shown within and above the bars.
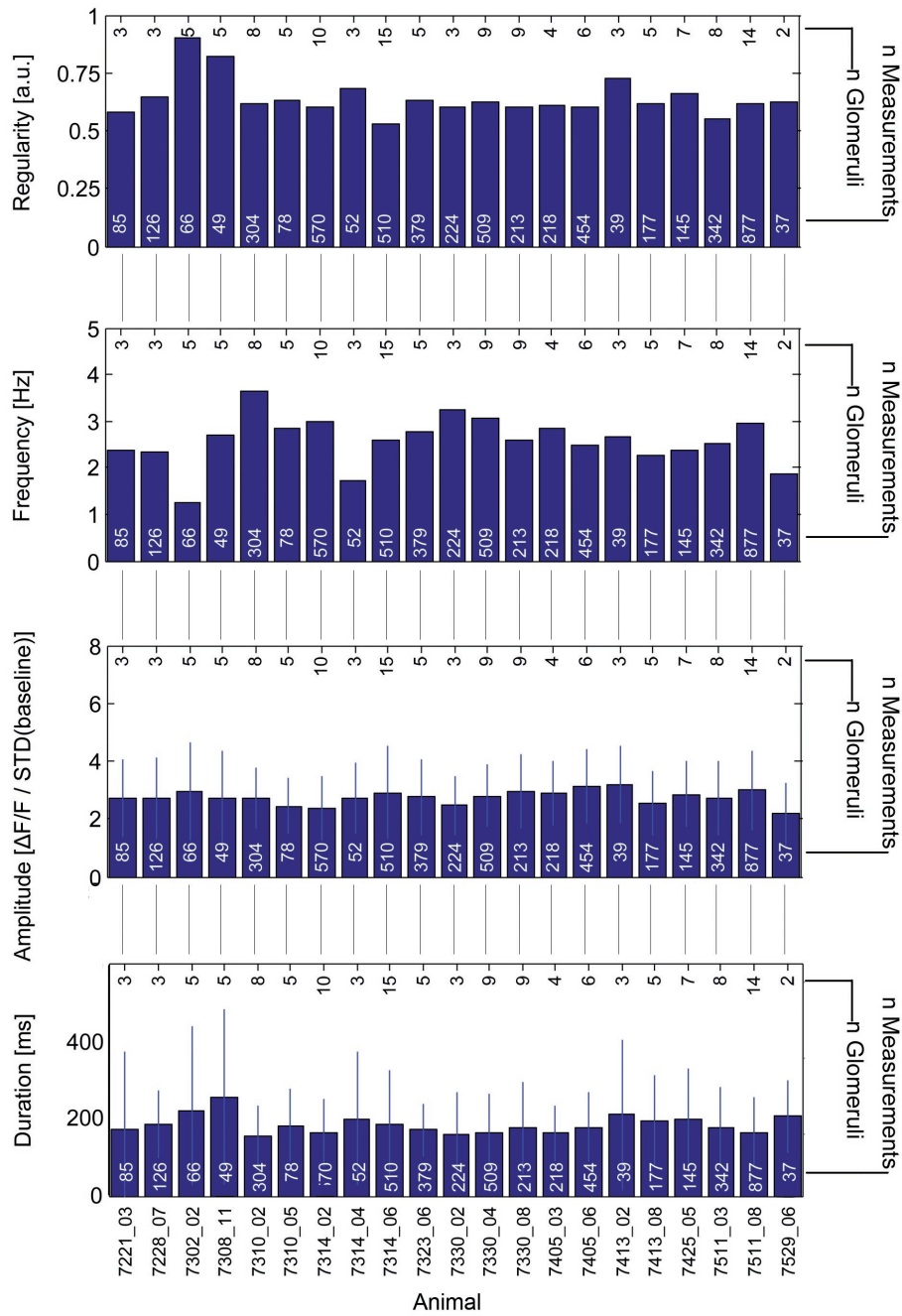
Figure 3.2.19: Amplitude, duration, frequency, and regularity of signals during the odor stimulation time window averaged per animal. Only signals of $\geq$ 1 standard deviation of baseline noise were included. The numbers of animals and measurements per glomerulus are shown within and above the bars.

Figure 3.2.18 on page 117 shows the results per glomerulus. When comparing the relative magnitudes of the bars per group to the corresponding bars of figures 3.2.4 and 3.2.10 on pages 96 and 104, where the same analysis was done on the basis of spontaneous signals, no obvious differences stand out. Two of the glomeruli did not achieve high enough frequencies of signals for the analysis of regularity and frequency in the current only 2 seconds long time window and are thus omitted in the graph. Otherwise, there are more common findings than differences: a glomerulus the displayed a higher frequency of spontaneous signals will very likely also display a higher frequency of signals in the time windows of odor stimulation; a glomerulus that produced large spontaneous signals before will do so too during the time window of odor stimulation. The durations of signals, and this is possibly the most astonishing result of this analysis, are around 200 ms also during the odor stimulation time window.

I repeated the analysis for data that was averaged per animal (figure 3.2.19 on page 118). Comparing this figure with figures 3.2.5 and 3.2.11 on pages 97 and 105 reveals that also here, no obvious differences exist between spontaneous signals and signals that occurred during the time window of odor stimulation. The similarity of signal parameters obtained in glomeruli is thus not caused by single animals that failed to display a response to the odor stimulus, but a general finding.

Next I analyzed the relation between the parameter pairs frequency vs. regularity and amplitude vs. duration (3.2.20 on page 120). I compared the scatter graphs and robust fits to their counter parts that dealt with spontaneous signals in figures 3.2.6 for the parameters regularity and frequency and 3.2.12 for the parameters amplitude and duration on pages 99 and 107. One important aspect in the comparison of regularity and frequency between spontaneous signals and signals during the odor stimulation time window is the opposed relation between the two parameters. While frequency and regularity appeared to be positively correlated during spontaneous activity, the opposite can be observed when signals obtained during the odor stimulation time window are analyzed. In both cases, the correlation has the same sign no matter if the data are organized by glomerulus or by test animal.

Table 3.2.3 on page 121 collects the means, standard deviations, medians, and inter quartile ranges of all signals during the odor stimulation time window. For comparison, I compiled out of the data presented in tables 3.2.1 and 3.2.2 on pages 98 and 106 a similarly structured table that recollects the data for sponta-

Glomeruli

R = −0.0055129 * F + 0.62112

Frequency [Hz]

Regularity [a.u.]

Animals

R = −0.014976 * F + 0.65701

Frequency [Hz]

Regularity [a.u.]

Glomeruli

Duration = −13.7982 * Amplitude + 214.5351

Duration [ms]

Amplitude [ΔF/F / STD(baseline)]

Animals

Duration = 6.363 * Amplitude + 164.3034

Duration [ms]

Amplitude [ΔF/F / STD(baseline)]
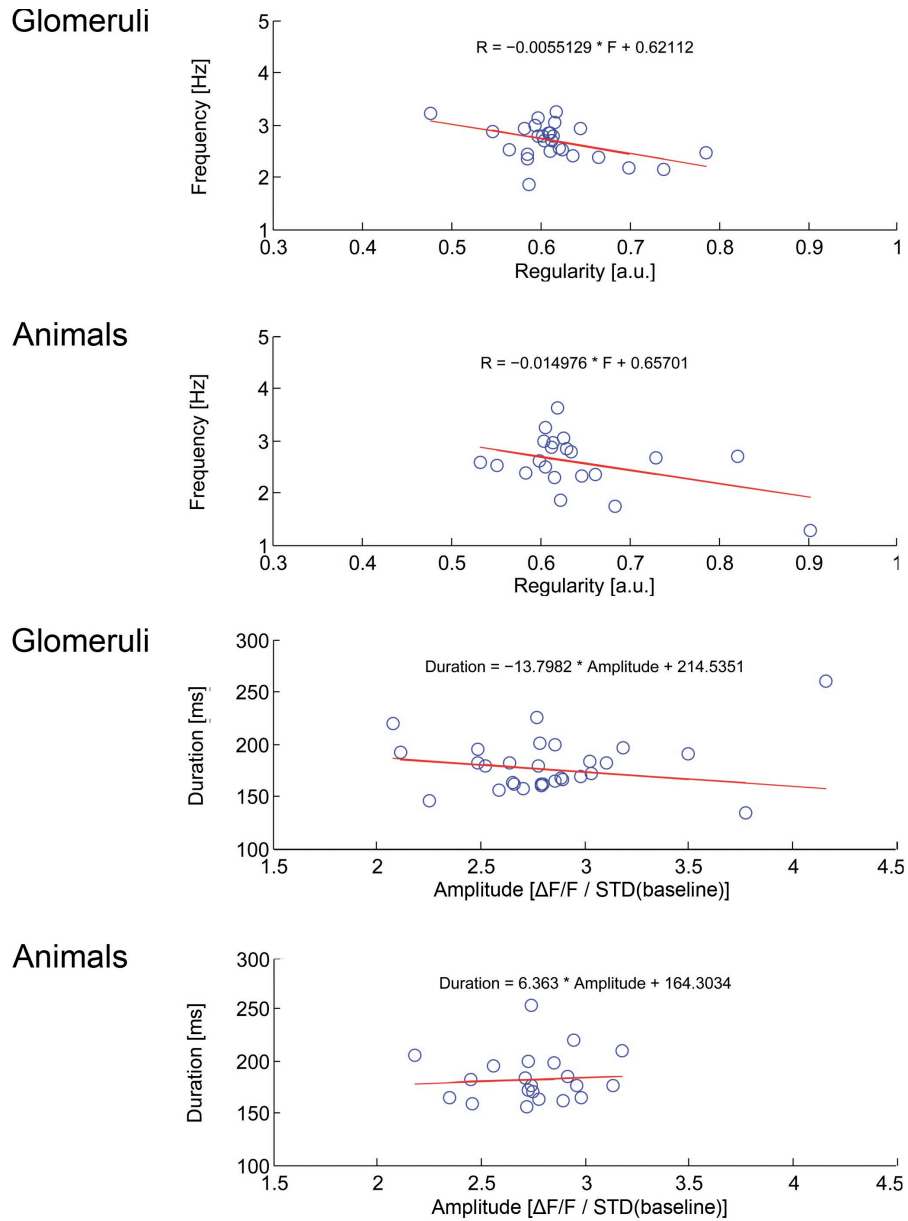
Figure 3.2.20: Scatter plots of frequency vs. regularity (top) and amplitude vs. duration (bottom) of signals of ≥ 1 standard deviations of baseline noise during the time window of odor stimulation. For each pair, two scatter plots are shown: the respective upper on contains the data averaged per glomerulus, the lower one contains the data averaged per animal. Formulae for the robust regressions are shown in the plot area.

Measure	Regularity	Frequency	Amplitude	Duration
Mean	0.642	2.575	2.749	184.17
Standard deviation	0.168	0.526	0.248	23.87
Median	0.608	2.601	2.739	176.24
Interquartile range	0.037	0.537	0.249	33.06

Table 3.2.3: Means, medians and the accompanying measures of spread of data for the parameters regularity, frequency, amplitude, and duration, based on signals of >1 standard deviation of baseline noise that were registered during the time window of odor stimulation.

Measure	Regularity	Frequency	Amplitude	Duration
Mean	0.543	2.240	2.729	188.32
Standard deviation	0.097	0.467	0.514	16.25
Median	0.568	2.416	2.606	187.40
Interquartile range	0.066	0.480	0.383	20.62

Table 3.2.4: Means, medians and the accompanying measures of spread of data for the parameters regularity, frequency, amplitude, and duration, based on signals of >1 standard deviation of baseline noise that were registered during the PRE time window of all measurements and AIR measurements.

neous signals (3.2.4 on page 121). The reported mean values of amplitude and duration reveal that the odor stimulus does not cause these signal parameters to change as compared to spontaneous signals. A high number of odor-evoked phasic-tonic signals would lead to a longer average signal duration. Stronger signals would lead to an increase of the average signal strength. Both effects can not be observed. The largest differences occur between the mean regularity values, which are 0.543 for spontaneous signals, but 0.642 for signals that occurred in the time window of odor stimulation. Thus, the odor stimulation imprints a higher regularity of signals onto glomeruli. Another difference is the standard deviation value of the amplitude parameter. The distribution of signal amplitudes is narrower during the time window of odor stimulation.

To conclude: parameters of glomerular signals during the odor stimulation time window do not differ fundamentally from the parameters obtained from the analysis of spontaneous signals. This may partly be explained by the fact that in each of the groups, only a part of the odor stimuli used here actually evoked a response; it is thus possible that the averaging needed to perform the analysis in groups partly masks the effect that odor stimuli have onto the AL. Nevertheless it is noticeable that the average amplitude and duration of signals

do not change at all.

In the next section I will report on glomerular odor response profiles that emerge if the responses in each glomerulus are aggregated separately for the test odors. The results will be compared to the response profiles published in the functional AL atlas (Galizia *et al.*, 1999b).

3.2.2.2 Odor-response-profiles correspond to functional AL atlas

Wide-field imaging led to the creation of the functional atlas of honeybee glomeruli, in which glomerular activity patterns evoked by a panel of odors were presented (Galizia *et al.*, 1999c). The atlas patterns are unique for each of the 60 odors tested so far. To compare the general features of the data measured in this work with the odor response profiles of glomeruli present in the atlas, I complied the linear scan data into glomerular odor response profiles.

Figures 3.2.21 and 3.2.22 on pages 123 and 124 show the odor response profiles of the glomeruli that were measured with linear scans. Both the reliability and the average signal amplitude are shown in separate bars for each combination of glomerulus and odor.

Reliability (less saturated colors) and amplitudes (saturated colors) were calculated as described in the methods part, section 2.5.3 on page 74. The number of responses that were registered is shown in the central line of numbers at the top of each bar; the numbers directly below show the total number of test trials. The topmost numbers show the number of animals in each group. The standard deviation of the mean peak amplitudes is shown as an error bar of 2 standard deviations in length. This procedure is similar to the approach used in Sachse and Galizia (2002), but there the reliability was not shown.

My data can reproduce the odor response profiles of that the atlas reports for the frontal glomeruli of the honeybee AL. Glomeruli 17 and 33, for instance, are reliably activated by the 3 alcohols in the odor set used, and also by the binary mixture of NO1 and OC1. Other glomeruli are more strongly and reliably activated by the only non-alcohol in my odor set, LIO, e. g. glomeruli 43 and 48.

Mixture effects are found: In glomeruli 28, 33, and 42, reliability and amplitude of signals appear reduced in the binary mixture of HX1 and LIO, LIX, as compared to the pure odors; in glomerulus 30 the same phenomenon occurs in the mixture of NO1 and OC1, MIX. This effect is known as mixture suppression. In the examples quoted, the ideal case of mixture suppression, in which the
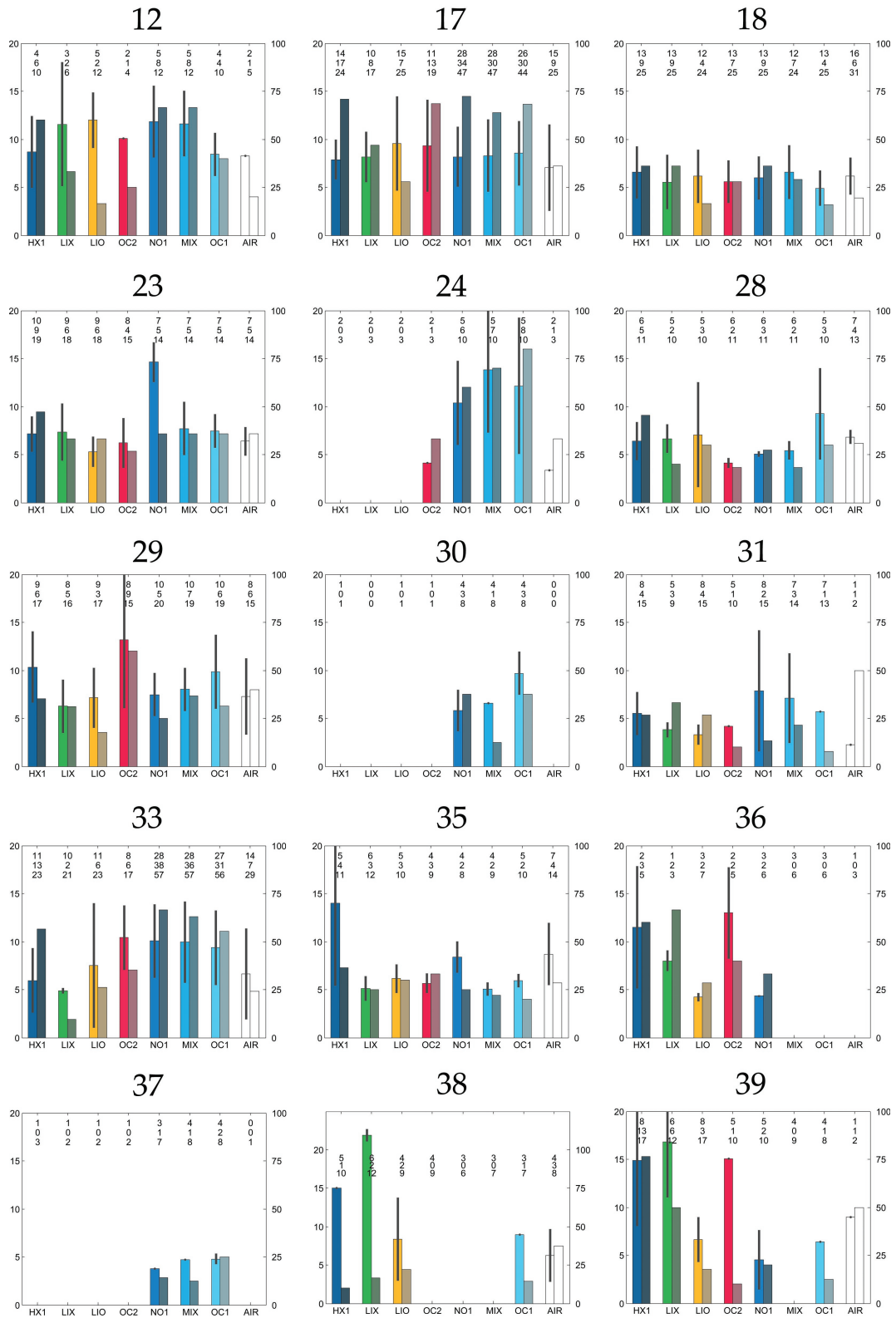
Figure 3.2.21: Odor response profiles of glomeruli 12 to 39. Refer to figure 3.2.22 on page 124 for a figure legend.
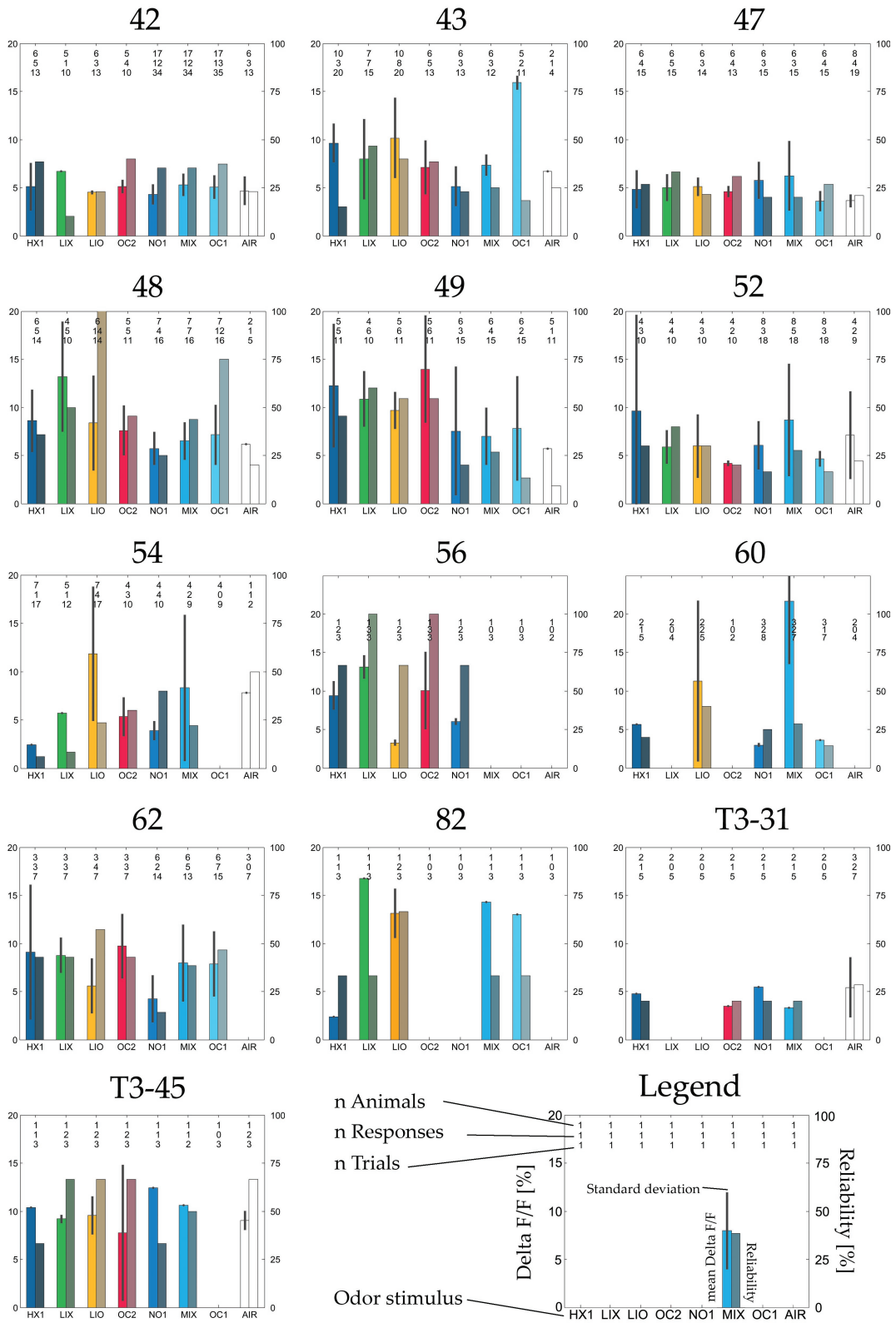
Figure 3.2.22: Odor response profiles of glomeruli 42 to T3-45. Legend is shown at the bottom right of this figure.

responses to the pure odorant are equally strong, is fulfilled. Nevertheless, also the case in which the response to the mixture is as weak as the response to the weaker of the two pure components qualifies as mixture suppression. The phenomenon can be observed in glomerulus 48: this glomerulus is most strongly activated by pure OC1, but the response to the mixture of NO1 and OC1, MIX is almost as weak as the response to the pure odor NO1. In this case the presence of the weaker component in the mixture, which on its own does not elicit a strong response, apparently suppresses the response to the stronger component in the mixture. Additive mixture effects, in which the response to the odor mixture is stronger than the response to any of the two pure components, can be observed in glomerulus 56 (LIX) and glomeruli 52 and 60 (MIX). Hypoadditivity is given if the response strength elicited by the mixture is as strong as the stronger of the responses elicited by any of the pure stimulants. This mixture effect has been observed the most frequently.

In the following sections exemplary raw data traces are shown that reveal in how far odors influence the glomerular signals. It becomes apparent that only a very advanced algorithm could detect all influences that odor stimuli have onto glomerular signaling.

3.2.2.3 Phasic-tonic responses are rare

Most signals that occurred during the odor stimulation time window were shorter in time than the 2 s stimulus interval. In many cases, a prominent off-response marked the end of the odor stimulus. At the level of the PN dendrite, the signals appear to have lost the tonic component that is regularly found in electro-antennogram recordings, sensillum recordings, and also in wide-field imaging studies where a bath-applied acetoxymethylester (AM) dye like Calcium Green-2 AM is applied.

Figure 3.2.23 on page 126 shows exemplary traces from several simultaneously measured glomeruli from three different animals. The top left sub-figure proves with the pronounced tonic signal in glomerulus 39 that the scarcity of tonic responses in the data presented here is not due to technical or other experimental reasons. Tonic signals are rare, but if there is one, the method can show it. In the other glomeruli that were measured simultaneously, however, the signals are more typical. Glomerulus 54 is spontaneously active before the stimulus with a low frequency of large signals. One slightly longer signal occurs
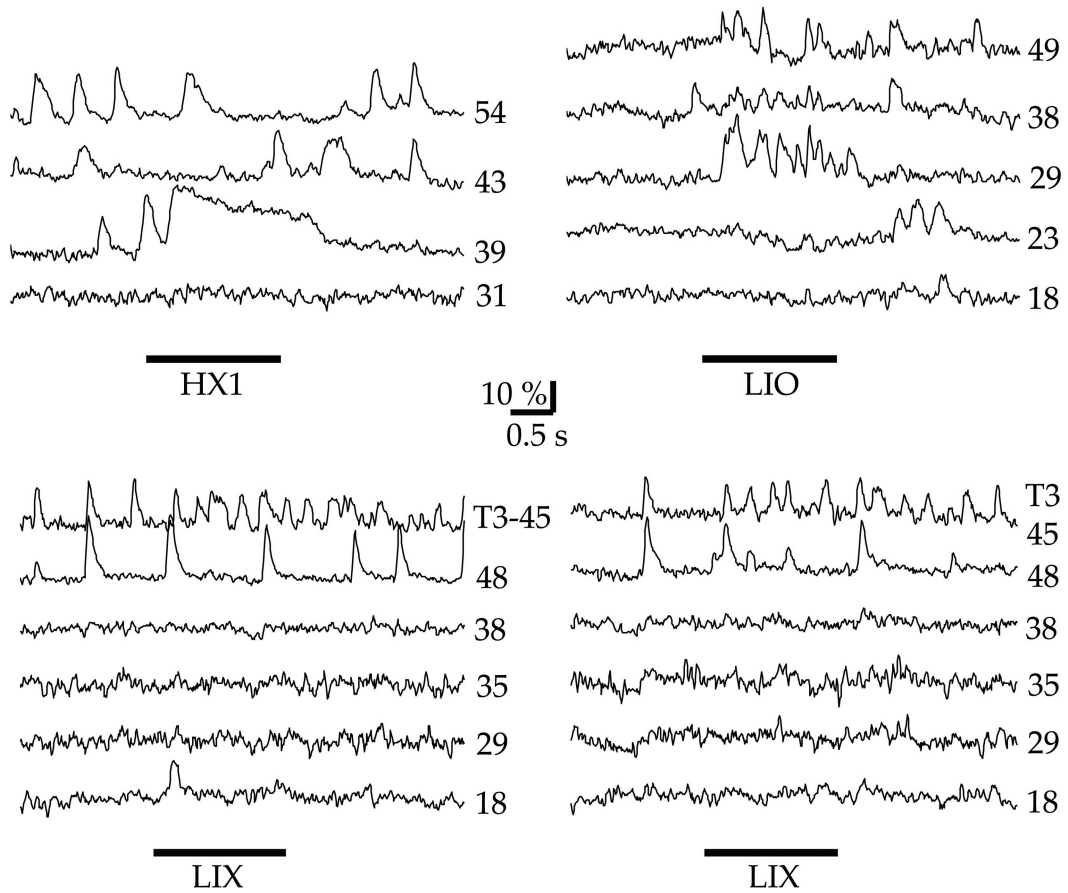
Figure 3.2.23: Exemplary traces showing the signals that occurred in 4 measurements. For each measurement, the traces from all glomeruli that were transected by the scanning line are shown, the respective glomerulus number is found to the right of the traces. Top left: Animal 7314_06, top right: Animal 7323_06, bottom left and right: two measurements in animal 7511_08, which were acquired 16 minutes apart. The odor stimuli are marked by long bars and odor names. The scale bar in the center of the figure shows axes of 10% $\Delta F/F$ height and 0.5 s length.

during the stimulation, followed by a pause. A package of small and large signals marks the end of the pause. An off response can be seen in the trace of glomerulus 43.

The two measurements shown at the bottom left and right in figure 3.2.23 originate from the same animal, but were recorded 16 minutes apart. The glomeruli 18, 29, 35, and 38 do not show pronounced signals, but both signal detection algorithms that were used in this work would register many signals also in these traces. The apparent randomness, the noise level, and the small size (at the scale of the figure) of signals are misleading for the human eye. In glomerulus 48, and 99, the odor mixture LIX evokes a signal: glomerulus 48 shows one signal after odor onset and one signal after odor offset; in glomerulus T3-45 the frequency of bust-like signals is increased during the stimulation compared to the time window before. The signals recorded in these two glomeruli illustrate how hard it can be to decide if a signal is elicited by the stimulus or if is a spontaneous signal. Especially in glomerulus 48 one would mistake the on and off-responses as spontaneous signals, if these responses were not recorded twice! Glomerulus T3-45 is interesting because it is one of two T3 glomeruli that I found to be stained by retrograde fills of the lACT. In this example T3-45 displays a higher rate of large burst-like signals than most T1-glomeruli, and the delay after odor onset is larger the delay in the simultaneously measured glomerulus 48.

The top right measurement in 3.2.23, lastly, shows the whole range of signal shapes that one can obtain in 2PLSM of honeybee PNs. Glomerulus 23 and potentially also glomerulus 12 display a signal of inhibition in the time window of odor stimulation. After the end of the stimulus, both glomeruli generate a delayed off-response. In glomerulus 49, some bust-like signals at odor onset ride on a signal of inhibition. Glomerulus 29 shows the clearest odor response with a train of burst-like signals that, if averaged in time, would look like a phasic-tonic signal. Glomerulus 38 generates small signals which are apparently synchronous to the signals in glomerulus 29, but smaller. Glomerulus 29 proves with the signals that occur after the stimulation that also larger signals can be generated. That the off-response of glomerulus 38 appears synchronous to one of the off-responses in glomerulus 49 may be coincidence.

To conclude: tonic signal components do occur in 2PLSM measurements of honeybee PNs, but these are rare. Phasic signals and signals of inhibition occur frequently. Odor-evoked signals are not larger than spontaneous signals and sometimes delayed, which makes it difficult to speak about odor-evoked signals.

Off-responses are frequent and sometimes appear synchronized between several of the glomeruli measured. Also spontaneous signals coincide frequently.

3.2.2.4 Inhibition can be revealed in 2PLSM

Strong inhibitory input onto a silent PN can be detected directly by calcium imaging of PNs as a drop in the baseline of a recorded glomerulus. However, this has not been observed as often as one would assume, given that inhibitory LINs are numerous in honeybees, and that the publications on electrophysiological measurements of LINs and PNs concur on the notion of that LINs are direct postsynaptic partners of RNs (see section 1.2.3 Connectivity on page 15 of the introduction). PNs are sometimes inhibited without a clear signal of inhibition as a drop in the baseline, as figure 3.2.24 on page 128 demonstrates. Shown are examples of recordings in which inhibition leads to decreased $\Delta F/F$ amplitude in some cases (see first and third stimulation with HX1). More importantly, in the same glomerulus and animal another indicator of presynaptic inhibition can be found, namely the suppression of otherwise regular burst-like signals (see OC2 stimulations 2 to 4).
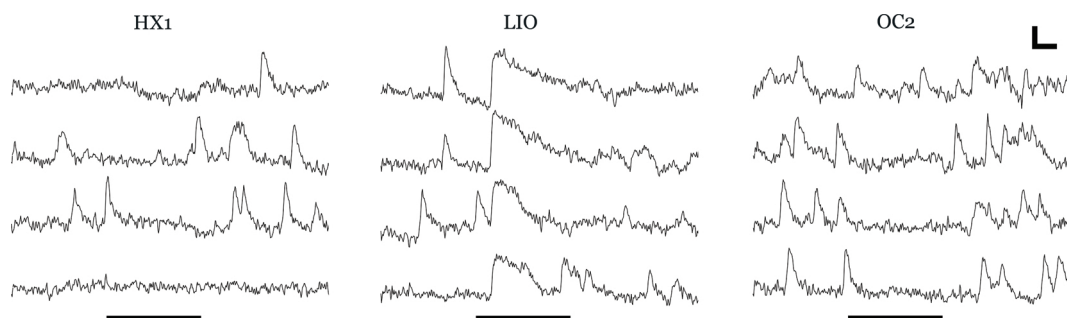
Figure 3.2.24: Examples for inhibitory signals. All measurement traces are from animal 7314_06, glomerulus 43. The stimulating odors were HX1, LIO, and OC2, as indicated above the traces. Each measurement was repeated 4 times. The first measurements are in the top row. The black bars at the bottom of the figure mark the 2-second odor stimulation interval. The scale bar on the top right of the figure shows 0.5 s in time in the horizontal and 5% $\Delta F/F$ in the vertical axis.

Figure 3.2.25 on page 129 shows two more exemplary measurements in which signals of inhibition are obvious. In the measurement shown at left, a large signal of inhibition occurs simultaneously on the traces of glomeruli 33 and 42. This is measurement is one of a few rare examples for signals of inhibition

that match the amplitude and fast rise-time that signals of excitation very often exhibit. The trace from glomerulus 17 that was recorded at the same time shows a normal signal of excitation. This may be seen as a proof for the absence of a measurement artifact.
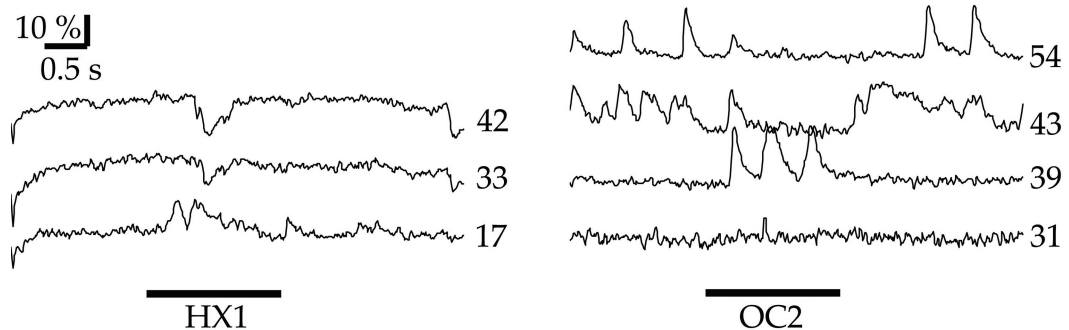
Figure 3.2.25: Exemplary traces from two test animals showing signals of inhibition. For each of the two measurements, the traces from all glomeruli that were transected by the scanning line are shown, the respective glomerulus number is found to the right of the traces. Left: animal 7302_02, right: animal 7323_06. The odor stimuli are marked by long bars and odor names. The scale bar in the top left of the figure shows axes of 10% $\Delta F/F$ height and 0.5 s length.

The measurement on the right illustrates once more how the absence of regular spontaneous signals reveals likely inhibition of two glomeruli, namely 43 and 54. Both exhibit responses after the stimulus offset, and these signals differ in shape: while the two burst-like signals in glomerulus 54 look exactly like the spontaneous signals before the odor stimulus, the pronounced signal of excitation seen in glomerulus 43 resembles more a typical tonic signal as odor stimuli can evoke them. This example also shows how it may come about that I see, on the one hand, many events in my recordings that can be correlated with the odor stimulation, but on the other hand the cumulative analyses of spontaneous signals vs. signals during the odor stimulation time window did not reveal large deviations in the four extracted parameters regularity, frequency, duration, and amplitude of signals. Glomeruli 43 and 39, when summed up, would not show an influence of the stimulating odor, but in fact there are clear signs for odor-evokes signals in the single traces.

To conclude: Inhibition is detectable by 2PLSM, but how much and which part of the action of the inhibitory networks become apparent in 2PLSM can not be answered. Because signals of inhibition are mostly much smaller and

less defined than signals of excitation, a cumulative analysis of such signals is difficult - the outcome of such an analysis would be largely defined by the detection threshold. I anyway did perform an analysis that yields results specifically for episodes of the measurement traces where signals of inhibition could be found by the template correlation algorithm TCA; it can be found in section 3.3.4.3 Correlation during signals of inhibition on page 153.

3.2.2.5 Some response shapes are odor-specific

As pointed out in the introduction, I divided my efforts between the goals to describe PN signaling in as many glomeruli as possible, but to also obtain numerous recordings from glomeruli 17 and 33 to determine the reproducibility of signals recorded in the 2PLSM. Shown in figure 3.2.26 on page 131 are exemplary recordings from two of the test animals during stimulations with the odors NO1, MIX, and OC1. The pure odors and their binary mixture are known to elicit responses in glomeruli 17 and 33. The recordings illustrate a finding that was often less pronounced or absent, but which occurred with high specificity more often than chance can explain, namely the finding that the response shapes that glomeruli exhibit during stimulation with an odor can be odor-specific.

Glomeruli 17 and 33 often respond to the application of the odor NO1 with a phasic-tonic signal. Phasic-tonic signals were rare in other glomeruli, so the rather reliable occurrence of these is already an interesting finding. The topmost recordings in figure 3.2.26 show examples for phasic-tonic responses in glomeruli 17 and 33 during application of NO1. NO1 was also part of the binary mixture with OC1 in the stimulant MIX. The responses to MIX, in the second row of the figure, show more phasic components. In both animals and both glomeruli, the signal returns to a $\Delta F/F$ value comparable to baseline already during the odor stimulus, then rises again before the stimulus has ended, but does not develop a pronounced off-response. In the measurements with OC1, animal 7221_02 responds with an even more phasic response, in which the initial peak after odor onset is sharper, the pause until the rise longer, and the rise continues until the end of the odor stimulus. A delayed, small off-response is visible in the traces from both glomeruli. Animal 7314_02 displays a more complex response shape during stimulation with OC1, but the direction is the same: the response is more phasic than the response to MIX, and an off-response
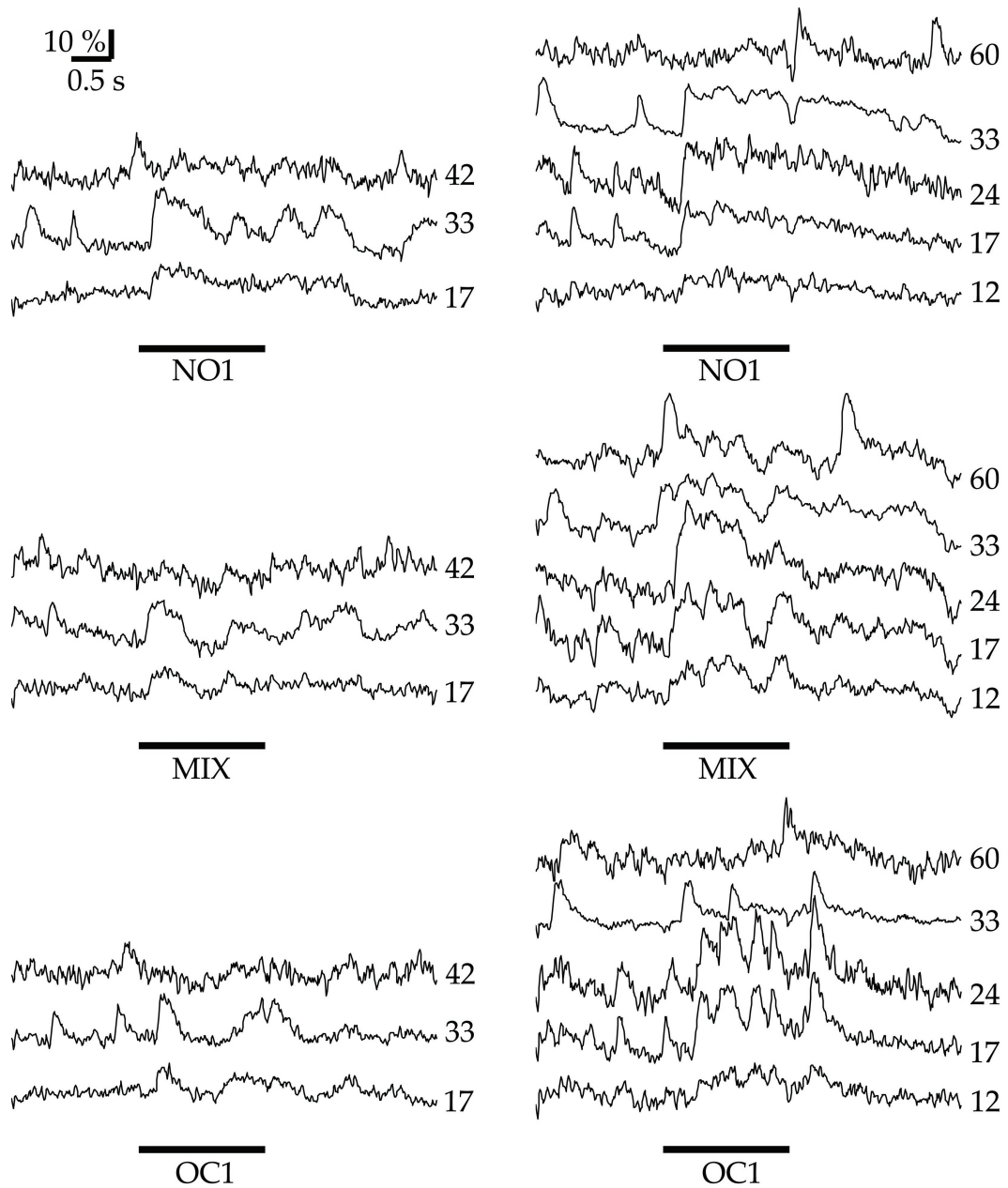
Figure 3.2.26: Exemplary traces from two test animals odor-specific response shapes. For each of the six measurements, the traces from all glomeruli that were transected by the scanning lines are shown. The respective glomerulus number is found to the right of the traces. Left: animal 7221_02, right: animal 7314_02. The odor stimuli are marked by long bars and odor names. The scale bar in the top left of the figure shows axes of 10% $\Delta F / F$ height and 0.5 s length.

is generated.

It is interesting that the phasic and tonic components of the responses in glomeruli 17 and 33 are not only triggered in an odor-specific way, but also appear to be graded: The response to the mixture of NO1 and OC1 is the perfect intermediate between the extremes.

3.2.2.6 Conclusive remarks on activity during odor stimulation

The analyses and examples presented in the previous sections reveal several important facts about odor-evoked signals in PNs. The fundamental findings are summarized in the following list.

- Signal parameters of signals that occurred during the time window of odor stimulation do not reveal fundamental differences towards spontaneous signals. Thus, the way in which glomeruli code for odors is not a *general* increase or decrease of any of the parameters regularity, frequency, amplitude, or duration.

- Nevertheless I could, by the same means as done previously with wide-filed imaging data, calculate odor response profiles that resemble the response profiles published in the functional AL atlas. Also mixture effects that had previously been found in glomeruli could be observed in the 2PLSM data.

- The exemplary measurement traces demonstrate several different effects that odor stimuli have on glomerular signaling, among these phasic responses, inhibition, off-responses, and simultaneous rate increase and decrease in different glomeruli. Thus, the effect of the odor stimulus is in most examples clearly identifiable for the human eye, but when these diverse signal types are summed up or averaged, the effects of the odor stimulus are masked.

- I could demonstrate in two examples that odor stimuli induced recognizable odor-specific response shapes.

3.3 Projection neurons are synchronized within glomeruli

3.3.1 Synchrony occurs already at the level of glomeruli

The analysis on the level of identified neurons and branches will concentrate on the correlation coefficient, which is a good measure for synchrony of a given pair of traces. Synchrony can also be observed between glomeruli, as figure 3.3.1 on page 134 shows in a representative example of a linear scan measurement. The raw linear scan recording is depicted alongside it's AOI overview image. At the right side, the signal traces from 5 glomeruli in three measurements are shown. Note that in both AIR measurements some, but far from all signals appear to be synchronized between several glomeruli. In the measurement with odor stimulus, a simultaneous response occurs in 4 out of the 5 glomeruli measured. Obviously, synchrony is not only evoked by odor stimuli that lead to simultaneous activity in several RN::PN chains, but also spontaneous activity is a property of the AL network rather than a secluded within-glomerulus phenomenon.

The following sections of the results part will deal with the synchrony within and between glomeruli. I will show that not only in examples, but also when the results from many animals and measurements are combined, there is on the one hand striking evidence for synchrony between PNs of separate glomeruli, and on the other hand I show de-correlation of PNs within single glomeruli.

3.3.2 Single projection neurons can be identified

It was in 7 out of 21 animals possible to reconstruct individual PNs on the basis of image stacks that were acquired *in vivo* before and after the physiological measurements. See section 2.5.1 on page 69 in the methods part for details on the reconstruction process.

Reconstructions were feasible if the recordings and stacks met all of the
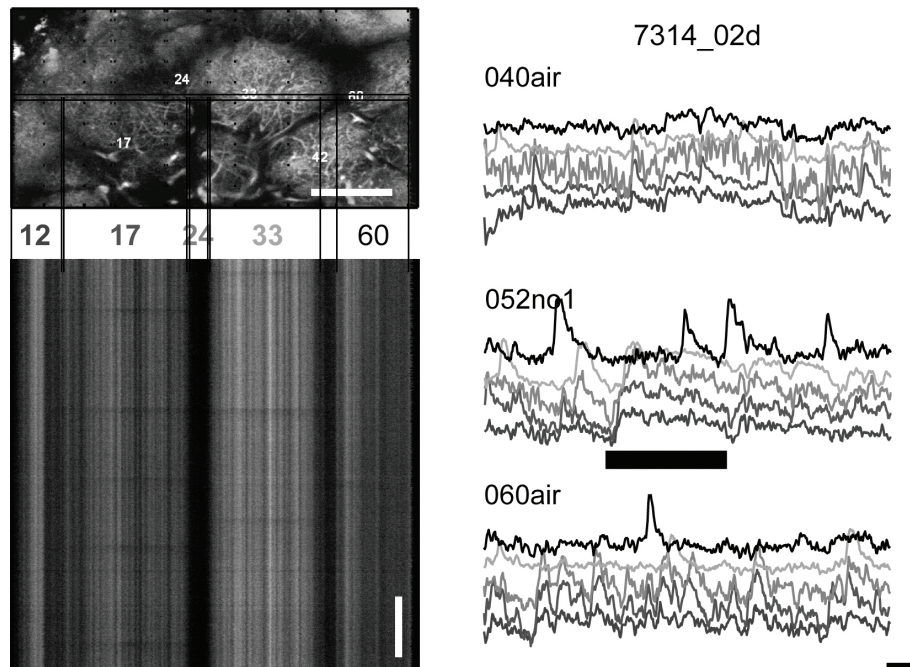
Figure 3.3.1: Linear scan on several dorso-frontal glomeruli. Top left: Overview image of the AOI. Scale bar is 50 μm. The scan line is indicated by two horizontal lines though the centre of the image. From left to right, the 5 glomeruli 12, 17, 24, 33, and 60 are transected by the scan line. Glomerulus 24 was transected only marginally and appeared very dark in the linear scans. Bottom left: raw linear scan recording, AIR measurement. The horizontal dimension of the image corresponds to the indicated scan line in the overview image. Time is from top to bottom, the vertical scale bar indicates 1 s. Signals show up as dark horizontal bands. Right: Quantification of % $\Delta F/F$ over time for all 5 glomeruli. The scale bar indicates 500 ms (horizontal) and 5 % $\Delta F/F$. Top right: same recording as shown in the bottom left panel. Bottom right: Another AIR measurement in the same region. Middle right: Measurement with odor stimulus (1-Nonanol). The thick horizontal bar indicates the stimulation time.

following requirements:

- At least one motion-free, bright, and not too noisy anatomical image stack was recorded

- Clear labeling of one or more PNs in one or more glomeruli

- No strong motions or drift during the entire time of odor recordings, especially along the depth axis

- Recording stable over several odor stimulations

Because most of these requirements are met (or not met) per animal rather than per glomerulus, it was in the animals with reconstructible PNs in one glomerulus often possible to reconstruct PNs in another glomerulus, too. Neurons in glomeruli 17 and 33 were measured and reconstructed most frequently, (1) because these are the glomeruli that I concentrated on (see section 2.3.3 on page 53 in the methods part for the reasoning behind measuring in these glomeruli), (2) because the large size of these glomeruli, and (3) because of frequent signals of inhibition in glomerulus 33 that has been observed in linear scans ans planar scans.

Figure 3.3.2 on page 137 shows traces that have been obtained at coordinates in a linear scan recording that correspond to 2 neurons with a total of 4 branches. The recording trace of the whole glomerulus is the result from spatially averaging over the complete length of the scan line that transected the glomerular volume of glomerulus 62. This trace reveals three obvious spontaneous signals that are in no temporal relation to the odor stimulus. The four traces of identified neuronal sub-branches display more "noise". Correlation was determined in 16 samples (210 ms) long time windows. Below the traces, a row of cross-correlograms is shown (16 colored sub-figures). The correlograms display, each for a separate time window, the results from pairwise cross-correlation of recording traces from the identified sub-branches. Please note that, during the spontaneous signals, correlation reaches very high values, which is marked by dark red colors in the correlograms. At bottom, a row of 16 histograms visualized the distribution of correlation coefficients from the correlograms. During the large signals, only correlation coefficients of 0.5 and larger occur, thus the histograms are shifted to the right side of the sub-figures. This is regularly observed if a signal is shared by all of the PN processes. In the phases

between signals, green and cold colors in the correlograms and broader distributions of correlation coefficients in the histograms reveal de-correlation and anti-correlation. In these phases, noise competes with small signals that are often not shared by all PN processes. The position of blue pixels in the correlograms identifies pairs of branches that are temporally anti-correlated. By close observation of trace episodes, one can identify the respective time windows in the traces, that lead to the registration of anti-correlation between a pair of processes. At time stamp 2.53 s, for example, the correlogram identifies two strongly anti-correlated branches, namely A1 and A2. Within the blue rectangle, the uppermost trace which belongs to A1 deflects upwards, while the other (A2, below) deflects downwards. This specific antipodal signaling is a prerequisite for registration of anti-correlation.

To conclude, both high correlation as high anti-correlation (negative values) are indicative of synchronous events. In the first case, the events are synchronous and trace deflection is parallel; in the latter case the events are synchronous but trace deflection is antipodal. All other events are registered as no correlation, or, as called in the rest of this document, de-correlation.

This example illustrates the duty of SWCA: determination of the number of correlation windows that yield significant correlation or anti-correlation from traces originating from identified PN processes. In the example, 4 branches are to be compared, but opposed to the comparison of all vs. all (as in the cross-correlogram), SWCA compares separately between distinct neurons and between branches of the same neuron. The comparisons would be in this case: A1::B1, A1::B2; A2::B2 for determining correlation between neurons, and A1::A2, B1::B2 for determining correlation between branches.

In the following 2 sections I will present results from the SWCA analysis of signals from identified sub-cellular processes of multiple simultaneously measured PNs. The analysis is largely based on the calculation of correlation coefficients from pairs of measurement traces. These coefficients are utilized as an indicator for synchrony of events in pairs of measurement traces.

To get you acquainted with the idea behind the method, I will first show and describe in detail exemplary data together with traces of coefficients that were derived from their pairwise correlation (section 3.3.3 "Correlation of signal traces from identified processes", starting on page 138). In the second section 3.3.4 "Quantification of the results from the sliding window correlation algorithm", starting on page 146, I will show the compiled result from the correlation
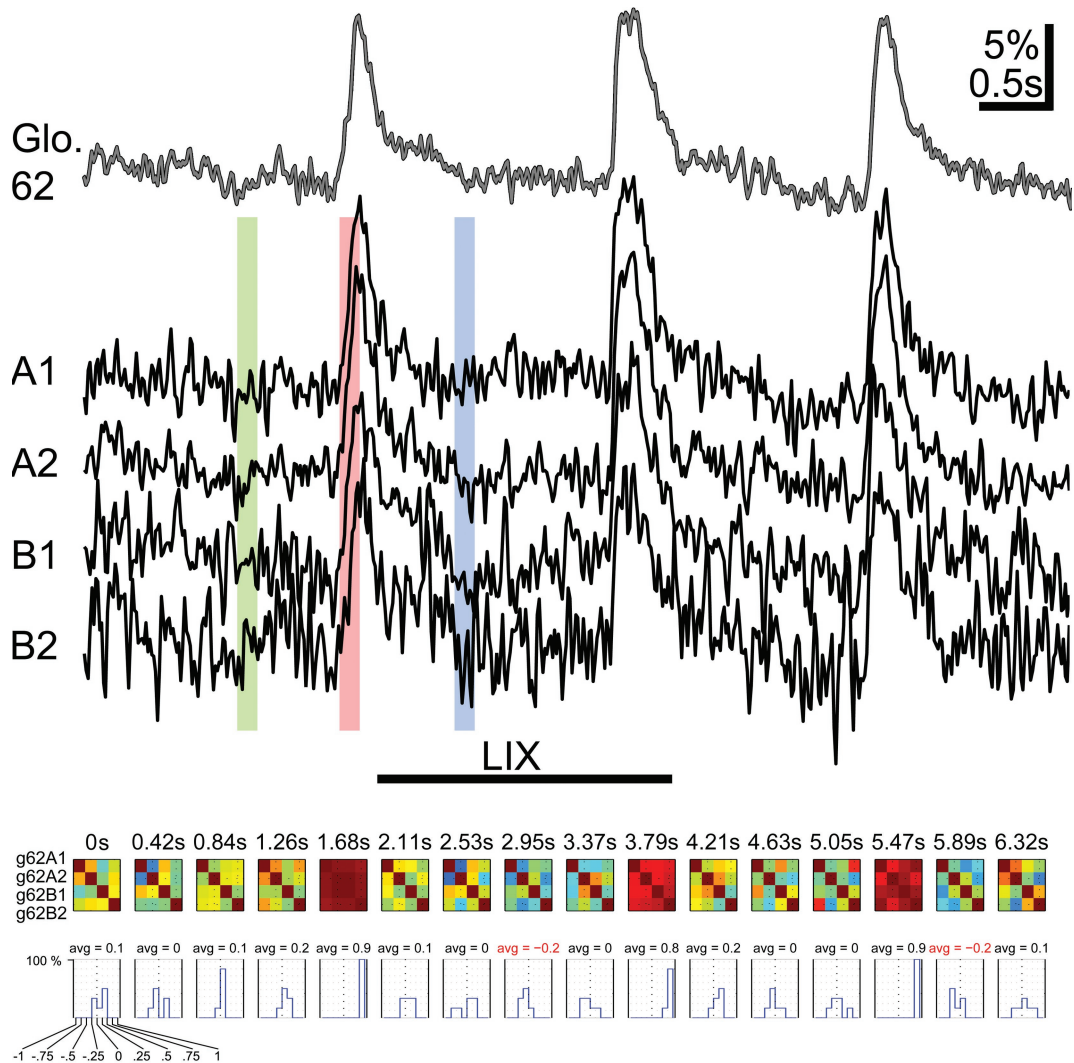
Figure 3.3.2: Exemplary recording traces from 2 PNs "A" and "B", each with 2 branches "1" and "2", from animal 7511_08. Odor stimulation with the odor LIX (horizontal bar with inscription) did not elicit a response. The topmost trace (gray) shows the spatially averaged glomerulus-wide signal. 4 traces below that show traces from the branches A1 through B2. Scale bar at top right of the figure indicates 5% $\Delta F/F$ (height) and 0.5 s (length). Rectangular color overlays mark (green) a phase of de-correlation, (red) a phase of strong correlation, and (blue) a phase of anti-correlation.

Row of cross-correlation matrices and row with histograms of correlation coefficients below the traces. Time index above the cross-correlograms. Branch descriptions at the left quote ['g' 'glomerulus number' 'neuron name' 'branch number']. Sequence in horizontal domain is (left to right) g62A1 to g62B2. Cold colors ≈ anti-correlation, green ≈ de-correlations, warm colors ≈ correlation. Horizontal arrangement of correlograms is in rough accordance with the time scale of the measurement traces. Average correlation between all branches is stated above the histograms. Bin size of histograms is .25. See tick labels below first histogram.

analyses performed in all 7 animals in which PNs could be identified.

3.3.3 Determining synchrony in pairs of recordings traces

Ultimately, the synchrony between sub-cellular processes will be described in this section. The level of synchrony between neuronal processes will be contrasted with the synchrony between glomeruli. The "Control" shows the amount of correlation in two traces that have not been recorded simultaneously. The amount of correlation and anti-correlation reported for the control represents the level of accidental synchrony between temporally unrelated traces.

3.3.3.1 Exemplary analysis of sliding window correlation traces

To visualize and analyze the correlation of measurement traces between sub-branches of PNs, I obtained the sliding window correlation between pairs of branches along all time points of a measurement. The sliding window correlation trace is a series of correlation coefficients that each result from the cross correlation of a small stretch of two measurement traces. The window is shifted along the original measurement traces in small steps, so that the stretches overlap. The temporal length of the stretches ("window size") has an important effect on the meaning and appearance of the resulting correlation trace. Very short time windows lead to large correlation and anti correlation values that alternate quickly between successive time points of the measurement. Synchrony of short term events and small baseline fluctuations of the calcium signals is represented in these correlation traces. Longer time windows lead to correlation traces that rather show the synchrony of strong, long lasting signals.

For this section of the results part it is important to differentiate between the terms correlation, de-correlation, and anti-correlation. The following list defines the terms in the context of the window correlation analysis:

- Correlation: The correlation coefficient of the observed stretch of the measurement traces is larger than zero. The signals in the two measurement traces are synchronous.

- De-correlation: The correlation coefficient of the observed stretch of the measurement traces is around zero. The signals in the two measurement traces are independent.

- Anti correlation: The correlation coefficient of the observed stretch of the measurement traces is smaller than zero. The signals in the two measurement traces are either synchronous but opposed, or there is a signal in one of the traces and none in the other.

Figures 3.3.3 and 3.3.4 on pages 140 and 141 contain examples of two pairs of raw measurement traces from an AIR measurement in preparation 7314_02 together with window correlation traces calculated at 5 different window sizes. These figures serve as examples for demonstrating the relation of pairs of raw $\Delta F/F$ traces to the correlation traces. In the following paragraphs, I will elucidate in length the features of the correlation analysis. This is crucial for the understanding of the cumulative analysis of data from identified neurons from several animals, which is presented in section 3.3.4 on page 146.

The $\Delta F/F$ traces in the top row of figure 3.3.3 are from two sub branches (d33B1 [blue] and d33B2 [green]) of the same identified neuron. Note that the three obvious spontaneous signals in the beginning, middle, and end of the measurement trace are synchronous and similarly shaped. In figure 3.3.4, one of the traces (d33B1 [blue]) is shown again, but together with a trace that was measured in another PN (d33D [green]). This pair of traces originates still from the same glomerulus, but now we are comparing neurons, nor sub-branches. Note that only some of the signals found in the trace from neuron d33B1 are present also in neuron d33D. The signal trace of PN d33D is not entirely different, but many deviations occur.

In both figures, the window correlations at five different time window sizes are shown (blue curves, window sizes from top to bottom: 8, 16, 32, 64, and 128 lines) below the $\Delta F/F$ traces. The green lines in the window correlation plots represent the correlation coefficients of differentiated signal traces and are of no further interest for the purpose of discussing the examples.

The shortest time window (8 samples, 105 ms kernel size) in figure 3.3.3, in which the sub-branches are compared, shows a high number of strongly correlated and anti correlated events. The average correlation of the raw signal traces from sub branches of the same PN is 0.156, standard deviation 0.490. The median correlation is 0.198, interquartile range 0.775. Thus the distribution of correlation coefficients is very broad and slightly skewed towards positive values. The pair of PNs from the same glomerulus, however, that is compared in figure 3.3.4, yields average and median values close to zero.

Figure 3.3.3: Correlation of signals in two branches of one PN within the same glomerulus (33). The measurement traces are from an AIR measurement (the same one as shown in the lower right panel of figure 3.3.1 on page 134). The upper graph shows the $\Delta F/F$ over time for the entire duration of the measurement (6.737s). One graph is drawn in blue, the other in green. The 5 graphs below the $\Delta F/F$ trace quantify the sliding window correlation between the two raw traces (blue) and between the differentiated traces (green).

Figure 3.3.4: Correlation of signals in two branches of two different PNs within the same glomerulus (33). The measurement traces are from an AIR measurement (the same one as shown in the lower right panel of figure 3.3.1 on page 134). The upper graph shows the $\Delta F/F$ over time for the entire duration of the measurement (6.737s). One graph is drawn in blue, the other in green. The 5 graphs below the $\Delta F/F$ trace quantify the sliding window correlation between the two raw traces (blue) and between the differentiated traces (green).

To test whether the median correlation coefficients and the interquartile ranges of pairs of measurements are a robust measure, I compared the distributions of correlation coefficients with 10,000 likewise calculated sets of correlation coefficients which were based on 2 x 10,000 fabricated traces of 512 random numbers each. Figure 3.3.5 on page 142 shows the distribution of mean and median values and the corresponding standard deviations and interquartile ranges. This was done for all 5 window sizes.
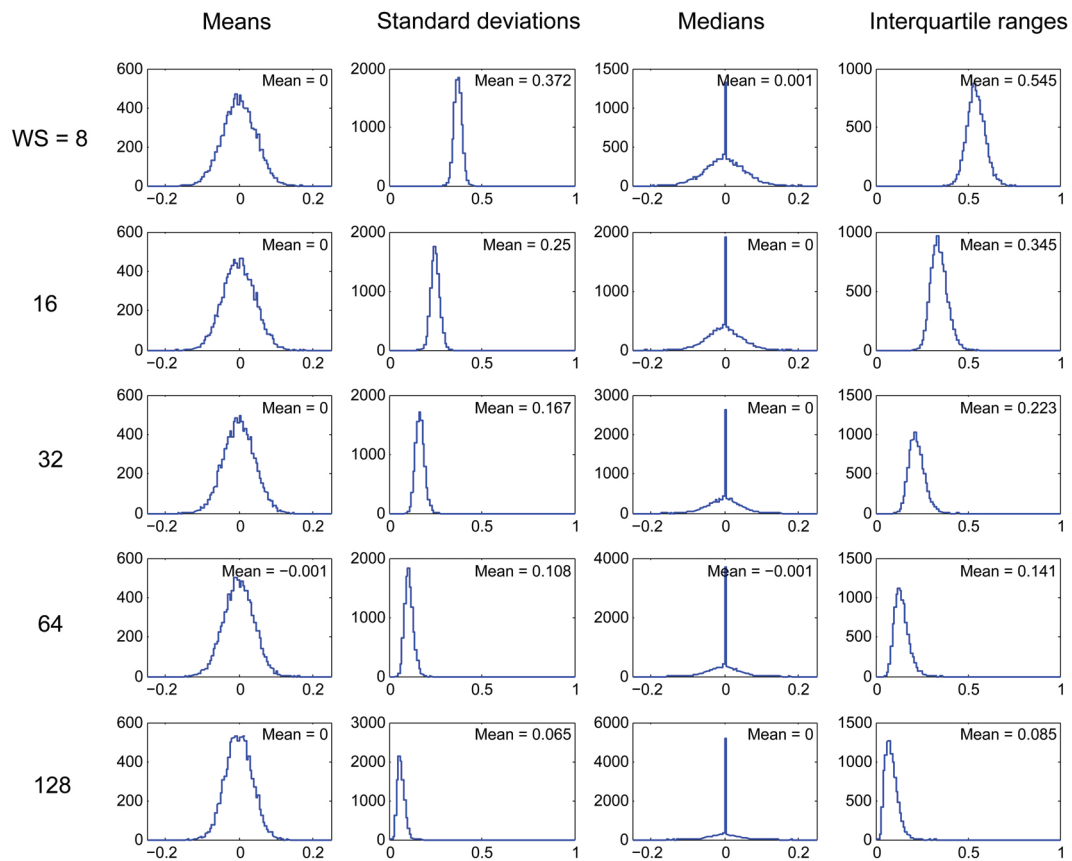
Figure 3.3.5: Means, standard deviations, medians, and interquartile ranges of the pairwise window correlation coefficients of a fabricated dataset of random noise.

The interquartile range of the correlation coefficients of the example traces shown in 3.3.3 on page 140 is 0.775 at a window size of 8. This is a larger value compared to the 0.545 that I determined for the same window size with pairs of random traces. *Thus the large amount of strongly correlated and strongly anti correlated phases in the window correlation is not due to noise.* The median correlation coefficient of 0.198 of the two example traces is in a range that is

unlikely to be have have happened by chance: as visible see in figure 3.3.5 on page 142 (distributions of median correlation coefficients at windows size = 8), a value of 0.198 or larger has been determined only in 2 out of the 10,000 pairs of random traces.

The correlation trace at a window size of 8 is largely determined by short term events. Small baseline signals that are synchronous lead to high correlation, asynchronous events to anti correlation. Larger signals do not stand out distinctively. The correlation trace shows that uncorrelated events are rare when two branches of the same neuron are compared. Rather, there is either strong correlation or strong anti correlation.

When two measurement traces from branches of separate neurons within the same glomerulus are compared, this picture changes. The $\Delta F/F$ traces in figure 3.3.4 on page 141 are from two branches (d33B1 [blue] and d33D [green]) of two different neurons. The raw signal traces show more deviations in the small baseline signals. The three large spontaneous signals that were rather congruent in the overlay of signals traces from branches of the same neuron, are not matched very well in this pair of traces.

The correlation trace at windows size of 8 still shows many correlated and anti correlated events. But the proportion of uncorrelated events is higher than in the comparison of branches from the same neuron. The average correlation of the raw signal traces from sub branches of the same PN is 0.003, standard deviation 0.493. The median correlation is -0.023, interquartile range 0.814. Thus the distribution of correlation coefficients is as broad as when comparing branches of the same PN, but not skewed in any direction.

In the larger window sizes, correlation between longer lasting signals is represented. Small baseline fluctuations in the measurement traces are represented less, so that synchronous signals of appropriate duration lead to more prominent amplitude changes of the correlation traces. The panels in the 3rd row of both figures discussed here show the correlation traces at a window size of 16 samples, corresponding to a kernel size of 211 ms. The average correlation between sub branches of the same PN is now 0.25, standard deviation 0.378. The median correlation is 0.232, interquartile range 0.58. The mean and median values of the correlation coefficients are larger at a window size of 211 ms compared to the results at a window size of 105 ms. When comparing branches from different PNs, the average correlation is now 0.066, the standard deviation 0.35, the median 0.04, and the interquartile range 0.489. Again, the spread of the

data is comparable, but the skewedness towards positive values is negligible.

In the 32, 64, and 128 samples long window sizes (corresponding to a kernel of 421, 842, and 1684 ms), the trend of higher skewedness and lower spread of the distribution of correlation coefficients is continued. The mean and median correlation values of branches from the same neurons get larger, the correlation values for branches from two different neurons stay small. With increasing window size the difference between the correlation traces of the differentiated measurement traces (green curves) vs. raw measurement traces (blue curves) becomes larger.

In the given example the analysis of mean / median correlation coefficient and the standard deviation / interquartile range values of the window correlation traces reveals differences in the measurement traces of separate neurons within the same glomerulus. Branches of the same neuron are more correlated than branches from different neurons. Nevertheless, not only correlation but also anti correlation can be observed in both cases. Even branches of the same neuron show many phases of anti correlation. During longer lasting and strong spontaneous signals (as opposed to short-term baseline fluctuations) the correlation is always high.

It is tempting to understand the baseline fluctuations as signals of local synaptic events on the dendrite of the PN, while the larger, longer lasting signals might be caused by back propagating spikes. It is intuitive that passively conducted currents of local synaptic events would lead to brief and locally constrained calcium influx/efflux events. The optic measurement of calcium concentration changes might not be suitable to fully resolve these single synaptic events, but the distribution of correlation / anti correlation events is different from the distribution that pure noise on the two measurement traces would cause. The large signals, which are usually strongly correlated between all PNs within the same glomerulus, are always positive (= calcium concentration increase), with quick rise-time, mostly phasic, and sometimes phasic-tonic. I never observed signals like this in the negative (= calcium concentration decrease) direction. This is in favour of (back propagating -) action potentials as the source of these signals.

For the analysis of the bunch of the data it is necessary to quantify and statistically test the correlation between sub structures within and between glomeruli. Median value and interquartile range of the sliding window correlation analysis are a simple, robust measure and thus a good starting point. Figure 3.3.6 on page
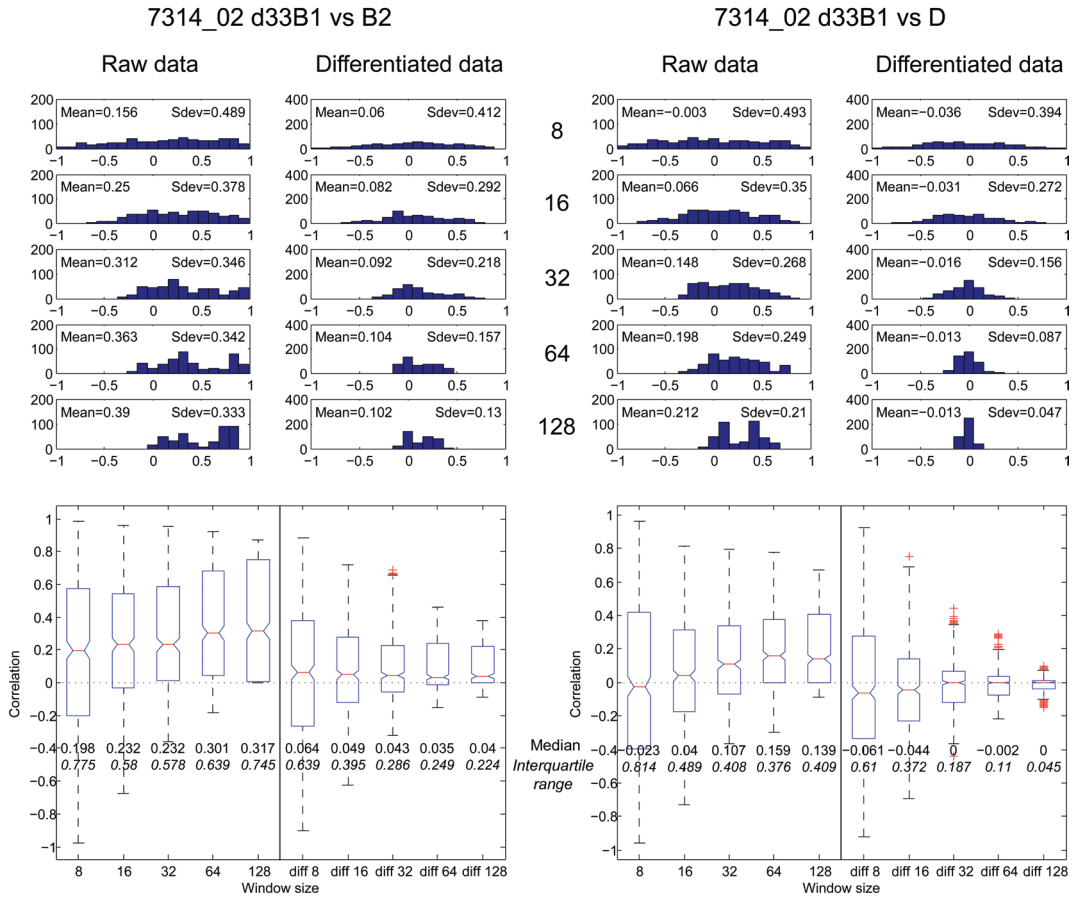
Figure 3.3.6: Visualizations of the distributions of correlation coefficients obtained by comparing the signals of sub branches in preparation 7314_02, AIR measurement 60. Left half of the figure: Comparison of two branches of the same neuron. On top, histograms of the sliding window correlation coefficients are shown for each part of the correlation analysis: the left column of histograms shows the distribution of correlation coefficients for all time windows (from top to bottom: 8, 16, 32, 64, 128) when comparing the raw measurement traces; the right column is based the differentiated measurement traces. Below, the same data is presented as series of box plots. The left 5 box plots show the distribution of correlation coefficients from the comparison of raw measurement traces (from left to right: time windows 8, 16, 32, 64, 128); on the right the same analysis has been done on differentiated measurement traces. The right half of the figure shows the identical analyses performed on data from two branches that belong to two different neurons within the same glomerulus. Within the sub figures, the mean, standard deviation ("Sdev"), median, and interquartile range values are quoted.

145 concludes for the given example of the AIR measurement in preparation 7314_02 how the correlation measure changes with the different window sizes; both for the analysis based upon raw data and differentiated measurement traces.

When comparing the left and right halves of that figure, it becomes clear that the correlation of the two measurement traces from sub branches of the same neuron is higher than the correlation of sub branches from different neurons. This is true for all correlation window sizes, irrespective of the kind of data that the analysis is based upon (raw or differentiated) and irrespective of the two methods to visualize the distributions (histograms or box plots).

With other words: The demonstration showed that the traces of correlation coefficients are well suited for the visual detection of correlation and anti correlation in the pair of measurement traces. The mean value of the correlation trace is a good measure for general similarity of the two traces that were compared. Thereby, short time windows stress extract the similarity of the baseline fluctuations and brief signals, while longer time windows detect synchronous, pronounced signals.

The sliding window correlation algorithm SWCA (described in section 2.6.1 on page 78 in the methods part) has been written with the aim to extract not a mean measure of synchrony, but to quantify events significant correlation and anti-correlation. The next section describes the results from the SWCA analysis.

3.3.4 Quantification of results from SWCA reveals synchrony

The responses in multiple reconstructed PNs within the same glomerulus do not differ fundamentally. But, as demonstrated in the presentation of the exemplary measurement traces above (section 3.3.3 on page 138), subtle differences do exist, and these differences are not due to noise. Otherwise, no difference in the correlation could be observed between branches from the same vs. branches from different neurons. The examples also show that even between branches belonging to the same neuron, the correlation is not absolute. In visual inspection, the correlation traces reveal three sources for incomplete synchrony in the pair of raw signal traces: (1) one of the two branches carries a signal, while the other does not; (2) a signal that is present on both branches is not synchronous;

(3) the sign of a signal on one branch is inverted on the other branch (e. g. there is a synchronous, but antipodal signal). Interestingly, significant correlation or anti-correlation is sometimes not accompanied by one of the three phenotypes described above, but it can occur in absence of signals on any of the traces. Close inspection of the traces reveals that during these episodes, the phase of the otherwise independent and noise-like baseline fluctuations are either in phase or out of phase during the relevant time window.

The Sliding Window Correlation Algorithm detects episodes of significant correlation and anti-correlation, and counts the absolute number of such events into bins (see section 2.6.1 on page 78 in the methods part). As opposed to the extraction of a single descriptive variable (like mean correlation) for each pair of traces, this approach makes sure that correlation and anti-correlation do not cancel each other out.

I want to compare the levels of correlation in 5 time windows during each measurement. The time windows, or phases, are defined by the onset and offset of the odor stimulus (see section 2.5.2 on page 74 in the methods part). The SWCA sorts the counts of correlation and anti-correlation each into 5 bins according to the phases of the measurement. The correlation is expressed as percent significantly correlated time points vs. all other time points during the current phase. There are 4 different kinds of pairs of traces, for which I implemented the nomenclature Branches, Neurons, Glomeruli, and Control in section 2.6 on page 76 in the methods part.

When combined with the signal indices determined by the Template Correlation Algorithm (TCA) (see section 2.4.2 on page 61 in the methods part), it is possible to dissect the counts for correlation and anti-correlation further. I was interested to see if the relative amounts of correlation between the different phases of the measurements would change if only episodes of (1) signals of excitation, (2) signals of inhibition, or (3) no signal were compared. To begin with, I will walk you through the analysis of correlation in un-dissected measurement traces, so the correlation scores originate from stretches of measurement traces irrespective of occurrence of signals, they are merely binned according to the temporal phases during the measurement.
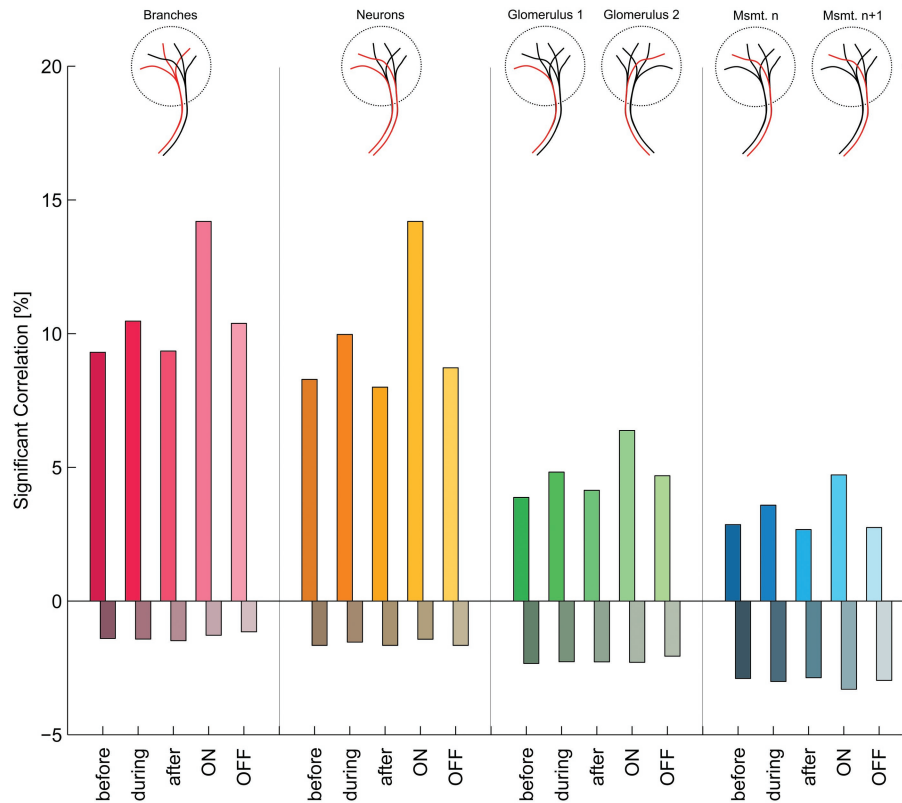
Figure 3.3.7: Percentages of measurement samples that are significantly correlated or anti-correlated. The 4 blocks of 10 bars summarize the correlation for each of the 4 kinds of pairs; the schematic drawings above the bar graph show which of the blocks belongs to which pairing. The 10 bars in each block visualize the percent significant correlation in each of the temporal phases of the measurement. Positive values are used for significant correlation, negative values and darker colors are used for significant anti-correlation. The bars are labeled according to the nomenclature introduced in the methods part, section 2.5.2 on page 74.

The measurement traces were not further subdivided by their signaling state, so these bars show the cumulative percentages of correlation and anti-correlation during odor-evoked and spontaneous signals as well as during inhibition and rest.

3.3.4.1 Quantification of correlation in whole recording traces

Figure 3.3.7 on page 148 shows the 40 numeric values that result from the comparisons between 4 kinds of pairs of branches. For each pairing, 10 values of % significant correlation and anti-correlationare are shown.

The red bars show for each temporal phase of the measurements the amount of significant correlation between Branches. "Before" and "After" the odor stimulus (1st and 3rd bar), 9.30% and 9.35% of measurement samples are significantly correlated. The odor stimulus increases the amount of correlation to 10.46% ("During"). In the short time window "OFF" after the odor stimulus, the correlation is 10.38%. The highest correlation is reached in the "ON" time window (14.19%). Thus, the odor stimulus leads to an increase in correlation between Branches. No difference between the correlation Before and After is imprinted onto the Branches by the odor stimulus, the scores are equal. In the ON time window, which coincides with the onset of odor-evoked signals, the correlation is higher than in the rest of the During time window. This translates into the notion that the odor stimulus leads to synchronous activation of the Branches especially at the signal onset. In the OFF phase, the correlation is as high as in the During phase, but lower than during the ON phase. In the comparison of the % significant anti-correlation, the phases ON and OFF score the lowest: 1.28% and 1.15% vs. 1.40%, 1.42%, and 1.48%. Taken togehter, the transition phase at the beginning and end of the odor stimulus evokes at the same time high correlation and low anti-correlation in Branches.

The yellow bars that conclude the significance values for the Neurons within the same glomerulus show a similar trend. The temporal phases ON and During score 9.97% and 14.19% significant correlation; these values are comparable to the values obtained in the comparison of Branches. Obviously, the common input to the glomerulus synchronizes branches from distinct neurons up to the same level as Branches. In the Before, After, and OFF phases, however, the correlation is lower (8.29%, 8.00%, and 8.72%). Symetrical to the lower scores for significant correlation, the anti-Correlation scores are higher in all temporal phases (mean of all phases 1.59% vs. 1.35% in Branches). As opposed to the situation in Branches, where the anti-correlation score is the lowest in the OFF phase, the anti-correlation score in the OFF phase of Neurons is exactly as high as in the Before and After phases: 1.66% to 1.66% to 1.66%. Thus, the OFF phase that imposed correlation as in the During phase in the Branch comparison and

simultaneously reduced the amount of anti-correlation, is less effective when distinct neurons are compared.

If compared with the red and yellow bars, the green bars appear like shrunken versions thereof. The bars show a similar relation of the correlation scores between the different phases of the measurements, but the bars are generally lower: The mean score for significant correlation in the Before, During, and After phases is 4.28% in Glomeruli vs. 9.70% in Branches and 8.75% in Neurons. If the neurons that are hosted in distinct glomeruli were completely independent, one would assume the there should be as much correlation as anti-correlation. This would be so especially in the Before phase, when no odor-evoked RN activity could impose simultaneous signals in the glomeruli that are compared. But the Anti-correlation score of 2.33% is much lower than the corresponding correlation score of 3.87%.

In the blue bars, however, of the signal traces that are compared are completely independent, because the pair of traces originates from two successive measurements (but from the same neuron/branch). Thus the correlation scores in the blue bars may serve as a Control: (1) these bars show the amount of false positive correlation and anti-correlation, and (2) they would reveal potential skewedness towards correlation or anti-correlation of the SWCA. Optimally, the correlation score in the Before phase should be identical to the anti-correlation score. This is the case: the correlation score is 2.86%, the anti-correlation score is 2.89%. In the During and ON phases, pseudo-correlation can be obsserved: PNs respond to several of the odor stimuli which were alsways delivered at the same relative time during the measurement. They appear correlated, because on both traces, a signal may have been evoked. The opposite effect can also be observed: PNs that do neither respond to all nor to none of the odor stimuli display pseudo-anti-correlation in the During and ON phases, because pairs of traces are compared in which a signal on one trace coincides with no signal on the other trace.

3.3.4.2 Quantification of correlation during signals of excitation

Figure 3.3.8 on page 151 shows the correlation scores that have been determined as described above, but only episodes of the measurement traces with an excitatory signal on either of the traces were used.

Most obviously, when compared to the same bars in figure 3.3.7 on page
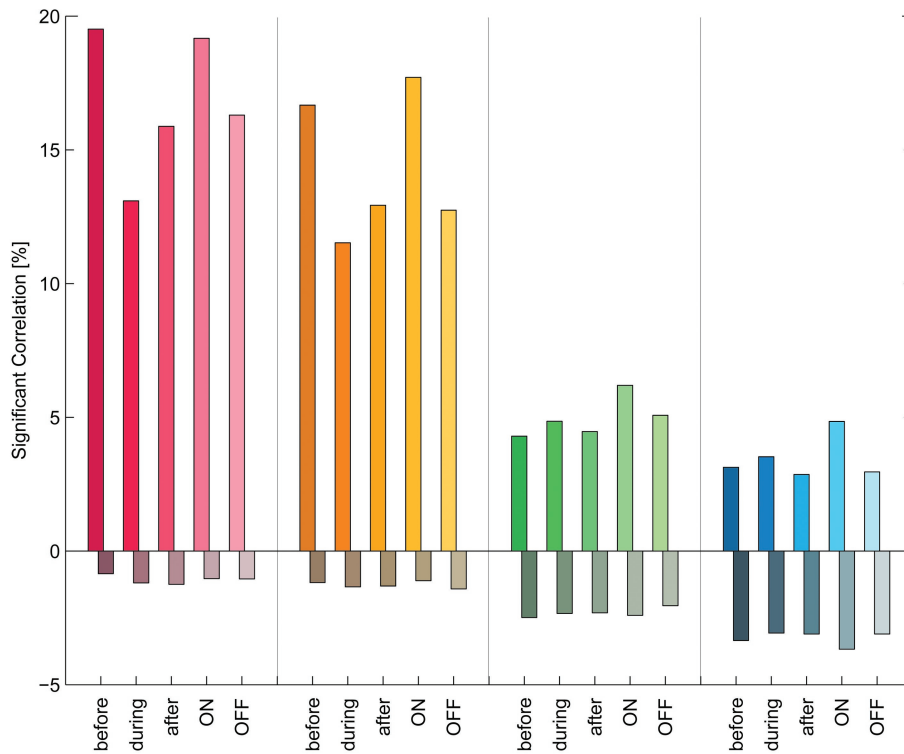
Figure 3.3.8: Please refer to the legend of figure 3.3.7 on page 148 for a description of the groups of data shown. In this graph the % significant correlation and anti-correlation have not been determined on the basis of the complete measurement traces, but only the episodes with excitatory signals (as detected by the TCA (see methods part section 2.4.2 on page 61) were evaluated in each of the temporal phases of the measurements.

148, the correlation scores are higher in the two within-glomeruli comparisons between pairs of Branches (red) and pairs of Neurons (yellow). Higher correlations scores were expected in the comparison of episodes carrying signals, because visual inspection of numerous exemplary pairs of traces (as shown in the figures 3.3.3 and 3.3.4 on pages 140 and 141) revealed that episodes of the measurement traces carrying signals were are often accompanied by high correlation scores.

The values reported by the green bars that conclude the correlation scores for comparisons between glomeruli, however, are indistinguishable from their siblings in figure 3.3.7: neither the average amplitudes of the phases Before, During, and After differ (4.53% for the excitatory signal episodes vs. 4.28% for all episodes), nor is the relation between the correlation scores changed. Both groups of bars indicate low correlation Before and After the odor stimulus and enhanced correlation During the odor stimulus and especially at odor ONset. The same is true for the blue bars. The mean amplitudes are comarable (3.17% vs. 3.04%, calculated from Before, During, After as above), as are the relations between the bars within each group.

The relations between the temporal phases in the within-glomerulus pairs Branches and Neurons, on the other hand, are different from the relations shown in figure 3.3.7. If only episodes carrying signals of excitation are compared, the correlation scores in the Before and After phase is higher than the correlation in the During phase, and as such inverted towards the relationship of the phases reported before. This result is extremely important, because it directly implies that *the synchrony of PNs during spontaneous signals is higher than the synchrony during odor-evoked signals.* This result also tells us an important fact about the signals in the phase After odor offset: the signals observed during this 2 second interval are obviously still influenced by the odor stimulus. They are not (or not all), spontaneous. Otherwise the synchrony would be identical to the level of synchrony detected in the Before phase. The enhanced synchrony of spontaneous vs. odor-evoked signals is not only found in the comparison between Branches, but also a characteristic of the pairs of Neurons and Branches within the same glomerulus. The scores of significant anti-correlation are lower during episodes of excitation as compared to complete recording traces; this shows that pairs of measurement traces in which at least one of both carries an excitatory signal rarely develop antipodal signals.

Conclusion: spontaneous PN signals are more synchronized than odor-

evoked signals. The synchrony is strong within all PNs hosted by the same glomerulus. The de-correlation of PN signals during the odor stimulus occurs not only between distinct neurons, but even between Branches of the same PN.

3.3.4.3 Quantification of correlation during signals of inhibition

Figure 3.3.9 on page 153 shows the correlation scores that have been determined as described above, but only episodes of the measurement traces with a signal of inhibition was detected on either of the traces.
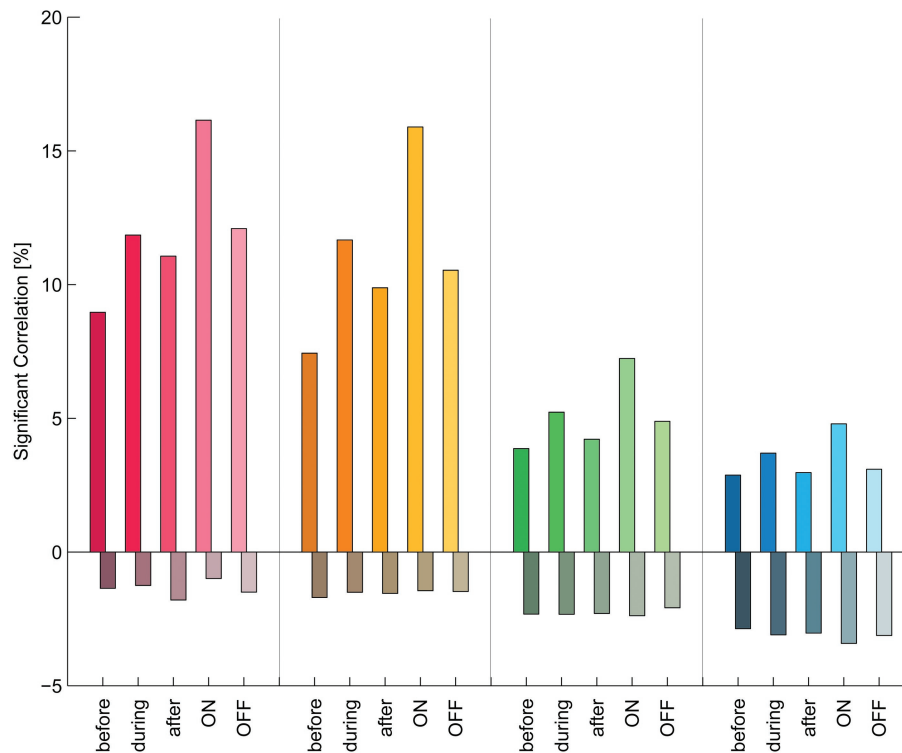
Figure 3.3.9: Please refer to the legend of figure 3.3.7 on page 148 for a description of the groups of data shown. In this graph the % significant correlation and anti-correlation have not been determined on the basis of the complete measurement traces, but only the episodes with signals of inhibition (as detected by the TCA (see methods part section 2.4.2 on page 61) were evaluated in each of the temporal phases of the measurements.

The relation of the bars within each group resembles the arrangement that we saw in figure 3.3.7 on page 148, where the correlation analysis did not exclude any signaling episodes, with one exception: The scores of significant correlation are reduced in the phases Before the odor stimulus in both groups of bars show-

ing within-glomerulus correlations (red and yellow). In figure 3.3.8 on page 151, in which only episodes of the measurement traces with an excitatory signal were evaluated, this temporal phase was the phase with the highest correlation scores. Obviously, the trend towards high correlation in spontaneous excitatory signals is inverted if only signals of inhibition are evaluated. This inversion continues in the During phase, where reduced synchrony was reported for the excitatory signals: inhibitory signals are correlated more strongly in the phase During odor stimulation as compared to Before and After.

To conclude: the odor stimulus leads to an increase of the synchrony of inhibitory signals. The synchrony of spontaneous signals of inhibition is low both when Branches or Neurons are compared.

3.3.4.4 Quantification of correlation in absence of detectable signals

Figure 3.3.10 on page 155 shows the correlation scores that have been determined as described above, but only episodes of the measurement traces without any signal on either of the traces were compared.

Strikingly, significant correlation still occurs also in the episodes between signals. The relative amplitudes of the bars shown in this graph are similar to the bars in figure 3.3.7 on page 148, where the correlation analysis did not exclude any signaling episodes, but the scores appear to be generally reduced. Thus, also if no detectable signal is induced, PNs display enhanced correlation in the During and ON phases. The episodes of the measurement traces where no signal occurred obviously do not contain only noise, otherwise there would not be a difference in the correlation scores between groups or between the scores of significant correlation and significant anti-correlation. Interestingly, one difference between the groups that was apparent in all of the other correlation analyses, namely the higher correlation scores of the Branches group compared to the Neurons group, is not present here.

3.3.4.5 The correlation window size does not matter

As mentioned in the methods part, section 2.6.1 on page 78, several **window sizes** were tested before finally the size of 16 samples was chosen for the correlation analysis. As mentioned there, the relative differences between the groups of data are not altered by the window size. This is shown in figure 3.3.11 on
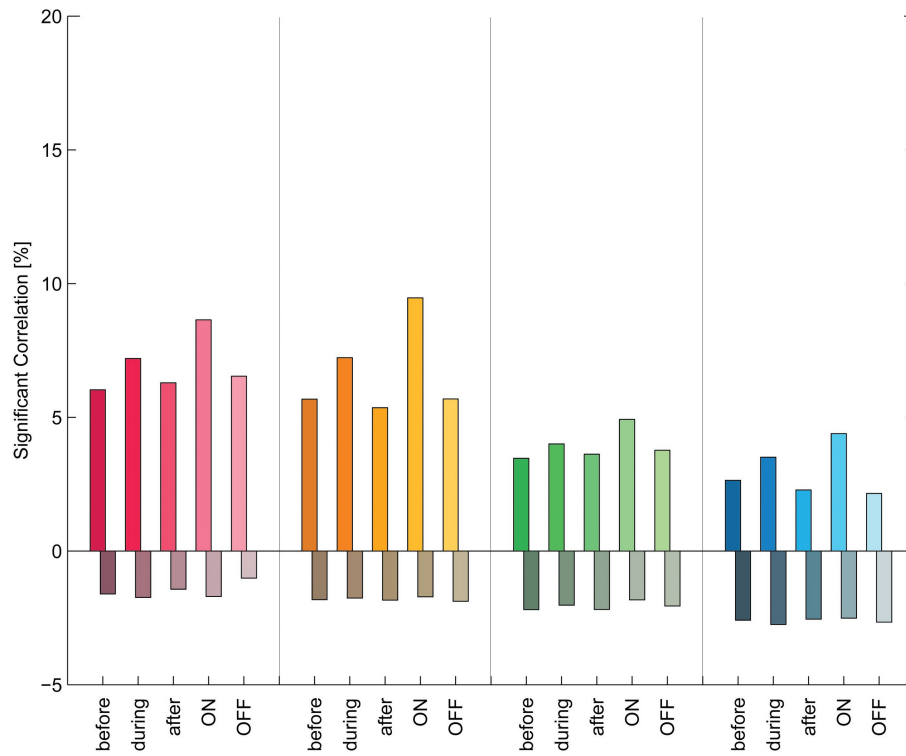
Figure 3.3.10: Please refer to the legend of figure 3.3.7 on page 148 for a description of the groups of data shown. In this graph the % significant correlation and anti-correlation have not been determined on the basis of the complete measurement traces, but only the episodes without a signal on any of the traces (as determined by the TCA (see methods part section 2.4.2 on page 61) were evaluated in each of the temporal phases of the measurements.

which concludes the effect of the windows size on the % significant correlation and anti-correlation.

3.3.4.6 Low-pass filtering abolishes group differences

When estimating parameters for the SWCA, I tried several kinds and strengths of **filtering of the raw data** before the correlation analysis. The assumption that led me to search for the optimal filtering was that correlations would get stronger when noise in the measurement traces was reduced by filtering. But, and this is an interesting finding in itself, any kind of filtering annihilates the difference between the two groups Branches and Neurons. All other relative differences between the groups and between the temporal phases are reduced as well. At the same time, the correlation scores are increased.

Figure 3.3.12 on page 158 shows the result of the SWCA after filtering of the raw data with a temporal running average of 4 samples (52.6 ms kernel size). Such a filter acts like a low-pass. Visual inspection of measurement traces that were smoothened in this way suggests that only noise is reduced by the filtering, while the fundamental properties of the signal (e. g. slopes, latencies, amplitudes) appear unchanged. But obviously one fundamental property of ON signaling is changed by low-pass filtering. This control demonstrates that the difference between the correlation of Branches and Neurons lies in exactly the high-frequency component of the raw signal traces that is destroyed by filtering. A part of the noise-like high-frequency signal component carries information that allows the SWCA to differentiate between processes that belong the the same neuron vs. processes that belong to distinct neurons.

The frequency range that this signal component occupies can be isolated: according to the Nyquist-Shannon sampling theorem the frequency cannot be higher than half of the sampling frequency of 76 Hz; the frequency is very likely higher than the cut-off frequency of a 4-samples running average filter, which is $1/0.0526$ s $\approx$19 Hz. Thus, the signal component that enables the SWCA to differentiate between Branches and Neurons must be in the range of 19-38 Hz.

3.3.4.7 Conclusion of the correlation analysis

The SWCA revealed a number of striking results that shall now be summarized.

- Odor-evoked signals of excitation within the same glomerulus are less
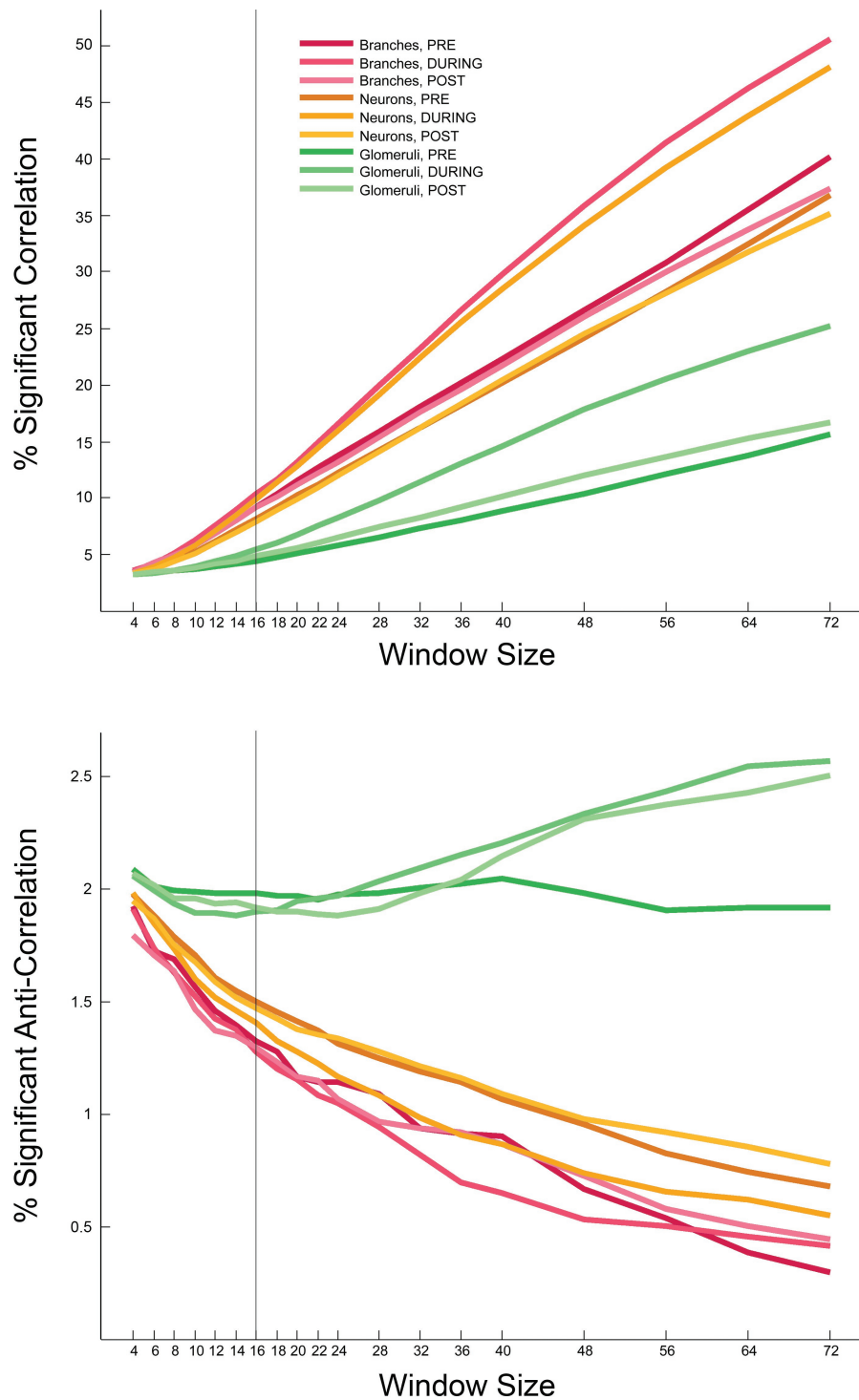
Figure 3.3.11: % significant correlation and anti-correlation in Branches, Neurons, and Glomeruli in the measurement phases Before, During, and After odor stimulation. The window size of 16 samples that was finally used for the SWCA is marked by a thin vertical line. Control and the temporal phases ON and OFF are ommitted for clarity. Please note that the scales differ between the lower and upper panel.

Branches :: Neurons difference is annihilated by filtering

All signaling states

Signals of excitation

Signals of inhibition

No signals
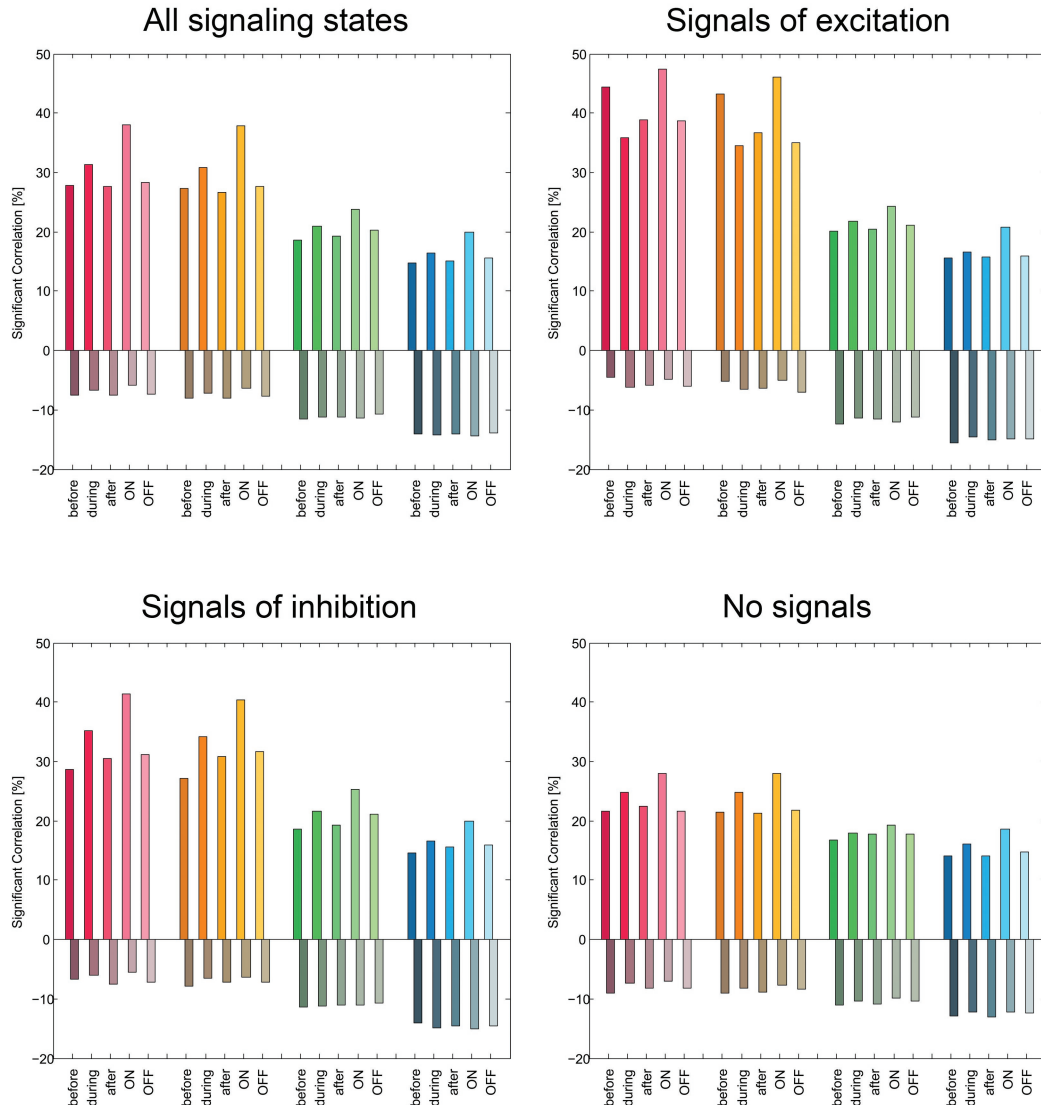
Figure 3.3.12: % significant correlation and anti-correlation after filtering with 4 sample sliding average filter. Please refer to the legend of figure 3.3.7 on page 148 for a description of the groups of data shown. This graph displays for all separate signaling episodes (see inscription above the bar graphs) the resulting correlation scores after filtering. Please not that the scale of the abscissa is different than in the previous graphs of this type.

correlated between branches and neurons than spontaneous excitatory signals.

- Odor-evoked signals of inhibition within the same glomerulus are more correlated between branches and neurons than spontaneous inhibitory signals.

- After the odor stimulus, signals are not (or not all) spontaneous, but yield correlation scores that lie in between the scores reached before and during the odor stimulus.

- Also in absence of signals on any of the pair of measurement traces, significant correlation is detectable.

- In none of the analyses did the SWCA produce skewed correlation scores.

- The difference in correlation scores between Branches and Neurons is sensitive to filtering of the raw data. A signal component in the range of 19-38 Hz is crucial for differentiation between Branches and Neurons.

- The relative correlation scores reported by the SWCA are insensitive to the window size used for the window correlation. The window size only affects the absolute magnitude of correlation.

3.3.4.8 % Correlation scores tabulated

For the numerical data behind the bar graphs 3.3.7, 3.3.8, 3.3.9, and 3.3.10 on pages 148, 151, 153, and 155 please refer to table 3.3.1 on page 160.

Before	During	After	ON	OFF	Mean*	Description
9.30	10.46	9.35	14.19	10.38	9.70	Branches, Corr, All
1.40	1.42	1.48	1.28	1.15	1.43	Branches, Anti, All
8.29	9.97	8.00	14.19	8.72	8.75	Neurons, Corr, All
1.66	1.54	1.66	1.43	1.66	1.62	Neurons, Anti, All
3.87	4.82	4.14	6.37	4.68	4.28	Glomeruli, Corr, All
2.33	2.27	2.27	2.29	2.06	2.29	Glomeruli, Anti, All
2.86	3.58	2.67	4.71	2.75	3.04	Control, Corr, All
2.89	3.01	2.87	3.30	2.97	2.97	Control, Anti, All
19.51	13.09	15.88	19.17	16.30	16.16	Branches, Corr, Ex
0.85	1.19	1.25	1.03	1.04	1.10	Branches, Anti, Ex
16.67	11.52	12.93	17.71	12.74	13.71	Neurons, Corr, Ex
1.18	1.34	1.31	1.11	1.42	1.28	Neurons, Anti, Ex
4.29	4.85	4.46	6.19	5.07	4.53	Glomeruli, Corr, Ex
2.49	2.34	2.31	2.41	2.05	2.38	Glomeruli, Anti, Ex
3.13	3.52	2.86	4.84	2.95	3.17	Control, Corr, Ex
3.35	3.07	3.11	3.67	3.10	3.18	Control, Anti, Ex
8.96	11.85	11.06	16.14	12.09	10.62	Branches, Corr, Inh
1.36	1.25	1.80	0.99	1.50	1.47	Branches, Anti, Inh
7.44	11.67	9.88	15.89	10.54	9.66	Neurons, Corr, Inh
1.70	1.51	1.54	1.45	1.48	1.58	Neurons, Anti, Inh
3.87	5.23	4.21	7.23	4.88	4.44	Glomeruli, Corr, Inh
2.32	2.33	2.30	2.38	2.08	2.32	Glomeruli, Anti, Inh
2.87	3.70	2.97	4.79	3.09	3.18	Control, Corr, Inh
2.86	3.10	3.03	3.42	3.12	3.00	Control, Anti, Inh
6.02	7.20	6.29	8.64	6.53	6.50	Branches, Corr, Rest
1.61	1.74	1.43	1.70	1.02	1.59	Branches, Anti, Rest
5.68	7.22	5.36	9.46	5.68	6.09	Neurons, Corr, Rest
1.82	1.76	1.83	1.71	1.88	1.80	Neurons, Anti, Rest
3.47	4.00	3.62	4.92	3.77	3.70	Glomeruli, Corr, Rest
2.20	2.03	2.19	1.82	2.06	2.14	Glomeruli, Anti, Rest
2.64	3.50	2.28	4.38	2.15	2.81	Control, Corr, Rest
2.59	2.75	2.55	2.51	2.66	2.63	Control, Anti, Rest

Table 3.3.1: Numerical data of % significant correlation in five temporal phases during the measurements, as sohwn in figures 3.3.7, 3.3.8, 3.3.9, and 3.3.10 on pages 148, 151, 153, and 155. No temporal filtering was applied to the raw data. The column "Description" indicates the level of comparison, **Corr**elation or **Anti**-correlation, and the signaling state (**All** states, only **Ex**citation, only **Inh**ibition, **Rest** = no signals).
* Mean is calculated from the phases Before, During, and After.

Part 4

Discussion

161

4.1 Spontaneous activity is a characteristic of PN signaling

I expected high levels of spontaneous activity and traces of inhibition to be encountered in linear scan recordings with 2PLSM. The wiring rules and the physiological data from electrophysiology suggested that PN responses are delayed, complex, and phasic, and that spontaneous activity is strong. Bursty spontaneous activity of PNs has been demonstrated before with electrophysiological (Sun *et al.* 1993; Müller *et al.* 2002; Krofczik *et al.* 2008) and optophysiological (Sachse and Galizia 2002; Sachse *et al.* 2006) methods. Unforeseen was the finding in this thesis that signals recorded during odor stimulation were so similar to spontaneous signals.

The results from the automated signal registration algorithm CSA show that spontaneous activity is a characteristic of PNs *per se*. The duration, amplitude, regularity, and frequency of spontaneous burst-like signals appears at the same time homogeneous and variable across glomeruli and test animals. The distributions of the extracted parameters are broad; the glomeruli and animals are alike in the broad range and variability of each of the extracted parameters.

I analyzed the relation between parameter pairs, firstly for frequency and regularity, secondly for amplitude and duration. Frequency and regularity appear coupled such that in a glomerulus or animal that displays a high frequency of spontaneous signals, also the regularity is high. The regularity measure was designed and tested such that it extracts relative, not absolute deviations of the train of signals from perfect regularity; thus the measure itself is frequency-independent. The reported correlation between frequency and regularity is therefore not trivial. Expressed the other way round, the likelihood to register a signal at the exact time point predicted by the time point of the previous signal and the average signal frequency rises disproportionally with the frequency of spontaneous signals. During odor stimuli, however, it is the other way round: now the regularity is generally somewhat higher, and the regularity actually rises when the frequency of signals falls.

The distribution of the signal parameters amplitude and duration are also broad. The finding that during the time window of odor stimulation the constant $\approx$200 ms signal duration and the $\approx$2.5 standard deviations signal amplitude that were already found during spontaneous activity are retained, is the most important and most unexpected result of the analysis of amplitudes and durations. Otherwise, there was a negative correlation of amplitude and duration of signals when the data were averaged per animal, but not when data were average per glomerulus. Thus, there appears to be a parameter that defines the relation of amplitude and duration of signals, and this parameter acts on the level of test animals, not on individual glomeruli.

Taking together the findings that (1) spontaneous activity matches in frequency, signal amplitude, and signal duration the activity during odor stimulation and (2) odor-evoked signals are only rarely phasic tonic but rather temporally complex, we have to draw the conclusion that the AL network transforms the representation of odors between RN input and PN output in a more fundamental way than hitherto assumed.

4.2 Odor-response-profiles of PNs *are* variable

The next section elucidates the repercussions of the comparatively high level of spontaneous on odor coding. The odor-response-spectra found here will be compared to the functional AL atlas. The methods 2PLSM, electrophysiology, and wide-field imaging will discussed with regard to the odor-response spectra reported.

Spontaneous activity was not an issue in the generation of data for the functional AL atlas (Galizia *et al.*, 1999c), because the response profiles there were acquired by imaging of bath-applied Calcium Green 2AM (Galizia *et al.*, 1998). The calcium imaging signal obtained with Calcium Green 2AM reflects the activity of RNs, but the slow kinetics of the signals and confocal images of brains stained with Calcium Green 2AM suggest that this signal is indirectly conveyed by the glial cells that ensheathe the AL neuropil. Both the fact that RNs are the source of the signals and the slow kinetics of the signals explain why no spontaneous signals can be detected with this technique.

As a control for the data obtained with the 2PLSM I tried to reproduce glomerular odor response patterns as they are reported in the functional AL atlas. For this analysis to be a valid control of the data obtained here, I calculated odor responses as in Sachse and Galizia (2002), where the same dye was used, but the measurements were performed with a wide-field fluorescence microscope. The atlas that I show in the results part (figures 3.2.21 and 3.2.22 on pages 123 and 124) can reproduce the fundamental findings of the publications on odor coding in the honeybee AL, namely the facts that glomeruli are activated by several of the test odors, and that each of the odors elicits responses in several of the glomeruli tested. Some of the glomeruli were activated by some odors with high reliability. This occurred preferentially in those combinations of odors and glomeruli that the atlas predicts.

The reliability of odor-evoked responses is however low. One trivial reason for this lies within the partly low number of animals per glomerulus. I concentrated on glomeruli 17 and 33 and mostly on odors that activate these glomeruli in my study. I obtained measurements in other glomeruli merely for the sake of

completeness and to justify the concentration on few glomeruli. The reliability that the frequently measured glomeruli 17 and 33 display shows how reliable the odor responses can get if odors that activate the glomeruli are comprised in the odor set and if enough animals are measured.

Another reason for low reliability is the maladaptation of the way in which responses are registered in the first step of the calculation of reliability and response strength. In this step, peak amplitudes are compared between the odor stimulation time window and the time window before odor stimulation. This worked well for Sachse and Galizia (2002), whose method I used here for the sake of comparability. Spontaneous signals appear smaller in amplitude in wide-field imaging. I will discuss in the next section possible reasons for this. In 2PLSM linear scan data, however, spontaneous signals reach the same amplitudes as odor-evoked signals. If the aim of this study were to characterize odor-response-spectra of the glomeruli tested, thereby exploiting all information on the temporal development of signals and including signals of inhibition, one would need to devise a different way to detect and to quantify odor-evoked responses. The examples of measurement traces that were given in sections 3.2.2.3 on page 125 *et secc.* illustrate what kinds of signals an adapted response detection algorithm would need to capture: obvious to the human eye, there are changes in glomerular signaling that are in temporal relationship to the odor stimulus. The changes occur (1) simultaneously with inversed sign in different glomeruli and/or (2) in temporal succession with inverted direction in the same glomerulus. Both phenomena occurred in the examples and were also otherwise characteristic for glomerular signaling: one glomerulus increases its rate of bursty signals, while another glomerulus is inhibited; one glomerulus responds with phasic on-responses to an odor stimulus but the phase of silence thereafter prevents the response in this glomerulus from contributing to a globally enhanced signal frequency or amplitude. A functional 2PLSM atlas that bundles the whole spectrum of odor-evoked signals would be incompatible with the published one, because a 2PLSM atlas would require more than one descriptive number per glomerulus; furthermore, to preserve the various response types that have been encountered in odor-glomerulus-combinations across several test animals, one would need to work with lists, rather than averages. It would be problematic to translate between the atlases The predictions that such an atlas makes would be likelihoods rather than certainties. Thus the informative value, notwithstanding the huge density of information within the atlas, would be

low. For these reasons I refrained from attempting to compile a new, functional 2PLSM atlas of glomerular odor-response-profiles.

Last but not least, it is a common finding in publications on the electrophysiology of PNs that a certain fraction of neurons recorded do not conform to the odor response spectrum that the innervated glomerulus is supposed to express according to the functional AL atlas. Müller *et al.* (2002) reported that lACT PNs, while displaying broader odor-response-spectra than mACT PNs, responded to less odors than the atlas predicts. Galizia and Kimmerle (2004) recorded intracellularly 9 PNs and stimulated with a panel of 8 odorants. In 2 glomeruli, no complete comparison with the atlas was possible because the odor response profiles of these glomeruli do not contain data for all of the odors used. 3 out of the remaining 7 PNs responded in concordance with the atlas. Further 2 PNs responded to an additional odor that was not expected. One PN did not respond to one of the odors that should have, according to the atlas, elicited a response. One PN did not respond to any of the odors. Also in the work of Menzel *et al.* (2005), intracellular recordings were compared to the honeybee AL atlas. The authors report that, as a general trend, the response spectra found in imaging experiments are broader than the response spectra of single PNs. Only in combinations of odor and glomerulus that yield, according to the atlas, a response of >50% of the maximum for the respective glomerulus, PNs responded reliably to the respective odor.

In the electrophysiological studies cited above, one neuron was recorded at a time. It was thus unclear if the remaining PNs that innervate the same glomerulus as the recorded neuron would show different sensitivities or deviant odor-response-spectra. In the 2PLSM recordings that were used for the creation of odor-response-spectra, responses from all (or almost all) PNs that innervate a glomerulus were accumulated by spatial averaging. The differences between the data recorded here and the atlas are still qualitatively similar to the deviance found in electrophysiological studies: additional responses to odors that are not predicted by the atlas occurred, e. g. the responses in glomerulus 33 to the odorant HX1; lacking, on the other hand, is for instance a clear preference of glomerulus 47 for the odor LIO. Therefore, linear scan 2PLSM recordings of whole glomeruli resemble sharp electrode recordings of single lACT PNs. Accumulating signals from many PN within one glomerulus does not lead to a more atlas-conform overall odor-response-spectrum as compared to single PN recordings. On the other hand, in this study, the congruity of the reported

odor-response-spectra increases with number of animals that were measured for a given glomerulus. It should thus be considered that the finding of complexity and aberrant odor responses in intracellular recording studies may be the result from (1) high temporal resolution, which makes complexity detectable in the first place, and (2) a low number of animals and trial repetitions. Or, expressed inversely, the extensive concordance of glomerular odor-response-profiles that is found when imaging studies are compared is primarily the result from a large number of animals and test trials. 2PLSM data, when analyzed in glomerular units, reflects the atlas-like patterns most properly in glomeruli that have been measured often and in many animals. Example traces from the 2PLSM and odor-response-spectra that are based on a low number of animals, however, resemble the situation in electrophysiological studies, where aberrant findings are not averaged out.

To conclude, glomerular odor-response-spectra obtained in this study resemble the spectra that are reported in the honeybee AL atlas, notwithstanding the problems mentioned of the data evaluation approach and the apparent complexity of responses. This proves that the 2PLSM produces measurement results are not fundamentally different from, but merely more rich in information than wide-field fluorescence imaging recordings. I consider this result a validation of the 2PLSM technique as it was used here. Technical considerations on the differences between wide-field imaging data and 2PLSM recordings are discussed in section 4.3.1 on page 169.

"Complexity" is not randomness

The analysis of glomerulus-wide signal by use of a 2PLSM reveals temporal complexity that has not been anticipated. I pointed out in the previous section that the odor-response-spectra can still be detected with previously used methods despite of the background of strong spontaneous activity. Generating nervous signals, however, is costly; repressing spontaneous signals is in theory easily achieved within the nervous system. Therefore we must assume that the complex signals that occur both during spontaneous activity as also during the time window of odor stimulation must have a functional role.

The complexity in spontaneous activity and during the odor stimulation time window is potentially not random. The odor specific temporal response shapes shown in section 3.2.2.5 on page 130 of the results part demonstrate that tem-

porally complex responses can be reproducible. This finding points towards a coding scheme that exceeds the concept of odor coding in glomerular patterns of activity (Galizia and Menzel, 2000). The phenomenon shown there implies that not only the glomerular pattern of activity, but that also temporal patterns of activity within glomeruli might be a means to code for odor quality. Odor coding in temporal patterns has been discussed in the literature, but in most studies the latency of responses was evaluated rather than the development over time (Müller *et al.* 2002 Krofczik *et al.* 2008). Quantification of complexity is an almost impossible deed, firstly because until now there was not enough data at hand with sufficient temporal resolution for the analysis of specific temporal patterns. Examples for suspicious temporal patterns can e. g. found in the publications from Sun *et al.* (1993), Müller *et al.* (2002), and Galizia and Kimmerle (2004), where either neurons that innervate the same glomerulus displayed deviant temporal patterns between animals, or the response characteristics differed between consecutive presentations of different odors, as in my example. But these are more or less anecdotal findings. However, even when a large body of data is at hand as in this thesis, the question remains of how one can approach an understanding of the apparent complexity. I already mentioned the effort that would be needed to generate a functional atlas that relates several response shapes and signals of inhibition to specific odor-glomerulus-combinations. The information density in such an atlas would be enormous, but the explanatory value potentially low. What is lacking is obviously not more data of the same kind, but supporting information on e. g. the behavioral relevance of spontaneous activity, the source of it in terms of network connectivity, and information on the readout system. I will propose how to approach this issue in section...

4.3 Methodological considerations on the amount of spontaneous activity

Complexity and amount of spontaneous activity and activity during the time window of odor stimulation appear stronger in the 2PLSM recordings as compared to other recording methods. In this section I will elaborate explanations for this discrepancy. I will try to convince you of my presumption that the characteristics of PN signaling reported here represent with high fidelity the real situation, while electrophysiology and wide-field imaging are prone to drawing a simplified picture.

4.3.1 Spontaneous activity in 2PLSM vs. wide-field imaging: Imaging is slow

Why is spontaneous activity not captured in its entirety by wide-field fluorescence imaging with the same dye FURA2? Firstly, the temporal complexity in the responses to certain stimuli would not have shown up in recent analyses of the glomerular odor code in PNs (e. g. Sachse and Galizia 2002), because the measure for activity used there was usually the peak amplitude during the stimulation time window. Such an approach is blind to temporal complexity. Secondly, the average duration of spontaneous and odor-evoked signals has been determined to be $\approx$200 ms on the basis of my data, and this might still be overestimated because of artificial gain in recorded signal duration which might be induced by the dye FURA2 (see below). 200 ms is equal to the time per frame that is being used in wide-field imaging at a frame rate of 5 Hz. Frequencies of 5-6 Hz have been used in all studies that applied wide-field imaging to honeybee ALs. The likelihood for a 200 ms signal to be registered with its full amplitude is low under these circumstances, because in most cases the signal will fill a fraction of two measurement frames, with a decrement in registered amplitude that is inversely proportional to the fraction of the signal episode that is captured in the respective image.

Secondly, the frequency of spontaneous signals is too close to the frame rate that is commonly used in wide-field imaging. Wide-field fluorescence imaging is usually performed with a frame rate of 5 Hz (Peele *et al.* 2006; Sachse *et al.* 2006) or 6 Hz (Sachse and Galizia 2002; Sachse and Galizia 2003). Spontaneous signal frequency of 2.5 Hz there would be, on average, one half-signal in every frame of the measurement. The resulting signal would at best show a sawtooth pattern, in which the amplitudes are subject again to the fit of the signal into the illumination time window.

A third argument for the maladaptation of wide-field imaging with the dye FURA2 for recording spontaneous activity concerns the dye and its calcium binding properties. Is is often stressed in publications as the imaging papers cited above, that the frame rate be enough to capture PN signals; this is then justified with the notion that the release of calcium from the dye, which defines how fast the measured signal returns to baseline irrespective of the real declining slope of the signal, is so slow in case of FURA2 that a higher recording frame rate would not reveal any additional information on cellular calcium levels, and thus activity. This means that a fundamental limitation of the combination of FURA2 and wide-field-imaging exists which prevents fast signals from being detectable. This is not so in 2PLSM, even if the same dye is used! (This notion will be pondered further below, in the section on calcium.)

4.3.2 Spontaneous activity in 2PLSM vs. electrophysiology: Temperature matters

Even if compared to temporally high-resolving electrophysiological data, the levels of spontaneous activity reported in this thesis appear very high. PNs were recorded with sharp electrodes e. g. in Sun *et al.* (1993), Müller *et al.* (2002), Galizia and Kimmerle (2004), and Krofczik *et al.* (2008). All of these studies also observed that the spontaneous activity of PNs is not regular and homogeneous as in RNs (Akers and Getz, 1992), but that bursts of action potentials alternate with longer periods of no activity. Judging from the traces that are shown in the figures of those publications and reasoning from the data evaluation methods, the spontaneous activity that occurred in all of the studies mentioned must have been lower, and thus the repercussions of odor stimuli were often more clearly

visible in the recoding traces shown.

Temperature is an important factor for spontaneous activity

So why is the observed spontaneous activity in this study stronger as compared to electrophysiology both in terms of frequency and in terms of amplitude? An important factor may be the room temperature. It is well possible that a certain critical temperature must be reached for strong spontaneous activity to occur. Honeybees actively generate high thoracial temperatures of >30 °C, for example while flying (Roberts and Harrison, 1999), foraging, and attack (Heinrich, 1979). Also inside of the hive, where a temperature of ≈35 °C is maintained by the bees, the brains are warmer than in the typical imaging setup, where the animals cannot raise their body temperature above room temperature through movements of the flight muscles and, more importantly, abdomen movements which pump warm hemolymph from the thorax into the head capsule. I chose a stable temperature of 27±0.5 °C for my experiments. This temperature is a closer to the temperature maintained by the bees themselves, but still not too far away from the room temperature that was chosen as the background in other imaging studies; therefore my data are not entirely incomparable to the data reported in other imaging studies. But the higher temperature can explain the richer spontaneous activity.

The high amount of spontaneous signals is thus caused by (1) the higher temperature at which the recordings were obtained, and (2) by the enhanced detectability of brief spontaneous signals due to the high temporal resolution available in linear scans. Thus the spontaneous activity is not an artifact; rather did the low room temperature in most of the studies cited impose artificially low levels of spontaneous activity.

4.3.3 Calcium imaging of the dye FURA2: Fast only when a 2PLSM is used

This section explains why FURA2, which is a high affinity calcium chelator and as such normally displays a very slow rate of calcium release, is faster when imaged with a 2PLSM.

Is is often stressed in publications that report on wide field imaging that low frame rates of ≤6 Hz suffice to capture faithfully the calcium signals as

they are reported by the dye. This claim is justified; calcium sensors share the characteristic that calcium binding has a shorter time constant than calcium release. Especially the high-affinity dyes like FURA2, which are approaching saturation of the signaling range already at intracellular calcium concentrations of 1 μM, have long dissociation constants (Molecular Probes Fura and Indo Ratiometric Calcium Indicators, Product Information (2005), and see figure 2.1.2 which shows the dose-response curve of FURA2 with various calcium concentrations in the methods part on page 38), leading in the worst case to signals that appear longer than the underlying fluctuation in calcium concentration. A higher recording frame rate would thus not reveal any additional information on cellular calcium levels. In wide-field imaging, the dye rather than the frame rate define how long the reported duration of signals is, and how steep the declining slope at the end of the signal is.

FURA2::calcium complex is dissociated by the pulsed laser

The large signals with fast decay times shown in this thesis prove that FURA2 has shorter decay times when recorded in a 2PLSM. This is not only demonstrated by the brief decay times of exemplary signals, but also by the fact that the duration of signals is independent on signal amplitude. A possible explanation has been provided by Valeur and Leray (2000), who reviewed commonly used fluorescent molecular sensors with respect to their photochemistry. According to this study, the FURA2::calcium complex is much less stable in the photo-excited state. It is speculated that the calcium binding cavity of the dye molecule might even invert its charge and get positively polarized while the dye is excited with a strong pulse of light. By such way, 2-photonic, focused IR laser radiation might be very effective in dissociating the dye::calcium complex; wide-field imaging, on the other hand, does not reach the required spatio-temporal illumination intensity, because (1) the light is not pulsed, and (2) because a field of view rather than a focal spot is illuminated. Thus, while the dissociation constant of FURA2 defines the decay time of calcium signals in wide-field imaging, in 2PLSM a correlation between signal duration and the amount of excitation light might exist. We attempted to illuminate all test animals with similar parameters. The pulsed IR laser was kept at an output power of roughly 400 mW, and the focal power was further attenuated using the Pockel's Cell to a value of 20-25 mW. Nevertheless, it has been reported in this thesis that the signal duration

at rest is to a part a function of the test animal, and the explanation for this observation might be small differences in incident light intensities.

It shall be mentioned that the photo-activated calcium ejection is not a common finding, but specific to the dye. Yaksi and Friedrich (2006) performed 2PLSM imaging experiments in zebrafish with the calcium sensors Oregon Green 488 BAPTA-1 and rhod-1 and simultaneous electrophysiology. He noted that the decline of signals always had a fixed slope with both dyes used. Conversely, the combination of 2PLSM with the dye FURA2 is an especially lucky one.

To conclude, the brevity of cellular calcium transients is obviously reproduced by FURA2 with high fidelity, thanks to the photo-induced ejection of calcium from illuminated dye molecules.

The amplitude of calcium signals is not trustworthy

Interpretation of recorded calcium signal amplitudes is a complicated story. It may be that the measured signal amplitude does not faithfully reflect the absolute calcium concentration changes. The measured signal amplitude is subject to...

- ...the volume of the cellular compartment that is analyzed.

  Assuming (1) that calcium enters the cell *via* channels in the plasma membrane, (2) that the calcium concentration increase is a local phenomenon of the cytoplasm close to the membrane (because calcium is e. g. chelated, actively removed, and diluted once it enters the cell) and (3) that the calcium sensor FURA2 is distributed evenly in the cytoplasm, the relation between surface and volume of a cellular compartment can influence the signal amplitude. The signal that is measured in imaging of FURA2 is a compound signal originating from hundreds of FURA molecules distributed in a volume of typically 0.5^3 μm^3 of cytoplasm. The relative amount of FURA2 molecules that bind calcium compared to a certain baseline is the determinant of signal amplitude. In a large volume of cytoplasm, it may be that a fraction of FURA molecules can not sense the calcium concentration increase which is strongest at the plasma membrane. As a consequence, we must conclude that the broad range of signal amplitudes observed in this study might in part be explained by differences in the mean local volume of PNs in the measurement area. That the signal am-

plitudes appear rather constant within the same animal and glomerulus is in accordance with this argument.

- ...the concentration of FURA2 molecules.

The amount of dye taken up by the retrogradely staining of PNs is variable from preparation to preparation. ALs with different staining intensity in different glomeruli have been observed. The concentration of dye differed also between glomeruli within the same animal. The distribution of dye in the stained cells, the binding properties, and the cellular calcium kinetics should not be correlated with the number of dye molecules in a given volume; a non-linearity in the correlation of calcium concentration and fluorescence intensity might, however, be induced by a floor-effect: At a given illumination intensity (and, as pointed out above, I attempted to keep the illumination intensity constant at all times), neurons with a low staining intensity can only be visualized with higher detector gain. Higher gain does not necessarily lead to enhanced image contrast, because the brightness of unstained background structures is increased with a higher factor than the stained neurons. During measurements of calcium signals, I did not want to alter the characteristic (i. e. use the logarithmizer stage) of the analog signal amplifier (see section 2.1.3 on page 34 in the methods part), because doing so would have induced further non-linearities in the measurement system. Therefore, the contrast in space and in time of neurons with lower staining intensity was lower, which in turn registers as reduced maximal signal amplitude, thus capping of large signals.

Very high staining intensity can, conversely, induce a ceiling-effect. When working with bright stainings, I reduced the sensor gain with the aim to obtain the same mean brightness of the resulting images as obtained in other stainings. The noise level was then obviously lower. At the absorption wavelength stimulated with the IR laser (see methods part section 2.1.7.1 on page 36), FURA2 fluorescence intensity drops when calcium is bound. The lower background noise levels let the dark parts of the recorded images appear darker than in the average preparation, so signals appear enlarged due to less capping as compared to darker stainings.

To conclude, the correlation of calcium concentration and the signal ampli-

tude reported by the measurement system might be non-linear; therefore the range of signal amplitudes is not necessarily indicative of different calcium concentrations in the cells. The amplitude differences between animals and glomeruli might instead be the consequence of non-linearities caused by the factors discussed above. Differences between amplitudes of consecutive signals measured in the same glomerulus of the same animal, however, are more trustworthy and, last but not least, prove that calcium signals are indeed graded, and that the measurement system can detect this.

4.4 Source of signals: Action potentials vs. synaptic calcium

In this section I will elucidate the source for the two amplitudes of signals that were regularly observed in 2PLSM recordings. In all recordings, there were large, more or less uniform signals and smaller, more variable signals. Smaller signals were observed as deflections towards higher or lower % $\Delta F/F$, i. e. signals of excitation and inhibition. The larger signals were always signals of excitation. Are there separate sources for the calcium concentration fluctuations that underly the two (or three) basic signal forms? Answering this question requires more knowledge about the PNs than 2PLSM alone can convey, therefore (1) results from studies that combined calcium imaging with electrophysiology and (2) studies in which PNs were analyzed in primary culture with a range of treatments will be consulted.

Calcium imaging has been combined with electrophysiological recordings in a few published studies, e. g. in honeybee (Galizia and Kimmerle, 2004), zebrafish (Yaksi and Friedrich, 2006), and drosophila (Jayaraman and Laurent, 2007). The combination of methods reveals the nature of the correlation between calcium signals and action potentials; but please note that such correlations are valid only under identical conditions, e. g. microscopic technique and target brain areas / cell types. Unfortunately, the honeybee-study Galizia and Kimmerle involved a room temperature of 22 °C (this temperature was controlled within the head capsule through steady flow of cool saline) and imaging data were obtained in a wide-field fluorescence imaging setup. Furthermore, electrophysiological recordings were not obtained simultaneously with the imaging recordings. Thus the results can not be directly compared to the data obtained in this thesis. Nevertheless all three of these studies reported that there is a correspondence of action potentials and calcium signals. The studies conducted by Yaksi and Friedrich and Jayaraman and Laurent calculated the relation of action potentials and calcium imaging signal amplitudes, yielding exact formulae which were demonstrated to allow extrapolating the number and temporal arrangement of

action potentials from calcium signals. Therefore I assume that action potentials are detectable also in 2PLSM recordings in the honeybee. Even if the action potentials would not be temporally resolvable, it seems likely that signals obtained in the 2PLSM would be based on trains of action potentials.

But, as mentioned above, the analysis of signal parameters (results part sections 3.2 on page 92 *et seqq.*) showed that at least two populations of signals are detectable in the recordings, one with large, ≈200 ms long, burst-like signals, and one that comprises smaller signals of more variable durations. I tend to sort signals of inhibition into the latter group as well, because the amplitudes of signals of inhibition and smaller excitatory signals match. There is potentially a third class of signals, which will become apparent in the discussion on the SWCA analysis. For the time being it suffices to remind you of the 19-38 Hz signal component which is most synchronous within branches that belong to the same neuron. I will discuss in length the results from that analysis in section...

It is tempting to assume that the large, uniform signals in my recordings are signals caused by spikes, or, more precisely, by back-propagating action potentials. The smaller, graded signals might be signals of dendritic post-synaptic calcium influx. That the large signals are constant in their duration, while the the small, synaptic signals cover a large spectrum of durations, is in accordance with this hypothesis. The hypothesis is also in line with figure 3.2.8 on page 101 in the results part, where the distributions of amplitudes and durations are displayed as a scatter plot. This plot shows that the distribution of signal durations is broader for the smaller signals. One factor does not fit with the proposed hypothesis: There no large and long signals. If action potentials generate strong, short calcium signals, then a train of spikes would cause a pronounced and long calcium signal, and such signals are rare in the scatter plot in figure 3.2.8! Thus, is is advised to ponder alternative explanations.

(1) "**All is spikes**": The signals represent in their relative amplitude bursts with different rates of action potentials; synaptic potentials do not lead to detectable signals. The assumption of a constant spike rate and count in the burst-like signals has to be made, otherwise this interpretation would not explain the homogeneity of large calcium signal amplitudes and durations. A finding that argues against this explanation are the clear signals of inhibition which prove that more signals than only action potentials are detectable with 2PLSM. Nevertheless, these signals might be brief breaks in an otherwise constant background spike rate. Nevertheless, the assumption of constant spike

rate and burst duration is not in accordance with reports on the electrophysiology of PNs; as mentioned earlier, the spontaneous and odor-evoked bursts of action potentials found there were not homogeneous.

(2) "**Synaptic potentials are larger**": The ratio between calcium signal amplitudes of action potentials and synaptic potentials might be the other way round. Barbara *et al.* (2008) demonstrated that the nACh receptor that is found in primary cultures of honeybee AL neurons is not kation selective, and that the ratio of calcium to sodium permeability was 0.54. Thus, synaptic calcium influx might evoke a large increase in dendritic calcium. This increase might be stronger than the increase in intracellular calcium through voltage gated calcium currents (Grünewald, 2003), which are supposedly triggered by back-propagating action potentials. Christensen *et al.* (1993), finally, demonstrated in the moth *Manduca sexta* with intracellular recordings of AL interneurons, that a depolarization of the membrane potential of 20 mV is caused by electrical stimulation of the antenna even when action potential generation is suppressed through injection of negative currents. Thus, also synaptic input that does not lead to action potentials can potentially activate voltage gated calcium channels, which is in line with an observation made in Menzel *et al.* (2005), namely that only when the functional honeybee AL atlas states an odor-evoked signal of >50 % of the maximum signal recorded in this glomerulus for a given odor, one reglarly finds increased spike rates in intracellular recordings of PNs during stimulations with that odor. However, this interpretation cannot explain the large amplitude of spontaneous signals. Spontaneous signals are unlikely to be evoked by cholinergic neurotransmission from RNs, because the presynaptic cholinergic RNs do not exhibit the bursty nature of spontaneous signals that is seen in PNs. The spontaneous activity would thus be less complex if RNs were the driving force behind them. Furthermore, if the largest signals in the recordings were the signals induced by direct RN neurotranmission, then I should observe more tonic signal components, because it is known that RN responses are phasic-tonic (Akers and Getz, 1992).

All three interpretations lack an explanation for the sparseness of long, pronounced, odor-evoked signals. Otherwise, the first explanation offered has the least number of arguments against it. Conclusively, the most likely explanation for the observed signal amplitudes that evolves from the above considerations is that...

- ... large signals correspond to voltage gated calcium influx into the PN dendrite caused by back-propagating action potentials,

- ... smaller signals of excitation are caused by dendritic calcium influx mediated by either cholinergic conductances or voltage-gated calcium channels that are activated by strong postsynaptic potentials,

- ... signals of inhibition are caused by either a pause in calcium influx through cholinergic RN synapses (involves inhibition of the RN synapse!) and/or by hyperpolarization of the PN-dendritic membrane and thus reduced calcium influx through voltage gated calcium conductances.

Assumptions which are implied in the above interpretation are:

- Direct tonic neurotransmission from cholinergic RN synapses is rare,

- tonic spike trains are rare in PNs (at least at a temperature of $27°$ C!),

- calcium influx into PN dendrites is constant, but prone to inhibition (otherwise inhibition would not be visible in calcium signals).

4.5 SWCA reveals how synchrony of PN signals develops during stimulation

I will now discuss the analytic value of the SWCA analysis. The descriptive texts that accompany the correlation score bar graphs in section 3.3.4 on pages 146 and following are already exhaustive, so correlation scores or specific bars in the figures will not be indexed here. In this section, the predictive value of the analysis as a whole for the AL network will be determined. Let me quickly recollect the wording, which must be held specific in this context: by "groups" I refer to the groups of comparison, i. e. comparison between pairs of branches from the same neuron; or comparison between processes of neurons that reside in different glomeruli. "Signaling states" are the episodes during pairs of recording traces with a certain characteristic as determined by the TCA, i. e. stretches of recording traces that carry signals of inhibition, excitation, or no signal. "Temporal phases", lastly, refers to the five phases of each measurement, as they are defined by the odor stimulus, namely before, during, after, ON, and OFF.

Synchronization is not mediated by RN input

A recurrent finding across many groups and signaling states is the enhanced correlation during the time window of odor stimulation, especially during the first 500 ms. One might assume that this enhanced correlation were result from concerted RN input that leads to synchronized activity in PNs. But SWCA shows that this is not so: If odor-evoked RN input were the synchronizing force within the AL, why then are the correlation scores of spontaneous excitatory signals before the odor stimulus higher than the scores of excitatory signals that occur during the time window of odor stimulation? The proposed effect of synchrony invoked by RN input might be the driving force behind the high correlation score in the ON phases, but in the during phase (which actually contains the ON phases the first 500 ms of its 2 seconds duration!) the correlation is still lower than in absence of an odor stimulus. Conversely, the synchronizing

180

effect of the odor stimulus is apparent only in signaling episodes of inhibition and rest.

It will be discussed in length in the next section what level of the AL network de-correlates signals of excitation during the time window of odor stimulation, and why (see section 4.6 on page 184). Now the source of synchrony in absence of signals of excitation shall be pondered.

How is synchrony detected in the first place, if signals of excitation do not occur on either of the traces that are compared? For reference, study figure 3.3.2 on page 137 of the results part once more; there are many examples for high synchrony in absence of strong signals hidden in the exemplary traces. The key to finding them is (1) choosing *ad libitum* a red pixel in any of the 16 cross-correlograms, (2) memorizing the two branch names of the PN processes compared here, and (3) and scanning the respective pair of traces from PN processes for episodes where the noise like baseline signal oscillates in synchrony. This kind of correlation, or synchrony, is not a random encounter, but dependent on and enhanced by the odor stimulus. The fact that the odor-elicited synchrony enhancement is seen even if all correlation scores of all pairs of traces of one group are averaged makes this a general finding. Which parts of the AL network could mediate such an effect?

> ### Synchronization is mediated by the global inhibitory network

Obviously, because we excluded the RNs as source for synchrony due to the fact that they would cause signals of excitation, synchrony must be mediated by LINs. It has been hypothesized that there are two inhibitory networks, one GABAergic global, unspecific one that interconnects all glomeruli, and one specific, histaminergic local one that interconnects primarily small groups of glomeruli that are activated by similar odorants (Sachse and Galizia 2002; Linster *et al.* 2005). The global network is consists presumably of a large number of GABAergic hetero-LINs (Abel *et al.* 2001; Sachse and Galizia 2002) that each receive input from RNs in one glomerulus and convey their output to PNs in all (or many) other glomeruli. Hetero-LINs are most likely polar, and receive input in the densely innervated glomerulus (Galizia and Kimmerle, 2004). Thus the inhibitory output synapses are situated in the sparsely innervated glomeruli. The local inhibitory network has been assumed to be histaminergic, but Barbara *et al.* (2005) did not find histamine-induced currents in primary culture of AL

neurons, a notion that provoked the notion that histaminergic LINs might synapse onto RN terminals. Inhibition of presynaptic RNs, however, would not induce synchrony in PNs. I thus conclude that evidence exists that the GABAergic global inhibitory network causes the synchronization of PNs during episodes of rest. This interpretation is in accordance with the fact that also during signals of inhibition, the synchrony is stronger in the time window of odor stimulation. It is indeed most likely the global LIN input itself that causes both synchrony and inhibition in glomeruli that do not get excitatory input from RNs.

This interpretation could easily be verified by a similar experiment as the one described in this thesis, but using PTX to block GABAergic neurotransmission. I predict that, after application of PTX, synchrony levels during episodes of rest will be generally reduced. I furthermore predict that less signals of inhibition will be detected; this is trivial.

No trace of reciprocal inhibition of similar glomeruli

If pairs of glomeruli with mutual inhibition are accessible to the method applied here, I should be able to find anti-correlation between responses in pairs of PNs that are housed in different glomeruli. This anti-correlation should be strongest during odor stimulations. If the PN output synapses at the integrative segments of the glomeruli are the driving force for this LIN network, spontaneous signals should be anti-correlated as well. Assuming that RN::PN synapses are rare, and that inhibitory networks are activated from the spontaneous signals in RNs, anti-correlation should be detectable even in the recording phase before the odor stimulation.

Linster *et al.* (2005) proposed a network that reciprocally inhibits glomeruli with similar odor-response-profiles. With a computer model she could show that such a functional inhibition network explains the differences found between odor-response-spectra obtained from widefield imaging of a RN-based signals vs. PN-based signals. No experimental evidence exists as yet for the physical basis of this network.

Can evidence for mutual inhibition between glomeruli be found in the data presented here? The mode predicts that, while one glomerulus is active, one or several others would be simultaneously inhibited. Thus the action of the network would cause anti-correlation which would be strongest during odor

stimuli. As the results from the SWCA analysis show, this effect cannot be found. The anti-correlation scores for pairs pf PNs from distinct glomeruli are not higher during odor stimulation as compared to before or after.

Thus, based on the data acquired in this thesis, I conclude that mutual inhibition is either not existent in the honeybee AL, or not dependent on odor stimuli.

4.6 Correlation scores reveal constitutive reciprocal PN::PN inhibition

I now want to test two postulates on signals in multiple PNs within the same glomerulus which were mentioned in the introduction. Thereby I will elucidate why excitatory signals in PNs are less synchronized during the time window of odor stimulation as compared to spontaneous signals. Both postulates imply that the individual PNs generate independent output signals:

1. **Single PNs are deviant, but the summed signal matches with the functional atlas**

   Galizia and Kimmerle (2004) speculated, based on the finding of deviations in signal time courses in two PNs recorded in two animals in the same glomerulus, and based on deviation of the odor response profile in single PNs that they measured ("deviations" implying: different from the glomerular odor response profiles reported in the functional AL atlas), that these deviations might be indicative of individual odor-response-spectra of the PNs within one glomerulus, and that these different response spectra might be averaged out, generating the response spectrum that the atlas claims, as soon as all PNs from the same glomerulus were summed up.

2. **Odor learning mediates reciprocal inhibition between PNs**

   Randolf Menzel and Michael Schmuker formulated the idea that the memory trace after odor learning might in part be realized as specific de-correlation of PN responses through constitutively activated LINs which interconnect the PNs within the same glomerulus. I elaborated the elegance of this idea in the hypotheses section 1.4 on page 28 in the introduction.

Ad 1: With the data obtained in this thesis it is possible to reject the idea by Galizia and Kimmerle (2004). Firstly, the "aberrant" odor response profiles reported in that study are not sufficient reason to hypothesize various odor

response profiles among PNs within the same glomerulus. PN responses that diverge from the glomerular activity patterns that are concluded in the functional AL atlas have been found in all electrophysiological studies cited in this thesis. Up to now, all studies in which only one PN could be recorded at a time could only speculate on what the signals on the other PNs of this and other glomeruli would be; yet is is a known fact for a long time that, also in wide-field imaging, aberrant odor response profiles are common. The published AL atlas patterns emerge not before data from many animals are pooled. Nothing different was found in the present thesis: in the glomerulus-based analysis PNs within the same glomerulus were averaged together; the glomerular odor response profiles were aberrant as long as a low number of animals was available for the calculation thereof. Thus, the major source for deviations from the atlas in electrophysiological studies is the trivial fact that an insufficient body of data can be assembled to average out the naturally occurring deviations. Secondly, the data from identified PNs obtained here do not display differences as large as one would assume if the response properties of the PNs were different. Anti-correlation between recordings traces from different PNs did occur, but it was only scarcely larger than the level of anti-correlation that was present in branches of the same neuron, which I regard negligible. The source for the differences in correlation and anti-correlation between Neurons vs. Branches was demonstrated to be mediated by a high-frequency component of baseline noise. If PNs within the same glomerulus would differ more fundamentally, one would assume (1) that this difference is not abolished by application of a mild temporal low-pass filter and (2) that the correlation between these PNs would be lower, e. g. halfway between the correlation value reported for branches of the same neuron and branches from different neurons. Therefore, even if correlation analysis revealed that signals of excitation are slightly de-correlated by an odor stimulus, this effect is much smaller than the effect that an aberrant odor response spectrum in one of the PNs would invoke.

> All PNs in on glomerulus share the same odor-response-spectrum

I therefore conclude that PNs within the same glomerulus do not differ in their odor-response-spectra. Response spectra that are deviant from the functional AL atlas are commonly found, no matter which recordings method used. Most importantly, deviant response spectra are a glomerulus-wide phenomenon. It

vanishes, if a large number of animals and recordings are averaged.

Ad 2: Notwithstanding the fact that I did not condition the test animals to odors prior to imaging, the postulated PN difference might be detectable on a low level in the data presented here. It is possible that the reciprocal inhibition between PNs becomes apparent in the results from the correlation analysis. To generate a testable hypothesis on how traces of the reciprocal inhibitory network might be detected in my data, or in data that one could record with a 2PLSM, some assumptions are required.

> Assumptions on glomerular LINs

The hypothetic LINs in question should interconnect PNs within one glomerulus. Because the de-correlation should be glomerulus-specific, we have to assume that such LINs are glomerulus-specific, too; because LINs that innervate a single glomerulus only are unknown, we need to assume that we are facing a group of hetero-LINs here. We will ignore the sparse innervation in the remaining glomeruli. We will call these LINs "gLINs" ("g" for glomerular).

Once activated by input from a central neuron, gLINs shall de-correlate or even anti-correlate PN signals. The de-correlation of PNs would be more accessible to a read-out system if it occurred simultaneously in a pair or group of PNs, thus I assume that gLINs are not fed by RNs, but by an output synapse at the integrative segment of one of the PNs. The other PNs within the same glomerulus would receive inhibitory input by the gLINs. Alternatively, one might imagine a gLIN that is activated by RNs, modulated by a central neuron, and synapses onto two different PNs with an excitatory synapse at one, and an inhibitory synapse at the other group of PNs. Assuming that gLINs get their input at the integrative segment of a PN is, however, more parsimonious.

At which times during recordings would I have a chance to see the action of de-correlating gLINs? Potentially at all times during the recordings, because gLINs require PN input, and PNs are active during spontaneous signals, which are ubiquitous. Following the same argument, one would assume that the action of gLINs would best be detectable during episodes of signals of excitation, because only then the PNs are active, thus feeding the gLINs. One further assumption is necessary before we can check the diagrams in the section on the correlation analysis in the results part for concordance with the assumptions: the gLINs should have a means to tell apart odor-evoked signals from spontaneous

signals. Otherwise ongoing spontaneous activity would lead to false signals about the presence of a learnt odor. Thus the de-correlation by gLINs should be strongest during the time window of odor stimulation, when the majority of signals should be odor-evoked.

The prediction is tested

Now, can we see anti-correlation or decreased correlation between PNs within one glomerulus during signals of excitation in the time window of odor stimulation? Figure 3.3.8 on page 151 of the results part contains the necessary information. The bars in question are the second ones ("during") in the yellow group (distinct PNs within the same glomerulus). We have to take into account the positive bar for significant correlation and the negative one for significant anti-correlation. To judge if the observed values are indicative of a specific effect, the scores have to be compared with the neighboring bars from the same group. It is obvious that the correlation score is highest before the odor stimulus and in the 500 ms long ON phase. The lowest score is reached during odor stimulation. Is this a general trend in all signaling episodes? No, in the graphs that collect scores for the signaling episodes inhibition and rest (figures 3.3.9 and 3.3.10 on pages 153 and 155), as well as in the graph the collects scores for all signaling episodes (figure 3.3.7 on page 148), the arrangement is different. As a general trend in all signaling episodes and groups, the scores are highest during the ON phase as well as during the rest of the time window of odor stimulation. Only in episodes of excitatory signals is the correlation score lower during the time window of odor stimulation as compared to the time window before.

Correlation data are in accordance with the assumptions

This is in accordance with the assumptions: only during signals of excitation do the gLINs get strong input. They then inhibit a sub-population of PNs within the same glomerulus, which registers as reduced correlation, or increased de-correlation. Also in accordance with the postulate is the arrangement of correlation scores in the green and blue bars of the graph on the excitatory signaling episodes: Menzel&Schmuker claim that the de-correlation must be glomerulus-specific; thus it should not affect the respective "other" glomeruli, and also not the next measurement. Fittingly, the arrangement of correlation scores between PNs in distinct glomeruli (green) and between consecutive

measurements (blue) is identical to the arrangement in all other graphs, i. e. the score during odor stimulation is not influenced by de-correlation through gLINs. Thus, in these groups, the scores are larger during the time window of odor stimulation than before.

The arrangement of correlation scores between the phases of the measurements, signaling episodes, and groups is in agreement with the assumptions made. Even in naïve animals, PNs within the same glomerulus are specifically de-correlated during door stimuli as compared to spontaneously signals in the phase before odor stimulation. The effect is observed only between PN processes that innervate the same glomerulus. Between PNs that reside in distinct glomeruli (green bars), the de-correlation effect is absent. Likewise, the de-correlation of PNs is exclusive to episodes of excitatory signals; during episodes of inhibition or rest, pairs of PNs are not de-correlated during the time window of odor stimulation. Actually more evidence for the correctness of the assumptions can be found in the graph on inhibitory signaling episodes: inhibited PNs feed gLINs less, thus de-correlation should be reduced, or correlation enhanced. This is exactly what one can see in figure 3.3.9 on page 153: the correlation score during signals of inhibition that fall into the time window of odor stimulation is indeed higher than the score in the time window before. The correlation is enhanced to a higher degree than observed otherwise, i. e. between PNs that reside in different glomeruli.

One group of bars, however, is not in consistency with the assumptions: In figure 3.3.8 on page 151 which shows the correlation scores during excitatory signaling states, the de-correlation during the time window of odor stimulation is found also in pairs of branches that belong to the same PN (red bars). There is no obvious use in specifically de-correlating branches of the same neuron. A possible explanation might be that the gLINs convey de-correlating inhibitory input to PNs only *via* few synapses, so that in many pairs of branches from the same neuron, one of the two branches is inhibited more strongly than the other.

The Menzel&Schmuker postulate can not be contradicted

To conclude: Assumptions were unforcedly generated by extrapolating from the idea postulated by Menzel and Schmuker. The assumptions were tested by cross-checking of predicted effects with the pool of correlation scores that were generated by the SWCA. All of the predicted effects can be found in

exactly the predicted groups, time windows, and episodes. Therefore, it appears likely that glomerulus-specific reciprocal inhibition of PNs that reside within the same glomerulus exists, even in naïve animals. It can be expected that a similar analysis, performed with measurement data that has been acquired with conditioned animals, reveals an even stronger effect, i. e. enhanced anti-correlation instead of a mere reduction in correlation.

4.7 2PLSM is a unique tool for the analysis of networks of neurons

The data presented in this thesis have been acquired during a period of 3 months. This trivial observation stresses the fact that, once the requirements in terms of light-efficiency and usability are met, the 2PLSM technique is fit for routine measurements of the neural activity in living animals. I could show in this thesis that the 2PLSM surpasses wide-field fluorescence imaging in the honeybee in several fundamental points, the most important of these being the cellular resolution in combination with high sampling rate. Combining high-resolution image stacks for reconstruction of PNs with high temporal resolution of 76 Hz that was achieved with linear scans proved to be particularly profitable: the data provides us with detailed information on spontaneous and odor-evoked signals in multiple identified cells that were recorded in parallel. Recordings could last for hours without noticeable bleaching or detriment in signal quality. The temporal resolution and the control that the experimenter can exercise over a cell that is measured by means of intracellular electrodes are out of reach for optophysiologic techniques; yet 2PLSM overly compensates this detriment by offering facilitated navigation in the target tissue, simultaneous recordings of activity in tenths of identifiable cells, and prolonged recordings as compared with intracellular electrophysiology. Therefore, 2PLSM is indeed a methodological puzzle stone between widefield imaging and electrophysiology. For the analysis of networks of neurons it is indeed the best method at hand, because it allows, additionally to parallel, fast recordings, also the identification of cells.

4.8 Outlook

Still many peaces of information are lacking that would be required for a complete understanding of olfactory coding.

It is in my view advised to invest efforts into **recordings of RNs**: As I concluded in the introduction, it is well possible that the number of 375 RNs per glomerulus do convey redundant information to AL glomeruli. Populations of RNs should be checked for their dose-response-curves, odor-response-profiles, and for the amount and structure of spontaneous activity. Staining RNs with a protocol alike the one used in mice (Wachowiak and Cohen, 2001), involving Triton-X and a acetoxymethyl-ester dye (like Calcium Green-1 AM) would allow for imaging of RN terminals within glomeruli. Alternatively, the method for RN stainings developed by Kelber *et al.* (2006) might be adapted such that the RNs are not only stained but also remain functional. It would be advised to use a 2PLSM for imaging; chances are that RN terminals could be related to identifiable RN neurites, and that by this way multiple RN terminals from several RNs could be recorded simultaneously. Not before such a study has been conducted do we know what the input signal to glomeruli is.

Furthermore, our ignorance as to the **behavioral relevance of spontaneous activity** is most unfortunate. I could show in this thesis that, at a temperature of 27°C (which is still lower than the temperature that unconstrained bees actively produce), spontaneous activity is so strong that previously used methods to differentiate odor-evoked from spontaneous signals almost fail completely. What does it represent? Is spontaneous activity an indication for overly increased detector gain in an odor-less environment? Is spontaneous activity indicative of previous activity patterns, like an after-image in vision? Is spontaneous activity perceived by the animal, or is it a peripheral phenomenon that stays unnoticed? Because there is apparently a direct relation between temperature and the amount of spontaneous activity, one might attempt a simple experiment: condition bees prior to imaging. Monitor proboscis extension or motoneuron M17 activity during imaging recordings. Test several rather similar odors or mixtures, one of which the rewarded one. Test different groups of

191

bees at increasing temperature. Quantify generalization at each temperature step. Characterize spontaneous activity in the imaging recordings. Determine if there is a correlation between spontaneous activity and generalization. Such an experiment would show if the amount of spontaneous activity relates in any way to the recognition of odors or the amount of generalization. Likewise, one could quantify detection threshold or dose-response curves of conditioned odors by using concentration series instead of a panel of qualitatively different odorants.

This experiment, if performed in a 2PLSM, would furthermore reveal if PNs within the same glomerulus code for learnt odors with **differentially inhibited PN signals**, as proposed by Menzel&Schmuker.

Finally, I mentioned already in the introduction how helpful a more complete picture of the ultrastructure of the AL would be; I reckon that efforts to **model the AL network** *in silicio* must fail until we know more about (1) the input signal to the AL (see proposed RN measurements above) and (2) the quantity and physiology of synaptic connections between all participants.

4.9 Contributions

The present project could not have been undertaken without the devotion of several people, enterprises, and institutions. I consider it necessary to specify in detail the contributions of these. Plain listing in the acknowledgments part would not suffice for adequate appraisal of their contributions. The acknowledgments part can be found on page 196.

Repair and conversion of the scanning microscope

Dr. Peter Schneider from Leica Microsystems, Wetzlar, gave the critical hint when I worked on the video board of the microscope system with the aim to remove digital artifacts in the recorded images that haunted us until March 2004.

Winfried Goltz from Leica Microsystems brokered the acquisition of the new, externally mounted photomultiplier, which never was officially sold and thus difficult to order.

Dr. Werner Zuschratter from the Leibniz Institute for Neurobiology, Magdeburg, helped with the diagnosis of defects of the microscope. He was also of great help when we needed to understand the electrical interface of the new photomultiplier during the installation of power supply and amplifier / logarithmizer.

The basic concept of the conversion of the microscope is inspired by the work of Prof. Dr. Winfried Denk from the Max-Planck-Institute for biomedical research in Heidelberg, Germany, i.e. the mounting of the photomultiplier very close to the objective, and the use of a Pockel's Cell for attenuation of the laser light. I had the opportunity to collect first hand experience with one of Winfried Denk's microscopes during preliminary measurements at the work group of Dr. Rainer Friedrich, also in the Max-Planck-Institute for Biomedical Research in Heidelberg.

Light source

In Collaboration with Prof. Dr. Ludger Wöste's work group at the Department Of Physics of the FU Berlin the 2-photon microscope was built up next to its laser light source. Prof. Dr. Thorsten Bernhard and Prof. Dr. Torsten Siebert supervised Dr. Tobias Gleitsmann and Dr. Bruno Schmidt (PhD students at that time) while they adjusted the pulsed IR-laser for the needs of *in vivo* imaging, built up and adjusted a prism compressor, helped with adjusting the Pockel's cell, devised and constructed the optic path and the focusing of the laser beam into the microscope system, and performed control measurements of the pulse length with an auto-correlator. Dr. Bruno Schmidt was of great help during several phases of the project, e.g. in assisting me during the construction of the microscope table, and by providing me with the theoretical and practical background necessary for operating various parts of the light source.

Data evaluation

The PhD student Ashu Behl, currently studying mathematics at the Indian Institute of Technology, Delhi, introduced me to MatLab while he wrote algorithms for importing the measurement data into MatLab. Together we created an algorithm for movement- and bleaching-correction of the linear scan measurements.

The rest was done by me

In the first phase of the project, I repaired the used scanning microscope, conceived the conversion into a 2-photon microscope, constructed/acquired and installed all parts that needed to be attached for the conversion process, among these a Pockel's Cell with delay generator, a security laser shutter, a new scanning mirror, a new photomultiplier including power supply and amplifier/logarithmizer, a dichroic mirror for 2-photon imaging with the dye FURA2, an objective stepper including control apparatus and software and an high-N/A water immersion objective. I built a microscope table suited to hold *in vivo* honeybee preparations and designed a new, adapted version of Plexiglas stage for containment of the honeybee preparation during the measurements.

In the second phase, I adapted the honeybee preparation for imaging such that greater stability and less brain movements were provided, routinely preformed

the preparations and stainings, planned and performed the measurements, analyzed the data with self-written scripts in MatLab, and wrote this document.

4.10 Acknowledgements / Danksagung

Mitstreiter, ich danke Euch für Eure Hilfe, Anteilnahme und Kritik, für Zureden und auch offene Ohren. Um jeder/m von Euch gerecht zu werden, müßte ich nun jedem einen Absatz widmen. Das kann ich nicht, daher werde ich Euch im Folgenden auflisten: Meine lieben Kommilitonen und Kollegen Abid Hussaini, Alejandro Delorenzi, Alexander Galkin, Ana Silvering, Andreas Kirbach, Anja Fröse, Anke Friedrich, Anna Wertlen, Antonio Pazienti, Astrid Klawitter, Beate Eisermann, Bernd Grünewald, Bettina Stocker, Björn Brembs, Carsten Duch, Caspar Schöning, Cécile Faucher, Claudia Kühn, Claudia Niggebrügge, Daniel Münch, Daniel Wüstenberg, Dirk Müller, Daniela Pelz, Denise Berger, Dorothea Eisenhardt, Einar Heidel, Evren Pamir, Farzad Farkooi, Felix Ebers, Fernando Guerrieri, Fernando Vonhoff, Frank Schaupp, Gérard Leboule, Ina Klinke, Irina Plekhanova, Jan Sölter, Jana Börner, Jaqueline Fuchs, Johannes Felsenberg, Jürgen Rybak, Karin Gehring, Kathrin Marter, Konstantin Lehmann, Laurenz Müßig, Lisa Bogusch, Marcel Weidert, Marco Schubert, Mariana Gil, Marion Ganz, Martin Gühmann, Martin Nawrot, Mary Wurm, Mathias Ditzen, Melanie Hähnel, Michael Schmuker, Natalie Hempel De Ibarra, Nicola Stollhoff, Nobuhiro Yamagata, Paul Szyszka, Peter Knoll, Phillip Peele, Ravit Hadar, Reinhard Rößler, Rodrigo De Marco, Robert Brandt, Robert Finke, Ryuichi Okada, Sabine Franke, Sabine Funke, Sabine Krofczik, Silke Sachse, Silke Stach, Sonja Grün, Tina Roeske, Uli Müller, Uwe Greggers, Victoria Antemann, Zain Seyd:

Danke!

Dank (bzw. Sorry) gebührt auch meiner Familie, die es vor dieser Doktorarbeit noch gar nicht gab. Meine liebe Frau Sabine (geb. Schwarz), Leonard und Emilia: ihr wart langmütig und duldsam. Meine lieben Eltern Tina Schaefer und Hartwig Franke: Eure Geduld, Euer gutes Zureden, Euer Verständnis und Vertrauen waren stetiger Ansporn für mich, diese Arbeit zu beenden.

Bibliography

Abel, R., Rybak, J., and Menzel, R. 2001. Structure and response patterns of olfactory interneurons in the honeybee, *Apis mellifera. J Comp Neurol*, **437**(3), 363–383. (Pages 13, 181).

Akers, R. P. and Getz, W. M. 1992. A test of identified response classes among olfactory receptor neurons in the honey-bee worker. *Chem senses*, **17 no. 2**, 191–209. (Pages 12, 170, 178).

Apáthy, S. v. 1897. Das leitende Element der Nervensystems und seine topographischen Beziehungen zu den Zellen. *Mitt Zool Stn Neapel*, **12**, 495–748. (Page 2).

Arnold, G., Masson, C., and Budharugsa, S. 1985. Comparative study of the antennal lobes and their afferent pathway in the worker bee and the drone (*Apis mellifera*) . *Cell Tissue Res*, **242 No. 3**, 593–605. (Page 16).

Baier, H. and Korsching, S. 1994. Olfactory glomeruli in the zebrafish form an invariant pattern and are identifiable across animals. *J Neurosci*, **14**(1), 219–230. (Page 8).

Barbara, G. S., Zube, C., Rybak, J., Gauthier, M., and Grünewald, B. 2005. Acetylcholine, gaba and glutamate induce ionic currents in cultured antennal lobe neurons of the honeybee, apis mellifera. *J Comp Physiol A Neuroethol Sens Neural Behav Physiol*, **191**(9), 823–836. (Pages 18, 181).

Barbara, G. S., Grünewald, B., Paute, S., Gauthier, M., and Raymond-Delpech, V. 2008. Study of nicotinic acetylcholine receptors on cultured antennal lobe neurones from adult honeybee brains. *Invert Neurosci*, **8**(1), 19–29. (Page 178).

Bhandawat, V., Olsen, S. R., Gouwens, N. W., Schlief, M. L., and Wilson, R. I. 2007. Sensory processing in the drosophila antennal lobe increases reliability and separability of ensemble odor representations. *Nat Neurosci*, **10**(11), 1474–1482. (Page 17).

Bicker, G., Kreissl, S., and Hofbauer, A. 1993. Monoclonal antibody labels olfactory and visual pathways in drosophila and apis brains. *J Comp Neurol*, **335**(3), 413–424. (Pages 8, 13).

Bignetti, E. 1985. Purification and characterisation of an odorant-binding protein from cow nasal tissue. *Eur J Biochem*, **149**(1), 227–231. (Page 11).

Boeckh, J. and Tolbert, L. P. 1993. Synaptic organization and development of the antennal lobe in insects. *Microsc Res Tech*, **24**(3), 260–280. (Page 16).

Bornhauser, B. C. and Meyer, E. P. 1997. Histamine-like immunoreactivity in the visual system and brain of an orthopteran and a hymenopteran insect. *Cell Tissue Res*, **287**(1), 211–221. (Page 19).

Brockmann, A. and Brückner, D. 1995. Projection pattern of poreplate sensory neurones in honey bee worker, *Apis mellifera L.* (Hymenoptera : Apidae) . *Int J Insect Morphol*, **24 Issue 4**, 405–411. (Page 7).

Buck, L. and Axel, R. 1991. A novel multigene family may encode odorant receptors: a molecular basis for odor recognition. *Cell*, **65**(1), 175–187. (Page 6).

Christensen, T. A., Waldrop, B. R., Harrow, I. D., and Hildebrand, J. G. 1993. Local interneurons and information processing in the olfactory glomeruli of the moth *Manduca sexta. J Comp Physiol A*, **173**(4), 385–399. (Pages 16, 19, 21, 178).

Christensen, T. A., Harrow, I. D., Cuzzocrea, C., Randolph, P. W., and Hildebrand, J. G. 1995. Distinct projections of two populations of olfactory receptor axons in the antennal lobe of the sphinx moth *Manduca sexta. Chem Senses*, **20**(3), 313–323. (Page 7).

Cinelli, A. R., Hamilton, K. A., and Kauer, J. S. 1995. Salamander olfactory bulb neuronal activity observed by video rate, voltage-sensitive dye imaging. Spatial and temporal properties of responses evoked by odorant stimulation. *J Neurophysiol*, **73**(5), 2053–2071. (Page 8).

Clyne, P. J., Warr, C. G., Freeman, M. R., Lessing, D., Kim, J., and Carlson, J. R. 1999. A novel family of divergent seven-transmembrane proteins: candidate odorant receptors in drosophila. *Neuron*, **22**(2), 327–338. (Page 6).

Couto, A., Alenius, M., and Dickson, B. J. 2005. Molecular, anatomical, and functional organization of the drosophila olfactory system. *Curr Biol*, **15**(17), 1535–1547. (Pages 6, 7).

Dahanukar, A., Hallem, E. A., and Carlson, J. R. 2005. Insect chemoreception. *Curr Opin Neurobiol*, **15**(4), 423–430. (Page 11).

Denk, W. and Svoboda, K. 1997. Photon upmanship: why multiphoton imaging is more than a gimmick. *Neuron*, **18**(3), 351–357. (Page 25).

Denk, W., Strickler, J. H., and Webb, W. W. 1990. Two-photon laser scanning fluorescence microscopy. *Science*, **248**(4951), 73–76. (Pages 3, 26).

Denk, W., Delaney, K. R., Gelperin, A., Kleinfeld, D., Strowbridge, B. W., Tank, D. W., and Yuste, R. 1994. Anatomical and functional imaging of neurons using 2-photon laser scanning microscopy. *J Neurosci Methods*, **54**(2), 151–162. (Pages 3, 26).

Distler, P. 1989. Histochemical demonstration of GABA-like immunoreactivity in cobalt labeled neuron individuals in the insect olfactory pathway. *Histochemistry*, **91**(3), 245–249. (Page 18).

Diverse authors 2003. Tree of Life web project. Internet (URI: http://tolweb.org/tree/phylogeny.html). (Page 22).

Eisthen, H. L. 2002. Why are olfactory systems of different animals so similar? *Brain Behav Evol*, **59**(5-6), 273–293. (Page 22).

Flanagan, D. and Mercer, A. R. 1989. An atlas and 3D-reconstruction of the antennal lobes in the worker honey bee, *Apis mellifera L.* (Hymenoptera : Apidae). *Int J Insect Morphol*, **18 No 2/3**, 145–159. (Pages 7, 8, 13).

Fonta, C., Sun, X.-J., and Masson, C. 1993. Morphology and spatial distribution of bee antennal lobe interneurones responsive to odors. *Chem senses*, **18 no 2**, 101–119. (Page 14).

Friedrich, R. W. and Korsching, S. I. 1998. Chemotopic, combinatorial, and noncombinatorial odorant representations in the olfactory bulb revealed using a voltage-sensitive axon tracer. *J Neurosci*, **18**(23), 9977–9988. (Page 8).

Galizia and Menzel 2001. The role of glomeruli in the neural representation of odours: results from optical recording studies. *J Insect Physiol*, **47**(2), 115–130. (Page 8).

Galizia, Menzel, and Holldobler 1999a. Optical imaging of odor-evoked glomerular activity patterns in the antennal lobes of the ant *Camponotus rufipes. Naturwissenschaften*, **86**(11), 533–537. (Page 8).

Galizia, C. G. and Kimmerle, B. 2004. Physiological and morphological characterization of honeybee olfactory neurons combining electrophysiology, calcium imaging and confocal microscopy. *J Comp Physiol A Neuroethol Sens Neural Behav Physiol*, **190**(1), 21–38. (Pages 19, 21, 27, 166, 168, 170, 176, 181, 184).

Galizia, C. G. and Menzel, R. 2000. Odour perception in honeybees: coding information in glomerular patterns. *Curr Opin Neurobiol*, **10**(4), 504–510. (Pages 8, 168).

Galizia, C. G., Nägler, K., Hölldobler, B., and Menzel, R. 1998. Odour coding is bilaterally symmetrical in the antennal lobes of honeybees (*Apis mellifera*). *Eur J Neurosci*, **10**(9), 2964–2974. (Pages 7, 164).

Galizia, C. G., McIlwrath, S. L., and Menzel, R. 1999b. A digital three-dimensional atlas of the honeybee antennal lobe based on optical sections acquired by confocal microscopy. *Cell Tissue Res*, **295**(3), 383–394. (Pages 8, 13, 84, 116, 122).

Galizia, C. G., Sachse, S., Rappert, A., and Menzel, R. 1999c. The glomerular code for odor representation is species specific in the honeybee *Apis mellifera. Nat Neurosci*, **2**(5), 473–478. (Pages 8, 27, 49, 122, 164).

Gao, Q., Yuan, B., and Chess, A. 2000. Convergent projections of drosophila olfactory neurons to specific glomeruli in the antennal lobe. *Nat Neurosci*, **3**(8), 780–785. (Page 6).

Getz, W. M. and Akers, R. P. 1994. Honeybee olfactory sensilla behave as integrated processing units. *Behav Neural Biol*, **61**(2), 191–195. (Page 12).

Gouwens, N. W. and Wilson, R. I. 2009. Signal propagation in drosophila central neurons. *J Neurosci*, **29**(19), 6239–6249. (Pages 16, 17).

Grünewald, B. 2003. Differential expression of voltage-sensitive k+ and ca2+ currents in neurons of the honeybee olfactory pathway. *J Exp Biol*, **206**(Pt 1), 117–129. (Page 178).

Hallem, E. A., Ho, M. G., and Carlson, J. R. 2004. The molecular basis of odor coding in the drosophila antenna. *Cell*, **117**(7), 965–979. (Pages 7, 11).

Hallem, E. A., Dahanukar, A., and Carlson, J. R. 2006. Insect odor and taste receptors. *Annu Rev Entomol*, **51**, 113–135. (Page 11).

Hammer, M. 1993. An identified neuron mediates the unconditioned stimulus in associative olfactory learning in honeybees. *Nature*, **366**, 59–63. (Pages 14, 15).

Heinrich, B. 1979. Thermoregulation of african and european honeybees during foraging, attack, and hive exits and returns. *J Exp Biol*, **80**, 217–229. (Page 171).

Helmchen, F. and Denk, W. 2002. New developments in multiphoton microscopy. *Curr Opin Neurobiol*, **12**(5), 593–601. (Page 25).

Helmchen, F. and Denk, W. 2005. Deep tissue two-photon microscopy. *Nat Methods*, **2**(12), 932–940. (Page 25).

Helmchen, F., Fee, M. S., Tank, D. W., and Denk, W. 2001. A miniature head-mounted two-photon microscope. high-resolution brain imaging in freely moving animals. *Neuron*, **31**(6), 903–912. (Page 26).

Hildebrand, J. G. and Shepherd, G. M. 1997. Mechanisms of olfactory discrimination: converging evidence for common principles across phyla. *Annu Rev Neurosci*, **20**, 595–631. (Page 6).

Hildebrand, J. G., Christensen, T. A., Harrow, I. D., Homberg, U., Matsumoto, S. G., and Waldrop, B. R. 1992. The roles of local interneurons in the processing of olfactory information in the antennal lobes of the moth *Manduca sexta. Acta Biol Hung*, **43**(1-4), 167–174. (Pages 16, 21).

Hoskins, S. G., Homberg, U., Kingan, T. G., Christensen, T. A., and Hildebrand, J. G. 1986. Immunocytochemistry of GABA in the antennal lobes of the sphinx moth *Manduca sexta. Cell Tissue Res*, **244**(2), 243–252. (Page 18).

Iwama, A., Sugihara, D., and Shibuya, T. 1995. Morphology and physiology of neurons responding to the Nasonov pheromone in the antennal lobe of the honeybee, *Apis mellifera. Zool Science*, **12**, 207–218. (Page 15).

Jayaraman, V. and Laurent, G. 2007. Evaluating a genetically encoded optical sensor of neural activity using electrophysiology in intact adult fruit flies. *Front Neural Circuits*, **1**, 3. (Pages 26, 176).

Kazama, H. and Wilson, R. I. 2008. Homeostatic matching and nonlinear amplification at identified central synapses. *Neuron*, **58**(3), 401–413. (Page 17).

Kelber, C., Rössler, W., and Kleineidam, C. J. 2006. Multiple olfactory receptor neurons and their axonal projections in the antennal lobe of the honeybee *Apis mellifera. J Comp Neurol*, **496**(3), 395–405. (Pages 12, 191).

Kirschner, S., Kleineidam, C. J., Zube, C., Rybak, J., Grünewald, B., and Rössler, W. 2006. Dual olfactory pathway in the honeybee, *Apis mellifera. J Comp Neurol*, **499**(6), 933–952. (Page 15).

Krofczik, S., Menzel, R., and Nawrot, M. P. 2008. Rapid odor processing in the honeybee antennal lobe network. *Front Comput Neurosci*, **2**, 9. (Pages 17, 20, 21, 162, 168, 170).

Lacher, V. and Schneider, D. 1963. Elektrophysiologischer Nachweis der Riechfunktion von Porenplatten (sensilla placodea) auf den Antennen der Drohne und der Arbeitsbiene (*Apis mellifica L. J Comp Physiol A*, **47 No 3**, 274–278. (Page 6).

Linster, C., Sachse, S., and Galizia, C. G. 2005. Computational modeling suggests that response properties rather than spatial position determine connectivity between olfactory glomeruli. *J Neurophysiol*, **93**(6), 3410–3417. (Pages 18, 19, 29, 90, 181, 182).

Malun, D. 1991. Synaptic relationships between GABA-immunoreactive neurons and an identified uniglomerular projection neuron in the antennal lobe of *Periplaneta americana*: a double-labeling electron microscopic study. *Histochemistry*, **96**(3), 197–207. (Page 16).

Matsumoto, S. G. and Hildebrand, J. G. 1981. Olfactory mechanisms in the moth *Manduca sexta*: response characteristics and morphology of central neurons in the antennal lobes. *Proc R Soc Lond*, **213**, 249–277. (Page 17).

Menzel, R., Galizia, G., Müller, D., and Szyszka, P. 2005. Odor coding in projection neurons of the honeybee brain. *Chem Senses*, **30 Suppl 1**, i301–i302. (Pages 166, 178).

Müller, D., Abel, R., Brandt, R., Zöckler, M., and Menzel, R. 2002. Differential parallel processing of olfactory information in the honeybee, *Apis mellifera L. J Comp Physiol A Neuroethol Sens Neural Behav Physiol*, **188**(5), 359–370. (Pages 20, 92, 162, 166, 168, 170).

Molecular Probes Fura and Indo Ratiometric Calcium Indicators, Product Information 2005. *probes.invitrogen.com/media/pis/mp01200.pdf*. (Page 172).

Mombaerts, P. 2001. How smell develops. *Nat Neurosci*, **4 Suppl**, 1192–1198. (Page 7).

Mombaerts, P., Wang, F., Dulac, C., Chao, S. K., Nemes, A., Mendelsohn, M., Edmondson, J., and Axel, R. 1996. Visualizing an olfactory sensory map. *Cell*, **87**(4), 675–686. (Pages 6, 7).

Olsen, S. R., Bhandawat, V., and Wilson, R. I. 2007. Excitatory interactions between olfactory processing channels in the drosophila antennal lobe. *Neuron*, **54**(1), 89–103. (Page 19).

Peele, P., Ditzen, M., Menzel, R., and Galizia, C. G. 2006. Appetitive odor learning does not change olfactory coding in a subpopulation of honeybee antennal lobe neurons. *J Comp Physiol A Neuroethol Sens Neural Behav Physiol*, **192**(10), 1083–1103. (Page 170).

Pelz, D., Roeske, T., Syed, Z., de Bruyne, M., and Galizia, C. G. 2006. The molecular receptive range of an olfactory receptor in vivo (*Drosophila melanogaster* Or22a). *J Neurobiol*, **66**(14), 1544–1563. (Page 7).

Pevsner, J., Sklar, P. B., and Snyder, S. H. 1986. Odorant-binding protein: localization to nasal glands and secretions. *Proc Natl Acad Sci U S A*, **83**(13), 4942–4946. (Page 11).

Pevsner, J., Reed, R. R., Feinstein, P. G., and Snyder, S. H. 1988. Molecular cloning of odorant-binding protein: member of a ligand carrier family. *Science*, **241**(4863), 336–339. (Page 11).

Piston, D. W. 1999. Imaging living cells and tissues by two-photon excitation microscopy. *Trends Cell Biol*, **9**(2), 66–69. (Page 25).

Ramón y Cajal, S. 1903a. Consideraciones críticas sobre la teoría de A. Bethe acerca de la estructura y conexiones de las células nerviosas. *Trab Lab Investig Biol Univ Madr*, **2**, 101–128. (Page 2).

Ramón y Cajal, S. 1903b. Un sencillo método de coloración selectiva del retículo protoplásmico y sus efectos en los diversos órganos nerviosos. *Trab Lab Investig Biol Univ Madr*, **2**, 129–221. (Page 2).

Ramón y Cajal, S. 1923. *Recuerdos de mi Vida*. 3rd ed. Juan Pueyo, Madrid. (Page 3).

Ramón y Cajal, S. 1937. *Recollections of my Life*. American Philosophical Society, Philadelphia. (Craigie, E.H., transl., with the assistance of Cano, J., Reprint: MIT Press, Cambridge, 1989). (Page 3).

Remak, R. 1843. Über den Inhalt der Nervenprimitivröhren. *Archiv für Anatomie, Physiologie und wissenschaftliche Medizin*, **197**. (Page 2).

Remak, R. 1844. Neurologische Erläuterungen. *Archiv für Anatomie, Physiologie und wissenschaftliche Medizin*, pages 463–472. (Page 2).

Roberts and Harrison 1999. Mechanisms of thermal stability during flight in the honeybee apis mellifera. *J Exp Biol*, **202 (Pt 11)**, 1523–1533. (Page 171).

Robertson, H. M. and Wanner, K. W. 2006. The chemoreceptor superfamily in the honey bee, apis mellifera: expansion of the odorant, but not gustatory, receptor family. *Genome Res*, **16**(11), 1395–1403. (Page 11).

Root, C. M., Semmelhack, J. L., Wong, A. M., Flores, J., and Wang, J. W. 2007. Propagation of olfactory information in drosophila. *Proc Natl Acad Sci U S A*, **104**(28), 11826–11831. (Page 25).

Rubin, B. D. and Katz, L. C. 1999. Optical imaging of odorant representations in the mammalian olfactory bulb. *Neuron*, **23**(3), 499–511. (Page 8).

Rybak, J. and Eichmüller, S. 1993. Structural plasticity of an immunochemically identified set of honeybee olfactory interneurones. *Acta Biol Hung*, **44**(1), 61–65. (Pages 14, 15).

Sachse, S. and Galizia, C. G. 2002. Role of inhibition for temporal and spatial odor representation in olfactory output neurons: a calcium imaging study. *J Neurophysiol*, **87**(2), 1106–1117. (Pages 8, 19, 29, 74, 122, 162, 164, 165, 169, 170, 181).

Sachse, S. and Galizia, C. G. 2003. The coding of odour-intensity in the honeybee antennal lobe: local computation optimizes odour representation. *Eur J Neurosci*, **18**(8), 2119–2132. (Pages 9, 170).

Sachse, S., Rappert, A., and Galizia, C. G. 1999. The spatial representation of chemical structures in the antennal lobe of honeybees: steps towards the olfactory code. *Eur J Neurosci*, **11**(11), 3970–3982. (Page 8).

Sachse, S., Peele, P., Silbering, A. F., Gühmann, M., and Galizia, C. G. 2006. Role of histamine as a putative inhibitory transmitter in the honeybee antennal lobe. *Front Zool*, **3**, 22. (Pages 18, 19, 162, 170).

Saggau, P. 2006. New methods and uses for fast optical scanning. *Curr Opin Neurobiol*, **16**(5), 543–550. (Page 26).

Sandler, B. H., Nikonova, L., Leal, W. S., and Clardy, J. 2000. Sexual attraction in the silkworm moth: structure of the pheromone-binding-protein-bombykol complex. *Chem Biol*, **7**(2), 143–151. (Page 11).

Schäfer, S. and Bicker, G. 1986. Distribution of GABA-like immunoreactivity in the brain of the honeybee. *J Comp Neurol*, **246**(3), 287–300. (Page 18).

Schild, D. 1988. Principles of odor coding and a neural network for odor discrimination. *Biophys J*, **54**(6), 1001–1011. (Page 8).

Schröter, U., Malun, D., and Menzel, R. 2007. Innervation pattern of suboesophageal ventral unpaired median neurones in the honeybee brain. *Cell Tissue Res*, **327**(3), 647–667. (Page 15).

Schwarz, S. 2006. *Drosophila olfactory sensilla*. Ph.D. thesis, Freien Universität Berlin, Germany; FB Biologie, Chemie, Pharmazie. (Page 12).

Simarro Lacabra, L. 1900. Nuevo método histológico de impregnación por las sales fotográficas de plata. *Rev Trimest Microgr*, **5**, 45–71. (Page 2).

Stengl, M., Hatt, H., and Breer, H. 1992. Peripheral processes in insect olfaction. *Annu Rev Physiol*, **54**, 665–681. (Page 11).

Stosiek, C., Garaschuk, O., Holthoff, K., and Konnerth, A. 2003. In vivo two-photon calcium imaging of neuronal networks. *Proc Natl Acad Sci U S A*, **100**(12), 7319–7324. (Page 25).

Strausfeld, N. J. and Hildebrand, J. G. 1999. Olfactory systems: common design, uncommon origins? *Curr Opin Neurobiol*, **9**(5), 634–639. (Page 6).

Sun, X.-J., Fonta, C., and Masson, C. 1993. Odour quality processing by bee antennal lobe interneurones. *Chem senses*, **18 no. 4**, 355–377. (Pages 21, 92, 162, 168, 170).

Svoboda, K. and Yasuda, R. 2006. Principles of two-photon excitation microscopy and its applications to neuroscience. *Neuron*, **50**(6), 823–839. (Page 25).

Szyszka, P. 2005. *Odor coding and neural plasticity in the mushroom body of the honeybee*. Ph.D. thesis, Freien Universität Berlin, Germany; FB Biologie, Chemie, Pharmazie. (Page 26).

Tolbert, L. P. and Hildebrand, J. G. 1981. Organization and synaptic ultrastructure of glomeruli in the antennal lobes of the moth *Manduca sexta*: a study using thin sections and freeze-fracture. *Proc R Soc Lond*, **213**, 279–301. (Page 17).

Valeur, B. and Leray, I. 2000. Design principles of fluorescent molecular sensors for cation recognition. *Coordin Chem Rev*, **205**, 3–40. (Page 172).

Van der Goes van Naters and Carlson 2007. Receptors and neurons for fly odors in drosophila. *Curr Biol*, **17**(7), 606–612. Wynand Van der Goes van Naters and John R Carlson. (Page 11).

Vermeulen, A. and Rospars, J.-P. 2004. Why are insect olfactory receptor neurons grouped into sensilla? The teachings of a model investigating the effects of the electrical interaction between neurons on the transepithelial potential and

the neuronal transmembrane potential. *Eur Biophys J*, **33**(7), 633–643. (Page 12).

Vogt, R. G., Prestwich, G. D., and Lerner, M. R. 1991. Odorant-binding-protein subfamilies associate with distinct classes of olfactory receptor neurons in insects. *J Neurobiol*, **22**(1), 74–84. (Page 11).

Wachowiak, M. and Cohen, L. B. 2001. Representation of odorants by receptor neuron input to the mouse olfactory bulb. *Neuron*, **32**(4), 723–735. (Page 191).

Wachowiak, M., Denk, W., and Friedrich, R. W. 2004. Functional organization of sensory input to the olfactory bulb glomerulus analyzed by two-photon calcium imaging. *Proc Natl Acad Sci U S A*, **101**(24), 9097–9102. (Page 25).

Wang, J. W., Wong, A. M., Flores, J., Vosshall, L. B., and Axel, R. 2003. Two-photon calcium imaging reveals an odor-evoked map of activity in the fly brain. *Cell*, **112**(2), 271–282. (Pages 8, 25, 27).

Wang, Y., Guo, H.-F., Pologruto, T. A., Hannan, F., Hakker, I., Svoboda, K., and Zhong, Y. 2004. Stereotyped odor-evoked activity in the mushroom body of Drosophila revealed by green fluorescent protein-based Ca^{2+} imaging. *J Neurosci*, **24**(29), 6507–6514. (Page 25).

Wilson, R. I. and Laurent, G. 2005. Role of gabaergic inhibition in shaping odor-evoked spatiotemporal patterns in the drosophila antennal lobe. *J Neurosci*, **25**(40), 9069–9079. (Page 17).

Wilson, R. I., Turner, G. C., and Laurent, G. 2004. Transformation of olfactory representations in the drosophila antennal lobe. *Science*, **303**(5656), 366–370. (Page 17).

Witthöft, W. 1967. Absolute Anzahl und Verteilung der Zellen im Hirn der Honigbiene. *Zeitschrift für Morphologie der Tiere*, **61**, 160–184. (Pages 6, 8, 13, 14, 18).

Xu, C., Zipfel, W., Shear, J. B., Williams, R. M., and Webb, W. W. 1996. Multiphoton fluorescence excitation: new spectral windows for biological nonlinear microscopy. *Proc Natl Acad Sci U S A*, **93**(20), 10763–10768. (Page 38).

Xu, F., Liu, N., Kida, I., Rothman, D. L., Hyder, F., and Shepherd, G. M. 2003. Odor maps of aldehydes and esters revealed by functional mri in the glomerular layer of the mouse olfactory bulb. *Proc Natl Acad Sci U S A*, **100**(19), 11029–11034. (Page 8).

Yaksi, E. and Friedrich, R. W. 2006. Reconstruction of firing rate changes across neuronal populations by temporally deconvolved Ca^{2+} imaging. *Nat Methods*, **3**(5), 377–383. (Pages 26, 173, 176).

Zou, D.-J., Chesler, A., and Firestein, S. 2009. How the olfactory bulb got its glomeruli: a just so story? *Nat Rev Neurosci*, **10**(8), 611–618. (Pages 7, 10).